HEWLETT-PACKARD
JOURNAL

February 1993

HEWLETT
PACKARD

HEWLETT-PACKARD JOURNAL

Articles

Departments

In this Issue

This issue is devoted entirely to lightwave instrumentation, that is, instruments for testing, analyzing, and characterizing fiber-optic communications systems, the components of those systems, and the signals found in those systems. Leading off the issue, the paper on page 6 summarizes the contributions of HP Laboratories to HP's lightwave instrumentation program. Many of the high-performance lightwave instruments designed at HP since the mid-1980s depend on photonics technologies developed or refined at HP Laboratories. These technologies include quantum-well semiconductor lasers with low threshold current densities and improved temperature performance, extremely stable ring YAG lasers, tunable external-cavity lasers, optical isolators to protect lasers from reflections and backscatter, the first integrated optical modulator in a commercial instrument, high-speed photodetectors, a scheme to measure the state and degree of polarization of an optical signal, spread-spectrum optical time-domain reflectometry, and low-coherence, white-light interferometry for resolving reflections less than a centimeter apart. In the remainder of this issue, some of these technologies are seen again, playing important roles in the design of five different kinds of lightwave instruments.

A potentially revolutionary development in fiber-optic communication system capacity is the use of wideband fiber amplifiers as repeaters. Because of the wide bandwidth of these amplifiers, many channels separated by wavelength can be transmitted over a single fiber without the need to separate the channels at each repeater. Characterization of these amplifiers requires light at many wavelengths, which can be provided either by many light sources or by a single, tunable light source. Two tunable laser sources designed for such applications are described in the article on page 11. Based on fundamental research done at HP Laboratories on external-cavity lasers, the two sources cover the two major fiber wavelength windows, the HP 8167A operating from 1280 to 1330 nanometers and the 8168A from 1500 to 1565 nanometers. Two essential requirements for any tunable source are that it be tunable to any wavelength within its operating range and that it produce a single-mode or single-frequency output at each wavelength. Early external-cavity lasers had problems with both requirements, and it was the research done at HP Laboratories that worked out solutions (see page 35). The next step was to construct a reliable, hermetically sealed laser module, which meant dealing with tight mechanical tolerances and learning to make high-quality antireflection coatings (see page 32). To use this laser module as the basis for an external-cavity laser, problems of power stability, tuning linearity, and wavelength stability had to be solved. The optomechanical design, including the tunable diffraction-grating and side-mode filters, is discussed in the article on page 20, along with wavelength calibration. Temperature stabilization, power control, and power calibration are the subjects of the article on page 28.

It's important to locate and measure reflections in optical components and systems because they can cause bad effects. For example, a laser may become unstable if the light it generates is reflected back into it. The size of a reflection is expressed as optical return loss, which is the ratio (in dB) of the incoming optical power to the optical power reflected by an optical component—the higher the return loss, the smaller the reflection. Two of the instruments in this issue are designed solely or partly to locate and measure reflections. Another is designed to measure the return loss of components connected to it without regard to the number of reflections or their locations.

The HP 8504A precision reflectometer can locate and measure reflections within components. It has a 75-dB return loss measurement range and can resolve reflections that are only 25 micrometers apart. It uses a method called white-light interferometry, which combines the 100-year-old Michelson interferometer and a light-emitting diode source. The light isn't really white, it's infrared, centered at 1300 or 1550 nanometers. "White-light" simply distinguishes the broad-spectrum, low-coherence light used here from single-frequency, high-coherence laser light. The design of the HP 8504A is described in the article on page 39, while the principles of its white-light interferometry technique are explained in the article on page 52 along with practical considerations such as noise, polarization dependence, dispersion, and spurious responses. The latter article also compares various methods of measuring return loss, including optical time-domain reflectometry, optical frequency-domain reflectometry, and power meter methods, giving the advantages, limitations, and uses of each method. On page 49 the design, fabrication, and

performance of the high-speed photodiodes used in the HP 8504A's polarization diversity receiver (a device that helps eliminate polarization dependence) are presented.

If instead of a small optical component you want to check out a fiber that's used for transmission, you're interested in losses and attenuation as well as reflections, and the distances involved are meters or kilometers instead of micrometers or millimeters. In this case, the instrument you need is an optical time-domain reflectometer, or OTDR. The OTDR is like an optical radar. It sends a pulse of laser light into the fiber under test and detects the reflected and backscattered light that returns from the fiber. Its display shows the locations and magnitudes of reflections and losses and the attenuation of the fiber. The HP 8146A OTDR (page 60) is a full-featured fourth-generation OTDR that can automatically characterize either short-haul or long-haul fiber-optic links in less than ten seconds. It is configured for operation at 1310 nanometers, 1550 nanometers, or both wavelengths by means of plug-in modules. Each module can be switched between a short-pulse, wideband mode for high-resolution short-haul measurements (less than 5 kilometers) and a longer-pulse, narrower-band mode for high-dynamic-range long-haul measurements. A key element in the HP 8146A's performance is a high-speed, flexible data processing system based on three custom gate arrays and a commercial digital signal processor chip (page 63). The data processing system makes selective use of techniques such as averaging, interleaving, variable decimation, and stitching to achieve various performance goals. The HP 8146A receiver (page 69) has short-haul, long-haul, and return loss modes and a −97-dBm rms noise level to support the instrument's 30-dB (optical) one-way dynamic range. The user interface (page 72) is designed for easy localization. It provides the automatic scan trace capability for rapid fiber characterization, a return loss measurement facility, an algorithm that eliminates ghost reflections caused by too high a pulse rate, and printer control for easy measurement documentation. With an optional software package, a PC can be used to control the OTDR and do analysis and documentation.

If you have an optical component and you simply want to make a precise measurement of its overall optical return loss, you can do it with a stable laser source, a coupler with low polarization dependence, an accurate reference reflection, and an accurate optical power meter. The article on page 79 explains an easy method for measuring overall optical return loss, discusses the sources of measurement uncertainty, and describes the HP 81534A return loss module, a plug-in for the HP 8153A optical multimeter. The return loss module is designed to work with a laser source module in the multimeter's other plug-in slot and the power measurement capability of the multimeter mainframe. It can measure return loss to 60 dB at wavelengths from 1250 to 1600 nanometers. Measurements to 50 dB are accurate within 0.4 dB and measurements from 50 to 60 dB are accurate within 0.65 dB.

Information in a fiber-optic communication system is typically in the form of optical pulses—an optical carrier signal is intensity modulated by an electrical pulse train at rates from 100 to 2,500 megapulses per second (up to 20 gigapulses per second in developmental systems). A lot of information about the performance of a fiber-optic system can be obtained by demodulating the optical pulses with a lightwave detector and looking at the resulting electrical pulses with an oscilloscope. However, there's a trade-off: amplifying the detected waveform improves the sensitivity of the detector but degrades the accuracy of the detected pulse shapes. The HP 83440 Series lightwave detectors (page 83) are designed for customers who want the best possible pulse accuracy and don't need high sensitivity. These detectors use unamplified high-speed HP photodiodes to demodulate light at carrier wavelengths of 1200 to 1600 nanometers. Careful optical, electrical, mechanical, and manufacturing process development results in electrical bandwidths of 6, 20, and 32 gigahertz. The detectors mount directly on a sampling oscilloscope. To test and calibrate the higher-bandwidth detectors, new systems were needed, and HP engineers responded with three different approaches: an optical impulse system, an optical heterodyne system, and an optical modulator system (see page 87). Photodetector frequency response measurements made by the three systems are in close agreement.

R.P. Dolan
Editor

Photonic Technology for Lightwave Communications Test Applications

State-of-the-art fiber-optic, integrated-optic, bulk-optic, and optoelectronic devices and subsystems provide a technology base for high-speed, high-performance lightwave communications test instrumentation.

by Waguih S. Ishak, Kent W. Carey, Steven A. Newton, and William R. Trutna, Jr.

The fiber-optic systems that emerged during the decade of the 1980s have revolutionized high-speed communications by competing very well with more traditional systems as cost-effective means for information exchange. These systems can operate at speeds up to several gigabits per second, and experimental systems in Japan and the U.S.A. are aimed at 40-Gbit/s and 100-Gbit/s transmission rates. The development of high-performance optical components such as fiber amplifiers has resulted in communications networks with spans of hundreds of kilometers without electronic repeaters. These developments are continuing at research laboratories around the world and it looks very feasible to see installed > 10-Gbit/s fiber-optic communications systems in the near future.

As the technology advances, the trends toward higher speeds, lower effective cost per bit and mile, and higher performance will continue. Designers of components, subsystems, and systems for fiber-optic communications need to maximize the performance of each block in the systems and to minimize the adverse interactions among systems blocks. For this reason, the designers need new techniques and measurement tools to help them carry out their work.

At Hewlett-Packard, a major program to develop lightwave communications measurement solutions was launched in the mid-1980s. This program has resulted in an impressive set of high-performance instruments including fault locators (optical time-domain reflectometers, or OTDRs), optical sources (fixed-wavelength and tunable sources), optical signal characterization instruments (power meters, signal analyzers, polarization analyzers, and spectrum analyzers), and optical component analyzers (precision reflectometers and high-speed analyzers).

The development of these instruments required an intensive R&D program at Hewlett-Packard Laboratories and at divisional R&D laboratories to identify and develop key enabling photonics technologies for these instruments.

These technologies include integrated optic and optoelectronic devices as well as bulk-optic and fiber-optic components and subsystems. Some of these devices and subsystems have been used in some of the lightwave instruments described in this and previous issues of the HP Journal. Other devices have been used as internal characterization tools. It is the purpose of this paper to give an overview of some of these key technologies. In the first section, we will review some of the basic technologies for optical signal generation. In the

second and third sections, we will discuss technologies used for analysis of optical signals and characterization of optical components, respectively. Finally, we will briefly touch on two important characterization tools that made possible the development of high-performance photonic components.
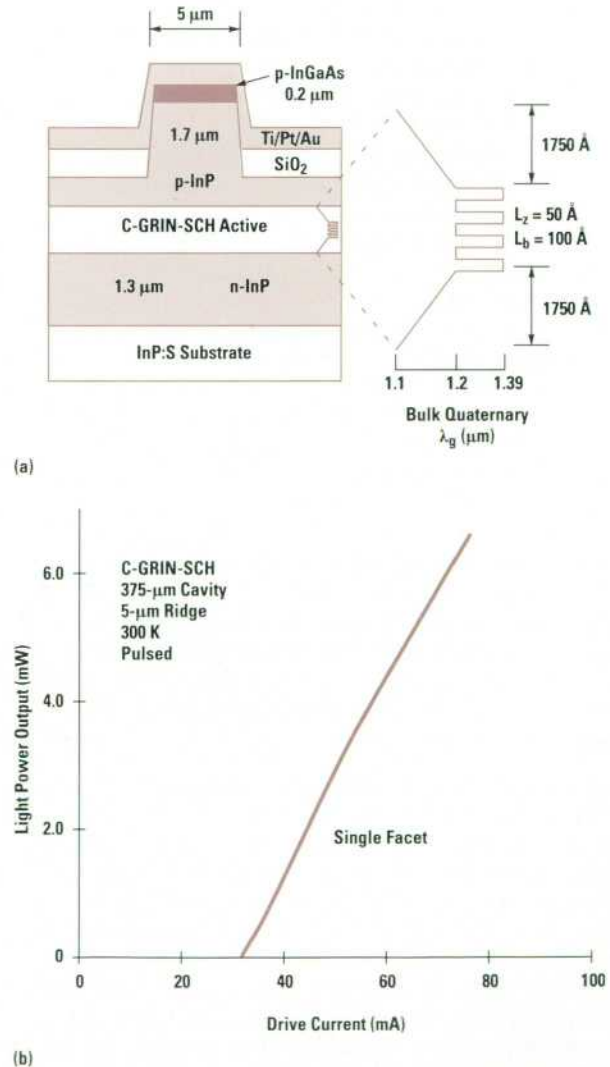

Fig. 1. (a) Schematic cross section of the C-GRIN-SCH multiple-quantum-well ridge waveguide laser. (b) Single-facet light output power of the device as a function of drive current.

Optical Signal Generation

Generating an Optical Signal—Semiconductor Lasers.
Semiconductor laser diodes play a very important role in test instruments for lightwave communications. While it is possible to purchase certain kinds of laser diodes (such as pigtailed distributed feedback lasers), it is not always possible to obtain bare laser chips with specific parameters suited for use in lightwave subsystems. The use of quantum wells in AlGaAs/GaAs lasers has resulted in impressive reductions of threshold current densities and improved temperature performance. Since then, many groups have been working to extend the quantum well technology to other material systems such as InGaAsP/InP for long-wavelength (1.3 and 1.55 mm) applications with impressive results. At HP Laboratories, as part of our epitaxial material technology development, we grew and fabricated graded-index separate confinement heterostructure (GRIN-SCH) quantum well ridge[1] and buried heterostructure (BH) lasers. Fig. 1(a) shows a cross section of a ridge laser with four quantum wells and Fig. 1(b) shows the output-light-versus-threshold-current characteristic of this laser.

Generating an Extremely Stable Optical Signal—YAG Lasers.
Monolithic diode-pumped unidirectional ring YAG lasers have extremely narrow linewidths and single-mode output spectra. This characteristic is useful for such applications as coherent communications and heterodyne component testing. A ring YAG laser developed earlier at HP Laboratories was very useful for the heterodyne characterization of high-speed photodetectors. For these and other applications, rapid tuning of the laser is desirable. Since the earlier ring laser was tuned by thermal expansion or by thermally stressing the crystal, the tuning speeds were relatively low. A two-piece piezoelectrically tuned ring laser, its design derived from the earlier one-piece ring laser, was developed.[2] This laser can be continuously tuned in milliseconds over more than 13 GHz. It consists of a YAG section and a magnetic glass section. The glass piece is mounted on a piezoelectric transducer. By driving the transducer at its fundamental resonance, the length of the gap between the YAG and the glass sections is changed, resulting in a change in the optical path length of the laser. This path length change produces a change in the output frequency of the laser. The laser produces more than 1 mW of single-mode output power at 1338 nm when pumped with a 30-mW AlGaAs semiconductor laser. Using a PZT (lead zirconate titanate) transducer, the laser was tuned over a 13.5-GHz range with a tuning rate limited only by the 4.6-kHz frequency response of the PZT.

Generating Tunable Optical Sources—External-Cavity Lasers.
As the performance of optical components is improved, new and improved measuring techniques and tools are needed. Particularly important are accurate measurements of the performance of components and systems as a function of wavelength. For example, with the rapid development of broadband erbium-doped fiber amplifiers in communications links, a widely tunable optical source is needed for wavelength characterization. The external-cavity semiconductor laser is a device that can satisfy this requirement. At HP Laboratories, we developed alignment-tolerant, single-mode, and widely-tunable external-cavity lasers in the 1.3 and 1.55-mm wavelength ranges. One of the interesting configurations of a grating-tuned external-cavity laser (Fig. 2)
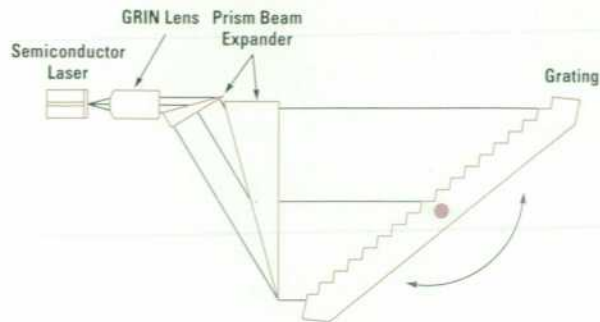
Fig. 2. Grating external-cavity semiconductor laser with a graded-index rod collimating lens and two silicon prism beam expanders at Brewster angle incidence.

incorporates a gradient-index rod lens and a pair of silicon prism beam expanders.[3] This laser achieves the following objectives simultaneously:

- Ability to operate at any external-cavity longitudinal mode without tuning gaps
- Stable feedback coupling between the laser diode and the external cavity
- Narrow optical linewidth
- A high degree of external cavity side-mode suppression
- A very wide tuning range.

The results obtained showed complete wavelength coverage over more than 100 nanometers with single-mode operation over most of the tuning range. The linewidth was less than 100 kHz and the side-mode suppression ratio was greater than 70 dB. We also developed other external-cavity laser configurations to tune over wider tuning ranges and to enhance the single-mode properties of the laser. One of these configurations forms the heart of the HP 8167A and 8168A tunable laser sources (see articles, pages 11 and 20).

Protecting the Optical Sources—Isolators.
High-performance optical isolators are playing an increasingly important role in lightwave instruments. Their purpose is to protect optical sources from reflections and backscattering that cause output instabilities or unwanted changes in the output spectra of the optical sources. The HP isolator combines rutile birefringent walk-off crystals and bismuth-doped yttrium iron garnet films (Bi-YIG) in a proprietary design that provides high isolation, low insertion loss, high return loss, and polarization independence over wide wavelength and temperature ranges.[4]

Modulating the Optical Sources—Modulators.
HP is credited with developing the world's first integrated optic modulator for a commercial instrument application.[5] The Mach-Zehnder lithium niobate ($LiNbO_3$) modulator used in the HP 8703A lightwave component analyzer uses titanium-diffused optical waveguides and exhibits a bandwidth of more than 20 GHz. The limitation on the bandwidth of this modulator is mainly the mismatch between the optical and microwave velocities. Building on the success of this 20-GHz modulator, HP Laboratories developed a new modulator configuration[6] that is velocity matched to frequencies in excess of 50 GHz with excellent loss-drive ratio and contrast characteristics over the 1.3-to-1.55-mm wavelength range. The modulator is a Mach-Zehnder type. It uses a thick-electrode, buffer-layer geometry that results in a device that achieves almost exact

velocity matching to the optical index, maintains high impedance, and has a very low voltage-length product. The structure uses a narrow ground plane whose width is only slightly larger than the electrode width, resulting in higher impedance and increased microwave velocity. This introduces an extra degree of freedom that allows exact matching of the optical and microwave indexes at a reasonably high impedance. The optical waveguides in the active section of the device are fabricated with a high enough index difference to be multimode at 1.3 mm. The input and output waveguide sections are reduced in width so as to be single-mode over the entire range from 1.3 to 1.55 mm. The symmetric, adiabatic nature of the Y junction connecting these two regions ensures that no coupling occurs to the higher-order modes of the active section.

Several cuts of LiNbO$_3$ wafers were used to verify the design of this modulator and excellent agreement with theory was obtained. Fig. 3a shows a cross section of the modulator design and Fig. 3b shows the exceptional bandwidth characteristics of this device. Measurements showed more than 60 GHz of bandwidth with a voltage-length product as low as 8.3 volt-cm over the 1.3-to-1.55-mm range.

Optical Signal Analysis
Measuring the Amplitude of Optical Signals—Photodetectors.
One of the first challenges facing HP Laboratories designers was to develop a high-speed infrared (1200 to 1600 nm) photodetector, which would form the basis for the optical receivers needed for many lightwave instruments. This required high-quality epitaxially grown layers of indium

gallium arsenide (InGaAs) on indium phosphide (InP) substrates and careful device design to minimize spurious capacitance and maximize the photodetector responsivity. For material growth, metalorganic chemical vapor deposition (MOCVD) was the method of choice because of the uniform thickness and low defect density in the grown films. A front-illuminated, circular, p-i-n device structure was chosen, and the layer thicknesses were designed to produce the 22-GHz response needed for the first-generation lightwave receivers. The InGaAs/InP p-i-n photodetector technology has been extended to develop and produce higher-frequency detectors (up to 50 GHz). Other work in GaInAs/InP photodetectors has concentrated on special needs for extended wavelength response (600 to 1600 nm achieved), and custom configurations such as a chip with two photodiodes with a precise separation for a polarization diversity receiver. This dual photodetector is used in the HP 8504A precision reflectometer (see article, page 39).

Measuring the Polarization of Optical Signals—Polarimeters. To measure the polarization sensitivity of optical components, an efficient real-time technique for accurately measuring the state of polarization and degree of polarization of an optical signal is needed. A scheme to measure the state of polarization and degree of polarization in real time was developed at HP Laboratories. This approach forms the basis for the HP 8509A lightwave polarization analyzer. The signal under test is transmitted out of an optical fiber and diverges onto four mirrors in a specific arrangement. The reflected beams are processed using bulk optic components and then transformed into electrical signals by four photodetectors to produce the needed Stokes parameters.[7] From these parameters, the final state of polarization is determined using electronic postprocessing. The results are displayed in various formats (polarization ellipse or Poincaré sphere) on a personal computer capable of providing the user with menu-driven software suited for several important polarization measurements.[8]

Optical Component Characterization
The optical sources and optical receivers described above can be used to build optical component analyzers such as the HP 8702A and 8703A.[9,10] These instruments are broadband optical subcarrier network analyzers that are capable of measuring the RF response of optical or optoelectronic components and networks out to a frequency of 20 GHz in the case of the HP 8703A. By calculating the inverse Fourier transform of these responses, a time-domain picture of the network under test can be obtained. Thus, these instruments can also serve as optical frequency-domain reflectometers (OFDRs) that are capable (in the case of the HP 8703A) of resolving reflections spaced less than a centimeter apart.

Coherent FMCW (frequency modulated continuous wave) reflectometry techniques can provide high sensitivity coupled with high resolution. Using tunable miniature YAG lasers, we were able to implement an FMCW reflectometer capable of resolving reflections spaced 5 cm apart.
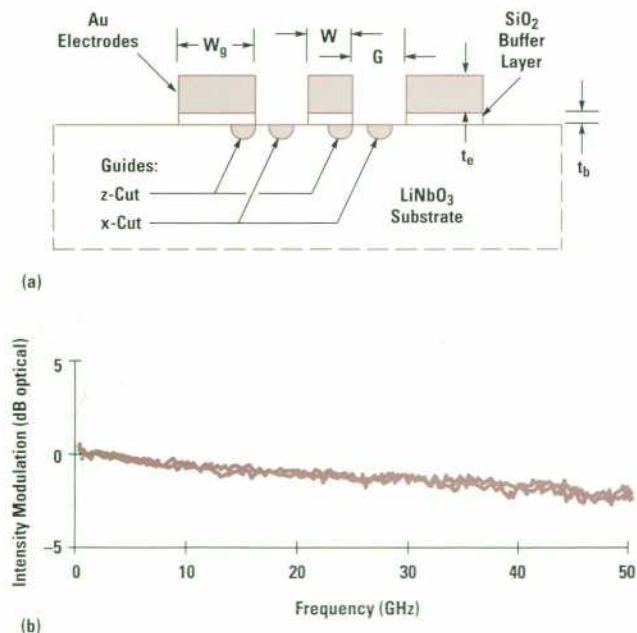
Fig. 3. (a) Cross section of the microwave coplanar modulator structure. (b) Frequency response of a 1-cm x-cut device.

Some reflectometry applications require that a user be able to look inside of a component, that is, to resolve reflections that are spaced less than 1 mm apart. The HP 8504A precision reflectometer (see article, page 39) was developed in response to these needs. This instrument is based on the well-known principle of white-light interferometry, in which coherent interference between reflections in each of two arms of an interferometer can be detected only if their distances to the splitting and recombining point are equal, to within the coherence length of the source. By locating the device under test at the end of one interferometer arm, scanning the position of a reference mirror at the end of the other, and detecting the positions where coherent interference takes place, the instrument effectively scans through the device under test, mapping out the positions and amplitudes of reflections. By using a broadband source with a short coherence length, reflections spaced less than 50 micrometers apart can be resolved. Using proprietary calibration techniques, accurate measurements of reflection amplitudes as small as −80 dB can be obtained. This resolution and reflection sensitivity are orders of magnitude better than those of other commercially available reflectometers.

The research team at HP Laboratories is a world leader in this technology. Early in 1992, they reported a reflectometry experiment[11] in which they demonstrated a world-record reflection sensitivity of −148 dB as shown in Fig. 4.

Characterization Tools

Two important characterization tools made possible the development of the photonics devices mentioned in this article. The first is photoluminescence and the second is electrooptic sampling. Photoluminescence (continuous wave and time-resolved) is used to characterize III-V compound semiconductor epitaxial films and is crucial to the development of high-quality films. For example, Fig. 5 shows time-resolved photoluminescence from AlGaInP structures for five excitation energies. The persistence of the long decay times at the low energy levels indicates high

Fig. 5. Photoluminescence data for AlGaInP quantum well devices.

material quality. This AlGaInP is used in HP's new high-brightness yellow and orange LEDs.

Electrooptic sampling is a tool for characterization of high-speed devices. It was very important to the time-domain characterization of the InGaAs photodetectors. At HP Laboratories, we continue to invest in photoluminescence measurements and electrooptical sampling to enhance their capabilities.

Conclusions

The success of the Hewlett-Packard lightwave instruments program is due in part to the strong photonics technology base at HP Laboratories and the healthy coupling and interaction between HP Laboratories and the divisional R&D programs. This interaction will continue to be an integral factor in the success of the program and the new products that are yet to come.

Acknowledgments

Fig. 4. Spatially averaged Rayleigh backscattering data using low-coherence reflectometry with 3.4-mm resolution.

References

1. M.J. Ludowise, T.R. Ranganath, and A. Fischer-Colbrie, "Continuously graded-index separate confinement heterostructure multi-quantum well $Ga_{1-x}In_xAs_{1-y}P_y$/InP ridge waveguide lasers grown by low-pressure metalorganic chemical vapor deposition with lattice-matched quaternary wells and barriers," *Applied Physics Letters*, Vol. 57, no. 15, October 8, 1990, p. 1493.

2. W.R. Trutna, Jr. and D.K. Donald, "Two piece, piezoelectrically tuned, single-mode Nd:YAG ring laser," *Optics Letters*, Vol. 15, 1990, pp. 369-371.

3. P. Zorabedian, "Characteristics of a grating-external-cavity semiconductor laser containing intracavity prism beam expanders," *Journal of Lightwave Technology*, Vol. 10, March 1992, pp. 330-335.

4. K.W. Chang, et al, "A High-Performance Optical Isolator for Lightwave Systems," *Hewlett-Packard Journal*, Vol. 42, no. 1, February 1991, pp. 45-50.

5. R.L. Jungerman and D.J. McQuate, "Development of an Optical Modulator for a High-Speed Lightwave Component Analyzer, *ibid*, pp. 41-45.

6. D.W. Dolfi and T.R. Ranganath, "50 GHz velocity-matched, broadband wavelength $LiNbO_3$ modulator with multimode active section," *Electronics Letters*, 1992.

7. P. Hernday and R. Cross, "Polarization Measurements in Lightwave Applications Using a New Real-Time Polarization Analyzer," *Hewlett-Packard Lightwave Test Seminar*, 1992.

8. R. Cross, B. Heffner, and P. Hernday, "Polarization measurement goes automatic," *Lasers and Optotronics*, November 1991, pp. 1-4.

9. R.W. Wong, et al "High-Speed Lightwave Component Analysis," *Hewlett-Packard Journal*, Vol. 40, no. 3, June 1989, pp. 35-51.

10. P.R. Hernday, et al "Design of a 20-GHz Lightwave Component Analyzer," *Hewlett-Packard Journal*, Vol. 42, no. 1, February 1991, pp. 13-22.

11. W.V. Sorin and D.M. Baney, "Measurement of Rayleigh backscattering at 1.55 mm with 32-mm spatial resolution," *Photonics Technology Letters*, Vol. 4, April 1992, pp. 374-376.

Cover

The colorful object shown in the background is a diffraction grating, a piece of glass with 1200 grooves per millimeter etched into its surface. In the new HP tunable laser sources, turning such a grating changes the wavelength of the light generated by the little laser module in the foreground. The laser light in this photo is simulated, of course; the real light is infrared and wouldn't be visible.

What's Ahead

The April issue will present the design stories of six products or groups of products:
- The HP 8370 Series and HP 70340 Series synthesized signal generators
- The HP 87350 Series sweep oscillators
- The HP 8133A 3-GHz pulse generator
- The HP 64700 embedded debug environment for the HP 64700 emulator system
- The HP 3569A portable real-time frequency analyzer
- The HP LanProbe II implementation of the Remote Monitoring Management Information Base (RMON MIB) of the Simple Network Management Protocol (SNMP).

Tunable Laser Sources for Optical Amplifier Testing

Two models of laser sources tune over wavelength ranges of 50 and 65 nanometers using grating-tuned external-cavity lasers with precisely controlled wavelength and power level. They are designed for testing wideband components such as erbium-doped fiber amplifiers.

by Bernd Maisenbacher, Edgar Leckel, Robert Jahn, and Michael Pott

Recently there has been great interest in using erbium-doped fiber amplifiers (EDFAs) as repeaters in lightwave transmission systems. These optical amplifiers are attractive alternatives to regenerative optoelectronic repeaters because they can amplify any optical signal within their bandwidth, independent of the modulation format, the bit rate, and the wavelength. Similar results can be obtained with semiconductor amplifiers, which are mainly used for the 1300-nm transmission window, and with praseodymium-doped fiber amplifiers.

The signal bandwidth of these optical amplifiers is extremely wide because the carrier is light. Therefore, their installation is expected to bring about a new revolution in optical communication system capacity. Many channels separated by wavelength can now be independently transmitted over a long piece of fiber without the need to separate these channels at each repeater. The channels are combined in the transmitter and redistributed at the receiver terminal by wavelength division multiplexers (WDMs), as shown in Fig. 1. With the WDM technique, the capacity of an installed fiber with EDFAs as repeaters can be enhanced by a factor of 10 or even 100.

When many EDFAs are cascaded, they must be extremely well-characterized so that their overall performance can be predicted. In WDM applications, each transmission channel should have nearly the same gain or loss performance at the receiving end, even after going through many amplifiers. Therefore, each amplifier must be characterized for gain, noise, and saturation level as functions of wavelength. This requires either many semiconductor light sources with different wavelengths or one tunable light source.

Lasers normally emit light at well-known and fixed wavelengths. A tunable laser, on the other hand, lets you select the wavelength. There are several ways of building tunable lasers, but for tuning ranges greater than 50 nm, which is the minimum required to characterize an EDFA system, only lasers with external cavities as resonators and diffraction gratings as wavelength selectors are suitable at this time.

Based on fundamental research done at HP Laboratories on external-cavity lasers, (see article, page 35), two tunable laser sources have been developed (see Fig. 2). The HP 8167A operates over the wavelength range from 1280 to 1330 nm and the HP 8168A operates from 1500 to 1565 nm.

Fig. 3 shows the operating ranges of the two tunable laser sources, the two fiber windows, the components that need to be characterized in each window, and the types of wavelength dependence that need to be measured. For characterization of passive components like filters, couplers, and wavelength division multiplexers, a tunable laser source
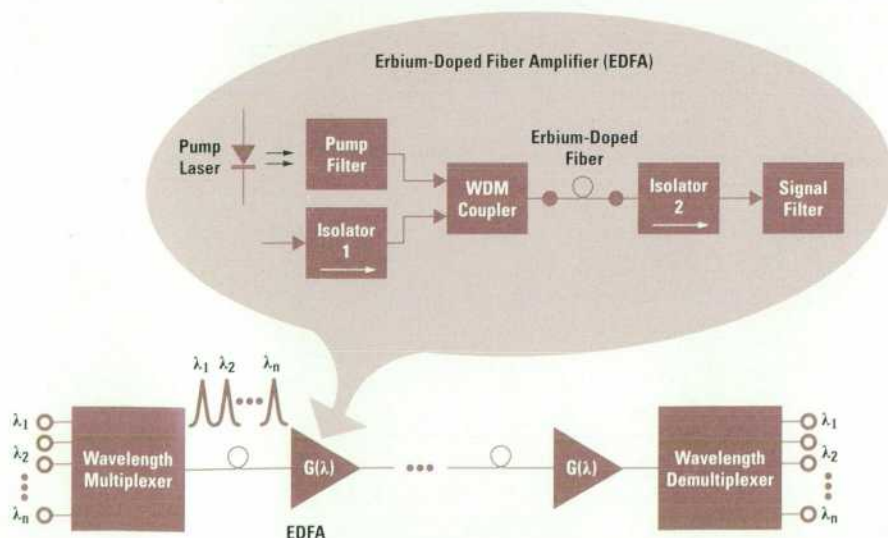
Fig. 1. Modern communication systems are using wavelength division multiplexers (WDMs) and erbium-doped fiber amplifiers (EDFAs) to increase capacity.

Fig. 2. The HP 8167A tunable laser source operates over the wavelength range from 1280 to 1330 nm. The HP 8168A, which is identical in appearance, operates from 1500 to 1565 nm.

needs a wide tuning range and fine wavelength resolution. For fiber amplifiers, low signal noise, high output power, and a single lasing mode are the dominant requirements. In general, for both production and R&D applications, customers want a power-stabilized output, a fast tuning speed, no reflections from the instrument output, ruggedness, and reliability.

Design Challenges

External-cavity lasers are in principle very sensitive to external influences. Temperature changes cause changes in the length of the external resonator, which change the frequency of the standing waves. The required wavelength stability for an external-cavity laser is on the order of 100 MHz or 1 picometer within 1 hour. How this is achieved is described in the article on page 20.

Reliability is hard to measure, but precautions such as hermetically sealing the semiconductor laser chip so that humidity can't destroy it can help ensure a long lifetime for the instrument. The design of the laser module for the tunable laser sources is described the article on page 32.

For the required tuning range of more than 50 nm for the 1300-nm window and more than 65 nm for the 1550-nm window, the semiconductor laser material must have a wide gain characteristic. A perfectly matched optomechanical

assembly and a high-reflection grating are also necessary. To get the highest possible output power, low loss is required, both in the lenses and for the coupling into a 9-µm single-mode fiber. A wavelength resolution of better than 1 pm is necessary for the evaluation of optical filters with a very narrow bandpass characteristic, such as etalons and Fabry-Perot filters. How these requirements were met is described in the article on page 20.

Low signal noise in a tunable laser requires that the laser cavity be isolated from any backreflections by blocking the backward traveling light with a double-stage isolator. Especially in EDFA applications, weak optical terminations have to be avoided because of their backreflections, which can form cavities with other reflection sources and can cause interference ripple on the measurement signal, thereby increasing the measurement uncertainty. High return loss is therefore required at the output of a tunable laser source.

The hardest goal for the design was to achieve a fast tuning speed. For steps below 1 nm a total settling time of better than 200 ms is required. Within that timeframe the new wavelength and power level has to be settled and stabilized at the output of the instrument. The design team optimized the task sharing between the microprocessor software and the electronic circuitry and achieved a settling time of better than 150 ms.
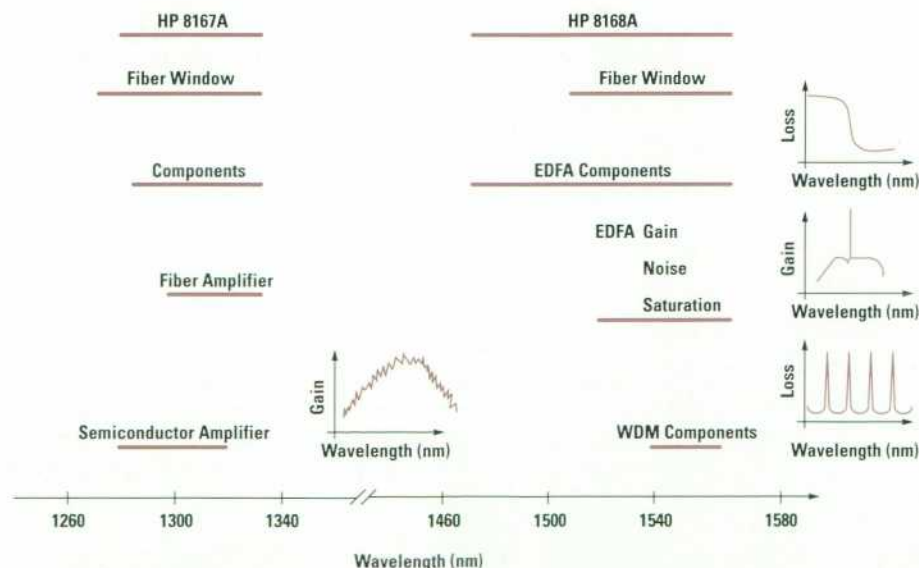
Fig. 3. Characterization of components over wavelength.
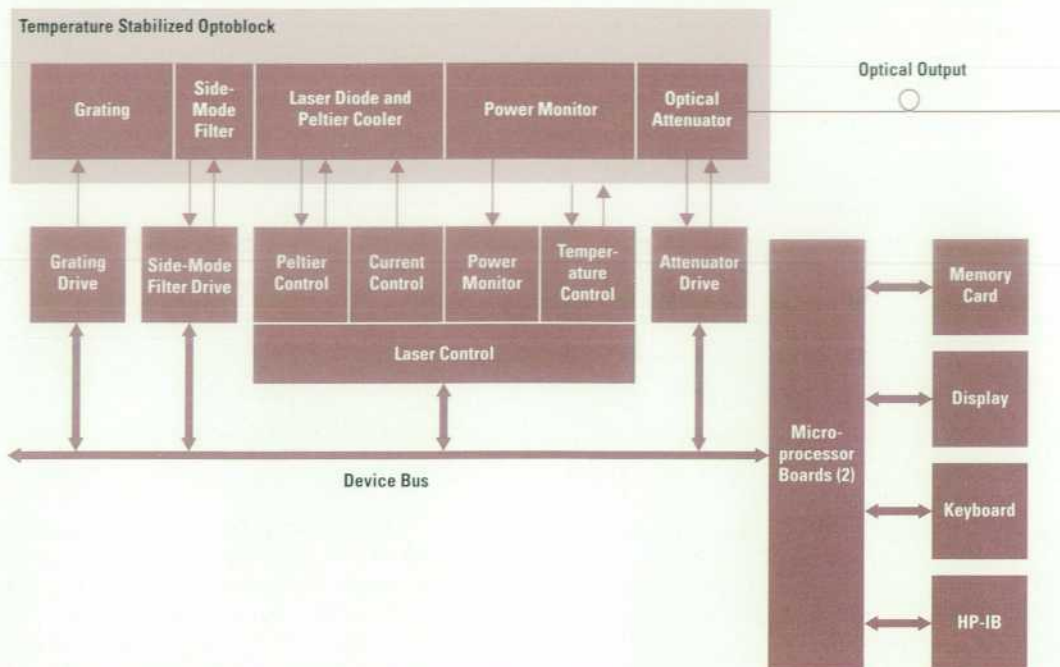
Fig. 4. Overall block diagram of the HP 8167A and 8168A tunable laser sources.

A pure single-mode laser output is needed. This means that spontaneous emissions of the laser and the side modes of the laser chip have to suppressed as much as possible. A side-mode suppression ratio of better than 40 dB is required. This number is very important in EDFA applications, where the amplified spontaneous emissions of the pumped erbium-doped fiber have to be measured for calculation of the gain and noise figure in transmission systems.

Architecture

Precise motor drivers, dedicated hardware, and robust calibration contribute to the performance of the HP 8167A and 8168A tunable laser sources. Performance is measured in three dimensions: power, wavelength, and time. Wavelength accuracy, repeatability, and linearity depend mainly on precise motor drivers and their calibration. Power flatness and repeatability depend on a high-resolution digital-to-analog converter (DAC) and calibration. Wavelength and power stability over time is achieved by hardware and software control loops. Fast tuning speed is achieved by optimizing motor driver speed and processing time.

Fig. 4 shows the block diagram of the instrument. The main part is the optoblock, which contains all the optical components (see article, page 20). There are two microprocessor boards, two motor driver boards, and an analog driver board. All boards are connected via the instrument device bus. The microprocessor supports the keyboard, display, HP-IB (IEEE 488, IEC 625), and memory card directly.

To rotate the grating to change the laser wavelength, a precise stepper motor with a control board is used. The side-mode filter (a Fabry-Perot etalon) and the optical attenuator are moved with dc motor/encoder setups and the necessary drivers. The laser control board hosts the current control for the laser diode and the power monitor loop. The laser chip

is temperature stabilized with the help of a Peltier cooler. The optoblock is also temperature stabilized.

Grating Drive
The grating drive is responsible for the wavelength resolution and the absolute wavelength accuracy of the instrument. A stepper motor with a micrometer leadscrew is used. Microstepping (10,000 microsteps/rev) provides a mechanical resolution of 50 nm. A lost-motion compensation function minimizes mechanical backlash and hysteresis effects and provides a bidirectional repeatability of ±100 nm over the entire range of travel. Acceleration and velocity can be chosen independently.

The stepper motor loses its current mechanical position after a power shutdown. To get an absolute reference point for the system an initial position is necessary. At power-on the stepper motor finds its initial position within ±100 nm with the help of a precision switch. This results in a absolute wavelength accuracy of better than 0.1 nm. Fig. 5 gives an overview of the key components of the grating drive.

The processor chip (a Z8) controls all elementary movements of the motor and communicates directly with the instrument device bus, the velocity and acceleration counter, the memory, and the DACs. The DACs control the two phases of the motor via power amplifiers. The switch indicates the zero position. Fig. 6 shows an example of the repeatability and accuracy of the stepper motor system.

Side-Mode Filter Drive
The side-mode filter, a Fabry-Perot etalon, guarantees single-mode operation of the laser over the tuning range. It has to be well-synchronized with the grating drive. The side-mode filter drive consists of a dc motor and an encoder with 1024 tracks. Fig. 7 shows the block diagram of this arrangement. The motor controller chip is connected directly to the
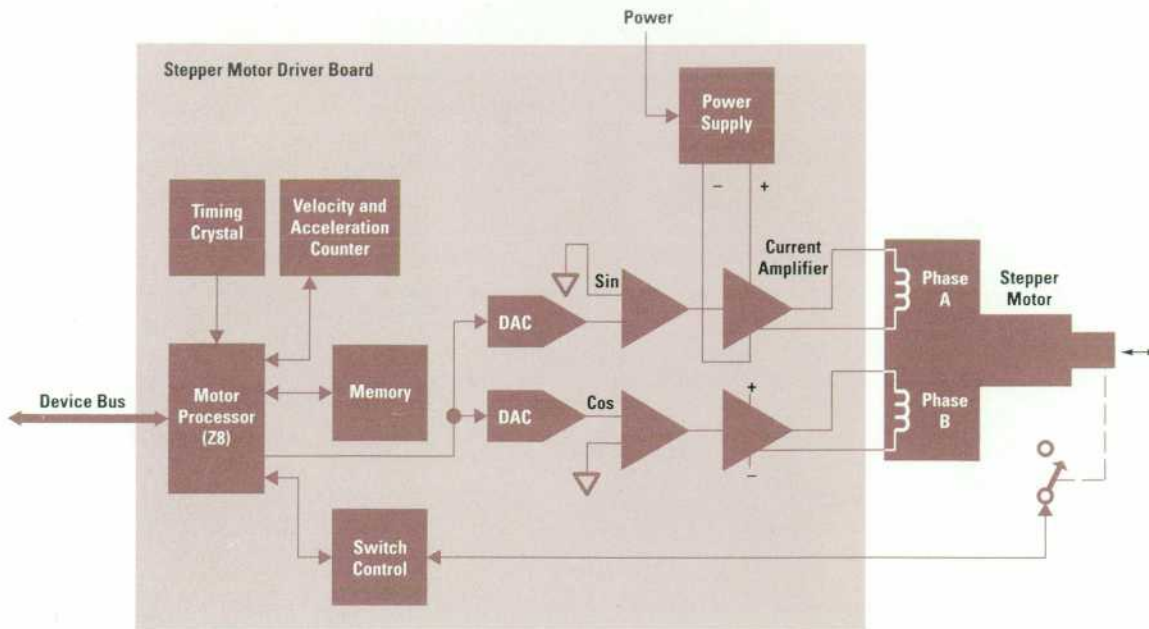
Fig. 5. Key components of the stepper motor driver, precision position reference switch, and stepper motor.

instrument device bus. The encoder signal is fed directly to the chip and the motor is driven by a bridge driver.

The motor controller profile generator lets the designer choose the acceleration and maximum velocity of the system. The maximum acceleration depends on the mechanical setup and the motor, and the maximum velocity depends on the encoder detection speed. Fig. 8 shows typical velocity profiles.

In our case we work in the position mode and therefore curve 2 in Fig. 8 must be used whenever possible to achieve the fastest moving speed. The velocity profile is compared with the encoder signal at every sampling point. The digital PID (proportional integral derivative) filter allows control of the behavior of the loop. The motor should follow the profile within one sample time to get the best tuning speed and transient behavior. The transfer function of the digital filter is:

$$U(n) = K_p e(n) + K_i \sum_{k=0}^{n} e(k) + K_d[e(n') - e(n' - 1)],$$
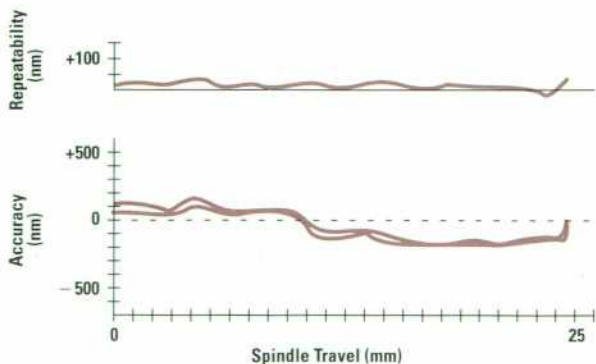
<div align="center">
proportional   integral   derivative term
term   term
</div>

where n is the current sample number. For calculating the derivative term, the current samples can be used, but often it is possible to use sample values taken several sample times earlier. Thus, sometimes $n' = n$, but usually $n' \neq n$.

The system is optimized for zero position error, no chatter in the final position, and minimum moving time. Typically, the final position will be within ±1 count of the desired position 100% of the time and will exactly match the desired position 99.9% of the time. The moving time is typically 100 ms.

Optical Attenuator Drive

The optical attenuator provides an attenuation range of 40 dB with a resolution of 0.1 dB. The attenuator drive has the same arrangement as the side-mode filter drive, but the motor encoder has only 512 tracks. This drive is optimized for a maximum overshoot or undershoot of ±0.03 dB (approximately ±1 count).

Fig. 6. Repeatability and accuracy of the stepper motor system.
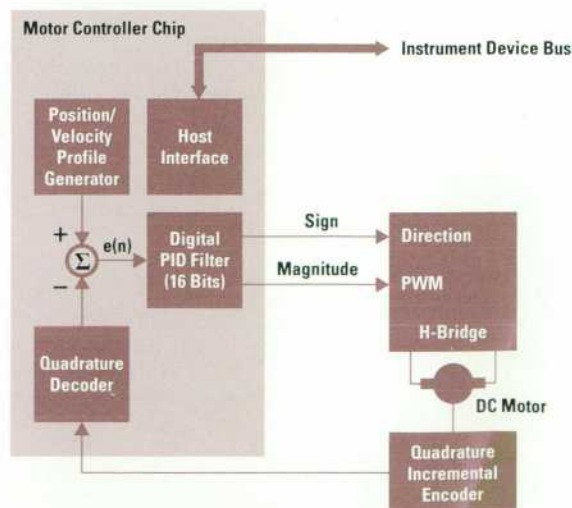
Fig. 7. Block diagram of the side-mode filter drive.
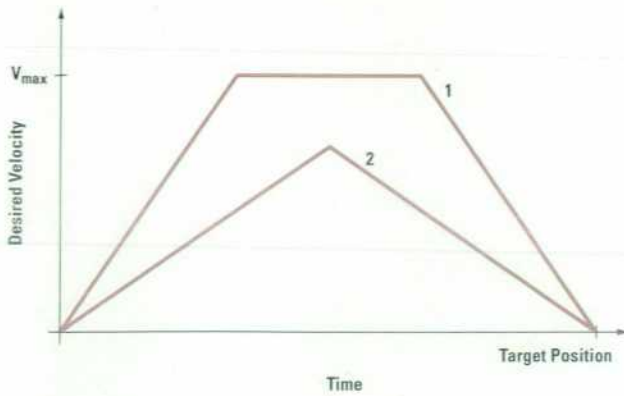
Fig. 8. Velocity profiles of the motor controller.

Microprocessor Hardware and Firmware

The main objectives in the firmware and microprocessor hardware design and development of the HP 8167A and 8168A tunable laser sources were an easy-to-handle firmware update capability, a flexible user interface for future extensions, and all preparations necessary for integrating the instruments into an automated measurement environment. We wanted to make it easy to satisfy future customer requirements by enhancing the instruments' capabilities with additional options.

Microprocessor Hardware

Fig. 9 gives an overview of the processor hardware. The main functional blocks are:

- A 68000 CPU with logic for clock and reset generation, address decoding, and wait state generation. The number of wait cycles of the I/O (e.g., for the HP-IB) can be selected at execution time by using different access addresses.
- Up to 1.5M bytes of memory (flash EPROMs, static RAMs), sufficient for later firmware add-ons.
- Additional battery-buffered RAM for storing nonvolatile information such as parameter settings.
- Interface for connecting memory cards to the instrument.

- Special boot logic for downloading firmware from memory cards at power-on.
- Dot matrix display (256 by 64 pixels) for a flexible and attractive user interface.
- HP-IB (IEEE 488, IEC 625) interface with controller capabilities.
- Easy-to-use interface bus with interrupt capability for connecting other electronics (e.g., motor control, laser control) to the processor.
- All electronics necessary for making the instrument behave like an MSIB* mainframe.

Firmware Updates

The conventional practice for embedded firmware for stand-alone instruments is to put the compiled and linked firmware into EPROMs. These memories are duplicated in production and plugged into the individual instruments. If the firmware has to be replaced during firmware development or later at the customer location, it is a very time-consuming and expensive process.

To avoid these disadvantages we use flash EPROMs, allowing in-system programming. The only difficulty was to get the firmware into these memories without having any firmware code already in the instrument, that is, without a bootstrap loader. The solution was to supply the hardware with a boot switch capability used in conjunction with a memory card (see Fig. 10).

When the instrument is switched on, the flash EPROMs begin at address 0, where the CPU starts working. This is the normal case, but it only works if there is already firmware in the EPROMs. To get the firmware transferred to the flash memory, we use a memory card. With the memory card inserted, pressing a certain key combination on the front panel during power-up switches the address decoding so that the CPU starts executing the firmware on the memory card, which now lies at address 0.

---

* Modular System Interface Bus, the internal bus of the HP Modular Measurement System, now an open standard.
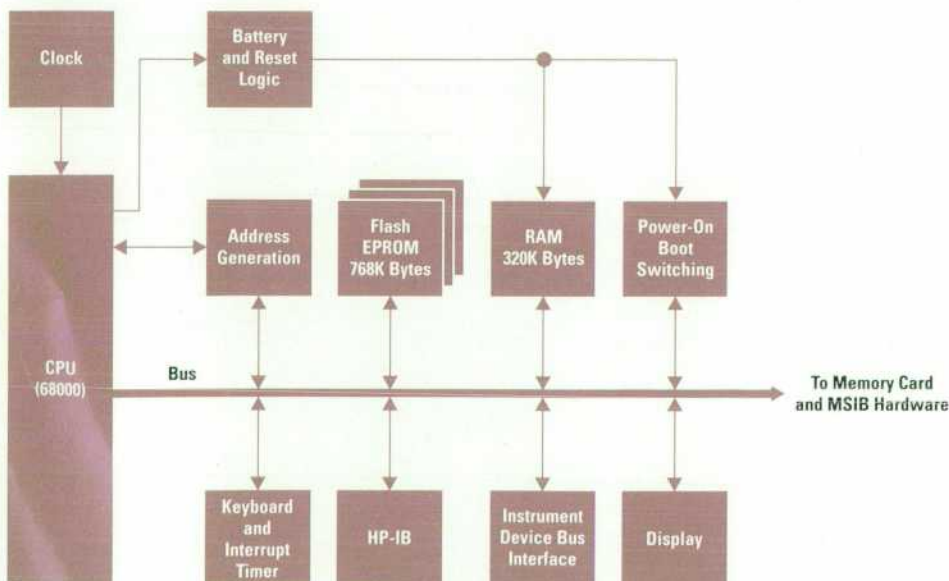
Fig. 9. Tunable laser source microprocessor hardware.
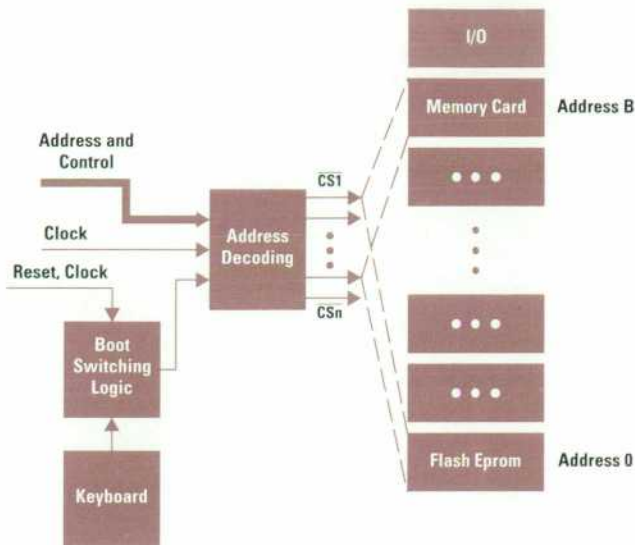
Fig. 10. Boot switching logic makes it possible to boot the firmware from a memory card instead of EPROM.

The firmware recognizes that it is running on the memory card and starts a special download function for copying itself to the flash EPROMs. When the copying is complete, the memory card is removed from the slot and the instrument boots normally, now disregarding the firmware download function. This can be done as often as needed.

Using this feature during the development of the instruments, we were able offer short response times for updating all development instruments with prerelease firmware revisions for testing and special purposes.

User Interface

The goal of the user interface development was to make the input of parameters from the front panel and feedback to the user on the display as intuitive as possible.

Main keyboard functions are grouped (data entry, parameter selection, softkeys) and the most important functions have hardkeys of different sizes associated with them. The main tasks can be done directly (e.g., switching the laser on and off), while other features are reachable with softkeys (e.g., switching the modulation on and off).

The programmable dot matrix display has a resolution of 256 by 64 pixels and supplies various output capabilities such as different character sizes, small curves, and scroll boxes. Fig. 11 shows some examples from the wide range of display organizations.

The softkeys together with the graphic display offer considerable flexibility for adding firmware options when new user interface requirements occur in the future.

Firmware Development Environment

The firmware was coded using HP 9000 workstations in a local area network. The programming language was C. HP 64000 emulators, together with tools such as a high-level language debugger, were used for developing, testing, and debugging the firmware.

Fig. 11. Examples of display formats.

The libraries used were a real-time operating system for embedded systems and a driver for programming the HP-IB according to the IEEE 488.2 standard.

Firmware Structure

Fig. 12 shows the general firmware structure. The platform on which the firmware is built is the real-time operating system. The main task of the firmware is to react to asynchronous environmental events (keyboard, rotary pulse generator, HP-IB, etc.). It processes the inputs and stimulates the hardware (motors, laser control) accordingly.

The low-level drivers are used to access the hardware (ADCs, motor control, display, etc.). They separate the higher functionality (data input, data verification, etc.) from the hardware dependent routines.

The instrument database saves all parameter values and accompanying limits, the instrument state, and the calibration data. It is divided into two identical parts, one for the hardware processes and another for the user interface process. All data exchange between processes is done by
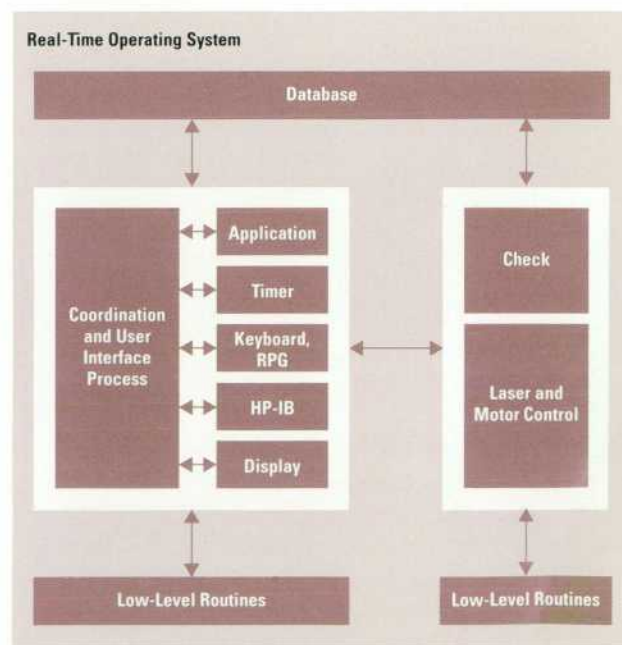
Fig. 12. Firmware processes.

means of mailboxes. Information hiding techniques are used to avoid direct (uncoordinated) accesses.

The task of the timer process is to manage some software timers by the use of a single hardware timer interrupt. Timers are used for data input timeouts and for guaranteeing constant sampling rates for the various control tasks (e.g., for stabilizing the temperature).

The keyboard, RPG (rotary pulse generator), and HP-IB processes are the firmware interface to the user. They accept inputs (e.g., a pressed key) and generate outputs (e.g., response strings from the HP-IB).

All input is reported to the control process. The application process is responsible for managing the wavelength sweep.

All message traffic from the other processes (keyboard, motor control, etc.) is coordinated by a single process called the coordination and user interface process. Its job is to synchronize the various input and output requests. After processing (e.g., display output), these messages are distributed to the correct destination processes. This ensures that conflicts are avoided when there are multiple requests for the same parameter at the same time. It also allows things like setting the wavelength via the HP-IB while the sweep is running.

The main tasks of this complex process are:
- Receive incoming messages from all other processes (keyboard, HP-IB, motor control, etc.) and analyze them
- Distribute handshake messages for synchronization purposes (e.g., to unblock the waiting HP-IB)
- Update the display, if necessary
- Supply editor functionality for all parameters
- Check parameter limits
- Convert values (e.g., from watts to dBm).

The measurement and motor control process converts parameter inputs (e.g., wavelength) into a hardware response (set the wavelength, control the laser chip, etc.). Its tasks are:
- Set the wavelength
- Set the laser power
- Set the attenuation
- Turn the laser on or off
- Turn the modulation on or off
- Set the modulation frequency.

To perform these tasks the measurement and control process has access to all necessary devices (grating, etalon, attenuator, ADCs, and DACs).

Hardware Drivers
The hardware drivers are implemented in a three-layer shell model (Fig. 13).

Level 0 only reads or writes a byte value from or to a specified address.

Level 1 specifies this address and makes it possible to read or write any device register in one-byte, two-byte, or four-byte mode (byte, word, long). For example, reading a grating position needs a four-byte access. A status register can be read in a one-byte access.

Level 2 realizes the individual features of every device. This level implements functions such as driving a motor, setting a DAC, and reading an ADC value.
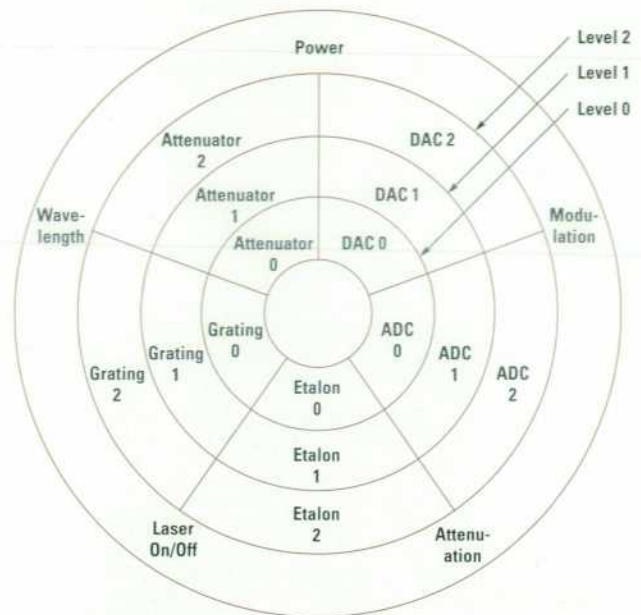
Fig. 13. Three-layer shell model of the hardware drivers.

There is no access from level 2 directly to level 0. All such accesses take place through level 1.

Every hardware driver can be debugged without an emulation station. It is only necessary to set the access flag via the HP-IB for the driver and the level you want to watch.

Setting the Wavelength
When a new wavelength is selected, the control process performs the following functions:
- Calculate the new grating position
- Calculate the new etalon position
- Calculate the new attenuator position
- Calculate the new power DAC value
- Move the grating motor
- Wait until the grating target position is reached
- Move the etalon motor
- Wait until the etalon target position is reached
- Move the attenuator motor
- Wait until the attenuator target position is reached.

For wavelength changes smaller than 1 nm, this process takes less than 150 ms from initiation until stable power is available at the output.

Achieving this tuning speed was a major challenge. The etalon and attenuator motors need moving times between 60 and 200 ms. The grating motor needs between 100 ms and 2000 ms. The calculation time for the new motor position and the new power value is between 60 ms and 120 ms. These calculation times essentially depend on floating-point operations for a linear interpolation algorithm between calibration points. Displaying the new wavelength and the new power takes about 40 ms. The processing of these procedures one after another generates a delay of more than 500 ms. For large wavelength steps (more than 50 nm) the tuning speed of the grating is the dominant factor. In these cases the tuning time reaches 1 to 2 seconds. However, for wavelength steps less than 10 nm, parallel motor processing and fast calculation can greatly reduce the tuning time (Fig. 14).

Calculate Grating Position (5 ms)

Calculate Etalon Position (5 ms)

Calculate Attenuator Position (5 ms)

Calculate Power (5 ms)

Update Display (40 ms)

Move Grating (100 ms)   Move Etalon (60 ms)   Move Attenuator (60 ms)   (Keyboard Handling)

Motors Are Ready

Stabilize Power

~ 120 ms Tuning Time
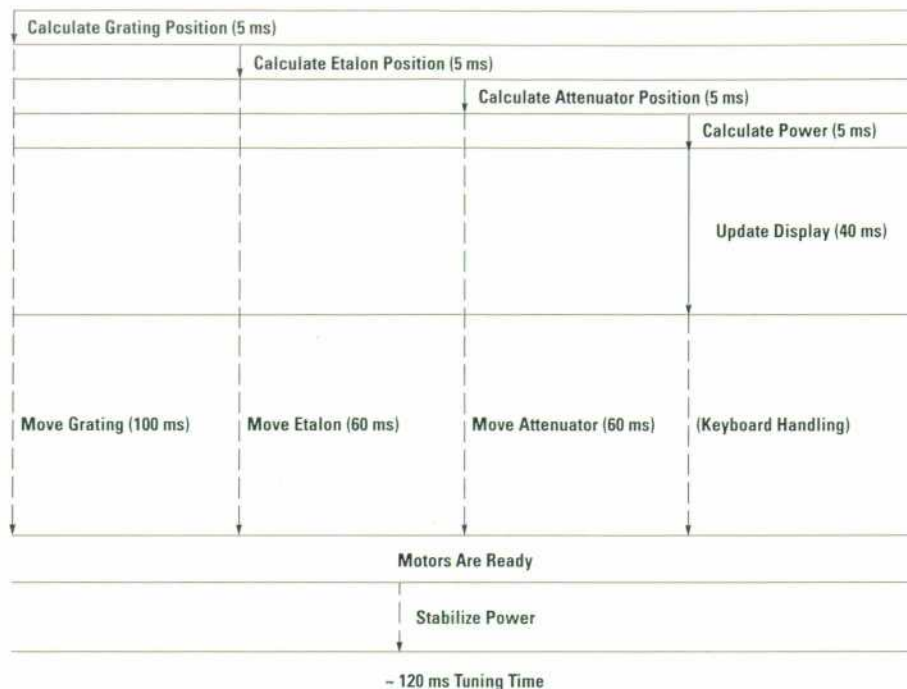
Fig. 14. Wavelength tuning time is minimized by parallel processing and motor movement.

Calculation Time. A new wavelength requires a new motor position. The firmware first finds the two points in the calibration data that bracket the new wavelength. To calculate the new position, it performs a linear interpolation between the calibrated base points:

$$y = mx + b$$

$$m = \frac{y_{\text{base point 2}} - y_{\text{base point 1}}}{x_{\text{base point 2}} - x_{\text{base point 1}}}.$$

The slope m between two calibration base points does not change, so this slope needs to be calculated only once, in the boot phase. This and the use of integer operations instead of floating-point operations help reduce the calibration time per motor to 5 ms from the 20 to 40 ms it would otherwise take.

Motor Processing Time. All motors (grating, etalon, and attenuator) are able to alert the processor by an interrupt when they have reached their target position. The firmware begins to calculate the grating position and starts to move the grating. After this, it calculates the etalon position and starts the motor, and the same for the attenuator motor.

While the motors are searching for their target positions, there is enough time to calculate the new power, update the display, and react to keyboard requests. The new wavelength setting is complete when all motors signal that they have reached their target positions and stable power is available at the output.

Measurement Features

The Maximum Power Curve

Because of different laser chip characteristics, every HP 8167A and 8168A tunable laser source has a different power-versus-wavelength behavior. In some applications, the user may want to choose values outside the specified wavelength

tuning range and the specified output power limits. These wider ranges may be out of specification, but suitable for the customer's specific needs.

To give the user a quick overview of the individual instrument's behavior, the instrument's power-versus-wavelength characteristic can be shown as a curve on the display. Fig. 15 is an example of this feature.

Wavelength Sweep

Besides the normal operation of selecting single wavelength values, the user can tune over a given wavelength range to automate measurements—for example, to measure the characteristics of a filter. When entering the sweep mode, the user can select and specify different sweep parameters by means of a pulldown menu (Fig. 16):
- Wavelength start value
- Wavelength stop value
- Wavelength step size
- Dwell time for the wavelength steps
- Number of cycles the sweep will execute.

The sweep direction can be reversed by simply exchanging the start and stop values. The sweep can run automatically, or by a keypress for every wavelength step for manually stepping through a specified range. In automatic sweep mode, each time the wavelength has settled, a trigger signal appears at the modulation output plug and the power and
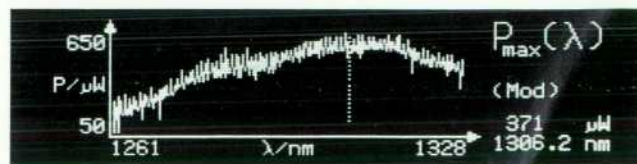
Fig. 15. Each instrument can display its maximum power as a function of wavelength.

Fig. 16. Menu for entering wavelength sweep parameters.

wavelength are held for the specified dwell time before the next wavelength value is set.

A power search algorithm (optional keystroke) looks for the maximum power available in the given sweep range, which guarantees constant power for the sweep.
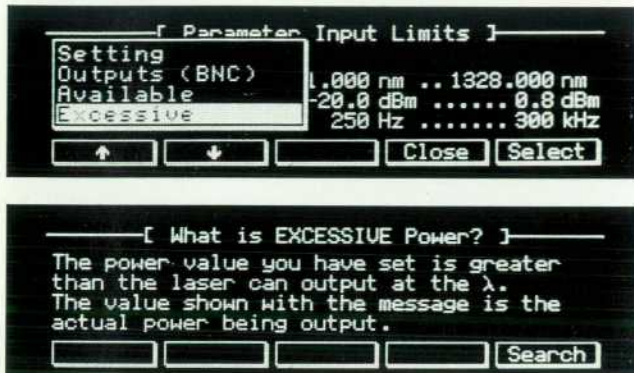
Fig. 17. An example of online help explaining the meaning of the EXCESSIVE warning.

Online Help

Online help texts supply detailed information about selected instrument topics, such as warning messages or working with the sweep application. For example, the user can get an explanation of the EXCESSIVE warning message without having to search through the manual (see Fig. 17).

Specific help is selected by walking through a select box, which contains a list of keywords for which help is available. The help texts can be of any size (more than one display page) and are easily expanded.

Acknowledgements

Correction

On page 103 of the December 1992 issue, the last two lines in the second column were missing. The complete paragraph reads:

Multiplexing the SCSI Bus between Nexuses

A device that disconnects from the SCSI bus during long delays in I/O processing enables other SCSI devices to use the bus. When the bus is relinquished by a given I/O process nexus, another I/O process nexus can connect to the SCSI bus and use it while the disconnected device continues I/O processing at the same time.

External-Cavity Laser Design and Wavelength Calibration

Sophisticated tuning and calibration methods coordinate the effects of a diffraction grating wavelength selector and a Fabry-Perot etalon side-mode suppression filter to ensure accurate wavelength selection and single-mode operation in the HP 8167A and 8168A tunable laser sources.

by Emmerich Müller, Wolfgang Reichert, Clemens Rück, and Rolf Steiner

To achieve the required tuning performance for the HP 8167A and 8168A tunable laser sources, it was decided to develop a tunable laser based on a semiconductor laser chip with an external cavity. There are several ways of building tunable lasers. For example, a three-electrode distributed feedback laser can be tuned over a wavelength range of approximately 10 nm. However, for tuning ranges of 50 nm or greater, lasers with external cavities as resonators and diffraction gratings as wavelength selectors are the solution of choice for most measurements. These lasers are called grating-tuned external-cavity lasers.

External-cavity lasers have been known as tunable sources for a long time and are often used in lab measurements, but have some disadvantages, such as poor power stability, tuning linearity, and wavelength stability. The goal of the tunable laser source development was to develop a stand-alone instrument without these shortcomings of existing external-cavity laser designs.

The two models of HP tunable laser sources are in principle built the same way. Both instruments are external-cavity-tuned laser sources. The differences are only in the gain media and some of the optical components. For the HP 8167A the gain is centered at about 1310 nm and the optical components are optimized for a wavelength range of 1250 nm to 1350 nm. In the HP 8168A, the maximum gain of the laser chip is centered at approximately 1540 nm. To cover the wavelength range from 1470 nm to 1565 nm with one instrument, the HP 8168A uses a laser chip that is selected to optimize several parameters. Fig. 1 gives an overview of the architecture and the major components.

Laser Cavity

The gain medium is a conventional laser diode in which the internal laser Fabry-Perot resonator is disabled by an antireflection coating on one laser facet. The coating design and performance are described in the article on page 32. The resonator is then rebuilt by adding an external reflector, the diffraction grating. The grating acts both as a plane mirror and as a wavelength-selective element.

The performance of an external-cavity laser is determined to a large extent by the external cavity. The laser output power, single-mode operation, tuning linearity, and wavelength stability are all are strongly related to the components used in the external resonator. Because of the temperature dependence of these components, the cavity and the laser chip have to be temperature stabilized.

For good performance, the external feedback from the cavity has to be as high as possible. Typical values in the current design are 20% to 30%. This means that the external resonator has roughly the same reflectivity as the former Fabry-Perot cavity. (The laser chip facet reflectivity is a result of Fresnel reflections. The reflectivity calculated from Fresnel's law is approximately 31%.)

The collimating lenses shown in Fig. 1 are needed because the laser chip emits a divergent output beam. The beam divergence (full angle at half maximum) of a laser can be as high as 45 degrees for conventional lasers. To capture most of the emitted light the lens has to be designed to handle numerical apertures up to 0.4 and it is required to have a controlled wavefront aberration better than $\lambda/4$.
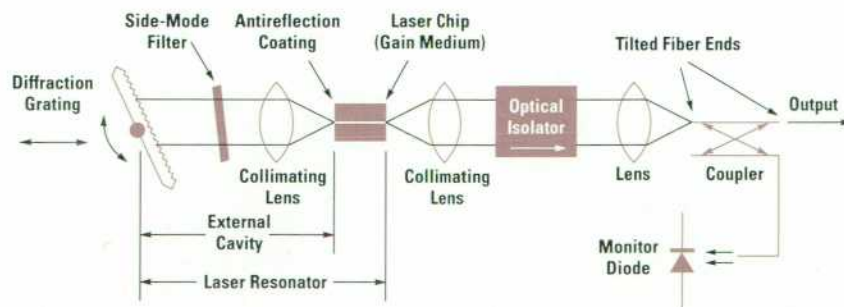
Fig. 1. Block diagram of the tunable laser in the HP 8167A and 8168A tunable laser sources.

The cavity design also includes a side-mode filter, which is needed to guarantee a high side-mode suppression ratio. The side-mode filter is a very narrowband wavelength filter that increases the wavelength selectivity compared to just a diffraction grating alone. Its operating concept and how it improves the performance of the external-cavity laser are explained later.

The control and calibration required to tune the side-mode filter and the grating synchronously were a significant challenge. The details are explained later in this article.

Principle of Operation

Fig. 2 shows the interaction between the gain medium, the resonator, the side-mode filter, and the diffraction grating. It also shows how variable wavelength selection is achieved. The grating is tuned by rotation, so the wavelength where
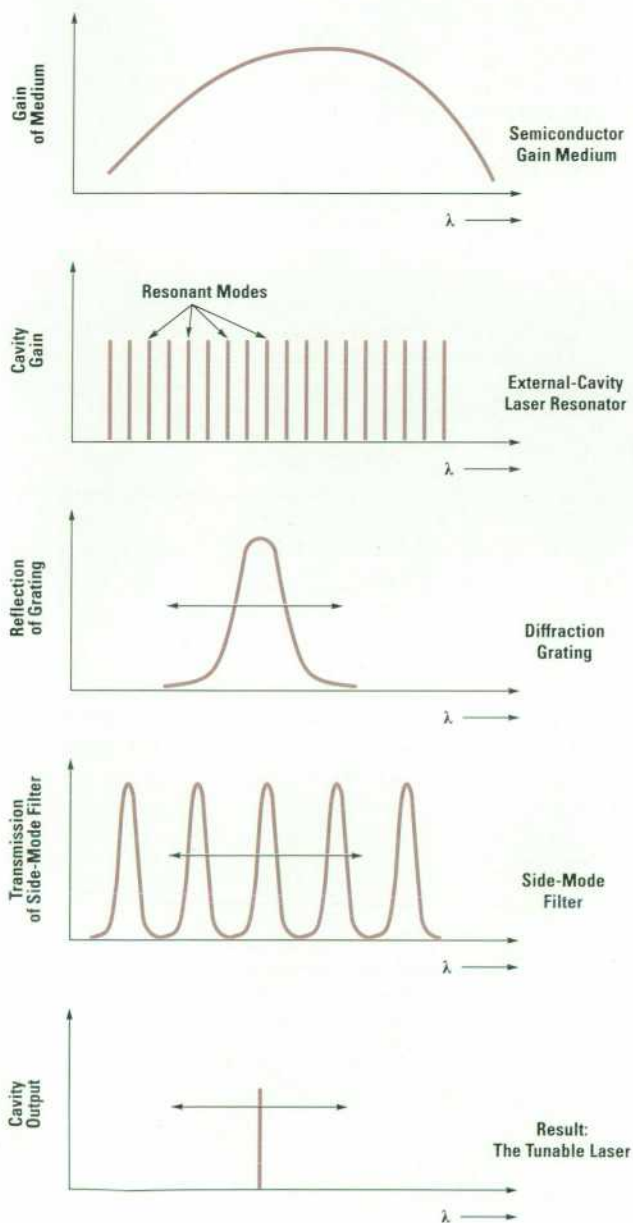
Fig. 2. Variable wavelength selection and side-mode suppression in the external-cavity laser.

the reflection is maximum is dependent on the angle of incidence of the emitted laser beam. The external-cavity laser resonator with its comb-like filter characteristic will allow a large number of possible lasing wavelengths. These possible lasing modes are called "cavity modes." The spacing between two modes is determined by the resonator length and can be calculated. The cavity length is chosen according to the needs of the other optical components and of some specific applications where the cavity mode spacing is important. The mode spacing is about 0.019 nm, corresponding to $\Delta f = 2.5$ GHz at a center wavelength of 1540 nm.

The diffraction grating filter bandwidth is determined by the optical beam diameter, the mechanical layout of the filter, and the spacing of the rulings. This is optimized for the external cavity requirements and for manufacturability. In practice, there is a trade-off between wavelength selectivity, reflection efficiency, and manufacturability. A selectivity of about 1 nm FWHM (full width at half maximum) gives good performance with this design.

From Fig. 2, it is easy to see that with just a diffraction grating filter, a more or less undefined mode is selected. Looking at the external-cavity mode spacing and the filter characteristic of the diffraction grating, it clear that a single-mode and stable laser output is not guaranteed. The result would be weak tunability and poor wavelength repeatability. Several modes have comparable gain conditions and are able to lase. This is one of the sources of multimoding and gives a high degree of instability. This might be less of a problem if the laser had an absolutely smooth and flat gain characteristic, but this is unrealistic and would require a perfect antireflection coating. In practice, there is some ripple in the laser gain characteristic, and although it is low in this case, it was still a big problem.

To improve the wavelength selectivity of the external cavity, the side-mode filter is added to the cavity. The requirements for this filter were at least 10 times higher selectivity than a stand-alone grating, nearly no feedback loss, reasonable component cost, and easy wavelength tunability. A solid glass Fabry-Perot etalon was designed to fulfill most of the requirements. With this type of optical filter it is easy to get the filter bandwidth down to less than 0.1 nm (about 12 GHz in frequency). The disadvantage of this filter is the comb-like filter characteristic (see Fig. 2), which requires a sophisticated tuning scheme and a complex calibration algorithm.

The wavelength tuning of the transmission maxima can be done in several ways; one is to tilt the etalon. To select a single lasing mode it is important to have the best possible match between the grating reflectivity maximum and the etalon transmission maxima; otherwise, the external feedback is reduced dramatically. To achieve this the requirements on the grating drive and the etalon drive are high resolution, good motion repeatability, and a stiff cavity arrangement. This match has to be certified at each wavelength over the entire tuning range.

Adjustment of the external cavity to achieve a specific output wavelength consists of selecting a particular angular position of the grating and a particular angular position of the etalon. To allow quasicontinuous tuning, the filter curve of the grating, the transmission maxima of the etalon, and

the resonant modes of the external-cavity laser resonator are shifted by the same wavelength increment. To accomplish this, the grating has to be rotated, the etalon tilted, and the cavity length adjusted by shifting the grating. The details of this adjustment are explained later.

Laser Output Side

The laser output side delivers the optical performance to the customer application. To avoid any problems with back-reflected light from customer applications it is necessary to have a built-in isolator. The isolator has to fulfil many tasks. The most important is to isolate the external cavity so that the laser performance is independent of external influences. Without a properly working optical isolator, backreflections into the laser could cause serious problems for wavelength and power stability. For most measurement systems it is important to have all system building blocks designed for low backreflections. Termination values of more than 50 dB return loss are needed to avoid trouble with Fabry-Perot cavities in the measurement setup. In the HP 8167A/68A, all internal fiber ends and the front-panel connector have at least 60 dB of return loss. This is accomplished by using custom fiber terminations and a new type of fiber optic connector designed by HP. The connector has more than 60 dB of return loss and is designed for good repeatability. The angled fiber ends are not in physical contact, so the connector cannot be destroyed by scratches or abrasion.

Output Power

So far, most of the design issues discussed here have addressed tunability and wavelength stability. There are also requirements on the output power of the tunable laser sources, including power stability over time and constant output power versus wavelength. With the addition of a fiber tap (fusion coupler) and a monitor diode near the fiber output port, the laser is driven under closed-loop control. A wavelength calibration of the entire monitoring system ensures stable and wavelength independent output power. These issues are discussed in the article on page 28.

Optical and Mechanical Design

The optical components of the external-cavity laser can be divided into two sections: parts belonging to the external cavity (grating, Fabry-Perot etalon) and parts belonging to the laser output assembly (isolator, fiber coupling, and power monitoring).

External Cavity

Coarse Filter. As mentioned earlier, there are two filters in the external cavity. First, a diffraction grating is used as a coarse filter. This kind of filter is basically a mirror upon which extremely narrowly spaced grooves are engraved. When the grating is illuminated, each groove generates a cylindrical wave, like a small radiation source. If the light is coherent, such as a laser beam, the superposition of these single waves produces a wavefront with large intensity only in those directions in which the path difference between the single waves is a multiple of the incoming wavelength (see Fig. 3a). Used as a wavelength-selective mirror in an optical resonator, as in the external-cavity laser, the grating reflects the first-order wavefront into the direction of the incident
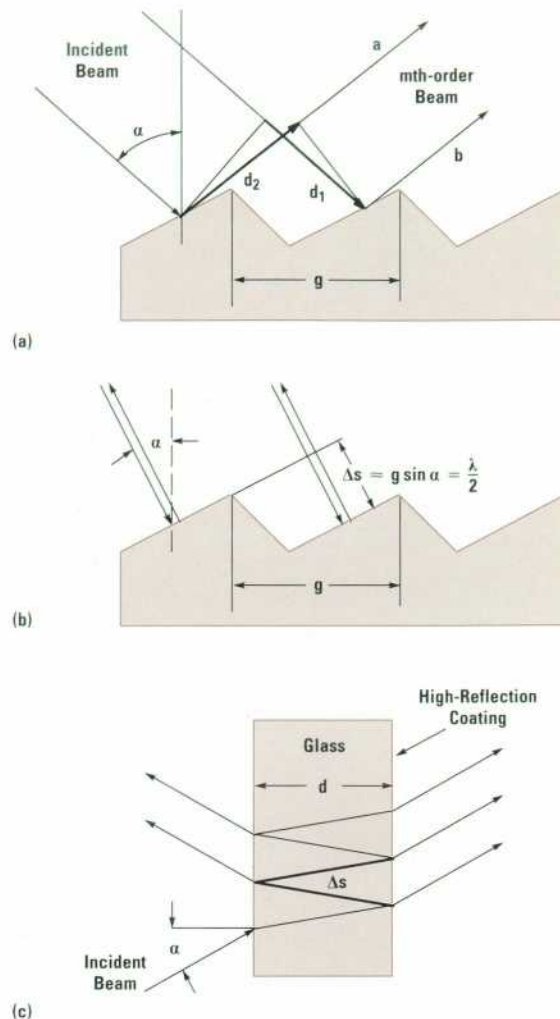
Fig. 3. (a) Optical path difference Δs of the reflected partial waves a and b in a diffraction grating. For the mth-order beam, $\Delta s = d_2 - d_1 = m\lambda$. (b) With the Littrow grating mount, the first-order reflected beam retraces the path of the incident beam. For this special case, $\Delta s = g\sin\alpha = \lambda/2$. (c) Principle of the Fabry-Perot etalon (ray angles exaggerated for clarity). For constructive interference, $\Delta s = 2d\sqrt{n^2 - \sin^2\alpha} = m\lambda$, where n is the refractive index of the etalon.

beam (Littrow grating mount, see Fig. 3b). For this special case there is a simple relationship between the angle of the grating relative to the incoming beam and the wavelength that will be reflected back into the laser chip:

$$\lambda = 2g\sin\alpha,$$

where α is the angle between the incident beam and the grating normal, g is the spacing between grooves, and λ is the incident wavelength.

In the HP 8167A the grating has 1200 grooves per millimeter, and in the HP 8168A, for the same mechanical geometry, the grating has 1020 grooves/mm. For a tuning range of 1280 to 1330 nm (HP 8167A) or 1500 to 1565 nm (HP 8168A) this defines the incident angle of the laser beam to be between 50 and 53 degrees. Besides the surface quality of the grating, the wavelength resolution depends linearly on the number of grooves reflecting the laser beam:

$$\Delta\lambda/\lambda = 1/(Nm),$$

where $\Delta\lambda$ is the wavelength difference that can be resolved, N is the number of grooves illuminated, and m is the order of the reflection. With a beam diameter of 0.9 nm and the chosen geometry, the resolution is about 1 nm.

Fine Filter. The second filter is a Fabry-Perot etalon. In principle, it is also based on the coherent superposition of partial contributions. Here the single waves are generated by a parallel light beam going through a plane parallel glass plate and being partially reflected. Just as in the diffraction grating, the optical path difference between the partial waves has to be a multiple of the wavelength to get constructive interference (see Fig. 3c). In contrast to the diffraction grating, all outgoing beams that fulfill these conditions have the same direction, resulting in an ambiguous filter curve (see Fig. 2). The spacing between the transmission maxima is called the mode spacing or the free spectral range FSR:

$$\text{FSR} = \lambda^2/(2d(n^2 - \sin^2\alpha)^{1/2}),$$

where n is the refraction index of the etalon, d is the thickness of the etalon, and α is the angle between the incident beam and the surface normal.

To get very fine wavelength resolution it is necessary to generate many partial waves. A parameter often used to characterize the comblike filter curve (Fig. 2) is the finesse F, which defines the ratio of the free spectral range FSR to the width of the transmission maxima. For an ideal parallel plate with perfect surface quality the finesse is determined only by the reflectivity R:

$$F = \text{FSR}/\text{FWHM} = \pi R^{1/2}/(1-R),$$

where FWHM is the full width at half maximum of the transmission maxima.

To avoid lasing on more than one etalon mode, the FSR of the etalon has to be significantly greater than the wavelength resolution of the grating. In addition, to suppress all of the cavity modes (see page 21) except the desired one, the FWHM has to be smaller than 0.1 nm. To achieve this, the etalon chosen has a thickness d of 500 µm and reflectivity R of 75%. Thus the FSR is about 1.1 nm for the HP 8167A (1.6 nm for the HP 8168A) and the finesse F is approximately 11.

The wavelength for which the etalon has maximum transmission is a function of the angle α of the surface normal of the etalon relative to the optical axis (Fig. 3c). The following relationship applies:

$$m\lambda = 2d(n^2 - \sin^2\alpha)^{1/2},$$

where n, λ, and d are as above and m is the order of the transmission maximum.

Taumel* Etalon

Typically the wavelength is shifted by tilting the etalon around an axis perpendicular to the optical axis (changing α directly). With this method it is very costly and complex to get a wavelength resolution of a few picometers. For this reason a new tilting concept called the taumel etalon was developed. The etalon is mounted concentrically on a spindle that has a 2-degree inclined endface. The spindle is connected to the shaft of a dc motor which is coupled to an encoder with a resolution of 4096 steps per turn. This assembly is fixed in the optoblock in such a way that the angle between the motor shaft and the laser beam is about three degrees (see Fig. 4). If the etalon is turned, the angle between the surface normal and the laser beam is changed between 1 and 5 degrees, resulting in a maximum wavelength shift of about 3 nm. In Fig. 5a this wavelength shift is plotted as a function of the motor position, and Fig. 5b shows the wavelength shift per motor step.

The coarse filter is mounted on a lever which is seated in a turnable bearing. A two-phase stepper motor coupled with a precision micrometer leadscrew works as a linear drive for turning and moving the grating filter. Using the microstep capability of the stepper motor it is possible to achieve a travel resolution and accuracy of better than 0.1 micrometer.

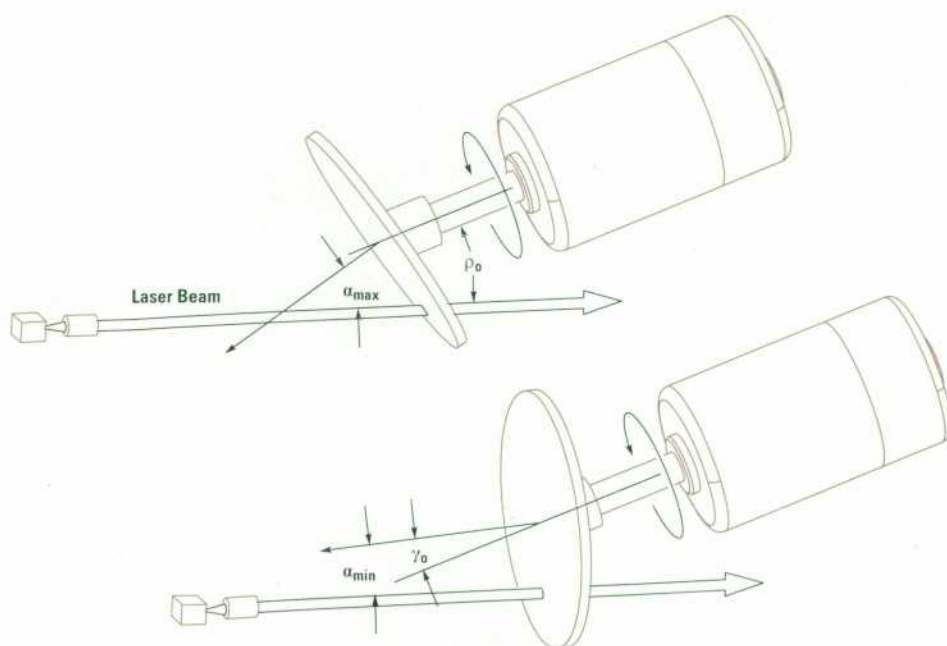* "Taumel" is the German expression for "reel" or "stagger."

Fig. 4. Geometry of the taumel etalon tuning scheme. For $\rho_0 = 3°$ and $\gamma_0 = 2°$, α is between 1 and 5 degrees. Rotation of the etalon by 180° shifts the wavelength of its transmission maxima by about 3 nm.

Laser Beam α_{max} ρ_0

α_{min} γ_0
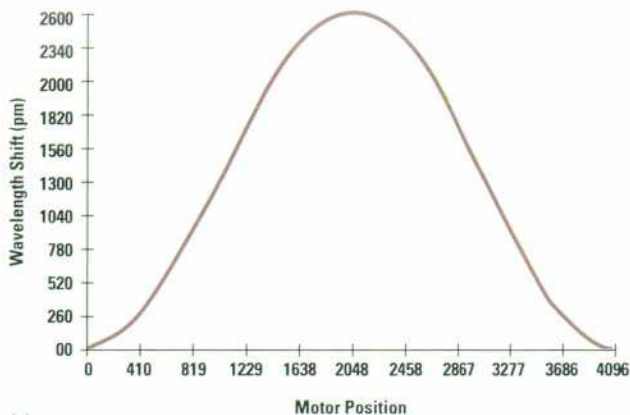
(a)
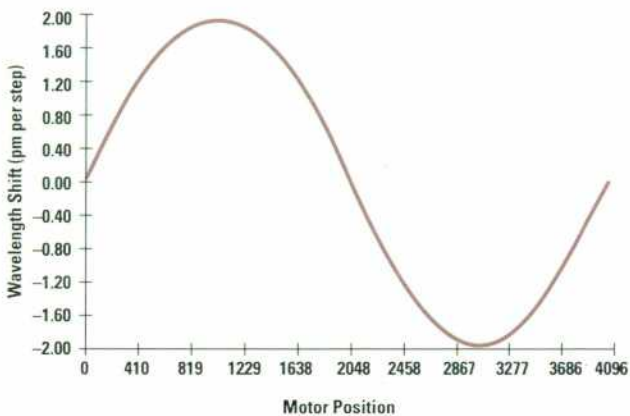
(b)

Fig. 5. Wavelength shift in the taumel etalon as a function of motor position.

The coarse filter has to have a known angular reference position after the instrument is switched on. A stepper motor is not able to provide this feature because it has no reference position. Therefore, a precision sensing switch is built into the cavity mechanism. As mentioned earlier, it is necessary to match the diffraction grating and the etalon when tuning the laser. This means that the reflection maximum of the grating has to be coincident with one of the transmission maxima of the etalon. It has been calculated that the maximum tolerable wavelength difference between the filter curves is less than 50 pm. Based on this, the accuracy of the switch has to be better than 1 micrometer.

The precision bearing is an important part that has a major influence on laser performance and reliability. Any kind of bearing clearance or tilt of the axis of rotation will cause mismatch of the filters. The objective was to find a bearing type that provides very good long-term stability. Using very hard materials that exhibit no or very little abrasion will guarantee a fixed position of the lever pivot under all conditions. At the same time it is essential to design all the movable mechanical parts of the cavity carefully. To keep the stress on the precision parts low, it is necessary to find the optimum weight and stability of the cavity structure.

Going through several design stages, it turned out that the best cavity design is achieved mainly by optimizing and

choosing the right material properties. In particular, the thermal expansion coefficients of the parts have to be well-balanced. Using exotic materials like Invar, Vacon, Carpenter, or Cerodur did not improve the results. If the temperature of the cavity changes, a drift in wavelength will occur, but the main contribution comes from the optical parts. The change in the thickness d of the etalon is the main determinant of the shift in wavelength, according to the simple formula:

$$\Delta\lambda/\lambda = \theta\Delta T,$$

where θ is the thermal expansion coefficient (typically 1×10^{-5}/K for fused silica) and ΔT is the temperature change in kelvin. For example, a temperature change of 1 kelvin will cause a drift of about 10 pm at a wavelength of 1.5 μm.

Laser Isolation and Fiber Coupling

Like the laser cavity, the laser output section of the HP 8167/68A tunable laser sources is also a bulk optical design. The laser light passes first through an optical isolator to protect the laser chip from backreflections coming from the coupling lens, fiber end, cable connectors, and other external disturbances. The isolator is a two-stage magnetooptic isolator. It is a preassembled unit that only has to be aligned according to the polarization axis of the laser light. The isolation is typically more than 60 dB and the insertion loss is less than 0.5 dB.

The laser beam is focused into a 9-μm fiber using a SELFLOC lens. For low insertion loss, the focal length is adjusted exactly to the focal length of the lens in the laser module and to the ratio of the numerical apertures of the laser chip and fiber. To obtain a high return loss the reflectivity of the fiber end is reduced by polishing the endface at an eight-degree angle. To avoid a mismatch of the optical axis and the fiber axis because of the slanted endface, the fiber is tilted about four degrees (see Fig. 6).

Also for high return loss, the front-panel connector is slanted by 10 degrees. To avoid damage of the fiber end by a badly mating connector, the connector used is a no-physical-contact type.

Optoblock Protective Housing

After the first experiments done on the optical block of the tunable laser sources it became obvious that the performance and reliability of the external cavity laser depends on the stability of the cavity in terms of unwanted motions of the optical filters caused by shock, vibration, and thermal expansion. One of the mechanical design goals was to come up with a rugged instrument package.

To achieve the highest optical signal accuracy, the optoblock needs a controlled environment and is therefore located in a separate housing, which is heated to 55°C. The optoblock housing acts as a shell and is a part of the temperature stabilization system. The base of the heat chamber is the chassis. It carries the heat chamber printed circuit board and the optoblock (Fig. 7). The optoblock is an independent and pretested subassembly, and is seated in the chassis using soft rubber spacers to reduce mechanical stress. Together with the mainframe, the design forms a two-stage shock absorbing system. As a result, the tunable laser sources are able to withstand use in both laboratory and production environments without special handling.
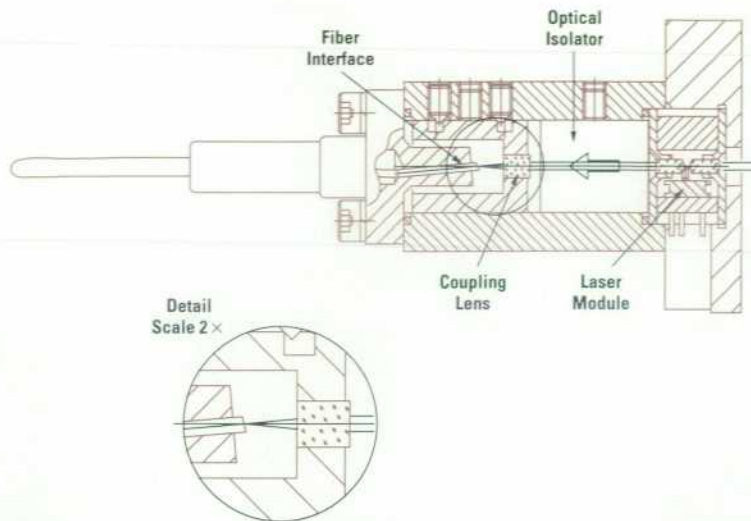
Fig. 6. Laser isolation and fiber coupling mechanism.

Fig. 7. Optical unit of the tunable laser source, showing the optoblock and some elements of the heat chamber.

Mainframe Design

The mainframe is a standard HP System II cabinet, 425.5 mm wide, 132.6 mm high, and 497.8 mm deep. The instrument weight is approximately 17 kg.

The optical unit takes a third of the mainframe volume. The cardcage of the tunable laser source provides six slots for printed circuit boards and the power supply module. It is made of zinc-plated steel and is strengthened at different points to withstand the acceleration forces of the heavy optical unit.

The mainframe power dissipation is approximately 150 watts. A dc fan located at the rear panel of the instrument keeps the temperature rise inside the cardcage and around the optical unit well below 15°C.

Wavelength Calibration

For wavelength calibration of the tunable laser sources, there are two dependent variables (the etalon and grating angles) that can be varied to get the desired wavelength with maximum output power.

One calibration method is to measure the motor positions for each wavelength setting. Assuming a tuning range of 100 nm and a wavelength resolution of 1 pm, this would require 100,000 calibration points. For each calibration point the two motors have to be moved so the desired wavelength is obtained with maximum output power. If each measurement takes only 10 seconds it would take about 12 days to complete a calibration.

Another way of calibrating is to calculate as much as possible and measure only a few reference points. The number of calibration points is then dependent on production tolerances and uncertainties. This is the method of calibration used for the tunable laser sources.

Grating Calibration

In the first step of the calibration process, the angular orientation of the grating (or position of the motor drive) is determined for several discrete wavelength values, such as λ_1 and λ_2 in Fig. 8. The laser output beam is coupled by an optical beamsplitter to a high-precision wavelength meter and to an optical power meter. Thus, the laser output wavelength and output power are measured simultaneously. The etalon is arranged at a fixed, but unknown angular position (λ_u). The grating is now moved within the tuning range of the laser (around 1540 nm for the HP 8168A) until the output power is at a local maximum. If this is the case, the maximum of the grating reflection curve is located at a transmission maximum of the etalon. This is illustrated in Fig. 8 where the maximum of the grating curve G_1 is at the etalon transmission maximum E_1. The corresponding wavelength λ_1 is determined with the wavelength meter. This wavelength and the grating position constitute the first data pair of the first calibration data array.

Finding the local maximum of the output power is not a trivial problem. The measured output power curve is very noisy because it includes the laser's gain ripple and some measurement uncertainties. To get an accurate transmission maximum, signal processing using fast Fourier transform and digital filtering techniques is necessary.

After the first data pair is measured, the grating is moved by a fixed amount (for example 10 nm) to a second position and is tuned until the output power is again a local maximum. This corresponds to the situation where the maximum
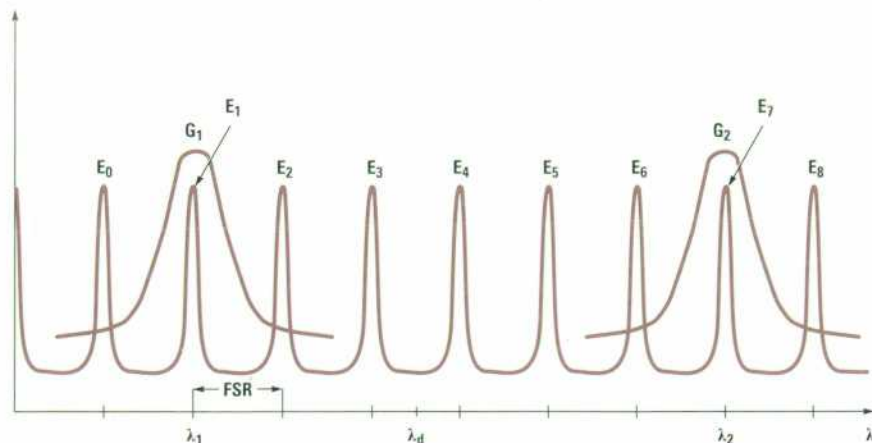
Fig. 8. The curve with the peaks labeled E_i indicates the transmitted power of the etalon as a function of wavelength. The peaks labeled G_1 and G_2 represent the reflectivity versus wavelength for two different angular positions of the grating. For maximum feedback the maximum of the reflectivity curve must coincide with a maximum of the transmission curve.

of grating curve G_2 in Fig. 8 is located at the etalon transmission maximum E_7. The corresponding wavelength λ_2 and the grating position are stored as the second data pair of the first calibration array. This procedure is repeated for the desired number of calibration points. The number of calibration points (about 10) is selected according to the total tuning range of the external-cavity laser. Later, when the laser is tuned to a desired wavelength that lies between two calibration wavelengths, a linear interpolation between these two wavelengths is done to determine the corresponding position of the grating drive. The linear interpolation is good enough because the transfer function (motor steps to grating angle) is nearly linear.

Etalon Calibration

As mentioned above, the etalon is arranged at a fixed but unknown position (λ_u) during the calibration of the grating. Calibration of the etalon rotation is also required for precisely adjusting a wavelength that is located between two transmission maxima of the etalon—for example, wavelength λ_d between the points λ_1 and λ_2 in Fig. 8. To ensure maximum laser output power at λ_d, a transmission maximum of the etalon has to be at a maximum of the grating reflection curve. Thus, in Fig. 8, the etalon transmission curve has to be shifted such that the transmission maximum E_3 is at the position λ_d. At the same time, the grating position has to be changed such that the grating reflection curve has its maximum at λ_d. The required grating position is derived by interpolation between the calibration points λ_1 and λ_2. The shift of the etalon transmission maximum to λ_d is accomplished by appropriate rotation of the motor axis on which the etalon is fixed. The angle by which the motor axis has to be rotated to shift the etalon transmission curve is taken from a second data array, which contains data pairs consisting of wavelength shifts and the corresponding angles of rotation.

To obtain the data pairs of the second array, first the reference position for the etalon ($\alpha = \alpha_{max}$ in Fig. 4) has to be found. This is done by tuning the etalon the way the wavelength decreases. At each setting the grating position is corrected as mentioned above. The reference position is found at the minimum wavelength position and corresponds to the zero point (wavelength shift = 0 in Fig. 5a).

Assume that the reference position corresponds to λ_2 in Fig. 8. Now, the motor axis is rotated by a fixed amount, for example 1 degree. The grating is then moved slightly to the

new wavelength measured by the wavemeter. Let the wavelength at this position of the etalon be λ_{calt}. The data pair consisting of the difference between λ_{calt} and λ_2 and the angle of rotation of the axis (1 degree in this example) is the first entry in the second data array. The rotation angle of the axis is expressed as the corresponding position of the motor position encoder and stored in this form in the second data array. Next, the axis is rotated further by the same fixed amount (1 degree in this example), the grating is again readjusted, the resulting wavelength is read, and the difference between this wavelength and λ_2 together with the total rotation angle (2 degrees) of the axis is stored in the second data array. This procedure is continued until the etalon has completed a rotation by 180 degrees.

The wavelength tuning of the etalon is dependent on the absolute wavelength. To minimize calibration time the tuning function is only measured at one wavelength and stored in the second data array. For the other transmission maxima this array is corrected by the following formula:

$$\text{Correction} = \frac{\pi - \arccos f(m_{act}, \ \Delta\lambda)}{\pi - \arccos f(m_1, \ \Delta\lambda)},$$

where m is the order of the etalon maximum and $\Delta\lambda$ is the wavelength shift. Using the calibration data of the second data array and this equation, it is possible to adjust any wavelength shift between two transmission maxima. The wavelength range that can be covered by the etalon rotation is determined by the parameters of the etalon. In the HP 8168A, this wavelength range is about 2.2 nm. If a desired wavelength shift lies between any two values in the second data array, a linear interpolation is done to obtain the proper rotation angle of the motor axis.

Absolute Wavelength Calibration

Returning to the task of adjusting the wavelength λ_d in Fig. 8, there is still one problem to solve. Even though it is now possible to shift the etalon transmission curve by a desired wavelength interval, it still has to be determined by what amount it has to be shifted so that an etalon transmission maximum (such as E_3) is at the position λ_d. For this purpose, it has to be determined at which absolute wavelength positions the etalon transmission maxima at the etalon position angle λ_u are located. This is done in the following way.

First, two wavelengths are chosen that have been accurately measured with a wavelength meter using the procedure for

determining the first data array. Assume that these two wavelengths are λ_1 and λ_2 as shown in Fig. 8. Several etalon transmission maxima E_2 to E_6 are located between λ_1 and λ_2. As explained earlier, the wavelength difference between adjacent maxima is the free spectral range of the etalon (FSR) and satisfies the following formula:

$$FSR = \lambda^2/(2d(n^2 - \sin^2\alpha)^{1/2}),$$

where λ is the wavelength transmitted through the etalon, n is the refractive index, and α is the angle of incidence. Since the angle of incidence α_u at the initial angular position of the etalon is not known and is typically small (a few degrees), the approximation can be made that the term $\sin^2\alpha$ is zero. Then:

$$FSR = \lambda^2/2dn.$$

As an approximation, λ is selected to be λ_1. This gives a preliminary value for the FSR. Denoting the orders of the etalon transmission maxima at λ_1 and λ_2 as m_1 and m_2, respectively, and the difference between m_1 and m_2 as Δm, the following applies:

$$\Delta m = \frac{\lambda_2 - \lambda_1}{FSR}.$$

With the constraint that Δm has to be an integer and with λ_1 and λ_2 known, this equation can be used to correct the preliminary value for the FSR.

The absolute value of m_1 can be calculated as:

$$m_1 = \frac{\Delta m}{1 - \lambda_1/\lambda_2}.$$

Now, using the following equation, the absolute wavelengths of the etalon transmission maxima subsequent to the maximum E_1 are calculated.

$$\lambda_1 m_1 = \lambda_2 m_2.$$

For example, the following applies for the wavelength λ_{E2} at etalon transmission maximum E_2, which is the first after the transmission maximum at λ_1 (corresponding to the order m_1):

$$\lambda_1 m_1 = \lambda_{E2}(m_1 - 1).$$

All subsequent transmission maxima are calculated by the stepwise decreasing of the order m of the transmission by 1.

Now the wavelength difference between the desired wavelength λ_d and the adjacent etalon transmission maximum (peak E_3) can be accurately determined. The rotation angle of the motor axis (or difference in motor encoder positions) corresponding to this wavelength difference is looked up in the second data array. This value is corrected as explained above and then the axis is rotated by the calculated amount.

This calibration method is fast and accurate, and takes into account the manufacturing tolerances of the optical and mechanical components.

External-Cavity Laser Temperature Stabilization and Power Control

The theory and operation of the laser temperature control and measurement circuits and the output power control and calibration of the HP 8167A/68A tunable laser sources are presented.

by Horst Schweikardt and Edgar Leckel

The operating temperature of the external-cavity laser of the HP 8167A and 8168A tunable laser sources is from +5°C to +35°C. To meet instrument specifications over this temperature range it is necessary to stabilize the temperature of the key internal components.

The simplest way to control temperature is to generate heat only, without forced cooling. This concept requires a cavity temperature T_{CAV} of about 55°C. Therefore, all components in the chain from the laser to the power measurement amplifier are located in a controlled temperature environment at approximately 55°C. On the other hand, for long laser lifetime and low threshold current, the laser chip temperature needs to be less than 25°C. In the HP 8167A/68A, a Peltier cooler is used because of its small dimensions and its heat pump capacity. This allows a laser chip temperature of approximately 20°C.

This article deals with the laser chip temperature control, the temperature sensing circuits, the output power control, and output power calibration. The hardware that performs these functions resides on the laser control board.

Laser Temperature Stabilization

Fig. 1 shows the laser temperature control loop. Laser chip temperature is measured by a thermistor chip which is
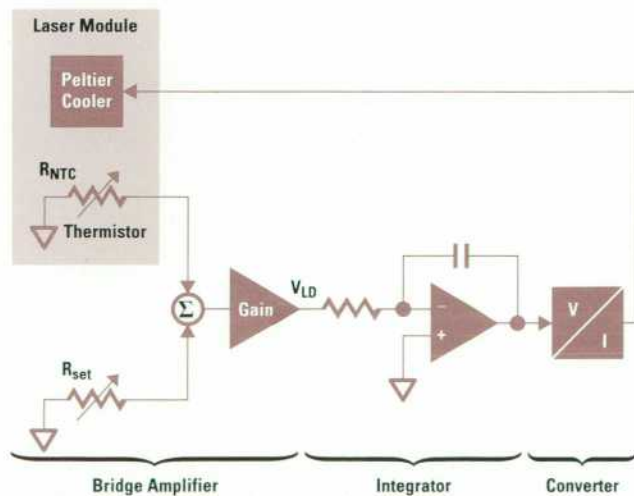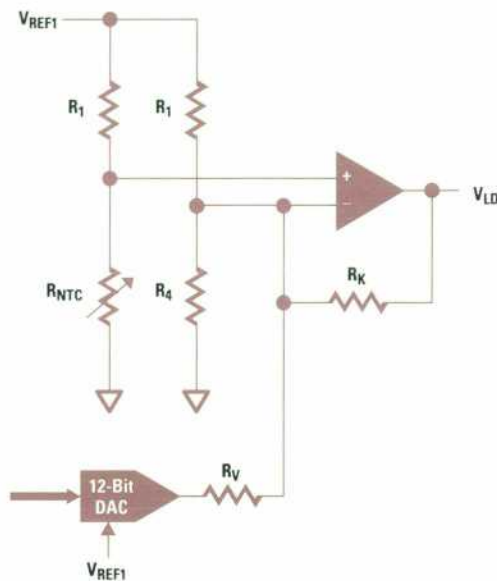
Fig. 2. Bridge amplifier with DAC (digital-to-analog converter).

mounted near the laser diode on the cold side of the thermoelectric Peltier cooler. A resistor bridge senses the deviation from the set voltage for the laser chip temperature. The amplified signal V_{LD} drives the input of an integrator. The integrator output feeds a voltage-to-current converter, which delivers the current for the thermoelectric cooler. This forces the cold side of the cooler to change its temperature until the thermistor value R_{NTC} is equal to R_{set}. At steady-state conditions, $R_{NTC} = R_{set}$ and the bridge amplifier output $V_{LD} = 0$ volts (no integrator input current).

The resistance R_{set} is adjusted using a DAC as shown in Fig. 2. The relationship between R_{set} and the DAC value is:

$$R_{set} = \frac{R_1(R_V/R_1 - DAC/4096)}{R_V(1/R_4 + 1/R_K + 1/R_V) + DAC/4096} \quad (1)$$

where: $R_1 = 38.3$ kΩ, $R_4 = 17.72$ kΩ, $R_K = 215$ kΩ, $R_V = 147$ kΩ, and $0 \le DAC \le 4095$. For example, if DAC = 2048, equation 1 gives $R_{set} = 12.2$ kΩ and the bridge amplifier gain is $dV_{LD}/dT = -1.41$V/°C. With DAC values from 0 to 4095, the laser chip temperature can be changed by more than 10°C to select a desired operating point.

Fig. 1. Laser temperature control loop.

The relation between the thermistor resistance and the thermistor temperature is described by the Steinhart-Hart equation, equation 2:

$$1/T = A + B(\ln R_{NTC}) + C(\ln R_{NTC})^3, \qquad (2)$$

where R_{NTC} is the thermistor resistance in ohms and T is the absolute temperature in Kelvin. The specifications for the thermistors used in the tunable laser sources are $R_{NTC}(20°C)$ = 12 kΩ ±10% and negative temperature coefficient NTC = $-0.038/°C$ at 20°C. Using these values and modeling by the Steinhart-Hart equation gives the curves in Fig. 3. For the nominal curve, A = 8.7636×10^{-4}, B = 2.5084×10^{-4}, and C = 2.1774×10^{-7}.

For DAC = 2219, the control loop will set $R_{NTC} = R_{set} = 12.0$ kΩ, independent of the thermistor curve. Thus Fig. 3 shows that the laser chip temperature T will be between 17.2°C and 22.5°C. This means that, depending on the particular thermistor, the cooler current change will be somewhere in a 200-mA range. This was considered too much variation. Therefore, instead of adjusting the DAC for R_{set} = 12.0 kΩ, the laser diode drive current is set at 30 mA and the DAC setting is adjusted for a thermoelectric cooler current of I_P = 800 mA, which corresponds to a cooler temperature of nominally 20°C. The temperature control loop then maintains a constant laser temperature.

Laser Temperature Measurement

To measure the absolute laser chip temperature T, another bridge amplifier is used. The parameters for this bridge amplifier are: R_1 = 38.3 kΩ, R_4 = 38.3 kΩ, R_K = 56.2 kΩ, R_V = infinite, V_{REF1} = 10V. R_{NTC} is calculated with equation 3:

$$R_{NTC} = \frac{R_1 V_{LD} + R_K V_{REF1}}{V_{REF1}(1 + R_K/R_4) - V_{LD}}. \qquad (3)$$

For example, reading bridge output voltage V_{LD} = -5.287V and inserting this value into equation 3 gives R_{NTC} = 12.0 kΩ. From equation 2 we get T = 20.0°C. The actual laser chip temperature will be T = 20.0 ±2.7°C because of the 10% thermistor tolerance.

Laser Power Control

A tunable laser source provides optical power over a specific wavelength range. Thus, in addition to depending on the same parameters as in a fixed-wavelength laser source
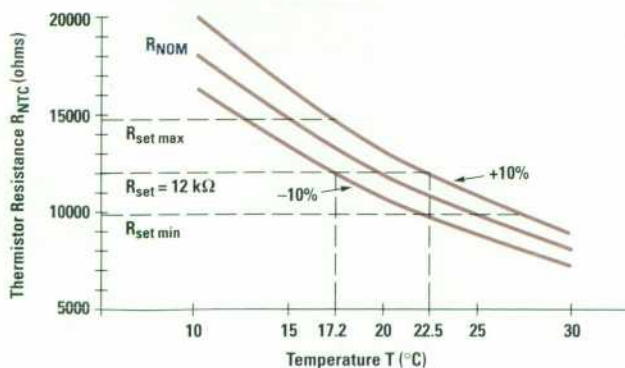
(temperature, coupling, materials, etc.), the output power is also a function of wavelength. To level the output power in the HP 8167A and 8168A tunable laser sources, a power control loop is used (see Fig. 4). The control loop is similar to that used in the laser sources for the HP 8153A optical power meter.[1] Because of gain variations with wavelength, a variable-gain amplifier is inserted in the loop instead of a fixed-gain amplifier.

Laser output power P_{las} is coupled into a fiber coupler with coupling ratio K_{ratio}. The coupling efficiency from a parallel beam into the fiber coupler is K_{fiber}. Thus the output power at the front-end connector is:

$$P_{ecl} = P_{las}K_{fiber}(1 - K_{ratio}). \qquad (4)$$

Nominal values are K_{ratio} = 0.06 and K_{fiber} = 0.5. The portion

$$P_{det} = P_{las}K_{fiber}K_{ratio} = \frac{P_{ecl}K_{ratio}}{(1 - K_{ratio})} \qquad (5)$$

is coupled to a germanium photodiode detector for output power monitoring. The detector feeds a transimpedance amplifier with output V_{XIMP}:

$$V_{XIMP} = P_{det}R_dR_{fb} \qquad (6)$$

where R_d is the responsivity of the photodiode (A/W), R_{fb} is the feedback resistor (ohms), and P_{det} is given by equation 5.

All components in the chain from the laser to the transimpedance amplifier are located in a heat chamber and are therefore in a controlled temperature environment at approximately 55°C. This reduces temperature dependence significantly by shifting the long-wavelength tail of the responsivity to wavelength values greater than 1550 nm with increasing temperature.

A multiplying DAC with gain $G_{mdac}(\lambda)$ provides the voltage V_{MON}:

$$V_{MON} = V_{XIMP}G_{mdac}(\lambda) \qquad (7)$$

A calibration procedure (see below) determines $G_{mdac}(\lambda)$ for each wavelength so that $V_{MON} = P_{ecl} \times 5V/mW$ independent of the wavelength. Since $G_{mdac}(\lambda)$ can only take values greater than 1, the transimpedance resistor R_{fb} must be selectable according to the change of responsivity at center wavelength (1310/1550 nm) and the coupling ratio specification of the fiber coupler to achieve 5V/mW for V_{MON}. A rocker switch provides values from 19.2 kΩ up to 178 kΩ.

The set voltage $V_{power\,dac}$ for the desired output power is generated with the 12-bit power DAC shown in Fig. 4 according to equation 8, giving a resolution better than 1 µW:

$$V_{power\,dac} = -P_{ecl} \times 5V/mW = -V_{REF1}MDAC/4096, \qquad (8)$$

where $0 < MDAC \le 4095$. The difference $-V_{MON} - V_{power\,dac}$ is the input of an integrator with time constant τ_{cw} = 1 ms. The integrator output controls the input voltage V_{CS} of a current source which generates the laser current I_{LD}. This creates optical power according to equation 9:

$$P_{las} = P_{thr} + S(I_{LD} - I_{thr}), \qquad (9)$$

where I_{thr} is the threshold current for lasing, P_{thr} is the optical power at I_{thr}, and S is the laser efficiency (µW/mA).

Fig. 3. Thermistor variations.
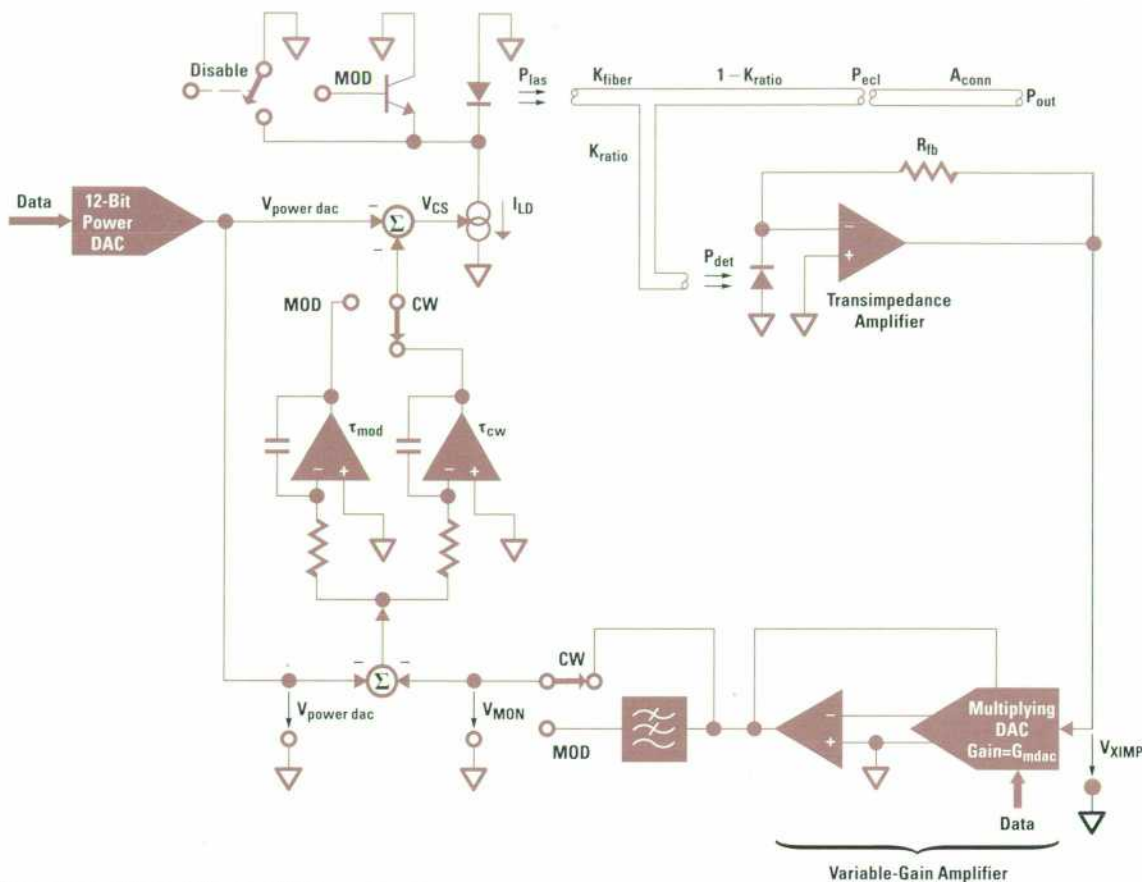
Fig. 4. Power control loop of the tunable laser source.

A typical measurement of output power versus time under changing operating conditions is shown in Fig. 5. The total change in the output power was 3 μW or 0.067 dB for a change of operating temperature from 25°C to 40°C.

Modulation is applied by switching the laser current I_{LD} on and off with a duty cycle of 50%. The modulated signal after the variable-gain amplifier is averaged by a low-pass filter (third-order Bessel with $f_g = 26$ Hz) with a gain of two, just canceling the 50% duty cycle. To get stable behavior in the modulated mode, the integrator time constant was chosen to be $\tau_{mod} = 76$ ms.

Since optical output power is specified after 2 m of fiber cable, the insertion loss A_{conn} of the output fiber must be taken into account. With $A_{conn} = 1.3$ dB, the set voltage $V_{power\ dac}$ is multiplied by $10^{1.3/10}$ to compensate for the worst-case insertion loss.

Output Power Calibration

Calibration of the optical output power of the tunable laser source is necessary to ensure constant output power and maximum laser output power as a function of wavelength. A typical characteristic for the output power of an external cavity laser at constant laser diode chip current is shown in Fig. 6.

To guarantee a long lifetime, the semiconductor laser chip can only be driven up to a maximum constant current level. This then determines the maximum power as a function of

Fig. 5. Power stability versus time for a change of ambient temperature from 25°C to 40°C.
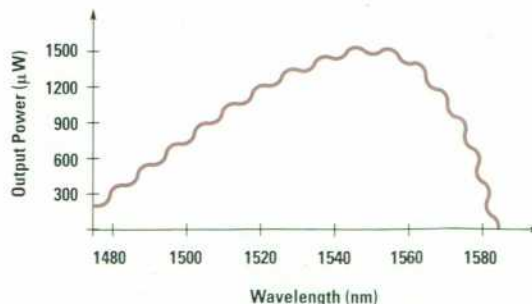
Fig. 6. Typical output power of an external-cavity laser at constant drive current as a function of wavelength.

wavelength. To stabilize the output power as a function of time the laser is operated in a power feedback loop. Because the loop is set for a particular power level, not a particular current level, we need to measure the maximum laser power as a function of wavelength to determine the maximum power available for a given power setting.

Several internal optical parameters, such as the photodiode responsivity and the splitting ratio of the coupler, are wavelength dependent. To guarantee the flatness of the output power as a function of wavelength, the whole arrangement has to be calibrated as a function of wavelength.

In the power control loop, the light coming from the laser diode is split by a coupler into the output power P_{ecl} and the power incident on the photodiode, P_{det}. After the transimpedance amplifier with fixed gain, the detected power signal is controlled by a multiplying DAC to generate a wavelength independent signal. This voltage is proportional to the optical output power and is compared with the desired voltage from the power DAC to control the laser current source. Calibration consists of determining the multiplying DAC setting for each wavelength to compensate for all of the wavelength dependent effects.

The gain of the multiplying DAC is

$$G_{mdac} = 4096/MDAC, \qquad (10)$$
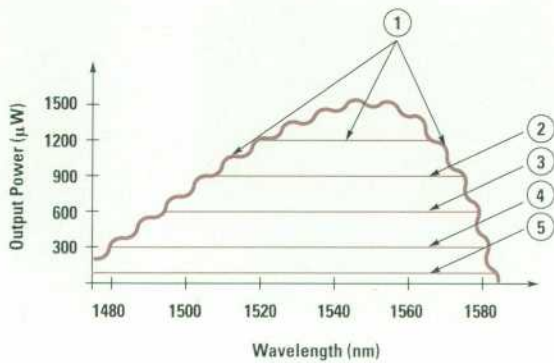
Fig. 7. Result of power flatness and maximum power calibration as a function of wavelength.

where $0 < MDAC \leq 4095$. For the calibration measurements we bypass the multiplying DAC, effectively setting $G_{mdac} = 1$, and adjust the output power so that $V_{MON} = V_{XIMP}G_{mdac} = $ constant. We determine the measured proportionality factor $R_{cali}(\lambda)$ in volts per watt by measuring P_{ecl} at each wavelength:

$$R_{cali}(\lambda) = \frac{V_{MON}}{P_{ecl}(\lambda)}. \qquad (11)$$

Then the gain of the multiplying DAC needed for any wavelength is:

$$G_{mdac}(\lambda) = \frac{V_{MON\ want}}{V_{MON\ cali}(\lambda)} = \frac{R_{want}}{R_{cali}(\lambda)} = \frac{5V/mW}{R_{cali}(\lambda)}. \qquad (12)$$

After this calibration the output power is easily chosen by setting the power DAC:

$$V_{power\ dac} = P_{want}R_{want} = P_{want} \times 5V/mW. \qquad (13)$$

The last calibration step is to detect the maximum power of the laser as a function of wavelength at the maximum drive current. The final power DAC value is then:

$$V_{power\ dac} = P_{want}R_{want},\ P_{want} < P_{max}(\lambda)$$
$$V_{power\ dac} = P_{max}(\lambda)R_{want},\ P_{want} \geq P_{max}(\lambda). \qquad (14)$$

Thus, to get constant power as a function of wavelength it is only necessary to change the gain of the multiplying DAC, and to get different output powers at a fixed wavelength it is only necessary to change the power DAC.

The result of the calibration is shown in Fig. 7. Curve 1 shows the maximum output power of one tunable laser source. 1.2 mW is the limit imposed by laser safety regulations. Curves 2 to 5 are examples of constant power-versus-wavelength curves.

The calibration setup requires only a power meter and a controller.

Reference
1. F.A. Maier, "Semiconductor Laser Sources with Superior Stability for Optical Loss Measurements," *Hewlett-Packard Journal*, Vol. 42, no. 1, February 1991, pp. 73-76.

Dual-Output Laser Module for a Tunable Laser Source

This reliable, hermetically sealed laser module is a key component in the HP 8167A and HP 8168A tunable laser sources. The semiconductor laser chip is precisely and stably aligned to two output lenses. One facet of the laser chip is antireflection-coated and has very low residual reflectivity.

by Roger L. Jungerman, David M. Braun, and Kari K. Salomaa

Wavelength-tunable light sources in the near-infrared wavelength band of 1300 to 1550 nm are finding increasing use in fiber optic instrumentation. Applications include characterization of gain in optical amplifiers as a function of wavelength and optical dispersion measurements in fiber systems. One method of making a widely tunable, narrow-linewidth optical source is to use an external-cavity laser (Fig. 1). This laser is wavelength-tuned by mechanically rotating a diffraction grating. A wavelength-selective side-mode filter ensures single-mode operation. As indicated in Fig. 1, an integral part of the external cavity laser is the laser module, which is described in this article. The design of the external-cavity tunable laser source as well as several instrument applications are covered in more detail in the articles on pages 11 and 20.

The laser module must maintain precise alignment between the laser diode and two collimating lenses and provide electrical connections for the laser chip drive current and the laser temperature controller. We have provided this functionality in a small, robust and hermetic package (Fig. 2). A schematic diagram of the laser module is shown in Fig. 3. A semiconductor laser chip with one facet antireflection-coated is solder-mounted to a submount and heat sink. The heat sink is temperature-controlled with a Peltier cooler using a thermistor to monitor the temperature. The reduced temperature extends the laser life and increases the optical output power for a given laser current. In addition, by minimizing temperature fluctuations, thermally induced refractive index changes in the chip are reduced. This improves the wavelength stability of the external-cavity laser.

Semiconductor lasers operating in a humid environment can have compromised reliability. This is particularly true when the laser is at a reduced temperature, which encourages water condensation on the laser surfaces. To avoid this problem in the module, hermetic solder seals are used throughout.

Semiconductor Laser Chip

The optical signal for the external-cavity laser is produced in a semiconductor laser diode chip. The laser diode is a quaternary InGaAsP index-guided buried-heterostructure device produced on an InP substrate. The center wavelength of the laser is determined by the quaternary material composition and can be varied to produce lasers with center wavelengths near the two wavelength bands of interest in telecommunications, 1300 nm and 1550 nm. The endfaces of the device are cleaved to produce semiconductor mirrors. Ohmic contacts on the top and bottom of the device are used to inject current, which produces optical gain and light output. Antireflection coating on the cavity-side facet of the laser diode reduces the feedback from this facet. This feedback must be minimized to give a broadband tuning range (> 100 nm). Reflections would introduce ripple in the power output spectrum of the external cavity source as described in the article on page 35. Small amounts of output power ripple can be compensated by varying the laser drive current in the instrument to achieve constant power. However, for maximum output power stability in the source while sweeping in wavelength, it is desirable to minimize the facet reflectivity as much as possible.

Very good antireflection coatings can have a reflectance below 0.1% across a 200-nm bandwidth. The ripple in the output spectrum of the laser can be used to measure the residual reflectivity of the coating.[1] First, the output spectral ripple of the uncoated chip is measured at a drive current
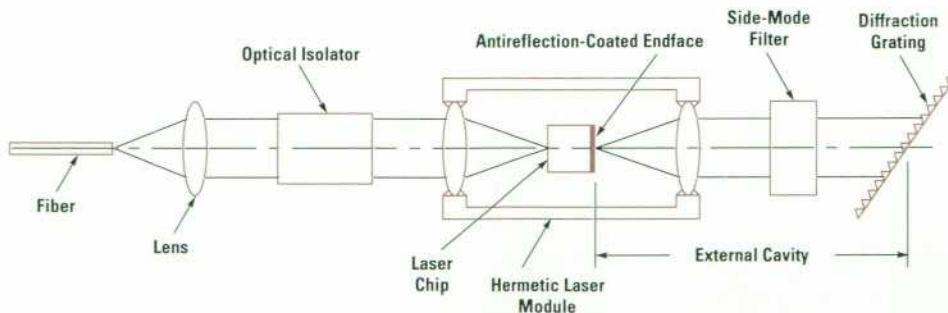
Fig. 1. Schematic diagram of a wavelength-tunable external cavity laser containing a hermetic laser module.

Labels in figure: Fiber, Lens, Optical Isolator, Antireflection-Coated Endface, Laser Chip, Hermetic Laser Module, Side-Mode Filter, Diffraction Grating, External Cavity
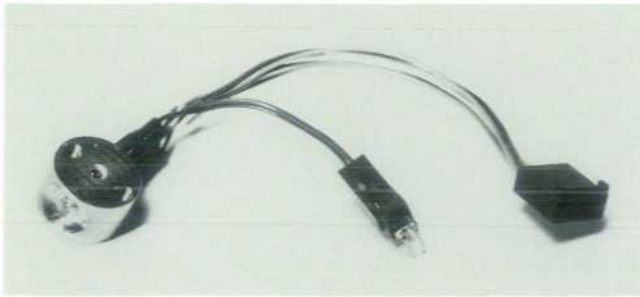
Fig. 2. Laser module with cables attached.

below the lasing threshold (Fig. 4). Knowing the uncoated facet reflectance and then measuring the ripple in the same chip after coating, it is possible to calculate the coating reflectance as a function of wavelength (Fig. 5). This result is for a three-layer coating of hard dielectric materials that are impervious to changes in humidity. This stable multilayer coating has a much wider range of wavelengths with low reflectance than can be produced with an ideal single-layer coating. The antireflection coating must be optimized separately for both 1300 nm and 1550 nm lasers.

Module Assembly

Before it is coated, the laser chip is soldered to a submount that has high thermal conductivity and provides a good thermal expansion match to the device. Both of these submount properties are critical for reliable long-term laser operation. The submount is soldered to a metal heat sink and attached to a Peltier cooler mounted on a metal carrier. A thermistor for temperature monitoring is mounted on the heat sink. The laser is then precisely aligned to the two lenses and all three components are soldered in place as shown in Fig. 3. Before fixing the components in place the module is tested in an external cavity to ensure stable single-mode operation with
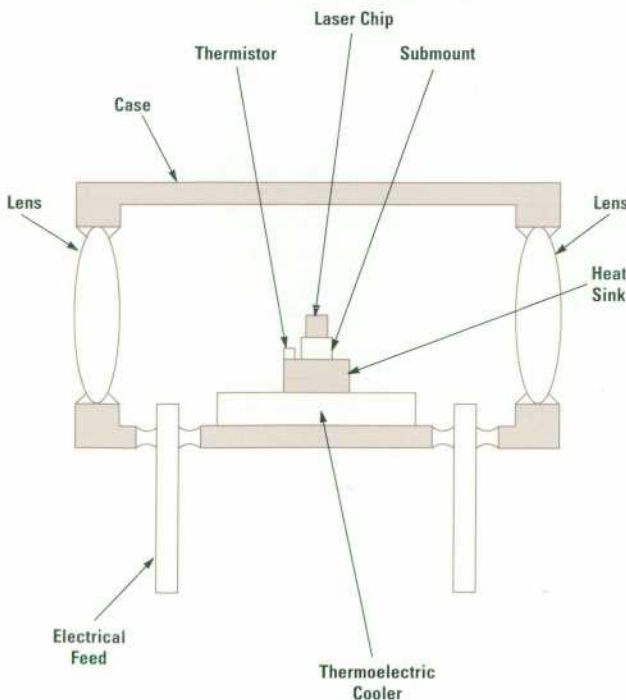
Fig. 3. Schematic diagram of the laser module.
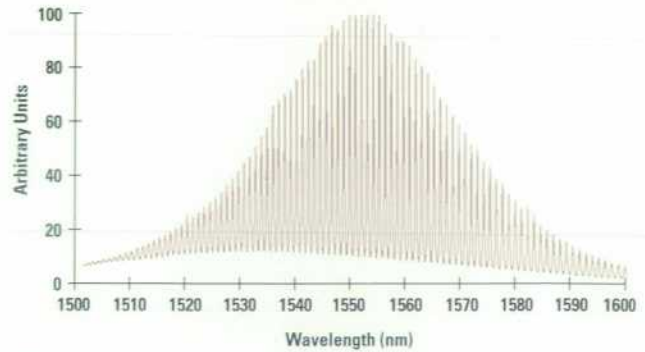
(a)
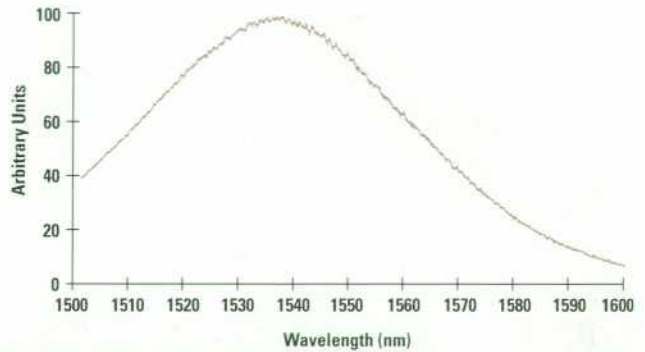
(b)

Fig. 4. Spectral ripple of an (a) uncoated and (b) antireflection-coated semiconductor laser measured below threshold.

the lowest possible threshold. Extremely precise laser-to-lens alignments are required for optimum instrument operation. Laser-to-lens misalignments of less than a few micrometers are required of both lenses before assembling the module into an instrument. Misalignment of the lens and the laser causes output beam defocusing or tilting. After the alignment is verified the package is checked for leaks using helium, backfilled with dry nitrogen, and solder sealed. A cable and an electrostatic discharge (ESD) protection plug are attached. Proper ESD procedures are observed throughout the process since ESD damage can cause latent laser failures, which degrade the long-term reliability of the module. Once the module is assembled and aligned in an instrument, the long-term alignment tolerances are even more severe—on the order of a few tenths of a micrometer. The Peltier cooler in the module and the heated and enclosed environment of the instrument help guard against thermal expansion of the package, which could produce misalignments and output power variations over the operating temperature range of the instrument.

Reliability

The laser modules described above have been stress tested as shown in Table I, with no failures. Temperature cycling and mechanical shock and vibration tests point out weak spots in the solder process, thermal mismatch problems, and unreliable wire bonds. For more sensitive humidity tests a small humidity sensor was placed in a module which then underwent high humidity followed by thermal cycling and an additional humidity test. No change in the internal package dew point ($< -20°C$) was observed. To test laser chip
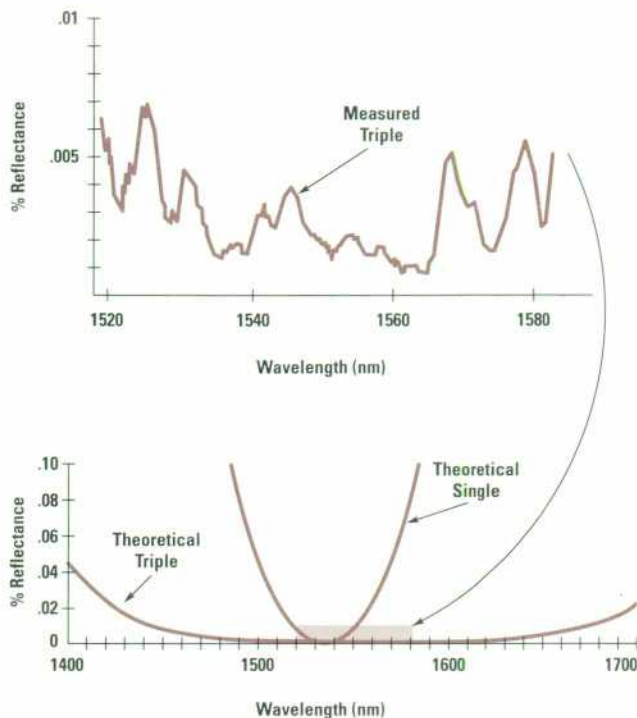
Fig. 5. Antireflection coating reflectivity as a function of wavelength calculated from the spectral ripple before and after coating. The coating consists of three layers of hard dielectric materials. Also shown are theoretical curves for a three-layer coating and an ideal single-layer coating. The use of more layers results in a broader-band antireflection coating.

reliability after antireflection coating, lasers at both 1300 nm and 1550 nm were stressed with high drive current at 70°C for 3000 hours. Less than 5% change in output power was observed.

**Table I
Laser Module Reliability Tests**

Test	Conditions	Duration
Temperature Cycle	–55 to +150°C	10 cycles
Vibration	0.02 g²/Hz 50-2000 Hz	15 min/axis
Humidity	85°C 85% RH	10 days

Summary

A laser module has been developed in which a semiconductor laser chip is precisely and stably aligned to two output lenses. One facet of the laser chip is antireflection-coated and has very low residual reflectivity. The package is hermetic and reliable. The module is a key component in the HP 8167A and HP 8168A tunable laser sources.

Acknowledgments

References

1. B.W. Hakki and T.L. Paoli, "Gain spectra in GaAs double-heterostructure injection lasers," *Journal of Applied Physics*, Vol. 46, no. 3, 1975, pp. 1299-1306.

Research on External-Cavity Lasers

The external-cavity laser is more complicated than it seems, showing both
bistability and multimoding behavior. Thorough detective work was
needed to understand this behavior and develop the light source for the
HP 8167A and HP 8168A tunable laser sources.

by William R. Trutna, Jr. and Paul Zorabedian

The tunable source in the HP 8167A and 8168A tunable laser
sources is an external-cavity semiconductor laser.[1] The
external-cavity laser is an optical oscillator, and like any
oscillator, it consists of an amplifier with feedback. The
external-cavity laser in its simplest form is sketched in
Fig. 1. It consists of a gain element—a semiconductor laser
chip—which is coupled to an external cavity that provides
wavelength-selective feedback.

A straight optical waveguide is built into the top surface of
the laser chip, running the length of the chip perpendicular
to the cleaved chip end facets. When the diode is forward
biased, gain in the waveguide is generated by optically stim-
ulated recombination of holes and electrons. Usually, the
feedback in semiconductor lasers is provided by reflections
from the cleaved facets, whose reflectivity is independent of
wavelength. In this simple form the emission wavelength is
the wavelength corresponding to the bandgap energy of the
semiconductor where the gain is the largest. However, the
gain bandwidth is typically 10% of the center wavelength,
and semiconductor lasers can be tuned provided that the
feedback wavelength is controlled. The tuning bands can be
varied by changing the semiconductor composition.

In the external-cavity laser, tunable feedback is provided by
the external cavity. However, the Q of the chip resonator
must first be spoiled by depositing an antireflection (AR)
coating on one of the facets. Light from the AR-coated facet
is then collimated by a lens. The collimated beam strikes a

Fig. 1. The external-cavity laser in the most common configuration,
using a diffraction grating to provide wavelength-selective feedback.

diffraction grating, which disperses different wavelength
components of the incident beam at different angles. Only a
narrow band of wavelengths, which depends on the grating
angle, is retroreflected back down the optical axis into the
laser waveguide. The feedback wavelength, and therefore
the oscillation wavelength, can be controlled by rotating the
grating.

Although the external-cavity laser appears to be a simple
device, a number of practical and fundamental problems
had to be overcome before the external-cavity laser could be
put into an instrument. The practical problems, such as tight
mechanical tolerances on the external cavity and the diffi-
culty of designing and manufacturing high quality AR coat-
ings, are covered in other papers in this issue (see pages 20
and 32). Here, the topic is the research that led to an under-
standing of how to control the spectrum of the external-
cavity laser reliably.

Spectral Characteristics

Two of the essential requirements of an instrument based on
an external-cavity laser are that it should be tunable to any
wavelength within its tuning range, and at each output wave-
length it should produce a single-frequency or single-mode
output. Early versions of the external-cavity laser met neither
of these requirements. Inadequate AR coatings prevented
tuning between the spurious chip-cavity modes. More myste-
rious was the seemingly unpredictable tendency of the laser
to produce multimode output at some wavelengths and
single-mode output at other wavelengths.

The modes referred to here are the modes of the external
cavity, which is long compared to the optical wavelength.
The cavity therefore oscillates on a very large harmonic
(mode number) of the cavity fundamental frequency. Several
thousand external cavity modes spaced by a few GHz lie
within the tuning range of the external-cavity laser. The job
of the external cavity is to select one and only one of the
cavity modes.

Most of the external-cavity laser tuning problems can ulti-
mately be traced to a competition between the external cav-
ity and the laser chip cavity for control of the oscillator.
Unfortunately, the chip cavity cannot be totally eliminated
because AR coatings with zero reflectivity cannot be made.
Two of the more troublesome consequences of the residual
chip cavity are bistability and multimoding.
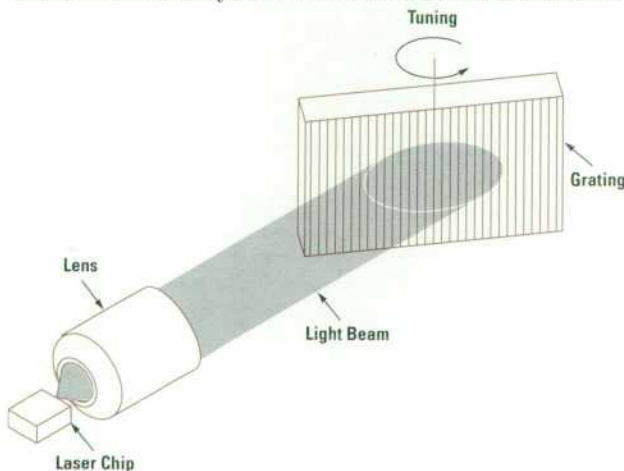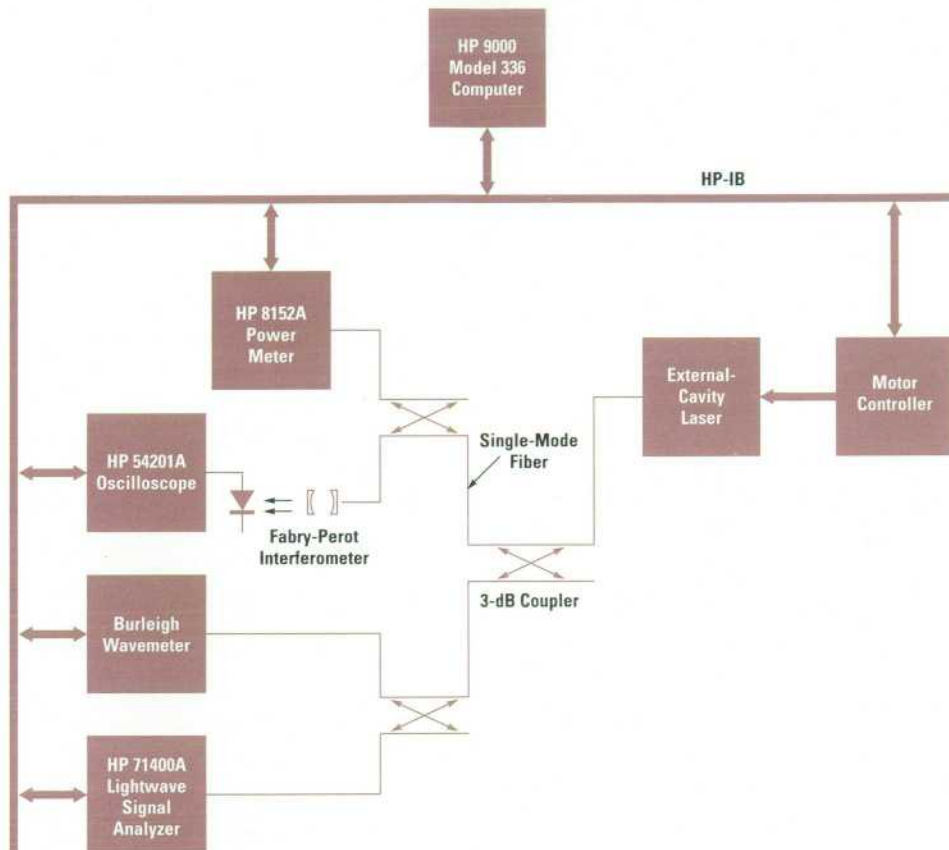
Fig. 2. A schematic of the external-cavity laser control and diagnostic system.

Control and Diagnostic System

The information provided by the measurement system sketched in Fig. 2 made it possible to make sense of the laser behavior. An HP 8152A power meter monitored the laser power output. A scanning Fabry-Perot interferometer was used as a high-resolution spectrum analyzer capable of resolving individual cavity modes. A Burleigh wavemeter measured the laser wavelength to an accuracy of 5 parts per million. The HP 71400A lightwave signal analyzer was used as a secondary, more sensitive method of detecting multimode signals. These instruments and the laser were controlled by an HP 9000 Model 336 computer, which collected the measurement data and tuned the laser.

Bistability

The first external-cavity lasers built in our laboratory contained laser chips with poor-quality AR coatings, that is, the facet reflectivity was reduced from the uncoated facet reflectivity of 30% to only about 4%. While this is sufficient to permit tuning of the laser to wavelengths between the chip cavity modes, the laser exhibited bistable behavior in some spectral regions.[2]

An example of a bistable external-cavity laser tuning curve (power versus wavelength) is shown in Fig. 3. The two experimental curves are the output power of the external-cavity laser as a function of wavelength plotted for wavelength scans up and down in wavelength. The drive current is constant and equal to 1.15 times the threshold current of the laser chip without external cavity feedback (the threshold current is the minimum current for laser action). The output power is normalized to the laser power without feedback. There are clearly some spectral regions in which two values
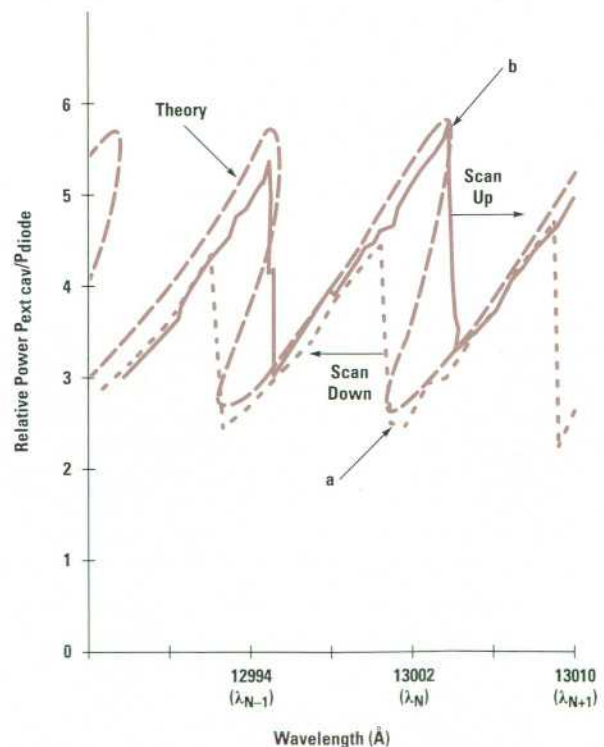
Fig. 3. Theoretical and experimental output power modulation normalized to zero-feedback output power, at 1.15 times zero-feedback threshold current, for 4% AR-coated facet reflectivity and 22% external-cavity feedback. (a) Minimum power, maximum threshold gain. (b) Maximum power, minimum threshold gain.
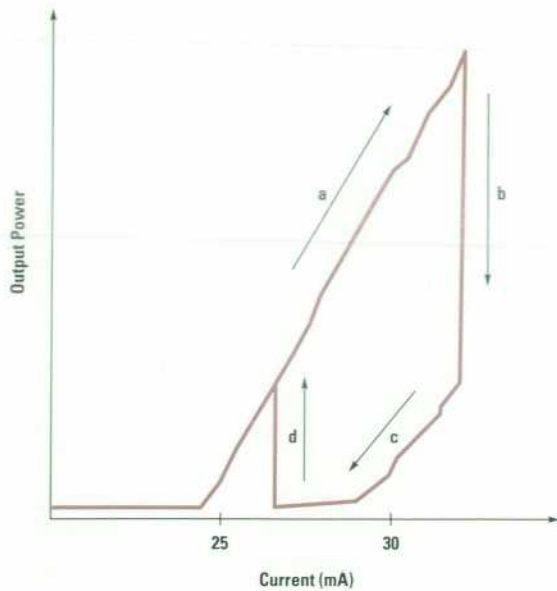
Fig. 4. Power as a function of current hysteresis. (a) Low-threshold state. (b) Low-to-high threshold transition caused by momentary feedback interruption. (c) High-threshold state, oscillation extinction by current reduction. (d) High-to-low threshold transition, reinitiation of oscillation by further current reduction.

of output power are possible; this is the condition given the name bistability. Furthermore, the output power is periodic in wavelength with a period equal to the mode spacing of the spurious laser chip cavity.

With the laser tuned to a bistable wavelength region, it is possible to switch the laser between the two states. In the bistable region, the laser exhibits power versus current hysteresis as shown in Fig. 4. When the current is increased from zero, the laser turns on in the low-threshold external-feedback state. A transition from the low-threshold state to the high-threshold state is triggered by momentarily blocking the external cavity. In this state, current reduction below the threshold current of the high-threshold state extinguishes the output. Further current reduction causes a spontaneous transition back to the low-threshold state.

The periodic nature of the bistable tuning curve in Fig. 3 is clearly a result of the residual chip cavity. The period is correct for the 285-μm laser chip cavity length, and the maximum power is expected when the optical signal is tuned to the cavity resonance. However, if this were the only physics involved, there would be no bistability and the power-versus-wavelength curve would be nearly sinusoidal. To explain bistability, the strong coupling between gain and laser refractive index must be included in the model.

The coupling of gain, which is proportional to carrier density, and refractive index can be explained by arguments similar to those used to model propagation of radio waves in plasmas.[3] In laser theory, the effect is quantified by a linewidth enhancement factor, α, which was originally introduced to explain the anomalously large spectral linewidths of semiconductor lasers.[4,5] When the α factor is included in the model of an external-cavity laser with a partially AR-coated facet, the output power-versus-wavelength curve distorts from a sinusoid to the multivalued theory curve in Fig. 3, which is in good agreement with the experiments. The α

factor is an inherent characteristic of the laser and cannot be reduced. However, bistability can be eliminated by improving the AR coatings and by increasing the external-cavity feedback.

Multimoding

Even when the AR coating reflectivity was reduced from a few percent to a few tenths of a percent, which cured the bistability problem, good tuning behavior could not be guaranteed. The external-cavity laser still suffered from a tendency to oscillate in multiple modes, particularly in certain spectral regions. Studying, explaining, and solving this problem was one of the most difficult and time-consuming aspects of the tunable source development project.

The multimode behavior of the external-cavity laser is well-illustrated by Fig. 5, which presents two sets of measurement data. The upper curve is a plot of the laser threshold current as a function of wavelength, showing the modulation effects of the laser chip cavity. The lower curve is a statistical measurement of the fraction of multimoding events detected on multiple sweeps. There is a clear correlation between multimoding and the threshold current modulation induced by the chip cavity.

The explanation for the periodic multimoding behavior of the external-cavity laser is centered around the saturation behavior of the laser. In the time domain, the multimode laser output is noisy and in some instances pulsates at the external-cavity round-trip time period. The amplifier saturation will normally tend to damp out these amplitude fluctuations. The damping occurs because, as the circulating power increases above the equilibrium level, the gain saturates, which in turn causes the power to decrease back toward the equilibrium level. Multimoding of the type illustrated in Fig. 5 is caused when the α factor and the residual chip cavity work together to switch off the saturation mechanism.

The details of the arguments leading to this conclusion are beyond the scope of this paper, but some results of the analysis are presented in Fig. 6, which again shows two curves. The first is a calculation of the threshold single-pass chip power gain under reasonable conditions of external-cavity feedback and AR-coated facet reflectivity. The horizontal axis is frequency normalized to one laser chip mode spacing. The second curve is related to the saturation behavior
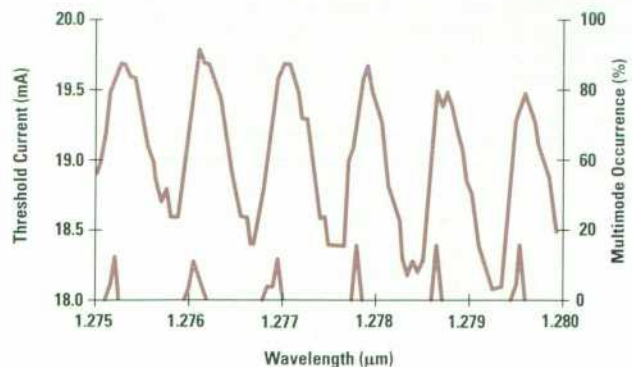
Fig. 5. The upper curve is the threshold current as a function of the laser wavelength, showing modulation resulting from the residual chip cavity. The lower curve is the multimoding probability as a function of wavelength.
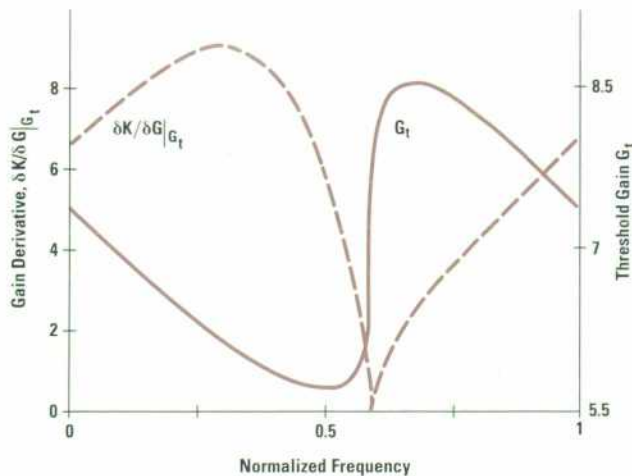
Fig. 6. The curve associated with the right vertical axis is the calculated threshold single-pass power gain (G_t) as a function of frequency normalized to a single chip mode period. AR-coating reflectivity is 0.32%, external feedback is 7.14%, and $\alpha = -5$. The second curve is $\left.\frac{\partial K}{\partial G}\right|_{G_t}$, where K is the external chip gain, G is the single-pass chip power gain, and G_t is the threshold gain.

of the laser. It is the derivative of the external chip power gain with respect to the internal chip gain. The external gain is defined as the ratio of the power coming out of the AR-coated facet to the incident power.

Unlike the internal gain, the external gain is strongly influenced by the laser chip cavity. A zero value of the derivative is an indication that the external gain is not changing as internal gain decreases as a result of carrier depletion. This is possible because even though carrier depletion reduces the internal gain, it also tunes the chip cavity because of the coupling of gain and refractive index. When the chip cavity is tuned closer to resonance by a carrier-depleting optical pulse, then the resonantly enhanced external gain can compensate for the reduction in internal gain. In effect, the amplifier has become unsaturable. In the spectral region where the derivative is small, the saturation of the amplifier has been reduced to the point where multimoding is likely.

The conclusion drawn from Fig. 6 is that multimoding is more likely in the spectral regions where the threshold gain curve has the steepest slope. This is indeed what was measured in Fig. 5.

There are two approaches to solving the multimoding problem. The first is simply to reduce the AR-coated facet reflectivity to the smallest manufacturable level and at the same time increase the external feedback to the largest practical level. It can be shown theoretically that multimoding will disappear if the facet reflectivity is sufficiently reduced.[6] The second approach is to reduce multimoding by changing the external cavity design. The idea here is to make the external cavity filter bandwidth narrow enough so that only one external cavity mode lies within the filter bandpass. Several cavity designs were investigated both analytically and

experimentally with this goal in mind. Our conclusion is that a sufficiently narrow filter cannot be made using the diffraction grating alone. For this reason a second filter element—a tilted etalon as described in the article on page 20—was added to solve the multimoding problem. Although the etalon complicates the external-cavity laser because the grating filter and the etalon must be tuned synchronously, the etalon proved to be the most reliable multimode suppression method.

Summary

Bistability and multimoding are two important phenomena that affect the control of external-cavity laser wavelength and spectral width. The investigations at HP Laboratories were done to develop a set of single-mode design specifications for AR coating reflectivity, feedback strength, and external filter bandwidth. Other investigations on cavity design,[7,8,9] mechanical tolerances, and phase-continuous tuning[10] were also completed. Altogether, the outcome of this work was a significant contribution to the development of the HP 8167A and HP 8168A tunable laser sources.

Acknowledgments

References

1. R. Wyatt and W.J. Devlin, "10 kHz linewidth 1.5 μm InGaAsP external cavity laser with 55 nm tuning range," *Electronics Letters*, Vol. 19, 1983, pp. 110-112.

2. P. Zorabedian, W.R. Trutna, and L. Cutler, "Bistability in Grating Tuned External-Cavity Semiconductor Lasers," *IEEE Journal of Quantum Electronics*, Vol. QE-23, 1987, pp. 1855-1860.

3. S. Ramo, J.R. Whinnery, and T. van Duzer, *Fields and Waves in Communication Electronics*, John Wiley & Sons, 1965, pp. 338-342.

4. C.H. Henry, "Theory of the linewidth of semiconductor lasers," *IEEE Journal of Quantum Electronics*, Vol. QE-19, 1982, pp. 259-264.

5. E. Patzak, A. Sugimura, S. Saito, T. Mukai, and H. Olesen, "Semiconductor laser linewidth in optical feedback configurations," *Electronics Letters*, Vol. 19, 1983, pp. 1026-1027.

6. P. Zorabedian, "Axial mode instability in external-cavity tunable semiconductor lasers," *submitted to IEEE Journal of Quantum Electronics*, publication date unkown.

7. P. Zorabedian and W.R. Trutna, Jr., "Alignment-stabilized grating-tuned external-cavity semiconductor laser," *Optics Letters*, Vol. 15, 1990, pp. 483-485.

8. P. Zorabedian and W.R. Trutna, "Interference-filter-tuned, alignment-stabilized semiconductor external cavity laser," *Optics Letters*, Vol. 13, 1988, pp. 826-828.

9. M. Nazarathy, P. Zorabedian, W.R. Trutna, Jr., and T. Ranganath, *Misalignment-Tolerant, Grating-Tuned External-Cavity Laser*, U.S. Patent number 4,942,583.

10. W.R. Trutna, Jr. and L. Stokes, "Continuously Tuned External Cavity Semiconductor Laser," *submitted to Journal of Lightwave Technology*, publication date unkown.

Design of a Precision Optical Low-Coherence Reflectometer

The HP 8504A precision reflectometer uses the classic Michelson interferometric measurement technique to allow designers and manufacturers to measure reflections easily in optical components and assemblies. Spatial resolution is on the order of tens of micrometers.

by D. Howard Booster, Harry Chou, Michael G. Hart, Steven J. Mifsud, and Rollin F. Rawson

An optical low-coherence reflectometer uses a Michelson interferometer configured with a broadband source to make spatially resolved measurements of reflections within optical components and assemblies. The short coherence length* of the source, usually a light-emitting diode, produces a spatial resolution on the order of tens of micrometers, while the measurement range is limited only by the travel of the reference mirror in the interferometer. The objective of the HP 8504A precision reflectometer project was to provide the lightwave industry with the first commercial implementation of the Michelson interferometric measurement technique in which all the components are provided in one package.

While white-light interferometry** has been around for some time in research labs, the measurement setup is complex, typically requiring an optical table and a very skilled person to make the measurement and interpret the results. To be successful, the commercial version of this measurement technique needs to be rugged, reliable, easy to use, and affordable for manufacturing applications. To meet this challenge within the constraints of a short development cycle and the requirement to minimize development cost, a small group of experienced engineers was assembled to build the HP 8504A. Off-the-shelf parts were used wherever possible and every opportunity to leverage previous designs was taken.

The article on page 52 provides a detailed discussion about the Michelson interferometer and white-light interferometry.

* Low coherence and short coherence length are two ways of describing the same fundamental characteristic of the LED source in the reflectometer. A low-coherence source has a broad spectral content and therefore it is noisy. The broad spectrum means that the source will have a short coherence length because the light beam travels only a short distance before it becomes incoherent.

** White-light interferometry uses a broadband, noisy source.
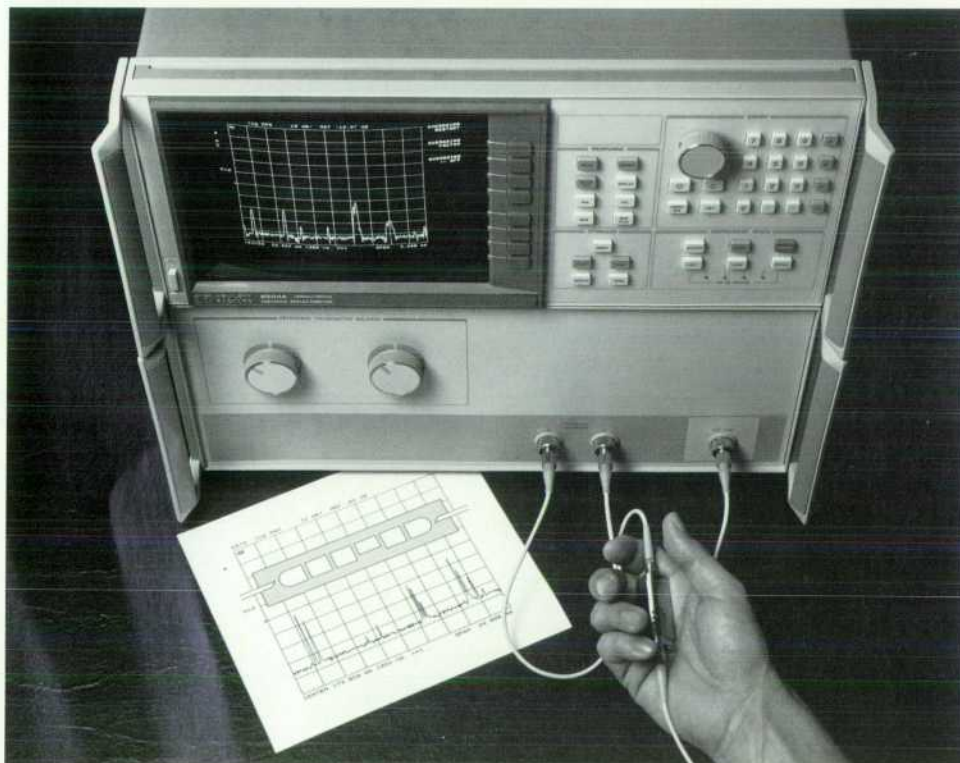
Fig. 1. The HP 8504A precision reflectometer. The top part is the display and signal processing section and the bottom part contains the optical and detection hardware.

Several instrument concepts were considered for the HP 8504A precision reflectometer, including a single, designed-from-scratch box and an upgrade or retrofit of an existing network analyzer. The final design consists of two packages of reasonable size and weight which can be transported separately and then reattached without losing factory calibration.

Measurement Example

Fig. 2 shows the display of a measurement taken with the HP 8504A precision reflectometer and an illustration of the device under test. The vertical axis of the display shows the magnitude of the optical reflections seen looking into the device and the horizontal axis shows the positions of the reflections.

In this case, the device is a small packaged laser. The first reflection is from the end of the fiber pigtail. The return loss is approximately 14 dB, which one would expect from the polished end of the fiber. The next two reflections are from

the two faces of the package window that provides the hermetic seal for the laser. The reflections are very low because these surfaces are coated with an antireflection film. Reflections from both sides of the spherical lens can also be seen. Because of the spherical shape of the lens the reflected light diverges, causing lens reflections to be small and limiting the amount of reflected light recaptured by the fiber. Finally, reflections from the front and rear facets of the laser chip are clearly visible.

Measurements of this type are nondestructive and valuable to both the component designer who wants to optimize each element of the component and the process engineer who wants to monitor the component's quality and assembly process consistency.

Block Diagram

Fig. 3 shows the block diagram of the HP 8504A precision reflectometer. In its standard configuration, the instrument contains two light-emitting diode sources, one at 1300 nm
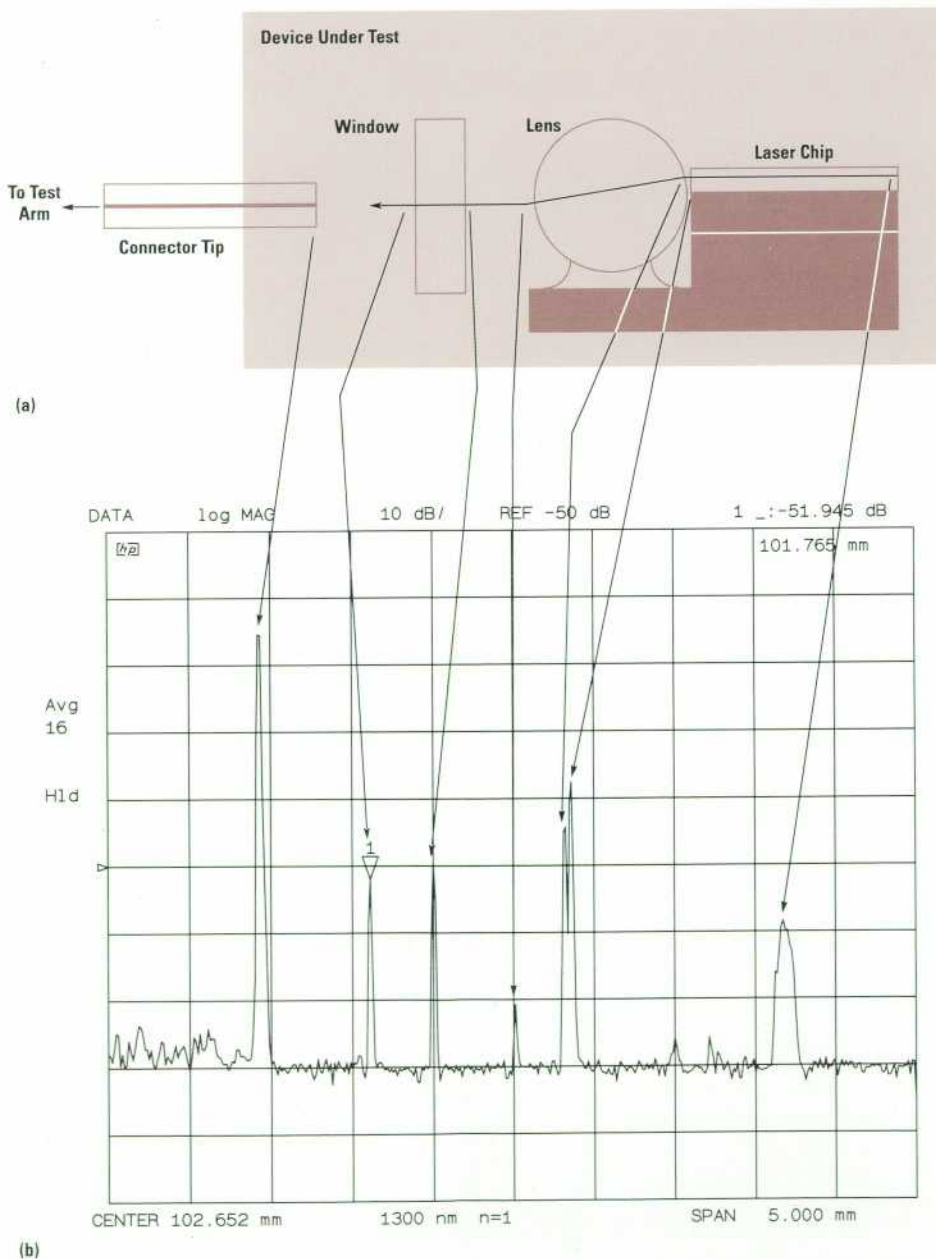
Fig. 2. Laser assembly measurement example showing the origins of the reflections that appear on the display. (a) The device under test. (b) The HP 8504 display showing the reflections in dB.
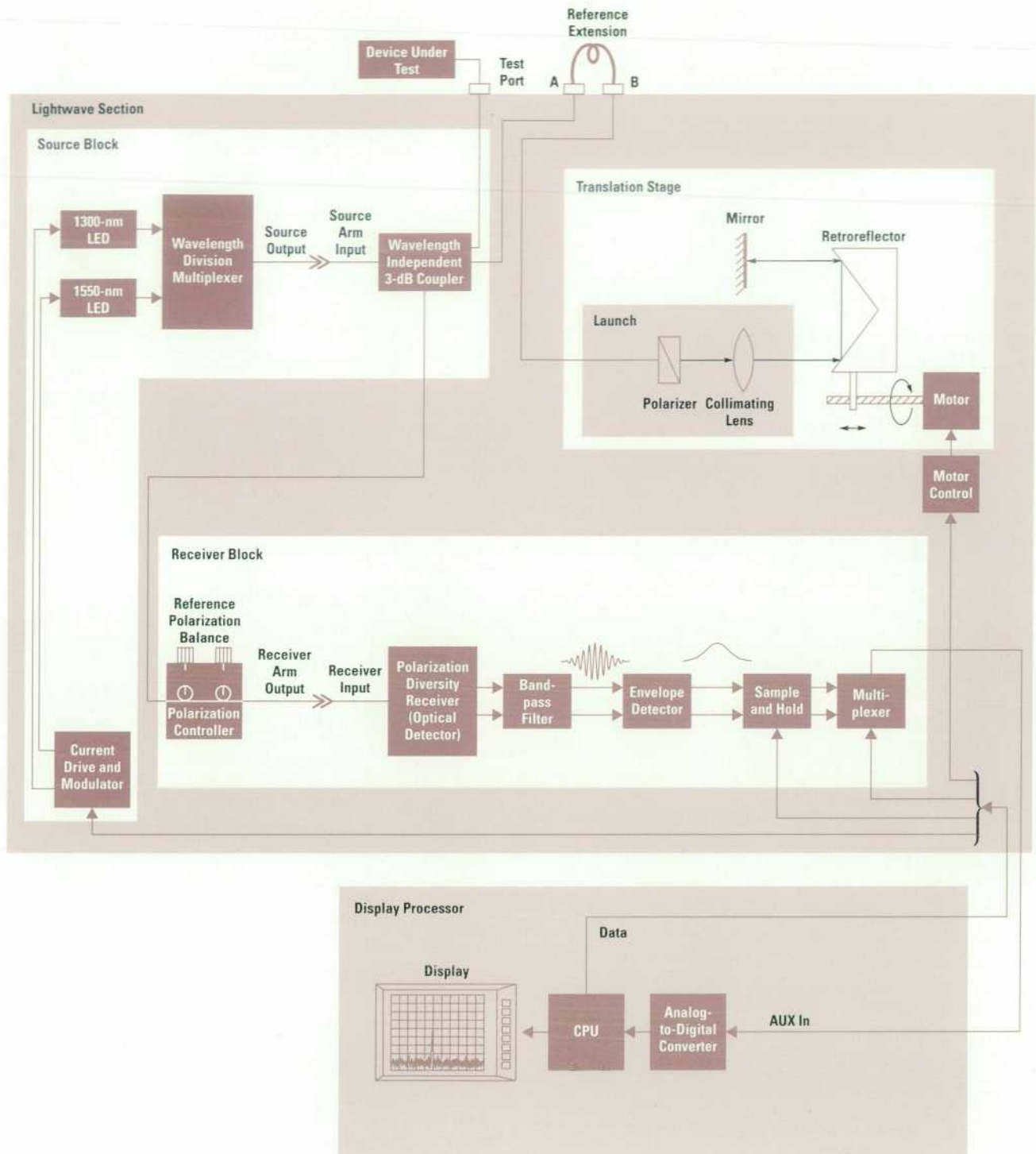
Fig. 3. HP 8504A block diagram.

and the other at 1550 nm. The outputs of the two sources are multiplexed by a wavelength division multiplexer. (Only one source is on at a time.) The output of the multiplexer is split into the two arms of the Michelson interferometer by a 3-dB directional coupler. The test arm is simply one leg of the directional coupler to which a test device can be connected. The reference arm output is polarized and collimated, and after going through a retroreflector, is reflected back along the same path by a stationary mirror and reenters the

fiber. This reflection from the reference arm is then combined with the reflection from the test arm by the directional coupler and sent to the receiver.

The retroreflector doubles the optical path length for a given mechanical travel and also improves the stability of the optical assembly. The reference arm also contains an extension cable that can be changed from the instrument front panel. By varying the length of this extension cable, the reference

plane of the measurement can be positioned at any desired point—that is, the measurement window can be offset to compensate for the fiber pigtail on the device under test.

The retroreflector scans during the measurement and hence the light reflected from the reference arm of the reflectometer is shifted in frequency (because of the Doppler effect) by an amount proportional to the scanning velocity of the retroreflector (a frequency shift of 27.7 kHz in this case). Thus, two beams of different optical frequencies are incident upon the polarization diversity receiver, and it is their difference frequency (or beat frequency) of 27.7 kHz that is processed by the receiver.

Provisions are made that allow the user to configure the HP 8504A into a general-purpose Michelson interferometer. The connector pair in the source arm makes it possible for the user to provide sources to be used with the interferometer and the connector in the receiver arm makes it possible for the user to supply external receivers. This opens up a wide variety of measurement applications. For example, the user can obtain the coherence function of a source by connecting it to the source arm input. The user can also connect an optical amplifier between the source arm connectors to improve the sensitivity of the instrument. In addition, the moving retroreflector and the zero-span feature built into the user interface allow the HP 8504A to be used as a programmable, variable, optical delay line with 1.3 ns of total range and 8 fs of resolution.

Receiver

The hardware blocks that make up the receiver portion of the HP 8504A are shown in Fig. 4. The polarization diversity receiver detects the optical interference signal generated by the combined reflections from the test arm and the reference arm of the interferometer. The electrical current output from the polarization diversity receiver is converted into a voltage by the transimpedance amplifier and fed to a bandpass filter to reduce unwanted frequency components.

Next, the envelope of the interference signal is detected by an active full-wave rectifier circuit followed by a low-pass filter. The resulting dc signal is fed to a sample-and-hold circuit, a multiplexer, and then on to the analog-to-digital converter in the display section of the instrument to be processed for display.

Polarization Diversity Receiver. The purpose of the polarization diversity receiver is to remove the undesirable dependence of the interference signal on polarization transformations in the test arm of the interferometer. In the HP 8504A, the polarization diversity receiver consists of a polarization splitter that splits the incoming optical fields into two orthogonal polarization components, each of which is imaged onto its own photodiode. These two photodiodes are described in the article on page 49.

During the instrument calibration procedure, the test port is first terminated with a low reflection, so that only the reference arm reflection is detected. The polarization controllers in the receiver arm are then adjusted such that the optical powers in the two orthogonal polarization axes are roughly equal. This ensures that an interference signal will occur regardless of the polarization state of the signal in the test arm. The device under test is then connected to the test port and the resulting interference signals are detected and converted to a current that consists of bursts of the 27.7-kHz beat frequency. The peak amplitude of these bursts is proportional to the square root of the magnitude of the reflectivity at the particular mirror position.

More detailed information about polarization and the polarization diversity receiver is given on page 55.

Transimpedance Amplifier. The transimpedance amplifier converts the output current from the photodiodes in the polarization diversity receiver into a voltage at the amplifier output (see Fig. 5). Since the information of interest is contained in a low-level 27.7-kHz signal, the amplifier must be capable of processing this frequency and also have good noise performance. However, as frequency increases, the reactance of the diode capacitance (C_D) and stray capacitance (C_{in}) shunts the negative feedback port of the operational amplifier, causing a potentially unstable condition. Adding capacitor C_1 across feedback resistor R_1 helps to compensate for this effect.

Noise performance is also improved by adding C_1.[1] The voltage gain for any noise appearing at the input of the amplifier is equal to:

$$\text{Voltage gain} = 1 + Z_1 / Z_{diode}.$$
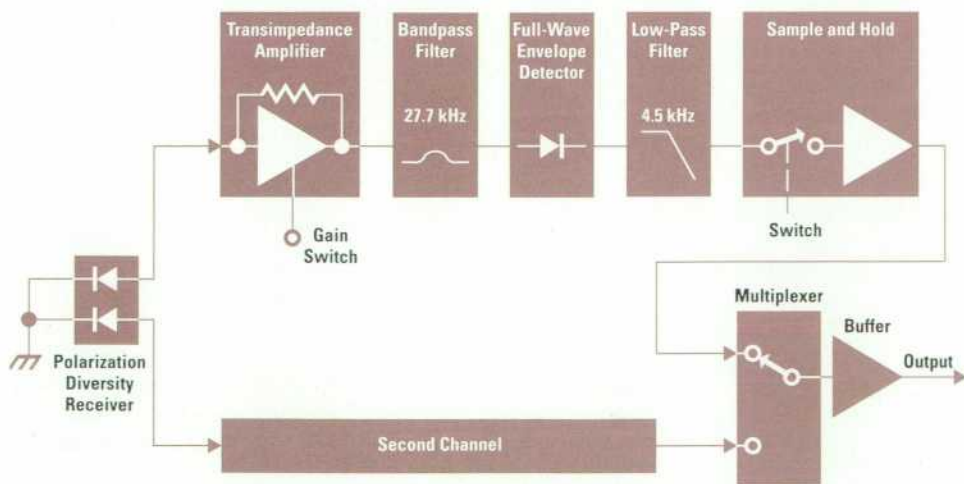
Fig. 4. Receiver block diagram.
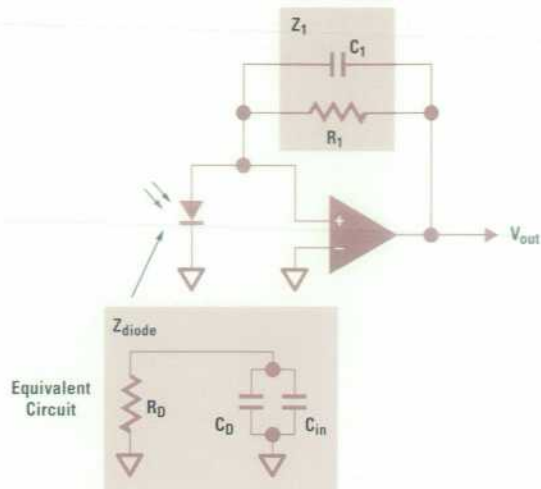
Fig. 5. Transimpedance amplifier circuit.

Fig. 7. Dynamic range of the envelope detector used in the receiver section of the HP 8504A.

This gain at dc is very nearly equal to one since the diode's equivalent resistance is very large compared to R_1. However, as the frequency increases, the diode impedance decreases because of the shunt capacitances. When the diode impedance equals R_1, the voltage gain increases at a rate of 6 dB per octave. Adding C_1 in parallel with R_1 reduces Z_1, thereby reducing the voltage gain.

A voltage amplifier with adjustable gain follows the transimpedance amplifier. This compensates for the LED device-to-device power variation and the wavelength sensitivity of the detector responsivity.

Bandpass Filter. The bandpass filter is an active, state-variable type of filter (see Fig. 6). If the gain of the operational amplifiers at the desired frequencies is sufficient, the characteristics of the filter are only dependent upon the passive components. So by choosing proper components, the filter can be made very stable with temperature.

Remaining Components. The envelope detector, sample-and-hold circuit, and multiplexer were all leveraged from other HP instruments. However, improved dynamic range was needed from the envelope detector. By optimizing the operating point of the envelope detector diodes and using a higher-frequency operational amplifier, the dynamic range was extended beyond 80 dB (see Fig. 7).

Fig. 6. Bandpass filter circuit.

Signal Processing

The top section of the HP 8504A shown in Fig. 1 is the display processor. It controls the lightwave section, digitizes the measurements, processes and displays the data, and provides the user interface. Control of the lightwave section includes initiating motor control, selecting the source, setting source power, and sampling measured signals.

The data processed by the display processor comes from the signals received by the two receiver channels. These signals are multiplexed and sent to a single, 16-bit analog-to-digital converter that produces a number that is proportional to the magnitude of the signal in the corresponding receiver channel. Then a constant, corresponding to the dc offset voltage in the particular receiver channel, is subtracted from each number. This data flow is shown in Fig. 8.

Next, the number of data points must be reduced to fit on the CRT. Data is measured approximately every 2.5 micrometers (in the 1300-nm case) and since the envelope generated by each reflection is approximately 15 micrometers wide, no reflection will be missed. However, in a full span of 400 mm this produces 160,000 data points. Only 400 points are displayed on the CRT, so the number of points must be reduced. This is accomplished using a maximum hold function. The number of measured points, which ranges from 400 to 160,000 as a function of the span, is divided into 400 groups. The data with the largest magnitude is found in each group and becomes the nominal value for the group. Consequently, in wide sweeps, a single response on the display may represent multiple reflection responses in the device under test. However, performing this function guarantees that every DUT reflection is represented. By reducing the span, multiple reflections can be resolved down to the 25-micrometer spacing.

Data averaging can be used to improve the noise floor. The averaging function in the processing sequence is an exponential average. The data being averaged consists of complex values representing the orthogonal polarization components of the detected signals. Each element of the complex data pair is averaged independently for each spatial position. An averaging factor, k, selected by the user, specifies how much of the current measurement is added to a complementary portion of the previous average to form the current average.

Averaging Measurements to Improve Sensitivity

Significant measurement sensitivity improvement can be realized if multiple measurements in narrow sweep widths are time averaged, reducing the level of the noise floor. Fig. 1 shows a reflection that is just above the noise floor in a single sweep, but is clearly visible after averaging. When using averaging to improve the noise floor, care must be taken to correctly interpret the results.

The HP 8504A measures reflections at discrete points spaced approximately 2.5 micrometers apart when using a 1300-nm source. The envelope of the response from each reflection is approximately 15 micrometers wide because of the coherence length of the LED source, so each reflection is sampled at a minimum of five points.

In the maximum sweep width of 400 mm, 160,000 data points are obtained, but only about 400 points can be displayed on the CRT. So in this case the 160,000 data points are divided into 400 groups of 400 data points each, and the largest value in each group is displayed on the CRT.

This technique of displaying the maximum value in each group of data points guarantees that any reflection that exists in the DUT will show up in the final measurement, ensuring that no DUT reflections are missed. However, it also means that averaging the data will improve the noise floor more in narrow sweeps than in wide ones.

(a)

(a)

(b)

(b)

(c)
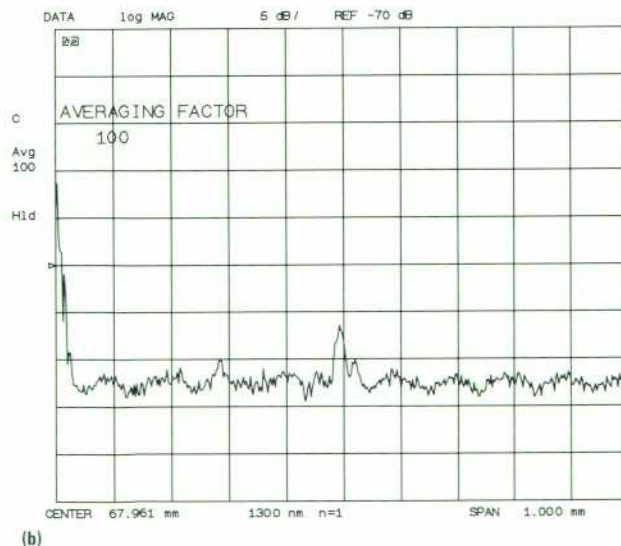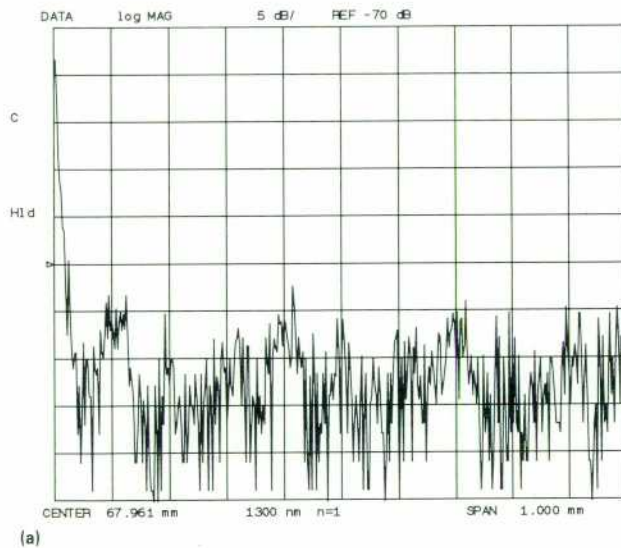
Fig. 1. A reflection that is just above the noise floor. (a) Before averaging. (b) After 100 averages.
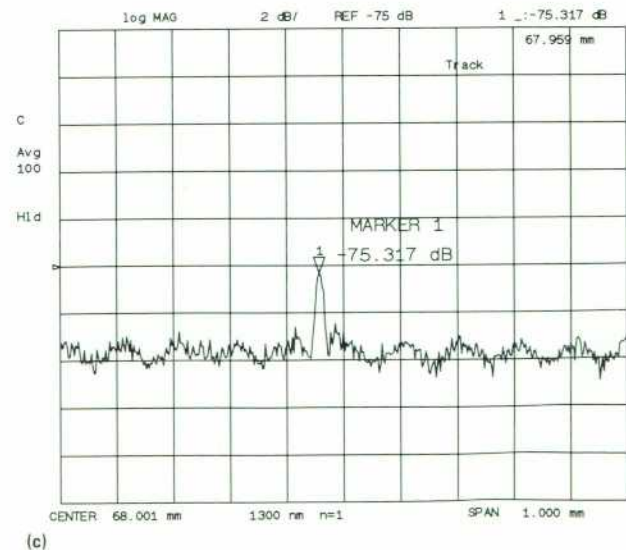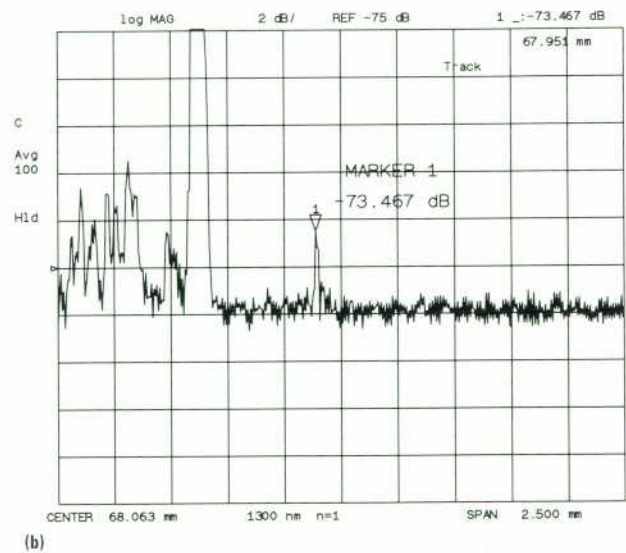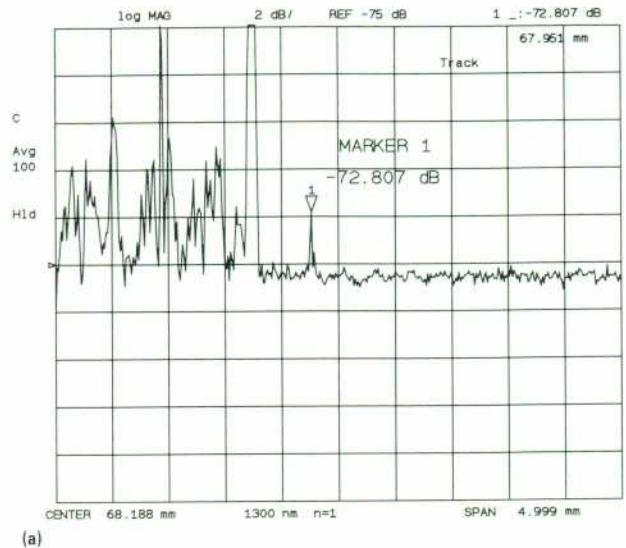
Fig. 2. Amplitude change with sweep width. (a) Sweep width (span) = 4.999 mm. (b) Sweep width = 2.5 mm. (c) Sweep width = 1.0 mm.

In the scheme just described, the largest signal in each of the groups of data points is the one that is displayed on the CRT and subsequently averaged. But noise is a random function, and in wide sweeps, which have a large number of data points in each group, there is a high probability of having a noise peak or spike show up in each group. It is this peak, the maximum value of the data points in the group, that is displayed on the CRT and used in the averaging algorithm. This has the effect of biasing the displayed noise floor upward, because it is the maximum value in each group that is kept and averaged. Decreasing the sweep width, and hence the number of data points in each group, decreases the probability that a noise peak will occur in any given group of data points. Thus, the displayed noise floor will be lower with narrower sweep widths with the optimum performance being achieved when there is only one data point per group.

This situation can lead to some confusing results when using averaging to pull signals out of the noise, particularly when measuring reflections that are below the level of the unaveraged noise floor peaks. As the sweep width* is narrowed, the level of the reflection will appear to decrease (See Fig. 2). This is because the maximum value of the reflection and the noise in each group is being averaged. In wide sweeps, the noise will dominate. As the sweep is narrowed, fewer noise peaks occur within each group and the desired reflection dominates the maximum value of the group.

So, for the best sensitivity and accuracy in the measurement of low level signals, the minimum sweep width should be used.

* Sweep width is also called measurement span.

The average for each element of the complex data is calculated as follows:

$$\text{Average}_n = \left(\frac{1}{k}\right) \times \text{Data}_{new} + \left[\frac{(k-1)}{k}\right] \times \text{Average}_{n-1}$$

where k is an averaging factor.

See "Averaging Measurements to Improve Sensitivity," on page 44 for more about measurement averaging.

Calibration

Calibration processes are used to remove systematic measurement errors and to reference measurements to a reflection of known magnitude. The calibration process consists of several steps. First the dc offsets in the receiver channels are measured. Next, with a low-reflection termination connected to the test port, the receiver polarization is balanced to divide the reference power equally between the two polarization diversity receiver photodiode detectors. The user interface provides a special display to indicate the ratio of power in the two detectors. The user manually adjusts a

two-paddle polarization controller until the trace on the display falls within a marked range. The final step is performed by connecting a known reflection to the test port. This known reflection standard is measured and used to calibrate the magnitude of the displayed reflection formed by the sum of the squares of the outputs of the two receiver channels. In addition, for measurements made at 1550 nm, the user can elect to correct for the dispersion effects of the fiber. The equation for calculating the value of a data item to take into account systematic measurement errors is:

$$\text{Data}_n = \left(k_{1_n} \times s_{1_n}^2\right) + \left(k_2 \times s_{2_n}^2\right)$$

where k_1 and k_2 are correction coefficients combining balance, magnitude, and dispersion factors and s_1 and s_2 are the data points for the two channels with the offsets removed.

Magnitude data is formatted either as linear data ranging from 0 to 1.0 for calibrated measurement, or as logarithmic data in dB. The absolute value of the logarithmic data is return loss. Before the data is displayed, it is scaled and the reference value and position are set.

Interferometer Details

The interferometer section of the HP 8504A consists of two major assemblies: the optical deck and the translation stage. The modular approach of these designs allows the interferometer section to be serviced in the field and to be manufactured separately.

Optical Deck. The optical deck houses the major interferometer devices (see Fig. 9). The LED sources, wavelength division multiplexer, coupler, and receiver are packaged within one sheet-metal tray. The fiber and each splice are routed through channels of neoprene foam to control bend radii and fiber stability and to manage fiber lengths. The front-panel connectors are attached directly to the tray, which aids in assembly.

Translation Stage. The translation stage serves two functions in making the return loss measurement. The first is to position the measurement window at the point of interest within the DUT. The translation stage has a maximum travel of 200 mm. By using a retroreflector to double the optical path length, 400 mm of measurement range is achieved. The measurement window, or span, can be as small as 1 mm or as large as 400 mm.
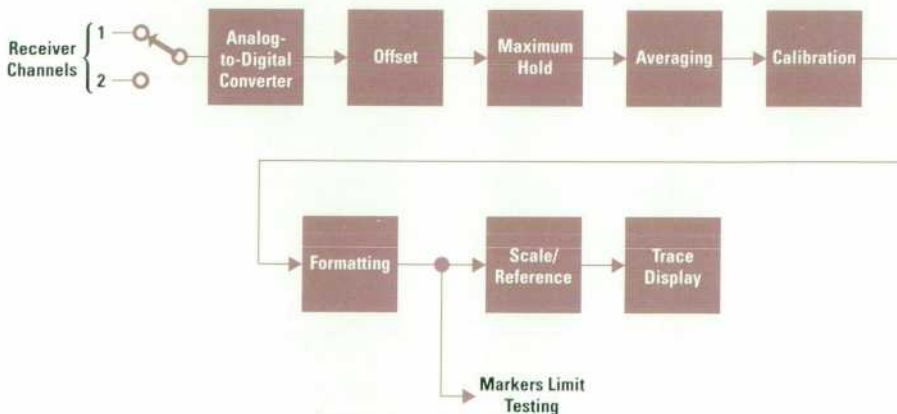
Fig. 8. Data processing flow.
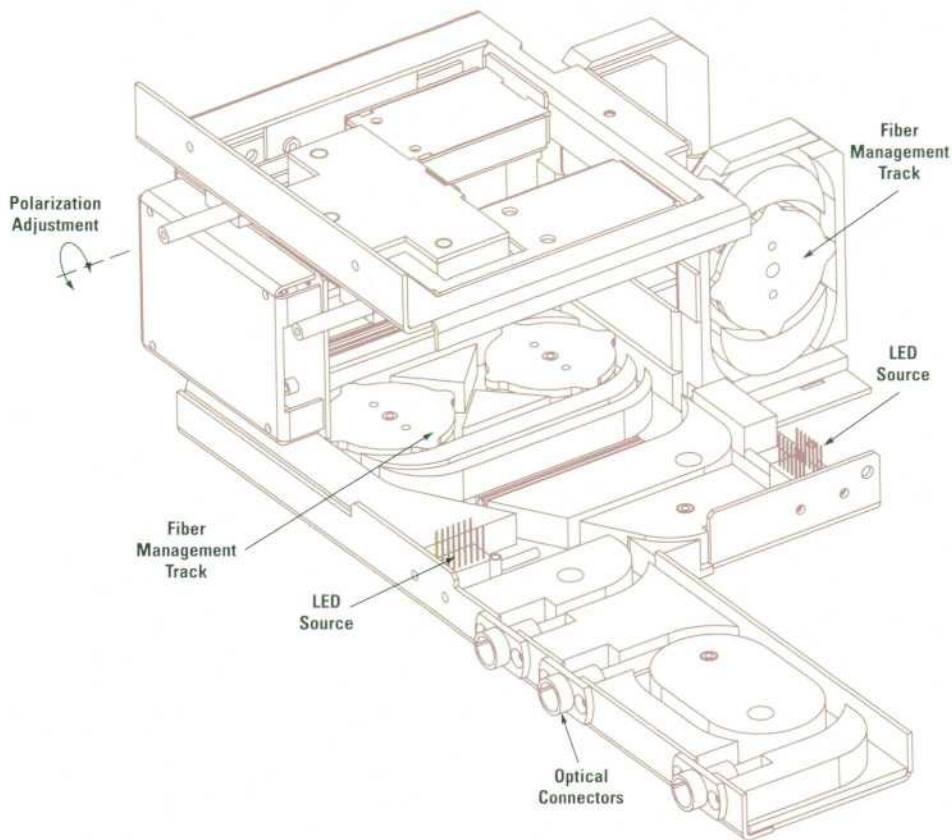
Fig. 9. Optical deck in the HP 8504A.

The second function of the translation stage is to move the retroreflector at a constant velocity. This produces a Doppler shift in the reference arm signal of 27.7 kHz. The distance between two reflections, measured during the same sweep, is calculated from the velocity and the elapsed time.

The translation stage consists of a preloaded ball-bearing linear slide driven by a leadscrew and a servo-controlled dc motor (see Fig. 10). The leadscrew moves the retroreflector along the linear slide. Light is launched from the fiber, passes through the polarizer and the collimating lens, and to one side of the retroreflector aperture. The light is then directed to a stationary flat mirror mounted adjacent to the fiber launch where it reflects back onto itself, retracing the forward path, and is recoupled into the fiber. By moving the position of the retroreflector, the open beam length is increased by twice the slide travel.

To minimize the time to market for the HP 8504A, standard components were used in the design wherever possible. The dc motor was leveraged from components used in other HP products, and the linear slide is a commercially available product. Most of the other optical components were also readily available, that is, they did not have to be specially designed.

The translation stage's most critical performance requirement is velocity control. Measurement repeatability, reflection position, and amplitude accuracy are all directly affected by the retroreflector's velocity. In addition, very low-amplitude vibrations can modulate the mirror or the retroreflector. This velocity "noise" appears as frequency modulation on the Doppler-shifted signal.
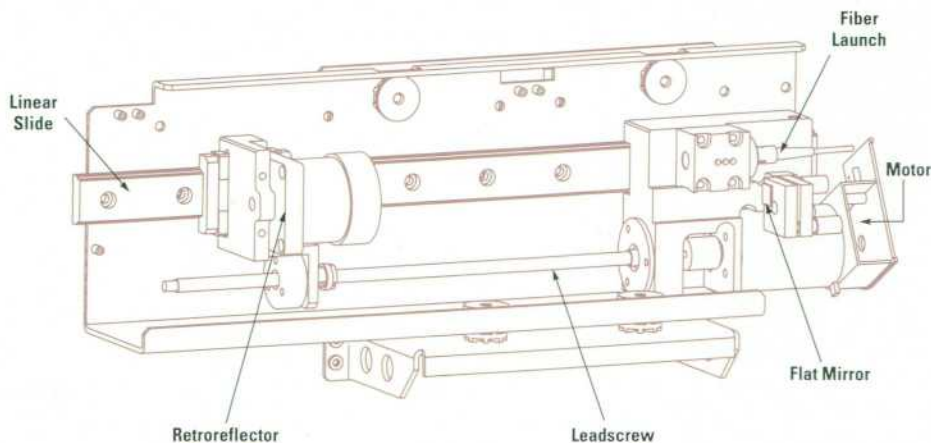
Fig. 10. Components in the translation stage.
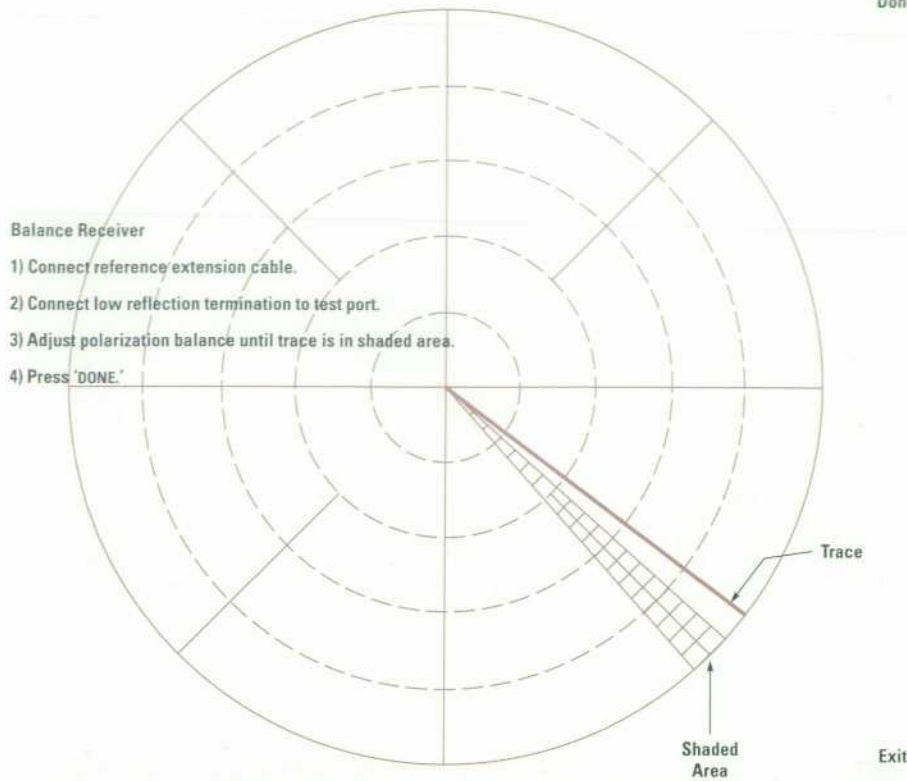
Fig. 11. Polarization receiver balance display.

Two separate approaches were used to minimize the system vibration. First, the loop was optimized for low-amplitude velocity noise at the expense of maximum system responsiveness. Second, the open-loop structural vibrations were suppressed by damping and using compliant coupling in the leadscrew design.

Optimizing translation stage performance required an unusual velocity measurement technique. The unwanted vibrations and velocity fluctuations of the optical surfaces on the stage needed to be measured precisely without influencing the dynamics of the system. Traditional approaches such as the use of a tachometer or accelerometer proved inadequate in this application. The solution was to use an external laser as the source for the interferometer and then monitor the period of the resulting fringes.

User Interface

Development of the HP 8504A user interface was facilitated by the reuse and leverage of firmware from the HP 8703A lightwave component analyzer. Both of these instruments, as well as the HP 8702 lightwave component analyzer, are used to characterize lightwave components. A common origin for the firmware helped maintain a consistent user interface for lightwave component measurements. In addition, development time was shortened by reusing firmware.

Most of the user interface and data display manipulation features of the HP 8504A are a subset of those found in HP's lightwave component analyzers. However, other features were added to meet the specific needs of the reflectometer. Two of the added features contribute significantly to the usability of the HP 8504A. The first of these is the peak search functions. The interpretation of measurements made with the HP 8504A involves locating the position and amplitude of impulse peaks corresponding to reflections in the

device under test. The user can easily position a trace marker on one of the peaks to determine reflection position and amplitude.

A second feature that aids usability is the polarization balance display (see Fig. 11). The user is provided with a graphical representation of polarization. The display gives real-time feedback as the user adjusts the polarization state. The display includes a shaded target area to indicate the acceptable range for polarization balance.

The HP 8504A includes a feature called guided setup, which is also found in other HP lightwave component analyzers. This feature greatly simplifies the use of the HP 8504A precision reflectometer. Graphics and text help the user through the important step of selecting and connecting the reference
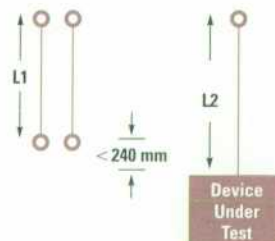
Fig. 12. Guided setup display.

extension cable (see Fig. 12). The user is also guided through receiver balance and magnitude calibration.

In addition to front-panel operation, the HP 8504A can be remotely controlled using a standard HP-IB interface. Hard copy of the data can be produced using plotters and printers connected via the HP-IB. Data and instrument states can be stored to disk via the HP-IB and retrieved for later use.

References
1. "Noise Model of Photodiode Applications," *Notes from Burr Brown Technical Seminar*, 1986.

Fabrication of Diffused Diodes for HP Lightwave Applications

The simple but robust p-i-n dual detector used in the receiver of the HP 8504A precision reflectometer has −17 dB return loss (2% reflection) operating at both 1300 nm and 1550 nm.

by Patricia A. Beck

The HP 8504A precision lightwave reflectometer uses a pair of cofabricated planar photodiodes as its receiver element (see article on page 39). One path of the split polarization beam strikes each diode and the resulting photocurrents are added vectorially. Although the InP/InGaAs detectors have been optimized for wavelengths from 1300 nm to 1550 nm, other operational configurations are possible.

P-i-n photodetectors convert optical inputs to electrical signals. A photon enters through the p-doped region, which is chosen to be transparent to the radiation, and is absorbed in the intrinsic (i) region. An electron-hole pair is formed. Carriers are moved from the intrinsic region to the p and n regions by the electric field induced by the applied voltage bias. The movement of charge is the detected photocurrent. This photodetector operation is shown in Fig. 1.

This article describes the design and process used to develop the diffused photodiodes used in the HP 8504A.
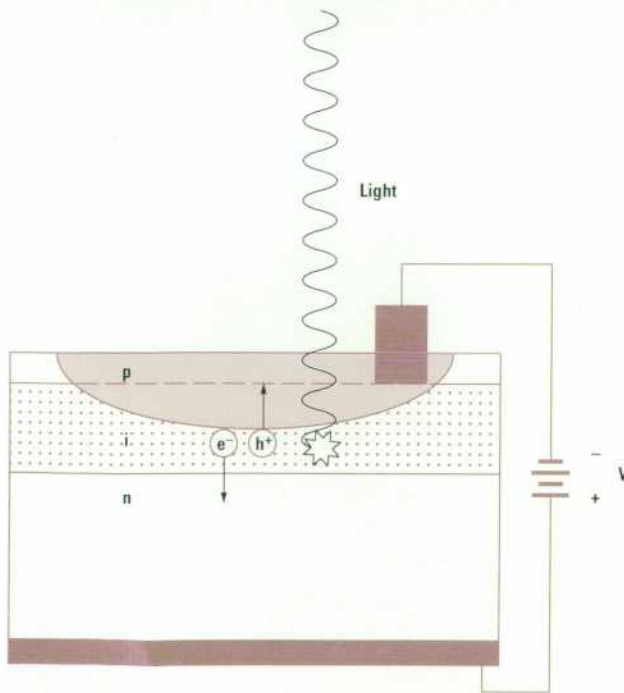
Types of Photodiodes

Two types of semiconductor photodiodes are used in HP lightwave products: mesa and diffused planar. While their operation is similar, their structures are different.

Mesa p-i-n diodes have their layers grown epitaxially with the dopants already in place. Extraneous material is then etched away to form the devices and provide isolation and separation from neighboring devices as shown in Fig. 2. The layers for the devices in question are: Zn-doped InP for the p region, sulphur-doped InP for the n region, and undoped (intrinsic) InGaAs for the i region.

Fig. 1. Photodetector operation.
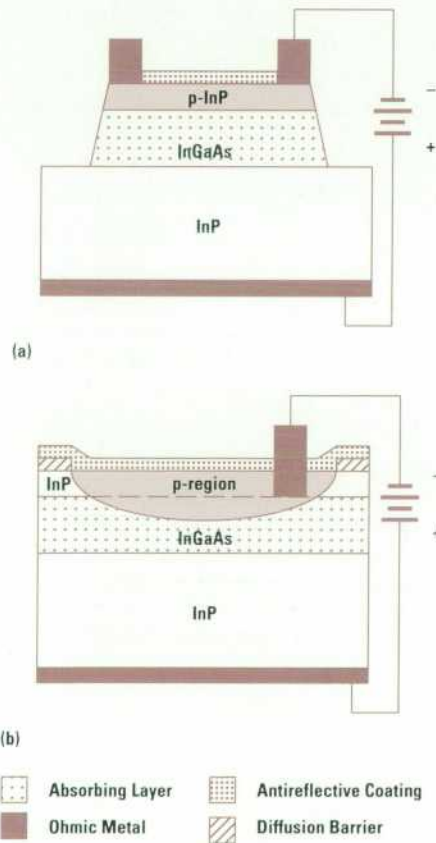
Fig. 2. P-i-n structures. (a) Mesa device. (b) Planar device.

Fig. 3. Closed ampoule diffusion.

Fig. 5. I-V curve of a 320-µm diameter diffused photodiode.
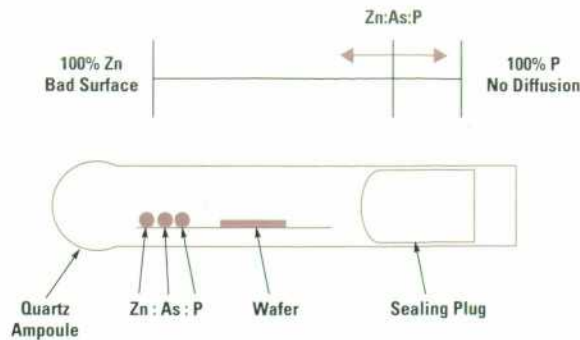
Planar p-i-n diodes also have their layers grown epitaxially, but the layers above the n-type substrate are undoped. The p region is formed later by diffusing dopants into the surface. After the epitaxial layers are grown, a diffusion barrier (in this case silicon nitride) is deposited and patterned. The openings in the diffusion barrier expose the InP surface to define and separate devices. The patterned wafer is sealed in a closed vessel with the solid dopants or placed in an OMVPE (organometallic vapor phase epitaxy) reactor with dopant gases flowing over its surface. This may be the same type of reactor used to grow the original epitaxial structure. Fig. 3 depicts a wafer resting in a quartz ampoule with elemental zinc (the p dopant), arsenic (to slow and control the zinc diffusion), and phosphorous (to provide an overpressure to keep the phosphorous in the InP from diffusing out at high temperatures). Out-diffusion causes severe surface pitting. The sliding bar in Fig. 3 illustrates the balance of Zn, As, and P in the ampoule. Holding the As concentrate constant while increasing the amount of Zn tends to cause a poor, pitted surface (100% Zn with 0% P is the extreme). At the other end of the scale, 100% P and 0% Zn will result in a smooth surface but no diffusion. The exact balance of elements depends on the process parameters for a specific device. The wafer is held at high temperature long enough for the solid sources to form a gas and drive the dopants to the InP/InGaAs junction. Although the time is more predictable in gas source diffusion because there is no solid phase with which to contend, closed ampoule diffusion is adequate for small production runs and is used in this process.

Diffused photodiodes can easily be sized from micrometers to millimeters, and can be closely spaced. The planar design offers easier fabrication and passivation with improved leakage characteristics and an abrupt turn-on. The particular birefringent crystal chosen for use in the HP 8504A splits the incident radiation into two beams whose polarizations are orthogonal. Two planar detectors fabricated on the same microchip offer advantages of matched spacing (to the beams) and matched responsivity (to each other). Fig. 4 shows the dual detector used in the HP 8504A. Bond pads lie off the active area above the diffusion barrier.
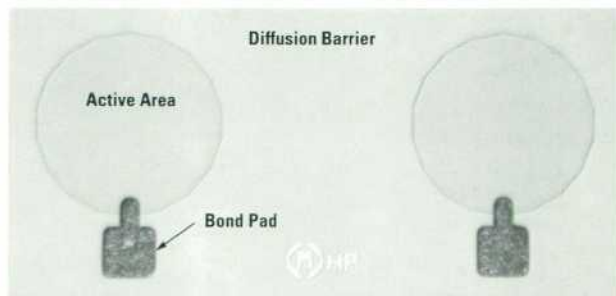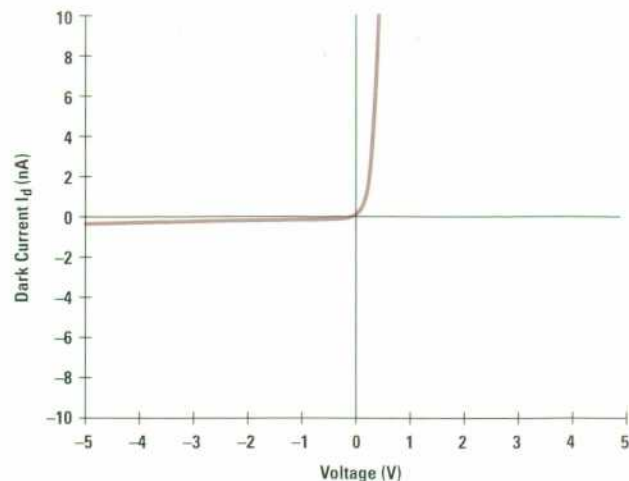
Processing and Development

To speed processing (both layout and alignment) and to increase yield, a simple tab contact to one side of the active region is used rather than an encircling ring of metal. If the diode is probed with a small light beam, response decreases slightly with distance from the contact. In the HP 8504A, the beam striking the surface is large compared to the diode, therefore, the tab design is adequate. Although it has higher capacitance and therefore lower frequency response than a mesa device with a similar intrinsic layer thickness, the diffused device is ideal for this broad-area application. Under reverse bias conditions the intrinsic layer of the diode is depleted of charge. In the absence of light only a small reverse leakage or dark current (I_d) flows. I_d is considered a measure of the noise floor of the receiver. Planar devices have lower dark currents than mesa devices. A typical 80-µm-diameter mesa device from this laboratory exhibits I_d less than 30 nA at −5V, while a similarly sized planar device would have an I_d of less than 1 nA. Dynamic resistance (extrapolated resistance through 0V) is greater than 200 MΩ. Responsivity is on the order of 0.9 to 1.1 A/W over the wavelengths of interest between 0V and −5V bias. Fig. 5 graphs typical current-versus-voltage characteristics.

Optical reflections prove important in component and system manufacturing. Therefore, antireflection coatings are applied to decrease these reflections. One coating is placed directly on the chip and another is placed on the window or lens of the package containing the photodiode. The coatings decrease the feedback to the laser source and increase the amount of light absorbed rather than reflected from the surface of the device.

Fig. 6 is a plot of the power reflected as a function of wavelength for a standard one-layer antireflection coating deposited on the chip. It is possible to obtain −17dB (2%) reflection at both 1300 nm and 1550 nm. Fig. 7 is a photo of the packaged receiver. The top of the TO39 can is windowed to

Fig. 4. Dual diffused detector.
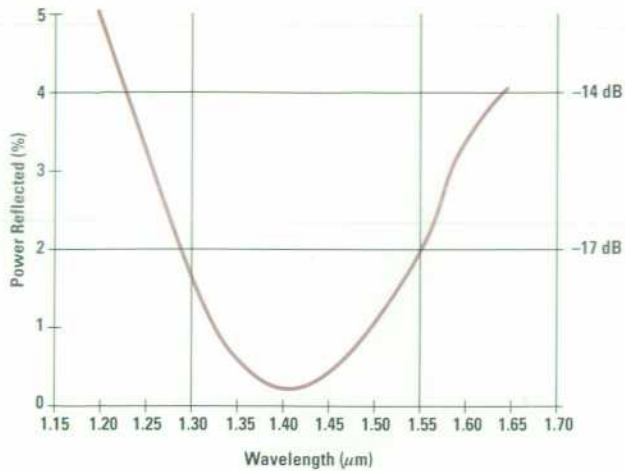
Fig. 6. Efficiency curve for diode antireflection coating.

allow light to pass through to the diode. The antireflection coating is applied to both sides of the window.

The diodes have been stressed at elevated temperature and bias, predicting a lifetime of 1×10^9 hours at 55°C instrument operation. Samples have also been subjected to a variety of environmental tests. They have been put through random vibration, shock tested to 1000g, subjected while under bias in their hermetic packages to 90% humidity for greater than one week while cycling temperature, and investigated at 0°C for variation in electrical characteristics and condensation. No significant changes in diode characteristics were produced. It was found that these devices are static-sensitive and can be shorted with the application of 200V reverse bias.

Conclusion

The large-format p-i-n dual detector used in the HP 8504A is simple but robust and with minimum care it will function
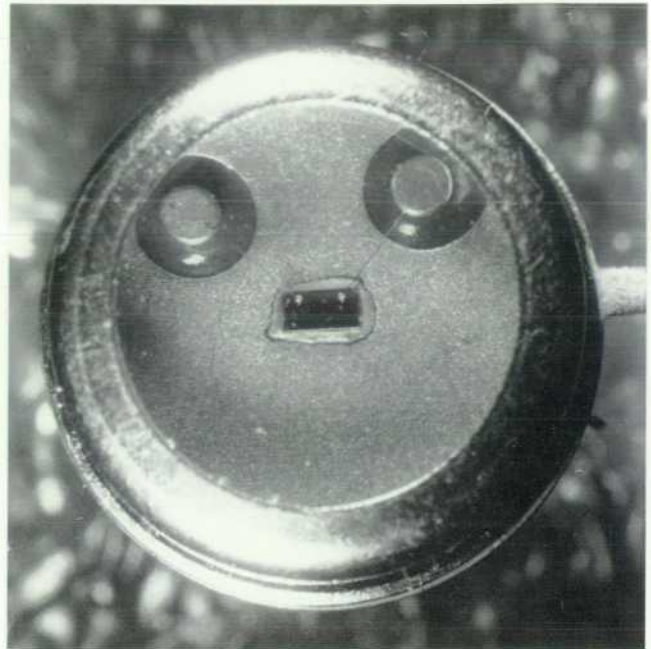
Fig. 7. Dual detector package. Diode and bonding posts are visible beneath the windowed lid.

well over the instrument's life. The use of highly leveraged design and processing has resulted in a very short time from concept through production to instrument release.

Acknowledgments

Production of a marketplace device has been a cross-divisional effort involving contributions from HP's Microwave Technology Division, Optical Communication Division, Optoelectronics Division, Network Measurement Division, Signal Analysis Division, and HP Laboratories.

High-Resolution and High-Sensitivity Optical Reflection Measurements Using White-Light Interferometry

In the HP 8504A precision reflectometer white-light interferometry is used as a nondestructive measurement technique for probing closely spaced reflections in optical devices.

by Harry Chou and Wayne V. Sorin

Reflections in optical components and systems often pose problems to the designer. For example, many laser sources become unstable when laser light is reflected back into the laser cavity. These reflections can cause abrupt frequency changes or increased intensity noise, even for reflectivities as low as 10^{-8} (−80 dB). Therefore, it is necessary for laser manufacturers to avoid any excess reflections within their laser packages. Reflecting surfaces can also set up optical resonances known as the Fabry-Perot effect, which converts the phase noise of the source (or length variation between the reflecting surfaces) into intensity noise. In analog communication links, reflections as small as 0.1% (−30 dB return loss) can significantly degrade system performance. The Fabry-Perot effect is a particularly acute problem for optical amplifiers that will be used in the next generation of optical fiber communication systems. In these amplifiers, a double reflection with an effective reflectivity (i.e., the product of their reflectivities) of 0.0001% (−60 dB) can degrade performance. Optical isolators can be used to circumvent this problem provided the isolators themselves have low reflectivities. These examples show the importance of locating and measuring reflections in optical devices.

A number of techniques exist for measuring optical reflections. Optical time-domain reflectometry (OTDR)[1] is commercially the most successful, and is suitable for finding faults in long lengths (meters to kilometers) of fibers. The technique consists of transmitting a pulse of light through the fiber under test and examining the time-dependent response of the resulting backscattered signal. The basic setup for an OTDR measurement is illustrated in Fig. 1. The output of a pulsed laser source is launched into the fiber under test
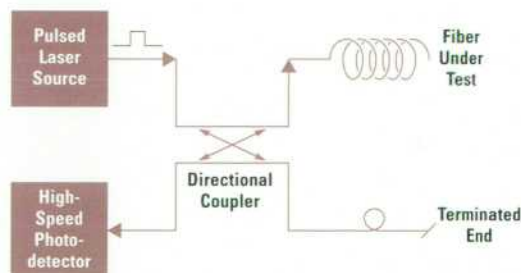
by a fused fiber-optic directional coupler, and the backscattered power is detected by a high-speed photodetector. The spatial resolution of an OTDR is limited by the width of the optical pulse. Typical resolutions of commercially available OTDRs vary from a few centimeters to hundreds of meters. For spatial resolutions below one meter, the usefulness of these conventional pulsed methods becomes limited because of the additional receiver noise required to detect the shorter optical pulses. The optical dynamic range of an OTDR is typically limited to about 60 dB to 70 dB, and is usually set by the dynamic range of the receiver circuitry.

A second reflectometry technique is optical frequency-domain reflectometry (OFDR).[2] With OFDR an intensity-modulated optical signal is applied to the device under test and the reflected signal is measured as a function of the modulation frequency. An inverse Fourier transformation is then applied to calculate the time-domain impulse response. The spatial resolution achievable with this method depends on the modulation bandwidth of the source. A two-point resolution of about 5 mm is possible with a 20-GHz modulation bandwidth. The dynamic range depends on source power and receiver noise. Typical dynamic range is 40 dB to 50 dB.

Another technique, based on using a power meter, is to measure the continuous-wave (CW) reflected light from the fiber under test. While strictly not a reflectometry technique because it does not spatially resolve the reflections, it has been widely used to measure the ratio of total reflected power to total incident power. The setup is similar to that shown in Fig. 1, except that the pulsed source is replaced by a CW source and the detector by a dc power meter. By measuring the CW reflected power, the total integrated return loss from the test device can be determined. The advantage of this method is its simplicity and accuracy, but since the reflections are not spatially resolved, it does not provide information about the source of the reflections.

The technique of white-light interferometry described in this paper is fundamentally different from the above techniques and offers greatly improved performance for high-resolution optical reflectometry. Compared to existing commercial techniques, several orders of magnitude of improvement in both spatial resolution and reflection sensitivity is achieved.

Fig. 1. The basic components used in optical time-domain reflectometry (OTDR).
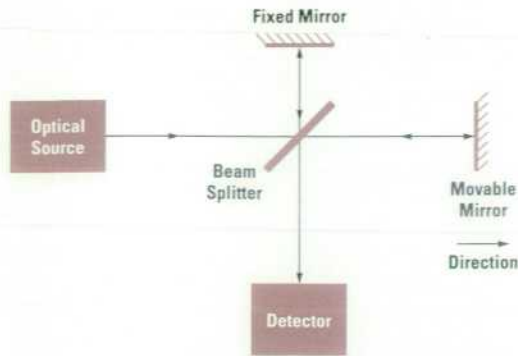
Fig. 2. The components of an open-beam Michelson interferometer. In this setup a beam of light from the optical source falls on the beam splitter. The reflected beam from the splitter passes to the fixed mirror where it is reflected back through the splitter to the detector. The other beam (transmitted beam) from the splitter goes to the movable mirror where it is also reflected back through the splitter to the detector.

The rest of this paper discusses the principles and practical considerations associated with white-light reflectometry, particularly as they relate to the HP 8504A precision reflectometer. The article on page 39 describes the design of the HP 8504A.

Fundamental Principles

The white-light measurement technique uses optical interference and is based on the use of a Michelson interferometer, which has been in existence for over 100 years. An open-beam version of a Michelson interferometer is shown in Fig. 2. Historically, this type of interferometer was used to try to detect the presence of an ether which was thought to be needed for light waves to propagate through. It was also used to define the length of a meter accurately with respect to various optical wavelengths. One of the uses of the Michelson interferometer is the measurement of the coherence length (or coherence function) of various optical sources. The HP 8504A precision reflectometer uses this concept of measuring coherence length to achieve high-performance optical reflectometry measurements.

The coherence length of an optical signal is the distance over which a correlation exists within the phase of the optical carrier. This correlation distance can be measured by monitoring the optical interference as the path length difference is scanned by the movable mirror in Fig. 2. For a long-coherence-length source, such as a helium-neon laser, this distance can be many kilometers, while for a broadband white-light source such as sunlight this distance is only a few micrometers. For these short-coherence-length sources, optical interference only occurs when the distance between the beam splitter and each of the two mirrors is matched to within a few optical wavelengths. The operation of the HP 8504A can be understood by replacing the fixed mirror in Fig. 2 with an optical component having multiple reflections and detecting the optical interference that occurs whenever the time delay to the moving mirror matches the delay to any of the component reflections. Although this seems reasonably straightforward, it was not until about 1987 that these ideas were first applied to the problem of optical reflectometry measurements.[3,4,5]

One way to understand the operation of the reflectometer is to think of the CW short-coherence-length source as continuously emitting "coherence wave packets" that propagate through the optical system in a manner identical to that of an optical pulse. The length of each of these wave packets is equal to the coherence length of the source. For the light-emitting diode (LED) sources used inside the HP 8504A precision reflectometer, these wave packets are on the order of a few tens of micrometers long.

A simplified fiber-optic version of a Michelson interferometer is shown in Fig. 3. The use of fiber optics offers advantages in the manufacturing of the product and is compatible with the fiber-optic pigtailed devices it is designed to measure. The low-coherence source is coupled into the input of the fiber-optic interferometer and is divided equally between the two arms of the interferometer by a fused 3-dB directional coupler. To simplify the description we will assume that the device under test (DUT) in the upper test arm consists of a single reflection with reflectivity R that reflects an optical power P_{dut} back towards the directional coupler. The lower arm provides, via a mirror that moves at a constant velocity (v), a reflected reference power (P_{ref}) with a variable time delay. The reflected powers from each arm are then added together using the 3-dB coupler and sent to a detector which generates a photocurrent (I_D) that is proportional to the square of the incident optical field.

For the case of a single reflection, the photocurrent can be written as:

$$I_D = R_d \left(P_{ref} + P_{dut} + 2\sqrt{P_{ref}P_{dut}} \cos \Delta\phi \right),$$

where $\Delta\phi$ is equal to the optical phase difference between the reflected signals from the two arms, and R_d, which has the units A/W, is the responsivity of the detector. The term $\Delta\phi$ is important in the operation of the reflectometer since it describes all the interference effects used in the measurement. When the path-length difference between the moving mirror and the DUT reflection is longer than the coherence length of the source, the returning optical phases are uncorrelated and the term $2\sqrt{P_{ref}P_{dut}} \cos \Delta\phi$ averages to zero. For path-length differences within the coherence length of the source, this term produces a beat frequency equal to the Doppler frequency shift of the moving mirror. Detection of this Doppler frequency signal allows the determination of
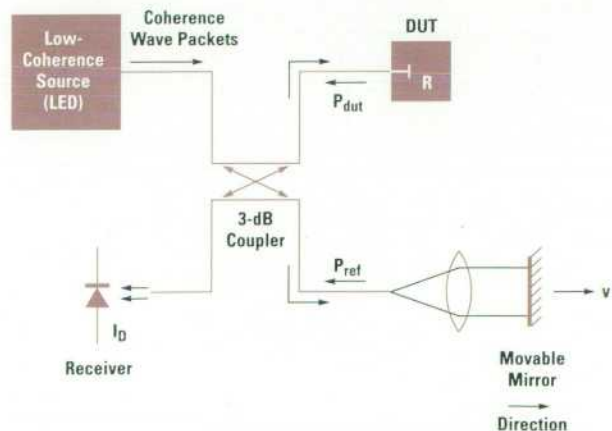
Fig. 3. A simplified fiber-optic version of a Michelson interferometer.
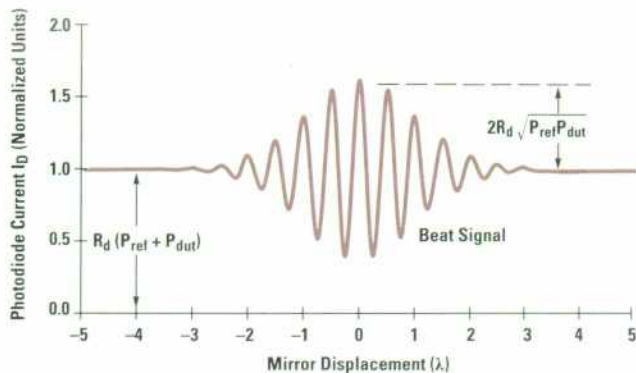
Fig. 4. Photocurrent response of the detector as the moving mirror passes through a reflection.

both the magnitude and the location (with respect to the movable mirror) of any reflection sites along the test arm.

The photocurrent response as the moving mirror passes through a reflection is illustrated in Fig. 4. The period of the sinusoidal current variations is equal to one-half the optical wavelength. The peak of the beat signal is proportional to the square root of the optical reflectivity. The width of the response determines the spatial resolution, and is related to the coherence length of the source. If we assume ideal conditions, that is, no wavelength dependent absorption or differential dispersion in the arms of the interferometer, then the photocurrent response is equal to the coherence function (autocorrelation of the optical electric field) of the source. This case gives the minimum spatial resolution for the measurement. By calculating the full width at half maximum (FWHM) of the coherence function squared we can relate the minimum spatial resolution to the spectral width of the source. For the case of a Gaussian spectrum the minimum spatial resolution is given by:

$$\Delta x = \frac{\sqrt{2}\ln 2}{\pi} \frac{v_g}{\Delta v}$$

where Δv is the FWHM of the source spectrum, v_g is the group velocity of the light, and Δx is the FWHM of the displayed reflection response. For a typical LED with a 60-nm spectral width operating at 1300 nm the minimum spatial resolution is about nine micrometers.

In the description above we have assumed that the returning polarization states from the two arms are matched so that full optical interference can take place. In practice, this assumption is usually not true because of the residual birefringence in optical fibers. To solve this problem, the HP 8504A precision reflectometer uses a polarization diversity receiver that allows accurate measurements to be performed regardless of the returning polarization state from the test arm. A more detailed description of the polarization diversity receiver will be given later in this paper.

The use of this optical interference method for measuring reflectivity has two major inherent advantages compared to the more popular pulsed OTDR techniques. The first advantage is greatly increased dynamic range and the second is much finer spatial resolution. The inherent improvement in dynamic range occurs because the photocurrent beat signal is proportional to the square root of the optical reflectivity and not just linearly related as in conventional pulsed

techniques. This means that the dynamic range for reflectivity measurements can be improved from about 60 dB to values on the order of 120 dB or more.

The improvement in spatial resolution is also an inherent difference because of the fact that the fiber dispersion can be canceled using the interference technique, but not with the pulsed technique. This cancellation occurs because the test and reference signals travel through the same medium (i.e., standard single-mode fiber) and therefore experience the same dispersion. Since the interferometric detection process compares time delays between the test and reference signals, any common delays because of dispersion are canceled out. For comparison, using standard single-mode fiber at a wavelength of 1.55 micrometers, an optical pulse needed to achieve a spatial resolution of 20 micrometers can only probe a fiber length of 7 cm before dispersion degrades its resolution to 40 micrometers. A discussion on the effects of dispersion differences in the two arms of the interferometer will be given later in this paper.

Practical Considerations

In implementing a white-light reflectometer, a number of physical phenomena must be considered. These considerations had an important impact on the design of the HP 8504A precision reflectometer.

Signal-to-Noise Ratio
Reflection sensitivity is determined by the amount of noise that passes through the bandpass filter centered at the photocurrent beat frequency. This noise comes from three major sources: thermal receiver noise, optical shot noise, and optical intensity noise. Both the shot noise and the intensity noise result from the large dc component of optical power (usually the reference power) incident on the receiver.

For a single reflection the signal-to-noise ratio (SNR) is:

$$\frac{2R_d^2 P_{ref} P_{dut}}{[4kT/R_e + 2qR_d P_t + RINR_d^2 P_t^2]\Delta f}$$

where the numerator contains the signal power, which is proportional to the square of the photocurrent, and the denominator contains the three major noise sources. The first term in the denominator accounts for the thermal noise where k is Boltzmann's constant, T is the temperature, and R_e is the effective receiver noise resistance. The second term is the shot noise, where q is the charge of an electron, R_d is the responsivity of the photodetector, and $P_t = P_{ref} + P_{dut}$ is the total reflected power from the reference and DUT arms. The last term accounts for the intensity noise, where RIN (relative intensity noise) is a measure of the fractional intensity noise within a one-hertz electrical bandwidth. The term Δf is the detection bandwidth.

In most cases in which a reasonable source power can be obtained, the shot noise or intensity noise will dominate the receiver noise. For example, if a 1-MΩ transimpedance receiver is used, a reflected reference power (P_{ref}) of only about 100 nW is required for the shot noise to start dominating the receiver noise. As the source power is increased, the shot noise will eventually be dominated by the intensity noise. This occurs because the intensity noise increases as

the square of the optical power while the shot noise grows only linearly. For typical LED sources, intensity noise starts to dominate for receiver powers on the order of a few microwatts. When intensity noise becomes dominant, reflection sensitivity is not improved as the source power is increased. This is because both the numerator and the denominator in the SNR are proportional to the source power squared. By making modifications to the basic Michelson interferometer configuration, schemes have been demonstrated that remove the effects of intensity noise.[6,7] The use of these schemes can become practical when source powers get significantly larger than a few tens of microwatts. Regardless of which noise source is dominant, the reflection sensitivity can always be improved by simply narrowing the bandpass filter of the receiver. However, this solution can lead to very long measurement times.

With optimum design, white-light reflectometry can have extremely good reflection sensitivity. For example, by combining a narrow receiver bandwidth (3 Hz) with a high-power source (10 mW) and intensity noise removal, reflection sensitivities as low as –148 dB have been experimentally demonstrated.[8]

Polarization Dependence

The magnitude of the optical reflectivity is obtained from the strength of the interferometric beat signal. This signal can be expressed as a dot product between the optical fields returning from the reference and test arms, taking into account their relative polarization states. If these two fields are in the same polarization state, then the interference produces a strong signal. On the other hand, if they are orthogonally polarized, the signal becomes zero. This illustrates that in determining optical reflectivity, the effects of polarization must be considered.

Although the precision reflectometer sends an unpolarized signal into the device under test, these polarization effects still occur. This can be understood by realizing that an unpolarized field is the linear superposition of two polarized fields, each of which can produce independent interferometric signals. Thus in an interferometric measurement, unpolarized light must be treated as though it were polarized.

Polarization dependence can present a serious problem when using conventional single-mode fiber because the polarization transformation properties of the fibers are unstable over time and under different environmental conditions. To remove the dependence of the detected signal on the polarization state of the test arm reflection, a special type of receiver called a polarization diversity receiver can be used. As shown in Fig. 5, the polarization diversity receiver contains a polarizing beam splitter that divides the incoming light into two orthogonal polarization components and directs these to the two photodiode detectors. The polarization split is set up such that the power reflected from the reference arm is equally divided between the detectors. This condition requires that the reference power be polarized, which can be accomplished by using a polarized source, or if the source is unpolarized, by placing a polarizer in the reference path.

Equal division of the reference power ensures that an interference signal will occur regardless of the polarization state from the test arm. For example, if the returning reference and test signals are orthogonal (the case of no interference when using a single detector), the polarizing beam splitter projects a portion of each signal onto each detector resulting in two separate interference signals. These two interference signals are 180 degrees out of phase and if they are simply summed would produce no signal. If instead we measure the amplitude of the beat signal envelope from each detector
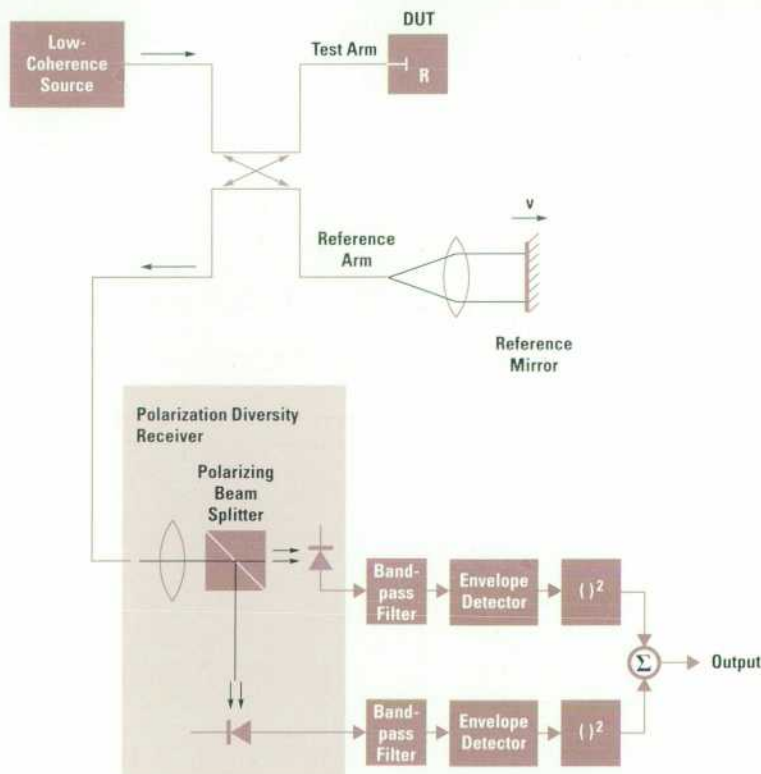
Fig. 5. The basic components of a polarization diversity receiver.

and add the squares of this quantity, an interference signal is obtained that is independent of the polarization state returning from the test arm of the interferometer.

To calibrate the polarization diversity receiver, it is necessary to know how the optical field from the reference arm is split between the two detectors. Each detector, however, produces a photocurrent proportional to the optical power and not the field incident on it. Even though it is possible to deduce the split of the fields from the split of the powers, such deduction requires detailed knowledge of all of the proportionality constants. A further complication is that typically the photocurrent is not directly measured but amplified into a voltage by a transimpedance amplifier, which may be followed by other signal processing electronics. The gain of each of these electronic stages becomes another proportionality constant to be characterized to convert power into optical field. Thus, it is highly desirable to have a simple and effective calibration procedure that removes the uncertainties in the combined proportionality constants. This can be accomplished by introducing a modulation on the source intensity at the Doppler frequency of the interference signal. By directing all the power returned from the reference arm into one or the other of the detectors using manual polarization controllers, the ratio of the effective electronic gains of the two polarization channels can be obtained. This ratio is a hardware-specific correction constant that can later be used to normalize the gain difference between the two polarization channels of the receiver. The same scheme can be used to measure the power split ratio in the two polarization channels. With both the gain ratio and the power split ratio, the split ratio of the optical fields can be calculated.

More details about the polarization diversity receiver used in the HP 8504A can be found on page 42.

Dispersion Effects

Dispersion refers to the variation in the propagation speed of a signal as a function of a quantity such as wavelength or polarization state. For the HP 8504A we were concerned with the impact of chromatic dispersion and polarization dispersion on measurement accuracy.

Since the velocity at which an optical pulse travels along a fiber depends on its wavelength, different colors contained in a light pulse propagate at different speeds. This effect is referred to as chromatic dispersion and results in broadening of the optical pulse.

Chromatic dispersion can play an important role in white-light reflectometers because of the broadband source spectrum needed to achieve high resolution. A mismatch between the chromatic dispersion properties of the two arms of the interferometer will result in the broadening of the beat signal and a reduction in its peak magnitude. This can lead to inaccuracies if the reflectivity is determined solely from the peak magnitude of the interference signal. A number of researchers have examined the effects of chromatic dispersion on white-light interferometers.[9-11] The general problem of recovering the true signal from the dispersion-broadened signal is described in reference 9.

A possible dispersion mismatch exists in the HP 8504A precision reflectometer because the reference arm has an air-filled section for the reference arm mirror to move through. The corresponding section in the test arm usually consists of the fiber pigtail connected to the device under test. At wavelengths centered around 1300 nm, where the chromatic dispersion in silica fiber is a minimum, the dispersion difference between the two interferometer arms is usually not significant. However, at wavelengths centered around 1550 nm, standard fiber has a dispersion of about 17 ps/(nm·km), which is significantly different from that of air. This dispersion mismatch can cause the measured peak reflectivity to become a function of the mirror position as the air path through the reference arm changes. Fig. 6 shows how this dispersion mismatch can affect the apparent reflectivity for a reflector located at different positions along the 400-mm scan range of the reference arm mirror. The source for the results in Fig. 6 was an LED that had a spectral width of 60 nm centered at about 1550 nm. To correct for this apparent drop in reflectivity, a model was developed to predict the signal drop as a function of mirror position.[11] This model is used in the HP 8504A precision reflectometer to alter the displayed data so that accurate reflectivity measurements can be made with its internal 1550-nm source.

The dispersion mismatch also increases the width of each reflection peak and therefore affects the spatial resolution. Fig. 7 shows how the spatial resolution in the HP 8504A degrades for measurements made with an LED operating at 1550 nm. Note, however, that the amount of broadening depends on the length of the mismatched portion of the reflectometer, not on the total length of the fiber in the system. This is different from optical time-domain reflectometry in which the pulse broadening is proportional to the total length of the fiber. The necessity for dispersion cancellation is an important requirement in high-resolution reflectometry. For this reason, white-light reflectometry offers a major advantage over high-resolution OTDR techniques.

White-light reflectometry can also be used to measure the amount of polarization dispersion in a component or length of fiber. Polarization dispersion is the differential time delay resulting from birefringence. Fig. 8 shows an example of

Fig. 6. The effect of dispersion mismatch on the peak interference signal from similar reflectors located at different locations with respect to the scan path of the movable mirror.
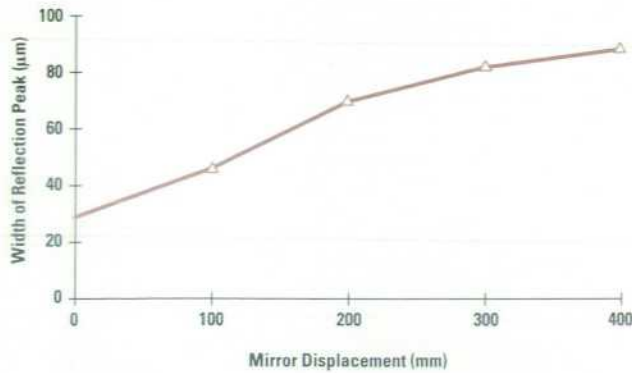
Fig. 7. Degradation of the spatial resolution in the HP 8504A precision reflectometer made with an LED source operating at 1550 mm.

Fig. 8. Measuring the group refractive indexes of the principal polarization states of the birefringent material rutile.

measuring the group refractive indexes of the principal polarization states of the birefringent material rutile (TiO_2). With light launched into both principal polarization axes of the crystal, there are two reflection peaks corresponding to the single back surface of the crystal. This is because the reflections of the two polarization states propagate at different speeds and therefore are separated in time. Because of the high resolution achievable with the reflectometer, the propagation speed difference and therefore the difference in the group refractive indexes are easily measured once the thickness of the material is known.

Spurious Responses

Because of the high sensitivity achievable using white-light interferometry, small secondary reflections within the system can also be detected. Secondary reflections can come from any component in the system, but since we are trying to measure the test arm, the device under test is not considered to be a source of spurious responses. Depending on which arm of the interferometer they originate from, secondary reflections can show up as symmetric or asymmetric sidelobes relative to a large reflection peak.

If the secondary reflections originate in the source or receiver arm of the interferometer, they will give rise to a symmetric spurious response. Fig. 9, which shows the secondary reflection originating from a double bounce within the source, illustrates why this spurious symmetric response is observed.

The secondary reflection produces a small delayed version of the coherence wave packet (pulse) from the source. When the reference arm is shorter than the test arm (movable mirror is closer to the beam splitter), the delayed secondary wave packet from the reference arm can combine with the primary wave packet from the test arm to produce a spurious response. When the reference arm delay is longer than the test arm (mirror is further from the beam splitter), the secondary wave packet going through the test arm can combine with the primary wave packet from the reference arm. Thus, one spurious response occurs before the true reflection (ⓐ in Fig 9) and the other after it (ⓑ in Fig. 9), symmetrically placed around the true reflection at a distance equal to the spacing between the reflectors that generated the secondary wave packet. The reflection ratio between the main signal and the spurious response is equal to the ratio of the powers of the primary and secondary wave packets.

Asymmetric spurious responses come from secondary reflections generated in either the reference or test arms. If the secondary reflection is in the reference arm, the spurious response is on the left side of the true response. Conversely, secondary reflections in the test arm produce spurious responses on the right side of the true reflection. Although multiple reflections can originate from the device

Fig. 9. Illustration of how spurious responses are generated because of secondary reflections.

under test, they are not considered spurious responses since they are a true measure of the optical reflectivity from the test device. In some devices containing many large reflections, it may be difficult to identify the reflective surfaces from the secondary reflections caused by them.

Effects of Water Vapor Absorption near 1.3 μm

In white-light interferometry, we often observe an asymmetric tail on the left side of a strong reflection when a 1360-nm light-emitting diode is used as the source. Fig. 10 shows a typical response. This tail results from ambient water vapor (OH⁻) absorption at about 1340 nm in the open beam of the reference arm under normal humidity conditions. The reason for this asymmetric tail can be understood if we use the fact that the displayed reflection peak is actually a crosscorrelation (in the time domain) of the optical fields from the two interferometric arms. This crosscorrelation can also be viewed in the frequency domain as a product of the frequency spectrums returning from each interferometric arm.

The sharp OH⁻ absorption lines cause abrupt delta function changes in the frequency spectrum which then result in long slow changes in the Fourier-transformed time-domain signal. These changes show up as asymmetric tails on the large reflection peaks because of the crosscorrelation of the fields from the two arms. A similar argument, when applied to absorption in the test arm, shows that the tail will be on the right side of the large reflection for that case. If the absorption is in the source or receiver arms, the tails are symmetric. The spatial extent of the tail is inversely proportional to the spectral width of the absorption lines.

Comparison to Power-Meter-Based Measurements

As described earlier, a relatively popular technique for measuring return loss (or percent of reflectivity) from components and connectors is simply to measure the amount of dc power reflected back from the device under test. Although easy to implement, this technique provides different information from the interferometric technique and has limitations that prevent it from being useful in many applications. These limitations include:

- Since the detected power is the integrated reflected and backscattered powers from the total measurement system, small reflections can be "masked" by large ones. For example, connector reflections can mask any reflected power from the test device. Other sources of unwanted reflectivity can occur from coupler directivity, the terminated (unused) coupler port, and Rayleigh backscatter from fiber pigtails. Even when special care is taken to address these problems, the power-meter measurement is limited to a return loss of about –60 dB or –70 dB.

- Accuracy can depend strongly on the coherence properties of the source used in the measurement. When a laser is used to measure a device with multiple reflections, the reflected optical fields can add constructively or destructively if the coherence length is longer than the distance between reflectors. If the reflected fields add destructively, the integrated return loss may not reveal the presence of large reflections.

Conclusion

White-light interferometry offers some unique advantages as a reflectometry technique. Excellent dynamic range and spatial resolution can be obtained with source powers as small as 10 microwatts. Resolution is limited primarily by optical coherence lengths, which can be on the order of tens of micrometers. Unlike pulsed techniques, resolution limits resulting from fiber dispersion can be canceled with the use of a reference delay and interferometric detection. Although polarization dependence of the interference signal introduces some complications, it can be minimized by using a polarization diversity receiver. Thus, white-light interferometry opens up a wide range of measurement applications in device design and testing, process control, and noninvasive diagnosis.
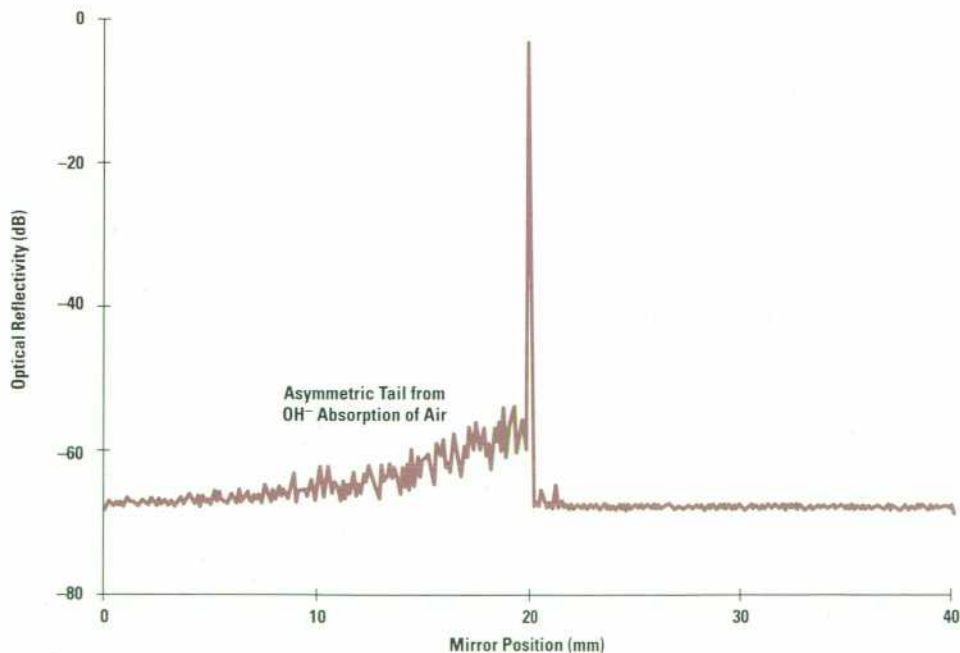
Fig. 10. Reflectivity response when a 1.3-μm LED is used as a source.

Acknowledgments

References

1. J. P. Healey, "Review of Long Wavelength Single-Mode Optical Fiber Reflectometry Techniques," *Journal of Lightwave Technology,* Vol. LT-3, no. 4, 1985, p. 876

2. D.M. Braun and K.W. Leyde, "Optical Reflection Measurement System using a Swept Modulation Frequency Technique," *Optical Engineering,* Vol. 28, no. 3, 1989, p. 286.

3. K. Takada, I. Yokohama, K. Chida and J. Noda, "New Measurement System for Fault Location in Optical Waveguide Devices Based on an Interferometric Technique," *Applied Optics,* Vol. 26, 1987, p. 1603.

4. B. L. Danielson and C. D. Whittenberg, "Guided-Wave Reflectometry with Micrometer Resolution," *Applied Optics,* Vol. 26, 1987, p. 2836.

5. R. C. Youngquist, S. Carr, and D. E. N. Davies, "Optical Coherence-Domain Reflectometry: a New Optical Evaluation Technique," *Optics Letters,* Vol. 12, 1987, p. 158.

6. K. Takada, K. Yukimatsu, M. Kobayashi and J. Noda, "Rayleigh Backscattering Measurement of Single-Mode Fibers by Low-Coherence Optical Time-Domain Reflectometer with 14 µm Spatial Resolution," *Applied Physics Letters,* Vol. 59, 1991, p. 143.

7. W. V. Sorin and D. M. Baney, "Improved Sensitivity for Optical Low-Coherence Reflectometry Using Reference Power Attenuation," *Symposium on Optical Fiber Measurements,* Boulder, Colorado, September 15-17, 1992.

8. W. V. Sorin and D. M. Baney, "Measurement of Rayleigh Backscattering at 1.55 µm with a 32 µm Spatial Resolution," *Photonics Technology Letters,* Vol. 4, 1992, p. 374.

9. E. Brinkmeyer and R. Ulrich, "High-Resolution OCDR in Dispersive Waveguides," *Electronic Letters,* Vol. 26, no. 6, 1990, p. 413.

10. A. Kohlhaas, C. Fromchen, and E. Brinkmeyer, "High-Resolution OCDR for Testing Integrated-Optical Waveguides: Dispersive-Corrupted Experimental Data Corrected by Numerical Algorithm," *Journal of Lightwave Technology,* Vol. 9, no. 11, 1991, p. 1493.

11. H. Chou, "Optical Low Coherence Reflectometry: Improving Reflectivity Accuracy in the Presence of Chromatic Dispersion," *Symposium on Optical Fiber Measurements,* Boulder, Colorado, September 15-17, 1992.

A Modular All-Haul Optical Time-Domain Reflectometer for Characterizing Fiber Links

The HP 8146A optical time-domain reflectometer provides good dynamic range and dead-zone performance and user interface features such as comprehensive documentation capabilities and automatic link characterization.

by Josef Beller and Wilfried Pless

Fiber optics has long been established in the communication world and so have the test tools that measure and characterize the equipment needed for fiber-optic transmission. Some of these test tools include:

- Highly accurate power meters to measure the output power of transmitters
- Optical sources (laser or LED) to stimulate transmitters
- Power meters and sources to characterize passive optical devices
- Optical spectrum analyzers to measure the wavelength of optical sources
- Return loss meters to measure the quality of connections
- Instruments to measure the state of polarization.

An instrument that is needed to qualify the performance of fiber used for transmission is the optical time-domain reflectometer (OTDR).

Fiber-optic manufacturers want to characterize their fibers in terms of mechanical parameters, dispersion, bandwidth, magnitude, and uniformity of loss and attenuation at lengths mainly below 5 km. Cable manufacturers want to measure the same parameters as the fiber manufacturer but at lengths above 5 km. Furthermore, cable manufacturers need to identify the location and quality of splices.

During the installation of fiber cables the installer must characterize the quality of the transmission link in terms of overall loss, attenuation of sections, position and through loss of splices, return loss and through loss of connections, link length, and location of breaks.

While the link is in use it has to be checked regularly for preventive maintenance. For these regular checks, measurements of the link are made to detect changes in link performance. Changes are detected by comparing the regular measurements to reference measurements that were made when the link was installed. By comparing the old and new link measurements it is possible to react to transmission degradation before it becomes critical.

The OTDR is capable of making most of these fiber measurements.
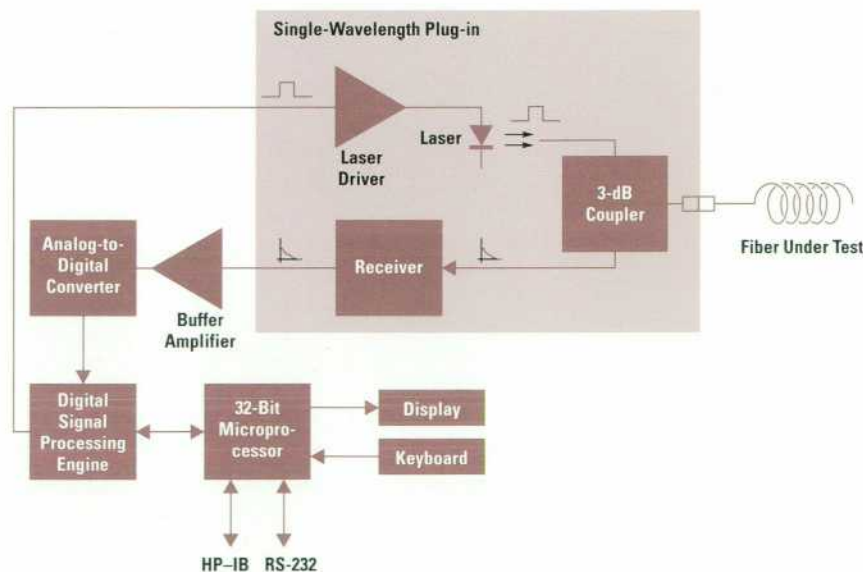
Fig. 1. The main components of the HP 8146A optical time-domain reflectometer (OTDR).

Overview of OTDR Operation

An OTDR measurement begins with a laser operating at a wavelength of 850 nm, 1300 nm, or 1550 nm. The OTDR probes a fiber attached to its connector by sending an optical pulse into the fiber via a 3-dB coupler (see Fig. 1). On its way through the fiber the light is partly reflected (Fresnel) and scattered (Rayleigh) back to the sending OTDR. By means of the optical coupler this backtraveling light is sent to a receiver that contains the components to convert the light into an electrical current. This current is converted to a voltage, which is amplified, sampled, converted to digital format, and then averaged by the digital signal processing engine. Knowing the speed of light, the index of refraction of the fiber, and the time between sending the pulse and receiving its echo, the OTDR can determine the distance of the backscattered light from the OTDR. The OTDR finally displays returned power versus distance on a semilogarithmic scale (see Fig. 2).

Fig. 2 shows that the OTDR tells the user the attenuation of a fiber over a certain distance (dB/km), places (indicated by step changes) where pieces of fibers are spliced together, and the loss from those splices. Also shown are peaks on
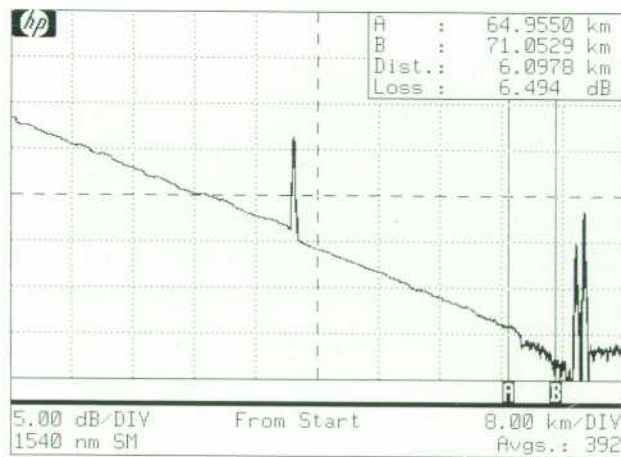
(a)
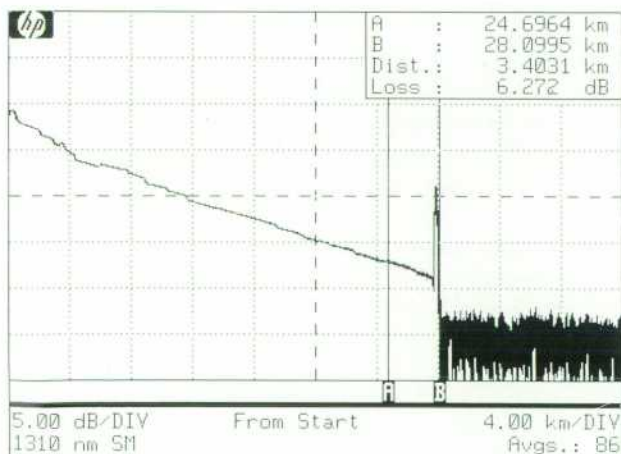
(b)

Fig. 2. An OTDR display showing the attenuation of a fiber in dB/km. (a) A single-mode fiber operating at a wavelength of 1540 nm. (b) A single-mode fiber operating at 1310 nm.

the trace resulting from Fresnel reflections which indicate poor connections and often lead to transmission problems in high-speed transmission links.

More information about the operation of OTDRs can be found in reference 1. The receiver shown in Fig. 1 is described in the article on page 69 and the digital signal processing engine in Fig. 1 is described in the article on page 63.

History of OTDRs

The first OTDR was developed about 15 years ago. These first-generation OTDRs were multimode instruments that used photomultiplier tubes to amplify the very weak input signal. Equipped with the simplest data sampling systems and external oscilloscope displays, these systems were heavy and required skilled technicians to operate them.

In the early 1980s, the second-generation OTDRs started to enter the market. They were still multimode instruments but offered simplified user control because of the use of 8-bit microprocessors. Most of these boxes were portable and could be used for maintenance and service applications. Digital data processing like storage and averaging was introduced. However, since only one sample per shot was acquired (only one sample was taken for each pulse launched), many repetitions of the pulse were needed to characterize a complete fiber trace. With this technique only modest noise reduction was achieved by averaging, even with long measurement times.

A big step forward in technical performance was achieved when third-generation OTDRs were introduced. With a microprocessor and dedicated hardware for digital signal processing, measurement speed was greatly increased by providing one complete trace per shot. Thus noise reduction by averaging improved considerably. Real-time monitoring became a standard feature because of fast display refresh. Some instruments offered pure single-mode capability for characterizing long fiber links, and others could be equipped with plug-in modules that provided flexibility in measurement range, resolution, and different fiber types. Features such as automatic splice loss, a built-in printer, or masking with an acoustooptical switch illustrated the development of universal tools covering a broad range of applications and customer needs.

About 1990, the fourth generation of OTDRs brought about a split into two different types of OTDRs: high-end and low-end OTDRs, which are mainly distinguished by performance and price.

In high-performance OTDRs, 32-bit microprocessors control the instrument and provide powerful data processing capabilities that increase measurement speed and implement new functions. It is now possible to provide all-haul OTDRs that cover both short-haul and long-haul measurement applications without having to change any module. Data storage on magnetic disk, interfacing to personal computers, user interfaces with screen windows, native language support for help screens, and scan trace algorithms are now available with these new instruments. The clear intention behind providing these features is to make the operation of an OTDR more user friendly and comfortable. However, performance improvement does cost. High-power lasers, low-noise avalanche
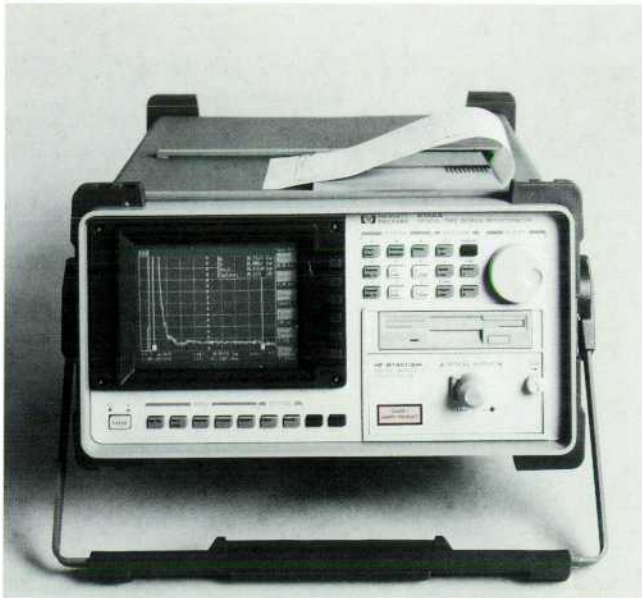
Fig. 3. The HP 8146A all-haul optical time-domain reflectometer.

diodes, powerful signal processors, and comprehensive equipment contribute strongly to a product's price.

For many customers these high-end instruments represent overkill for their applications. As a consequence, more and more manufacturers are offering simplified OTDRs such as fault locators or mini-OTDRs. Some of the properties that describe these portable, low-end instruments include: lightweight, handheld, battery operated, limited dynamic range and resolution, and low display resolution.

The HP 8146A (see Fig. 3) is a fourth-generation OTDR that offers the features and capabilities of high-end OTDRs.

Design Goals

With the improving quality of fibers, increasing bit rates, changes in fibers (from multimode fibers with core diameters of 50 μm and above to single-mode fibers with core diameters in the order of 9 μm), different wavelengths (850 nm, 1300 nm, and 1550 nm), and new fiber-optic application areas like LANs and FTTH (fiber to the home), the requirements for fiber-optic test equipment have changed.

When we started the development of the HP 8146A OTDR, we analyzed the OTDR market and came up with the following design goals:
* All-haul architecture to cover both long-haul and short-haul applications with just one plug-in
* 30-dB dynamic range at 10-μs pulse width within 3 min
* 0.5-m resolution in the short-haul mode
* Modularity to cover single-mode applications operating at wavelengths of 1300 nm and 1550 nm, multimode applications operating at 850 nm and 1300 nm with core diameters

of 50 μm, and fibers with 62.5-μm diameters operating at 1300 nm.

We also wanted to provide a user interface with the following features:
* A scan trace feature to identify automatically and quickly (in seconds) the locations of splices and breaks, the return loss and through loss of these events, and the attenuation between events of a complete link
* Support for beginning users that enables them to set up and start a complete, predefined measurement with just three keystrokes (not counting power on)
* Native language support and help screens
* MS-DOS®-compatible flexible disk drive or a memory card for harsh environments to enable users to store measurement data
* A built-in printer as well as an interface for external printers and plotters without using an additional controller
* PC software that allows users to analyze OTDR measurements easily
* A feature that allows users to compare the result of a previous measurement with the current measurement
* State-of-the-art analyzing functions for two-point loss, two-point attenuation, and least-squares approximation of attenuation.

Reflecting on all the different application areas in which an OTDR is used and especially all the different skill levels likely to use the instrument, the main motto for the definition of the HP 8146A user interface was: "Keep it simple for the novice user, but do not restrict the sophisticated user."

The user interface features of the HP 8146A are described in the article on page 72.

Besides the goals mentioned above other design goals for the HP 8146A OTDR included light weight, low power consumption to allow battery operation, and a wide temperature range to allow the OTDR to be used in all the extreme environmental conditions where a maintenance instrument might be used. Also, exchangeable connectors are offered to adapt to a variety of fiber connectors.

Acknowledgments

Reference

1. *Hewlett-Packard Journal*, Vol. 39, no. 6, December 1988, pp. 6-38.

MS-DOS is a U.S. registered trademark of Microsoft Corporation.

A High-Performance Signal Processing System for the HP 8146A Optical Time-Domain Reflectometer

Three custom integrated circuits and a powerful 24-bit digital signal processor offload data processing from the instrument's host processor.

by Josef Beller

The digital signal processing unit of the HP 8146A OTDR acquires and processes data coming from the optical front end after the data has been amplified and converted from analog signals to digital numbers. This data represents the response of an optical fiber under test to a probe from a laser pulse. After further processing and linear-to-logarithmic conversion, the fiber response is transferred to the instrument's host processor and displayed on the OTDR's screen as a function of distance.

The fiber response always depends on two physical effects: Fresnel reflections and Rayleigh scattering. Reflections occur at locations with refractive index discontinuities. Scattering, which is the dominant loss mechanism in single-mode fibers, is generated uniformly along the fiber. One main challenge of an OTDR is the wide range of the input signal level. High power levels occur because of reflections whereas backscattering produces very weak signals which are almost always covered by noise. To detect and identify clearly events that are hidden by noise (to be able to do long-distance measurements), any means of improving signal-to-noise-ratio (SNR) must be applied. Some increase in SNR is achieved by using an avalanche photodiode in the optical receiver instead of a p-i-n diode. Remarkable improvements are possible with digital signal averaging (see "Improving SNR by Averaging," on page 65).

With digital averaging as a standard processing scheme in OTDRs, SNR improvements of up to 30 dB can be obtained during a three-minute measurement. This corresponds to one million averages since the increase of SNR is proportional to the square root of the number of averages. This processing requires a certain amount of hardware because each fiber trace consists of several thousand data samples.

Since the early days of the development and manufacture of OTDRs, engineers have had to struggle with the fundamental OTDR range/resolution trade-off. The high spatial resolution needed in short-haul applications can only be achieved with short laser pulses and a wide receiver bandwidth. This means a low dynamic range. A high dynamic range for long-distance measurements is possible only with long laser pulses and low receiver bandwidth. One of the first questions in the design of an OTDR is where to place the instrument along this range/resolution line and how to balance the properties to fit customer needs in the best manner. It was this question

that convinced the HP 8146A development team to build an all-haul instrument that combines both worlds and covers all typical applications.

Digital Averaging and Processing

Digital averaging and processing require sampling and analog-to-digital conversion of the analog signal supplied by the OTDR receiver (see Fig. 1). The analog-to-digital converter (ADC) is one of the key components in an OTDR since its conversion rate and word width influence measurement speed, spatial resolution, and achievable dynamic range. In general, speed goes inversely as resolution (accuracy) at a given cost. In principle, a low-speed ADC with 16-bit resolution would fit into an all-haul OTDR. It provides a high dynamic range for measuring long and lossy optical links. On the other end, high spatial resolution can be achieved (if the analog bandwidth is sufficiently high) by applying the interleaving principle (see Fig. 2). However, this resolution is achieved at the cost of measurement time and thereby of noise reduction. To overcome this disadvantage it was decided to use a high-speed, 8-bit flash ADC in the HP 8146A. Its performance is very applicable to short-range applications. To cover long-distance and high-dynamic-range measurements, variable decimation (Fig. 3) and sophisticated stitching (Fig. 4) are implemented to overcome the limited conversion range of the high-speed flash ADC.
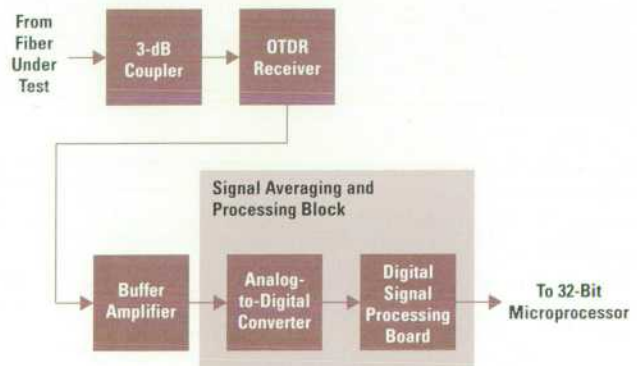
Fig. 1. The components of the HP 8146A involved in processing the signal from the fiber under test.
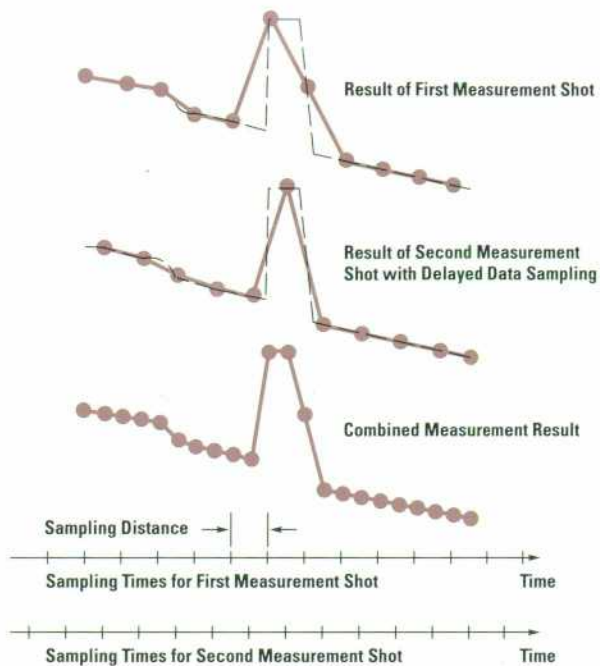
Fig. 2. Using interleaving to improve spatial resolution by a factor of two by combining two successive measurement shots. The second acquired trace is sampled with a time delay of half the sampling distance relative to the first trace.

With variable decimation two adjacent data samples are summed to one new data point. The geometrical spacing between the resulting data points increases, resulting in a greater measurement span. Decimation or downsampling can be performed with any number of successive samples. An advantage of this method is that it results in additional noise reduction because decimation calculates the mean value of consecutive samples, having the effect of low-pass filtering.

Stitching increases the conversion range of an ADC by executing one measurement with a low gain setting and a second measurement with a high gain setting in the amplifier path. The clipped part of the high-gain measurement is replaced by the corresponding detail of the nonclipped
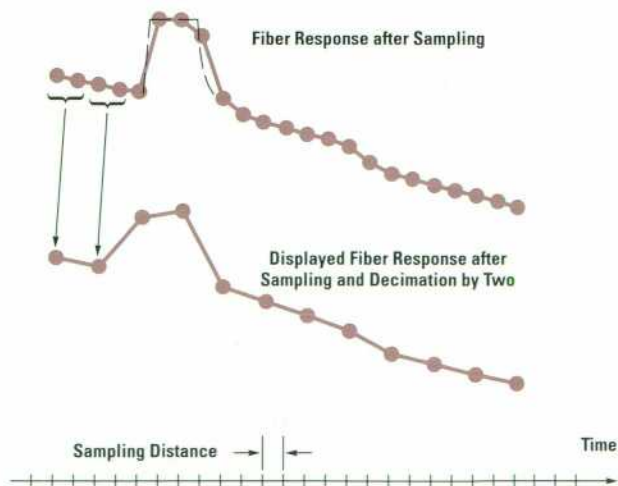
Fig. 3. An illustration of using variable decimation to overcome the limited range of the high-speed flash ADC.
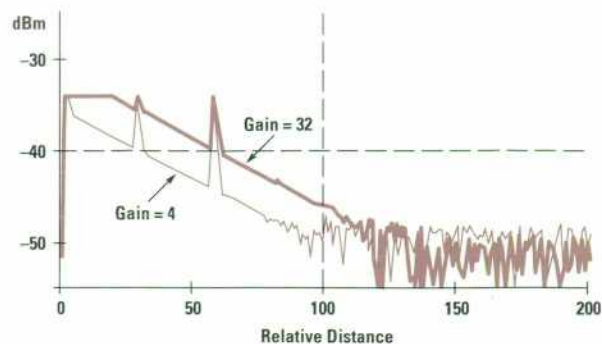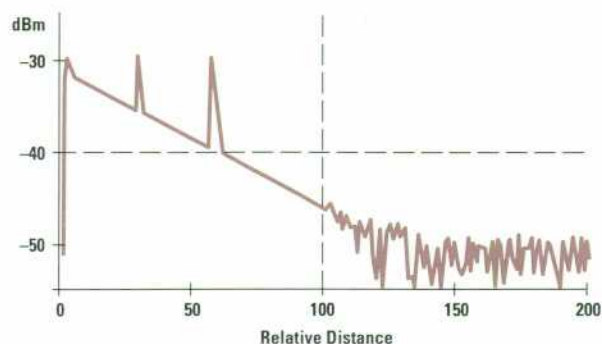
Fig. 4. Stitching to increase the range of an ADC. (a) Measurements made with high and low amplifier gain settings. (b) The signal after stitching.

measurement multiplied by the ratio of the gain factors. The transition region of the resulting fiber trace is invisible to the user since the gain ratio is calculated from the two individual traces to eliminate any gain variation of the analog amplifiers and because the transition region is computed as a weighted moving average.

Key specifications like resolution, dynamic range, and all-haul capabilities were determined or influenced by the architecture of the HP 8146A's digital signal processing system and the instrument's data acquisition speed and data processing power. From the beginning of the project it was clear that the contribution of the new all-haul feature could only be realized by the development of a flexible and powerful digital signal processing board. Friendly user interface features like obtaining a printout and getting a fast zoom while a new measurement is running are simpler to implement if the host processor is relieved of computationally intensive tasks by a high-throughput digital signal processing system.

A signal processing system can be highly efficient only if the acquired data is processed at the highest speed possible. After data acquisition the next main operation of signal processing is real-time averaging with positive or negative signs (addition and subtraction). Because even a digital signal processor can't perform averaging and decimation at clock rates of tens of MHz, we determined that an ASIC that included high-speed data acquisition, averaging, and decimation had to be developed. With a 16-bit word length in the first processing stage we calculated that an instruction cycle of 40 ns (25-MHz clock) would be feasible if a CMOS 1.55-μm process for a gate array were used.

Improving SNR by Averaging

Signal averaging in OTDRs sums repetitions of measurement shots using an accurate time reference for synchronization. To see how averaging improves signal-to-noise ratio (SNR) we represent a single shot measurement result $r_i(t)$ as a signal part $s(t)$ and an uncorrelated noise element $n_i(t)$:

$$r_i(t) = s(t) + n_i(t).$$

The sum $r_{avg}(t)$ of N repetitive measurement shots divided by N is:

$$r_{avg}(t) = \frac{1}{N}\sum_{i=1}^{N} r_i(t) = \frac{1}{N}\sum_{i=1}^{N} s(t) + \frac{1}{N}\sum_{i=1}^{N} n_i(t) = s(t) + \frac{1}{N}\sum_{i=1}^{N} n_i(t).$$

It can be seen that the correlated signal parts $s(t)$ add up proportionally, but the noise sum needs more detailed consideration.

The rms noise level or standard deviation σ_i of $n_i(t)$ can be described as:

$$\sigma_i = \sqrt{E\left[\overline{n_i(t)} - n_i(t)\right]^2} = \sqrt{E\left[n_i^2(t)\right] - E\left[n_i(t)\right]^2}$$

where E is the expected value. If we assume a zero mean noise the rms level of the noise sum σ_Σ gives the result:

$$\sigma_\Sigma = \sqrt{E\left[\frac{1}{N}\sum_{i=1}^{N} n_i(t)\right]^2} = \sqrt{E\left[\frac{1}{N^2}\sum_{k=1}^{N} n_k(t) \cdot \sum_{l=1}^{N} n_l(t)\right]}.$$

If the individual noise terms $n_i(t)$ are uncorrelated then all product terms with indexes $k \neq l$ disappear. Thus we get:

$$\sigma_\Sigma = \frac{1}{N}\sqrt{E\left[\sum_{i=1}^{N} n_i^2(t)\right]} = \frac{1}{N}\sqrt{N \cdot E\left[n_i^2(t)\right]}.$$

Substituting σ_i from above yields:

$$\sigma_\Sigma = \frac{1}{N}\sqrt{N\sigma_i^2} = \frac{\sigma_i}{\sqrt{N}}.$$

The sum of coherent signals builds up linearly with the number of measurements (or repetitions), N, while uncorrelated noise builds up only as $\sqrt{N}$. Thus the signal-to-noise ratio improves as $\sqrt{N}$.

A sample spacing of 40 ns is equivalent to a spatial resolution of about 4 m in an optical fiber since an OTDR performs round-trip measurements. This did not seem sufficient for short-haul applications even though higher resolution can be realized by interleaving at the expense of measurement time. By using two gate arrays for data acquisition, an average processing speed of 50 MHz can be achieved if the gate arrays are supplied with input signals mutually delayed by 20 ns. With this configuration, one gate array processes all input samples with even indexes and the other processes all odd-numbered samples. In this case spatial resolution improves to 2 m for real-time measurements. Further improvement of resolution down to 1 m or even 0.5 m can be realized by interleaving within an acceptable measurement time. The advantages of a sampling rate this high are a high spatial resolution in a short measurement time and additional noise reduction by decimation when longer measurement spans are selected. So as not to lose any performance and to limit memory depth, this decimation must execute in real time.

The two gate arrays cannot perform all the necessary signal processing operations by themselves because word length is limited to 16 bits and because speed requirements

limit complexity. Therefore, several main circuit blocks work together to provide an efficient data flow without incurring much overhead, as described below.

Digital Signal Processing Board

The architecture of the digital signal processing board is shown in Fig. 5. Its operation is controlled by the instrument's host processor via the device bus interface.

Device Bus Interface. The bus interface is a 16-bit bidirectional interface that provides access to the host microprocessor for all of the instrument's main function blocks. Registers and memory of the bus interface are mapped into the host processor's memory by address decoders. Data and address buses are buffered to minimize loading the host interface and to switch the direction of the data path.

Time Base and Pulse Generator. Since the instrument's distance accuracy is directly influenced by the stability and precision of the internal time reference, a crystal-controlled oscillator is used as a time base for the HP 8146A. The oscillator frequency is 200 MHz (5-ns period), which has the advantage that all timing parameters like measurement start and stop, the shortest sample spacing (0.5 m), and the pulse width (5 ns), can be directly controlled by the time base. Therefore, pulse width and sample spacing are very accurate and distance accuracy depends mainly on the refractive index and cabling factor uncertainties of the fiber.

The pulse generator is programmable to provide pulse widths ranging from 5 ns (high resolution) to 10 μs (high dynamic range) for short-haul and long-haul measurements.

Data Acquisition Block. Considerable design effort went into the development of the data acquisition architecture (see Fig. 6) to optimize the averaging process of the measured fiber signatures.

The input data coming from the ADC is fed to two registers that provide at their outputs two 8-bit data streams which are mutually delayed by 20 ns. Each of these outputs is connected to a data acquisition gate array running at 25 MHz. These gate arrays are fabricated with a 1.55-μm CMOS process and packaged in a 124-pin PGA. Each contains a 9-bit adder, a 16-bit wide ALU, a decimation counter plus register, an address counter with memory control circuitry, and an arbiter block to control acquisition-RAM access either by
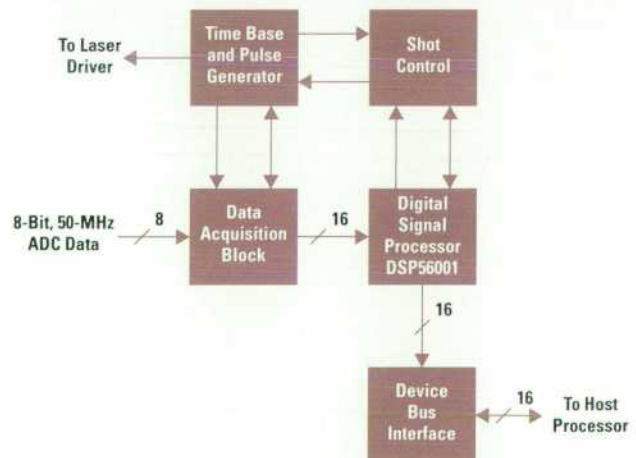
Fig. 5. Block diagram of the digital signal processing board.
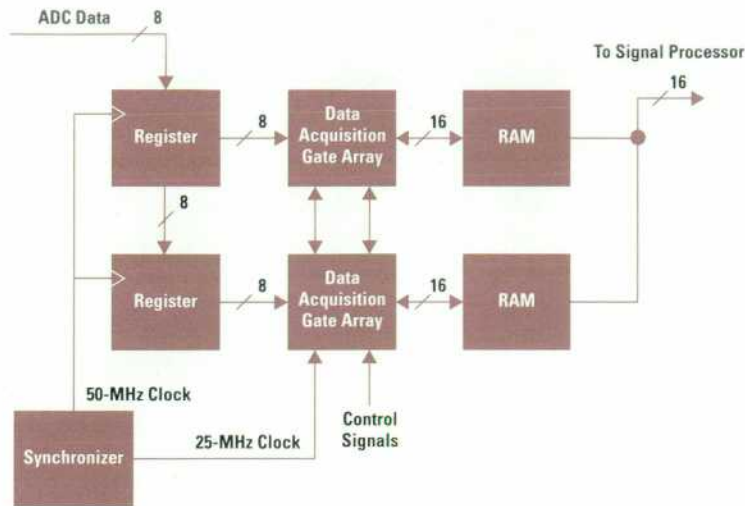
Fig. 6. Block diagram of the data acquisition block.

the gate arrays or the digital signal processor. The 9-bit adder is activated only for measurements in which decimation is used. When it is used it sums the two successive 8-bit data words of the 50-MHz data sequence, providing an intermediate result each 40 ns as input to the 16-bit ALU. This corresponds to a decimation by two. Higher decimations for longer measurement spans are realized by an 8-bit presettable counter and by data looping within the main ALU block. It can be seen that for decimated measurements (sample spacing greater than 2 m), one data acquisition gate array is sufficient. For high-resolution measurements with sample spacing of 2 m or below both gate arrays are necessary. In this case one of the gate arrays processes even-numbered data samples and the other gate array processes odd-numbered samples.

Data averaging runs along until the word width reaches 16 bits, a limit set by the ALU design and by the external fast SRAM. Depending on the decimation factor, this is the case after at most 256 measurement shots.

The Digital Signal Processor. The Motorola DSP56001 is a 24-bit fixed-point, high-performance digital signal processor with separate data and address ALUs operating at 100-ns instruction cycle time. With its 48-bit long-word processing capabilities, the processor is ideally suited for applications requiring extensive data averaging. Different measurement (and test) programs can be copied from an EPROM into the processor's internal program RAM according to the particular measurement situation. Data memory is organized as 2×24-bit $\times$ 16K SRAM with an access time of 35 ns. Two I/O ports are configured to deliver control signals to other circuit blocks. This processor does further averaging and postprocessing on the fiber trace data and provides prepared data to be displayed on the CRT.

Shot Control Block. The major components of the shot control block include a gate array, a 12-bit shot counter, and an 8-bit shot RAM. The gate array was developed because of the shortage of board space and not for performance reasons. It replaces about 40 TTL ICs and is made up of six 16-bit comparators, six 16-bit registers, a presettable 16-bit counter, and miscellaneous glue logic. The gate-array registers can be read by the host processor via the device bus interface to determine information such as the start and stop distance of the measured fiber trace and the time of the laser trigger and its repetition rate. The shot counter is triggered repetitively

shot by shot by the gate array and uses its count state to address successive locations in the shot RAM. The data in the shot RAM, which is programmed by the host processor during initialization, determines the arithmetical function of the data acquisition gate arrays, whether the laser is enabled or disabled, and whether the acquisition RAM is to be cleared. These programmable functions illustrate one part of the ability to adapt the digital signal processor to various measurement tasks.

Functional Description
Pressing the **START** key on the instrument's front panel initiates a new measurement process. The process begins with the instrument's host processor programming the digital signal processing board according to the measurement parameters selected by the user. The main parameters for the signal processing board that determine a particular measurement situation are pulse width, measurement start and stop, repetition time, sample spacing, and long-haul or short-haul operation. This group of parameters determines which one of several measurement programs stored in the board's EPROM should be loaded into the DSP56001 digital signal processor's RAM. The ability to select a program for the DSP56001 from among a variety of other programs is another part of the digital signal processing board's flexibility.

Programming the signal processing board by the host processor proceeds in the following manner:
- The decimation factor, which is derived from the measurement span, is transferred to the data acquisition gate array.
- A code for the selected pulse width is written into the appropriate register of the pulse generator and then codes for measurement start and stop, repetition time, and laser trigger time are transferred to the shot control gate array.
- The shot RAM is loaded with code for up to 256 individual measurement shots which are executed and repeated successively.
- The shot counter is set to the number of measurement shots that can be averaged without overflowing the acquisition block.
- Other information related to the measurement such as the interleaving factor, display update time interval, refresh or averaging measurement, and the measurement software to be used (e.g., long-haul or short-haul) is written into the SRAM of the digital signal processor, which is in a high-impedance state at that time.

By removing the master reset signal of the digital signal processing board, the DSP56001 starts to boot and load the specified measurement program from the EPROM into its internal program RAM. A flow chart of the signal processor software is shown in Fig. 7.

After the instrument passes self-test, a host interrupt A releases the signal processor from a wait loop and starts the repetitive measurement process on the signal processing board. The interrupt A service routine clears the 48-bit long-word averaging memory in the DSP56001 RAM and evaluates the measurement parameters for initializing the measurement loop. The number of loop iterations determines the display update time interval. In the measurement block loop the baseline signal is updated and the shot control circuit is triggered repetitively with each loop pass. (A variable baseline signal is added to the ADC input for improved linearity.)

The shot control starts the measurement process by providing control and trigger signals for the pulse generator and the data acquisition gate array. For each measurement shot the shot counter is decremented by one. When it reaches zero, the shot counter's terminal count pulse stops the acquisition process and interrupts the signal processor to fetch the averaged data from the data acquisition RAM. The DSP56001 transfers the fiber trace data to its own memory and does more averaging at the same time, converting the data to a 24-bit representation. If interleaving is used the signal processor sorts the data samples in the right sequence. The process up to this point is called a measurement block. The execution time of the measurement block can be calculated from the number of measurement shots and the repetition rate. Thus the amount of time allocated for the display update interval determines the number of measurement blocks or the number of measurement loop passes that are executed. All calculations for the number of measurement blocks and the number of shots per block take the processing time of the DSP56001 into account.

After finishing this measurement part, postprocessing of the fiber trace data starts. Offset calculation yields a result that is used for a closed-loop control to cancel any drift in the analog circuitry or the dc portion of the optical input signal. For self-test purposes, the rms noise level can be calculated. The intermediate measurement result that was obtained between two display updates is now added to previous fiber trace data and stored in a 48-bit integer long-word representation to avoid any data overflow with long measurement times. If necessary a finite impulse response (FIR) filter is applied to provide noise reduction and some trace smoothing for improved SNR. In a last step the measurement data is converted from a 48-bit linear representation to a 16-bit logarithmic representation using a conversion table, providing a resolution of 0.001 dB with an even better accuracy. The whole data acquisition process has a typical efficiency of 90% because only 10% of the time between two display updates is used for data transfers or signal processor calculations.

A measurement-ready interrupt to the host indicates to the main processor that a new measurement result is available. For each display update the host processor fetches the logarithmic fiber trace data from the signal processor RAM. Thus, the instrument's main processor is relieved of the whole signal and data processing burden, allowing it to focus on updating the display.
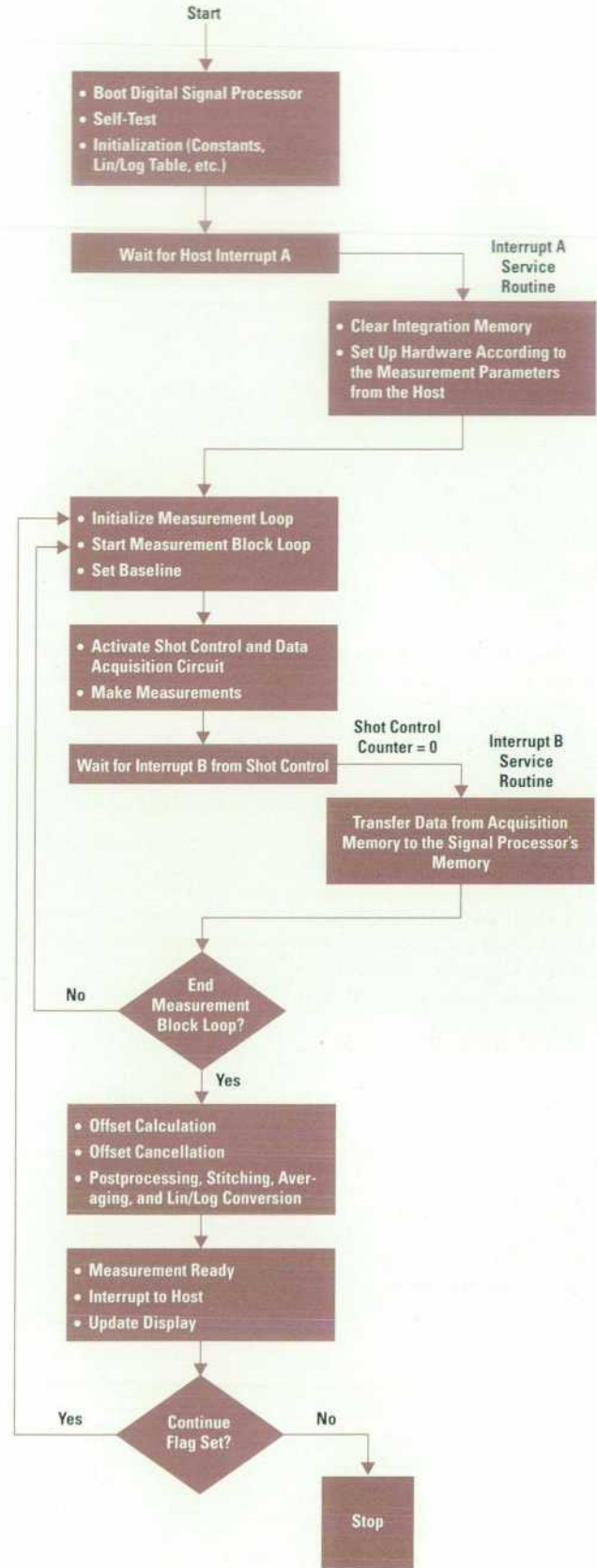
Fig. 7. Flow of activities in the HP 8146A during initialization, measurement, and display update.

Technical Data

The digital signal processing board is a six-layer, 192-mm-by-303-mm printed circuit board. The board layout was done with an internal design system for printed circuit boards. Critical traces of the pulse generator, the time base circuit, and the high-frequency clock lines were manually prerouted. About 85% of the traces were routed automatically. The online design rule checker was highly appreciated when manually editing the copper traces.

Power consumption of the board is about 18 watts. More than half of the power consumption is because of the ECL pulse generator which consists of 10KH series devices. For RFI reasons and because of functionality, high-speed components are grouped together to keep copper traces as short as possible. However, this arrangement causes some non-uniform power density on the board, requiring the air flow provided by the fan on the instrument's rear panel.

By using a +5.1V single supply voltage for both the TTL and ECL circuitry, we achieved some simplification in the power supply design and a contribution to cost reduction. However, proper grounding and decoupling are necessary to avoid performance degradation. One ground plane and two separate voltage supply planes for TTL and ECL devices ensure reliable operating conditions.

Summary

The architecture of the digital signal processing board sets a new level of performance and flexibility in OTDRs. Its real-time acquisition and processing rate of 50 Msamples/s represents a sixfold improvement over its predecessor the HP 8145A OTDR. The cooperation of three gate arrays and a digital signal processor increases data processing throughput by one to two orders of magnitude. Flexibility is provided because various measurement programs for the signal processor can be selected, even on the fly, and the arithmetic of the high-speed data acquisition process can be programmed to adapt to different applications.

Design Considerations for the HP 8146A OTDR Receiver

Low noise, high bandwidth, and good linearity are characteristics that guided the OTDR receiver circuit design.

by Frank Maier

The basic requirements for an all-haul OTDR receiver are low noise to achieve a high dynamic range, high bandwidth for excellent dead-zone performance, high linearity to ensure that the displayed data is valid, and the ability to make return loss measurements.

A tool that helps to visualize these requirements is a level diagram. The level diagram in Fig. 1 shows the performance of an OTDR operating on a single-mode fiber at 1310 nm. The laser source sending the pulse to the receiver has an optical power of 25 mW or 14 dBm. Because of the 3-dB bidirectional coupler shown in Fig. 2, the source power is attenuated by 3 dB. Therefore, as shown in the level diagram we have 11 dBm launch power into the fiber under test.

The OTDR must detect backscattered (Rayleigh) and reflected (Fresnel) signals. The highest power level is the Fresnel reflections from the OTDR output (glass-to-air interface). These reflections are 4% of the incident power level, or 14 dB lower. Taking into account the round-trip propagation of the signal, there is another 3-dB loss when the returning signal is split again in the coupler. The magnitude of the backscatter signal is dependent on the pulse width of the launched pulse. For a 10-μs pulse the backscatter is approximately 40 dB below launch power, and for a 10-ns pulse the

Fig. 2. The receiver and coupler blocks of the HP 8146A OTDR.

backscatter is 70 dB below launch power. Thus, the initial power at the receiving element of the OTDR is –32 dBm for a 10-μs pulse and –62 dBm for a 10-ns pulse.

We wanted to achieve a 30-dB dynamic range for the HP 8146A. The dynamic range is the difference between the initial backscatter level (at the longest pulse width) and the peak noise level (see Fig. 3). Both the launched pulse and the backscattered or reflected signal are attenuated by the fiber (typically 0.35 dB/km at 1310 nm single-mode). A required dynamic range of 30 dB results in a two-way 60-dB loss. Since the user is only interested in the one-way loss, the OTDR divides the measured two-way attenuation by two. Considering the 10-μs pulse width, which has a –32-dBm initial backscatter level, a peak noise level of –92 dBm (or a –97 dBm rms noise level) must be achieved to guarantee the required 30-dB dynamic range with a three-minute averaging time.

The Receiver Circuit

The dynamic range specification combined with the high-bandwidth requirements to achieve good dead-zone performance resulted in the receiver design shown in Fig. 4. The

Fig. 1. OTDR level diagram for a single-mode fiber operating at 1310 nm.
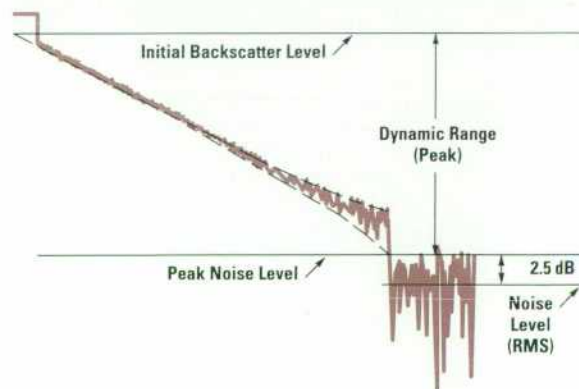
Fig. 3. The OTDR dynamic range parameter.
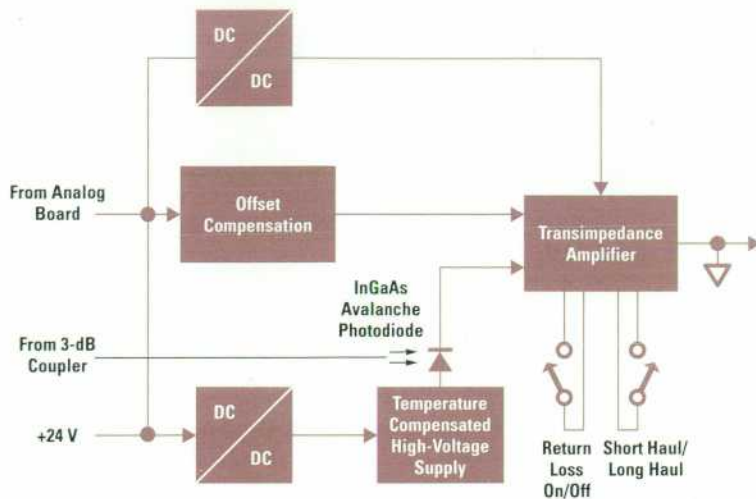
Fig. 4. HP 8146A receiver circuit block diagram.

optical-to-electrical conversion is made by an avalanche photodiode. The inner gain of this element helps to reduce the feedback resistance of the transimpedance amplifier, which increases the bandwidth. The disadvantage of the avalanche photodiode is the need to have a highly stable, temperature compensated high-voltage supply. To isolate the sensitive receiver from the noisy OTDR environment the whole receiver is supplied via dc-to-dc converters. All other basic noise considerations have been described in reference 1.

The receiver has the following modes:
- A return loss mode to measure reflections
- A short-haul mode for good dead-zone performance
- A low-noise, long-haul mode for high dynamic range.

The basic difference between these three modes is the different optical-to-electrical conversion gains. These modes can be characterized by the power that must be applied at the receiving element to reach the clip level of the analog-to-digital converter in the OTDR (see the clip levels in Fig. 1). In the return loss mode the gain saturation effects of the avalanche photodiode are taken into account to achieve a 3-dB increase of the return loss mode clip level. Even the return loss of Fresnel reflections can be measured if they are not located directly at the OTDR output.

In summary, the instrument covers a range of approximately 90 dB optical from the highest reflection being measured down to the noise level. Because of the direct conversion from optical power to voltage at the front-end amplifier, this equals 180 dB in the electrical domain.

OTDR Linearity

Another aspect of the OTDR performance is linearity. During development we found that the limiting element to good linearity is not the receiver as expected, but the analog-to-digital converter. One way of improving the resolution of the converter is by averaging the receiver noise with the assumption that it has a Gaussian distribution.[2] For a long averaging time the statistical distribution of the measurement values yields:

$$\overline{k} = \sum_k k\, p_k \qquad (1)$$

where each measurement value k is weighted by the relative frequency of occurrence p_k. The accuracy of $\overline{k}$ is affected by the differential nonlinearity (DNL) of the ADC, which is expressed as:

$$DNL_k = |\text{actual step size k} - 1\ \text{LSB}|. \qquad (2)$$

As shown in Fig. 5 for an ideal ADC with DNL equal to zero, $\overline{k} = n$. However, if the DNL is not equal to zero the distribution is distorted and $\overline{k}$ is not equal to n but to $n + \Delta n$.

This effect limits the achievable linearity. To improve the linearity of the OTDR a better ADC with lower differential nonlinearity could be chosen, but this leads to higher costs without significant improvement. A typical ADC differential nonlinearity value is 0.75 LSB (some have 0.5 LSB but cost three times as much). A better solution is to use more of the ADC range. Differential nonlinearity varies in a noise-like fashion over the ADC range. This leads to many different values for Δn, with the average value being closer to zero as more of the ADC range is used. This cannot be done by increasing the receiver noise because it would decrease the dynamic range. However, the measurement point can be shifted by a variable but known amount on each measurement, and then the measurements can be averaged taking into account the known shifts. This technique results in shifting the noise distribution over a wider range of the ADC, improving the OTDR linearity without decreasing the dynamic range.
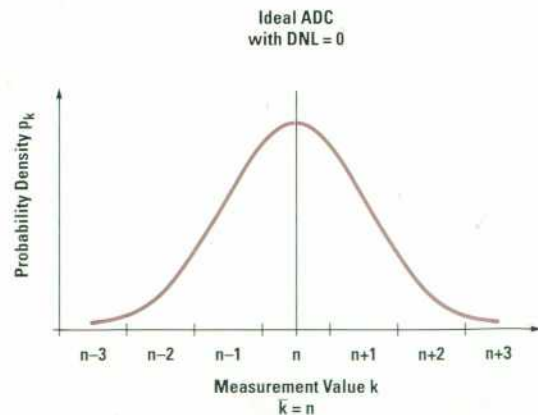
Fig. 5. For a signal with Gaussian noise and a value of n, the mean of the measured values equals n if the ADC has zero differential nonlinearity.
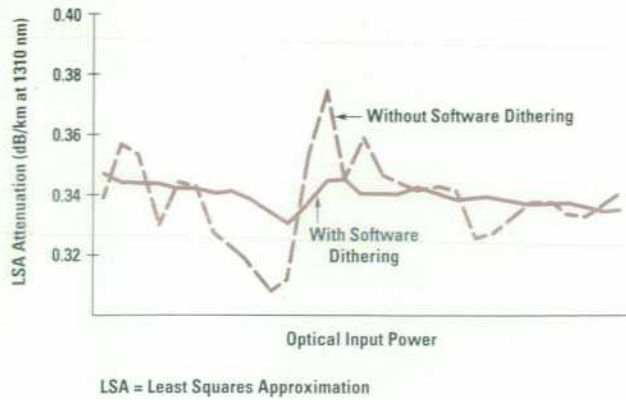
Fig. 6. Using software dithering to improve linearity.

In the HP 8146A, shifting the measurement value, which is also called software dithering, is handled by the digitally controlled offset compensation circuit shown in Fig. 4. An example of software dithering is shown in Fig. 6 where the fiber attenuation has been measured while varying the optical input power in 1-dB steps. The variation of the measured attenuation is improved by a factor to two to three.

References

1. J. Beck, S. Gross, and R. Giffard, "Optical Component Design for a Correlation-Based Optical Time-Domain Reflectometer," *Hewlett-Packard Journal*, Vol. 39, no. 6, December 1988, p. 22.
2. F. Sischka, S. Newton, and M. Nazarathy, "Complementary Correlation Optical Time-Domain Reflectometry," *Hewlett-Packard Journal*, Vol. 39, no. 6, December 1988, p. 14.

User Interface Design for the HP 8146A OTDR

Based on a multiprocessing operating system, the HP 8146A OTDR software can handle simultaneous execution of instrument operations, hide the complexity of instrument operations from the user, and provide a range of user-friendly features.

by Robert Jahn and Harald Seeger

Although many of the tasks performed by an instrument such as an OTDR may involve many complex operations, the user interface must provide the functionality to hide this complexity from the user. Trained operators must be able to do difficult measurements for characterization of optical links after installation. If a link is broken, the location of the break must be found quickly and precisely. In this situation ease of use is very important because the operator has no time to read a manual or become familiar with a complicated instrument.

The following are some of the user-accessible features and capabilities provided by the HP 8146A OTDR:
- Comprehensive documentation and storage of measured traces
- Automatic trace analysis and fault detection
- Help screens and native language support
- Automatic ghost detection and removal
- Remote operation.

OTDR Software

The binary code for revision 1.0 of the OTDR software is almost 500K bytes. The software runs on a Motorola 68010 microprocessor and is based on the real-time multiprocessing operating system pSOS-68k, which can coordinate multiple asynchronous activities. Thus, we have six independent processes running in parallel. Each process has its own data area and stack. A process communicates with others by sending signals or messages via the operating system. Information common to multiple processes is stored in databases, which are accessible only to driver routines. The processes are created after power-on by a special process called the root process. The root process spawns the other processes, creates their mailboxes, and then activates them.
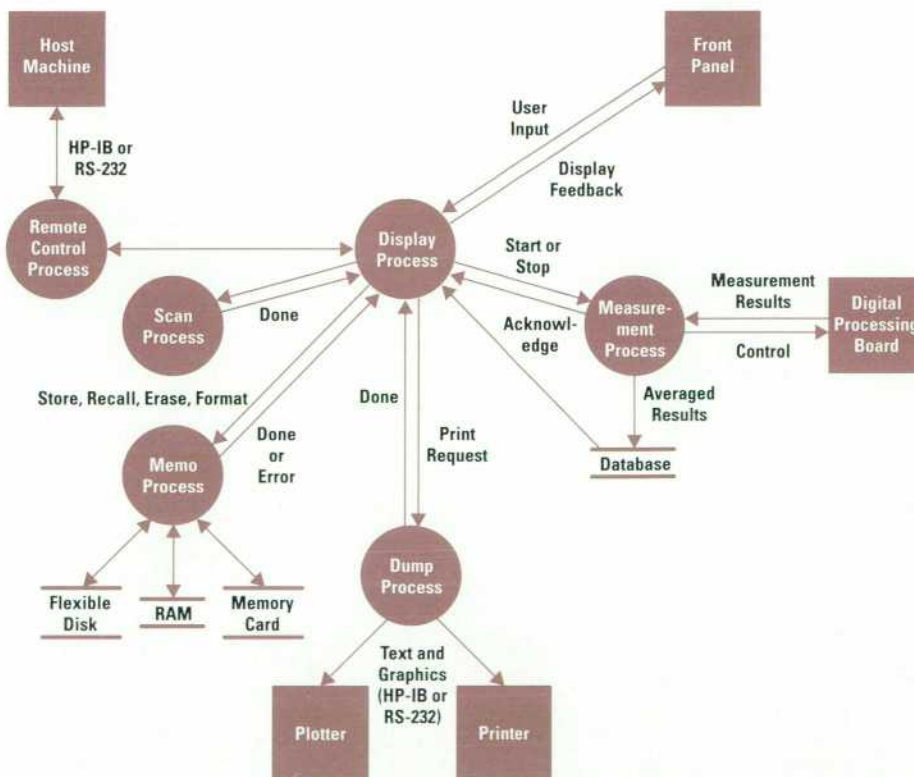
Fig. 1. The data flows and interactions between the software processes in the HP 8146A.

After all six processes are ready to run, the root process eliminates itself.

The display process handles most of the human interface activities such as accepting all input in local mode via the RPG and keystrokes, starting the requested actions, doing some analyses like calculating loss, attenuation, splice loss, and return loss, and drawing CRT text and graphics. Because of complexity, some tasks cannot be handled by the display process and so it passes requests to other processes to do the work.

The other five processes (or message exchanges) are: the measurement process, the dump process, the memo process, the scan process, and the remote control process. The interactions and data flows between these processes are illustrated in Fig. 1.

Measurement Process. To start and stop a measurement, messages are sent to the measurement process, which returns a positive or negative acknowledgment message. In the HP 8146A averaging mode, the measurement process transfers results from the digital signal processing system to

the database once every second. After every transfer a message is sent to the display process informing it that new data is available for display.

Dump Process. All communication with output devices such as the internal and external printers and plotter is done by the dump process. The dump process also configures the assigned interface (HP-IB or RS-232).

Memo Process. Every access to registers in battery-buffered RAM, flexible disk, or the memory card is executed by the memo process. When the memo process receives a request such as to store a result to disk, it will acknowledge with a request done message if the operation is successful; otherwise, it reports an error to the display process.

Scan Process. A complete automated analysis of fiber link measurement data is done by the scan process. Results of this scanning are stored in the register database.

Remote Control Process. Remote control of the OTDR is done via the remote control process. The remote control process configures the assigned interface and manages all I/O requests.

```
HELP_SETUP1 EQU $
    ADDTEXT "\I\2Set Up\N"
    ADDTEXT ""
    ADDTEXT ""
    ADDTEXT "\IStart Position\N chooses the distance of the first"
    ADDTEXT "measured point from the OTDR."
    ADDTEXT ""
    ADDTEXT "\IMeas. Span\N chooses the length of fiber that is"
    ADDTEXT "to be measured."
    ADDTEXT "        End = Start Position + Meas. Span"
    ADDTEXT "The measurement span affects the distance"
    ADDTEXT "between samples. This distance is shown at the"
    ADDTEXT "bottom of the screen while you edit Meas. Span"
    ADDTEXT ""
    ADDTEXT ""
    ADDTEXT "You cannot edit Start Position or Meas. Span if"
    ADDTEXT "the instrument is in compare mode."
    ADDTEXT ""
```

(a)

```
HELP_SETUP1 EQU $
    ADDTEXT "\I\2Set Up\N"
    ADDTEXT ""
    ADDTEXT ""
    ADDTEXT "\IStart Position\N permet de déterminer le"
    ADDTEXT "premier point de la mesure."
    ADDTEXT ""
    ADDTEXT "\IMeas. Span\N choisit la longueur de"
    ADDTEXT "la fibre à mesurer"
    ADDTEXT ""
    ADDTEXT "End = Start/début + Span/fenêtre"
    ADDTEXT "La fenêtre de mesure détermine la distance"
    ADDTEXT "entre chaque échantillon. Cette"
    ADDTEXT "distance est indiquée au bas de l'écran"
    ADDTEXT "lorsque vous appuyez sur Meas. Span."
    ADDTEXT ""
    ADDTEXT "Les fonctions  Start Position et Meas Span"
    ADDTEXT "ne sont pas utilisables en mode"
    ADDTEXT "comparaison (compare mode)."
```

(b)

```
HELP_SETUP1 EQU $
    ADDTEXT "\I\2Set Up\N"
    ADDTEXT ""
    ADDTEXT ""
    ADDTEXT "\IStart Position\N legt die Entfernung vom Meßgerät"
    ADDTEXT "fest, ab der Werte aufgenommen werden sollen."
    ADDTEXT ""
    ADDTEXT "\IMeas. Span\N bestimmt die Länge des"
    ADDTEXT "Meßbereichs. Es gilt:"
    ADDTEXT "        Ende = Start Position + Meas. Span"
    ADDTEXT "Meas. Span bestimmt auch den Abstand zwischen"
    ADDTEXT "den Messpunkten. Dieser Wert wird am Bildschirm"
    ADDTEXT "unten angezeigt, wenn Sie die Taste Meas. Span"
    ADDTEXT "angewählt haben."
    ADDTEXT ""
    ADDTEXT ""
    ADDTEXT "Im Vergleichs-Modus (Compare mode) kann weder"
    ADDTEXT "Start Position noch Meas. Span geändert werden."
    ADDTEXT ""
```

(c)

```
HELP_SETUP1 EQU $
    ADDTEXT "\I\2Set Up\N       \I\2USTAWIANIE\N"
    ADDTEXT ""
    ADDTEXT ""
    ADDTEXT "\IStart Position\N (Polozenie poczatku) pozwala"
    ADDTEXT "ustawic odleglosc miedzy reflektometrem a"
    ADDTEXT "pierwszym mierzonym punktem swiatlowodu."
    ADDTEXT ""
    ADDTEXT "\IMeas. Span\N (Zasieg pomiaru) pozwala ustawic"
    ADDTEXT "dlugosc mierzonego odcinka swiatlowodu."
    ADDTEXT "  \IPolozenie konca=Polozenie poczatku+Zasieg\N"
    ADDTEXT "Ustawiona wartosc zasiegu wplywa na odleglosc"
    ADDTEXT "miedzy kolejnymi punktami mierzonymi(probkami) w"
    ADDTEXT "swiatlowodzie. W czasie ustawiania zasiegu"
    ADDTEXT "odleglosc ta jest wyswietlana w dole ekranu."
    ADDTEXT ""
    ADDTEXT "W czasie pracy w trybie porownywania(compare)"
    ADDTEXT "nie ma mozliwosci zmiany polozenia poczatkowego"
    ADDTEXT "i zasiegu"
```

(d)

```
HELP_SETUP1 EQU $
    ADDTEXT "\I\2Set Up\N"
    ADDTEXT ""
    ADDTEXT ""
    ADDTEXT "\IStart Position\N selecciona la distancia del"
    ADDTEXT "primer punto medido respecto al OTDR."
    ADDTEXT ""
    ADDTEXT "\IMeas. Span\N selecciona la longitud de fibra"
    ADDTEXT "que se ha de medir."
    ADDTEXT ""
    ADDTEXT "  Pos. Final = Pos. Inicial + Campo de Medición"
    ADDTEXT ""
    ADDTEXT "El campo de medición afecta a la distancia entre"
    ADDTEXT "muestras. Esta distancia se indica en la parte"
    ADDTEXT "inferior de la pantalla, mientras se edita Meas."
    ADDTEXT "Span."
    ADDTEXT ""
    ADDTEXT "No se puede editar la posición inicial ni el"
    ADDTEXT "campo de medición si el OTDR está en modo de"
    ADDTEXT "comparación."
```

(e)

```
HELP_SETUP1 EQU $
    ADDTEXT "\I\2NASTAVENI\N"
    ADDTEXT " "
    ADDTEXT " "
    ADDTEXT "Po stisknuti tlacitka \IStart Position\N -(POCATEK)"
    ADDTEXT "lze nastavovat otocnym knoflikem vzdalenost"
    ADDTEXT "nejblizsiho mista trate, od nehoz zacina mereni."
    ADDTEXT " "
    ADDTEXT "Po stisknuti tlacitka \IMeas. Span\N -ROZPETI MER."
    ADDTEXT "lze otocnym knoflikem nastavit promerovanou"
    ADDTEXT "delku opticke trate."
    ADDTEXT " "
    ADDTEXT "Nejvzdalenejsi promerovane misto trate lezi ve"
    ADDTEXT "vzdalenosti dane souctem: \IPOCATEK\N + \IROZPETI MER\N."
    ADDTEXT "Hodnota \IROZPETI MER\N ovlivnuje hustotu mericich"
    ADDTEXT "vzorku. Jejich vzajemna vzdalenost se behem"
    ADDTEXT "nastavovani zobrazuje v dolni casti obrazovky."
    ADDTEXT " "
    ADDTEXT "Zmenu nastavenych hodnot \IPOCATEK\N a \IROZPETI MER\N"
    ADDTEXT "nelze provadet v rezimu \ICOMPARE -(POROVNAVANI)\N."
```

(f)

Fig. 2. Portions of the native language help text for (a) English. (b) French. (c) German. (d) Polish. (e) Spanish. (f) Czechoslovakian.

The benefit of using independent processes instead of simple function calls is parallelism. The dump process, for example, has a buffer large enough to hold one complete measurement result including parameter settings and results of the automated fiber scanning. The display process accepts the user request for printing the trace and then sends a print message to the dump process and waits for an acknowledgment message. After the dump process receives the print message, it tests the connection to the printer and the printer's status and then copies the trace from the display process's memory to its buffer. This takes some hundreds of milliseconds. Once the dump process is done copying the display data to its buffer, it sends an acknowledgment to the display process so that it can resume accepting user inputs. While running at a low priority in the background, the dump process sends the text and graphic data to the printer. Some OTDRs block all activity while printing or plotting, but the HP 8146A does not.

Help Text

To help users understand and use the instrument effectively we implemented an online help facility. This kind of short-form manual must be available in several languages. Therefore, we offer the capability to provide native language help text. In the field offices where the instrument is sold, engineers are provided with the tools to translate English text into the corresponding local language text and then link this translated text into the OTDR software. Currently we offer help text for English, French, German, Polish, Spanish, Czechoslovakian, Portuguese, and Italian (see Fig. 2).

To enable engineers to download help text to the instrument in the field, flash EPROMs are used to store software and text. With flash EPROMs the permanent software in the instrument is reduced to a software loader that reads software from an external device like a flexible disk, a memory card, or a host system (via the HP-IB) to program the flash EPROMs. This makes it easy to make software enhancements and support new laser modules. Native language help text can be implemented on demand and distributed by flexible disk or even electronic mail.

Scantrace

When users want to analyze their fiber links this typically means searching for nonreflective and reflective events* and the start and end of the fiber under test. They want to know the loss or gain resulting from splices and gain elements and the through loss and return loss of connectors. Scantrace is an automatic trace analysis and fault detection algorithm provided in the HP 8146A that does all these measurements in less than 10 seconds.

To understand the advantage of the Scantrace algorithm, consider the steps involved in manually making a splice measurement from just the plots that appear on the instrument display. The first step would be to position line segments on each side of the event on the trace (see Fig. 3). The line segments are least-squares approximations of the backscatter on either side of the splice. The line segment lengths can be adjusted by changing the two marker positions. The difference in the signal strength of the two line segments gives the splice loss. The correct position of the

---

* Nonreflective events include fusion splices and gain elements. Reflective events include connections. Mechanical splices cause small reflections.

Splices Loss = $X_2 - X_1$
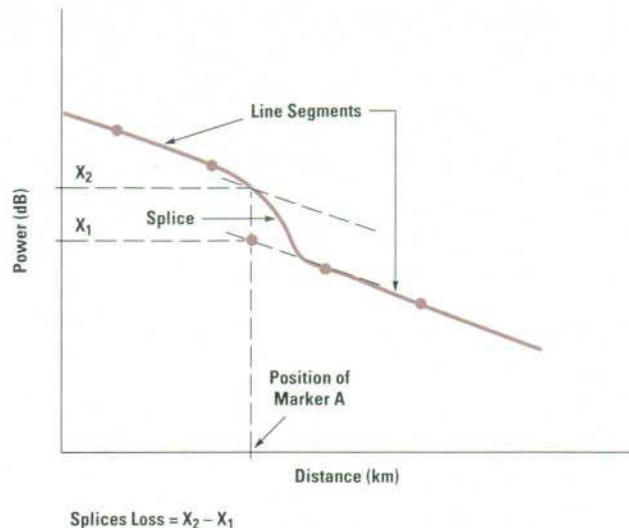
Fig. 3. Splice loss measurement.

splice is the the last point on the backscatter just before the event. In the same manner the through loss of reflective events can be measured and positioned. Three markers are necessary to measure the return loss of reflective events. Finally, a least-squares approximation measurement can be used to calculate the attenuation between the two events.

If we apply the above procedure to an 80-km fiber with splices every two kilometers, 40 splices would have to be calculated and 40 sections would have to be measured for attenuation. Also, the reflective event of the OTDR connector and the reflective event at the fiber end must be measured. All these measurements would take more than half an hour. With Scantrace these measurements can be done in less than 10 seconds. Fig. 4 shows a printout of a complete analysis of the 80-km fiber mentioned here.

Result Documentation

The HP 8146A provides two ways to document measurement results: hard copy or storage on external devices. To identify a measurement, an identification code, an operator name, and comments can be added before printing or storing. Hard copies can be made by an internal printer, an external printer, or a plotter. The internal printer is a thermal printer offering a resolution of 640 dots and a 4-inch printing width. The display resolution of 500×320 pixels is easily transferable to the printer's resolution after rotating the picture 90 degrees. Printing on the internal printer takes about 20 seconds. External devices are accessible via the HP-IB or RS-232 interfaces. When one interface is configured as the dump output port, the other interface is configured as a remote control port. All PCL-II compatible printers like ThinkJet, DeskJet, and others are supported by the OTDR. Plotters must be standard HP-GL-compatible. A series of traces stored on a flexible disk or a memory card can be printed to the internal or external printer.

Documenting measurement results on storage media is much more convenient than paper for carrying around measurement results (stacks of paper versus one 3.5-inch flexible disk). The HP 8146A OTDR supports 3.5-inch MS-DOS-compatible flexible disks with up to 1.44-Mbyte capacity. On a high-density disk, 141 measurement results, called *traces*,

```
ID Code: EXAMPLE: SCANTRACE
Meas. Date and Time: 91/01/30 09:40:03
Operator:
Comments:


MEAS. RANGE:        0.0 TO  80.0000 km
WAVELENGTH:         1540 nm   singlemode
GROUP INDEX:        1.4700
PULSEWIDTH:         3.0 us
DISTANCE RANGE:     longhaul
GRID CENTER:        -60.000 dBm

8146A / 0000G00053 / / PP2.3
```


(a)

```
MEAS. RANGE:        0.0 TO  80.0000 km
WAVELENGTH:         1540 nm   singlemode
GROUP INDEX:        1.4700
PULSEWIDTH:         3.0 us
DISTANCE RANGE:     longhaul
AVERAGES:           392
EVENT THRESHOLD:    0.00 dB

8146A / 0000G00053 / / PP2.3


EVENT TABLE
-----------

NO.  TYPE      LOCATION    THRULOSS dB  RETURNLOSS dB  ATT dB/km

 1: REFLECT      0.0 m      --.---        --.---        0.186
 2: NONREFL    1.5296 km    -0.120                      0.302
 3: NONREFL    2.9367 km     0.088                      0.322
 4: NONREFL    4.3439 km     0.072                      0.244
 5: NONREFL    6.3833 km     0.108                      0.353
 6: NONREFL    8.6675 km    -0.256                      0.319
 7: NONREFL   10.1358 km     0.315                      0.320
 8: NONREFL   11.5226 km    -0.323                      0.299
 9: NONREFL   12.9706 km     0.287                      0.343
10: NONREFL   13.5009 km     0.032                      0.347
11: NONREFL   14.3982 km     0.064                      0.276
12: NONREFL   17.3145 km     0.325                      0.256
13: NONREFL   18.7217 km    -0.221                      0.322
14: NONREFL   20.1697 km     0.096                      0.304
15: NONREFL   21.6177 km     0.294                      0.250
16: NONREFL   24.4525 km    -0.265                      0.309
17: NONREFL   27.3280 km    -0.153                      0.329
18: NONREFL   34.5679 km     0.105                      0.300
19: NONREFL   35.9955 km     0.290                      0.274
20: REFLECT   36.6073 km     0.858        26.683        0.396
21: NONREFL   38.2184 km     0.040                      0.332
22: NONREFL   39.0138 km     0.048                      0.329
23: NONREFL   54.2890 km     0.099                      0.270
24: NONREFL   54.7580 km     0.102                      0.238
25: NONREFL   56.2672 km     0.139                      0.246
26: NONREFL   57.3481 km    -0.030                      0.330
27: NONREFL   58.9592 km    -0.175                      0.413
28: NONREFL   60.4683 km     0.289
29: ENDSCAN   71.0529 km
30: REFLECT   73.3166 km    --.---        --.---
31: REFLECT   74.4587 km    --.---        --.---
32: REFLECT   75.3560 km    --.---        --.---
```

(b)

Fig. 4. The results of using the Scantrace algorithm for measuring an 80-km fiber. (a) The display. (b) The complete analysis.

can be stored. Since the BASIC programming language is widely used for programming instruments, we implemented a LIF-compatible (HP Logical Interchange Format) flexible disk driver. Finally we added a memory card interface according to PCMCIA Rel. 2.0 for users who think flexible disks are too sensitive to dust or humidity.

To help the user identify the measurement results stored on flexible disk, the HP 8146A builds a directory file that contains measurement parameters, date and time when a measurement was taken, and an identifier code (see Fig. 5).

Ghost Elimination

One key OTDR parameter is the dynamic range. Specifications are usually measured in compliance with the Bellcore standard which specifies that the instrument's dynamic range must be achievable within three minutes of averaging time. The repetition rate of laser pulses must be as high as possible since the dynamic range specification value rises with increasing repetition rate. However, there is an upper limit for repetition rate, which is based on the fact that the next laser pulse cannot be launched until the reflected light of the previous laser pulse has traveled back to the front connector. Launching laser pulses with higher repetition rates results in aliases or ghosts. The user would see a picture showing a reflection at a position where nothing but pure fiber exists. Also, attenuation measurements would be wrong, since backscattered signals of two laser pulses would overlap each other.

The HP 8146A OTDR eliminates ghosts by using a ghost elimination algorithm. The algorithm works by determining the length of a fiber link at the start of a measurement and then selecting a measurement span to get the appropriate repetition rate.

To determine the length of the fiber, at the start of a measurement the algorithm initiates a very short measurement with the longest possible measurement span (to ensure that the laser pulse goes beyond the end of the fiber). Beginning at the end of the sampled data the algorithm checks to find where the noise level is exceeded for the first time (see Fig. 6a). This location and the measurement span are used to calculate the repetition rate. Fig. 6b shows the ghost that appears when the ghost elimination algorithm is turned off, and Fig. 6c shows what happens when the algorithm is on and the pulse repetition rate is adjusted to eliminate ghost reflections.

```
[hp]

   FLOPPY DISK TRACE DIRECTORY
   _____

   1:   0.0 km TO  16.0 km   100 ns 1310 nm 07/05/92

   2:   0.0 km TO  16.0 km   100 ns 1310 nm 07/05/92

   3:   0.0 km TO   8.0 km   100 ns 1310 nm 06/26/91

   4:   0.0 km TO  80.0 km   3.0 us 1540 nm 01/30/91

   5:   0.0 km TO  40.0 km   1.0 us 1310 nm 11/02/90

   6:   0.0 km TO  16.0 km   100 ns 1315 nm 12/10/91
```

Fig. 5. Trace directory.

```
A     :    1.3818  km
B     :    6.0000  km
Dist.:    4.6182  km
Loss :    1.563   dB

5.00 dB/DIV     From Start        1.60 km/DIV
1315 nm SM                        Avgs.: 521
```

(a)


```
A     :    1.3818  km
B     :    6.0020  km
Dist.:    4.6203  km
Loss :    0.983   dB

5.00 dB/DIV     From Start        800  m/DIV
1315 nm SM                        Avgs.: 550
```

(b)


```
A     :    1.3824  km
B     :    6.0020  km
Dist.:    4.6196  km
Loss :    1.495   dB

5.00 dB/DIV     From Start        800  m/DIV
1310 nm SM                        Avgs.: 300
```
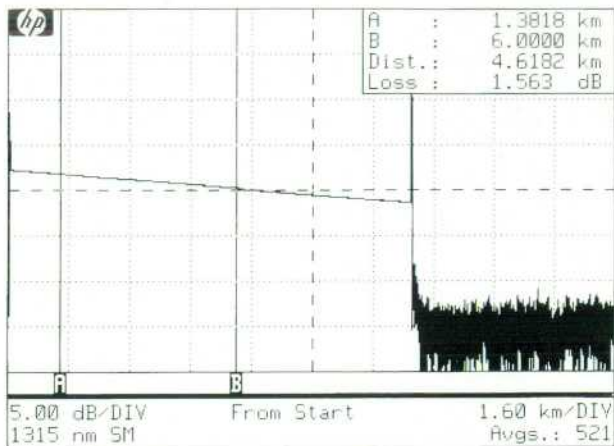
(c)

Fig. 6. Operation of the ghost elimination algorithm. (a) A 10.58-km fiber is measured with a measurement span of 16 km. (b) The same fiber using an 8-km measurement span without the ghost elimination algorithm and (c) with the ghost elimination algorithm.

To put this process into perspective, consider the case in which a user wants to measure a 5-km long fiber with a measurement span of 100 km. A lot of time is wasted because the time between measurement pulses will be long. There will be no ghosts because all reflections will be gone before the next pulse is fired. On the other hand if the user wants to measure a 100-km long fiber with a 5-km measurement span (for higher resolution), the ghost elimination algorithm must reduce the repetition rate to ensure that the user gets a clear picture on the display without ghosts.

Trace ID Code	
Measurement Date and Time	05/29/91 19:00:01
Operator	
Comments	
Measurement Span	0.000 to 4.000 km
Wavelength	1310 nm Singlemode
Group Index	1.458
Pulsewidth	100 ns
Distance Range	Shorthaul
Averages	255
Serial Number, Mainframe	3027G00062
Serial Number, Plug In	3104G00061
Software Version	1.0


```
5.000 dB/DIV        Around A         0.100 km/DIV
                   -107.582 dBm
```
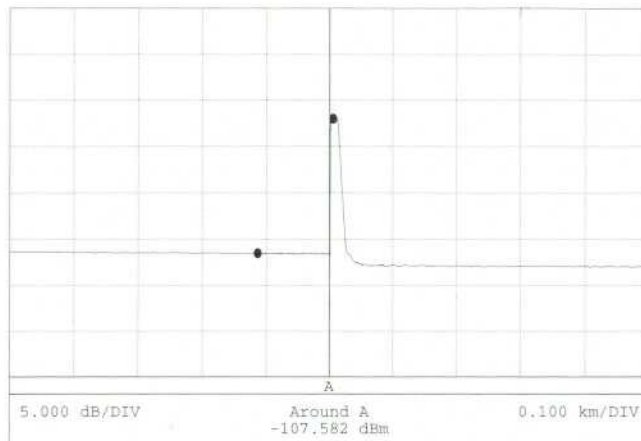
```
Marker Information:    A              1.145  km
                       B              3.997  km
                       Distance       2.852  km
                       Return Loss    23.940 dB
```

(a)


```
5.000 dB/DIV        Around A         0.100 km/DIV
                   -107.582 dBm
```
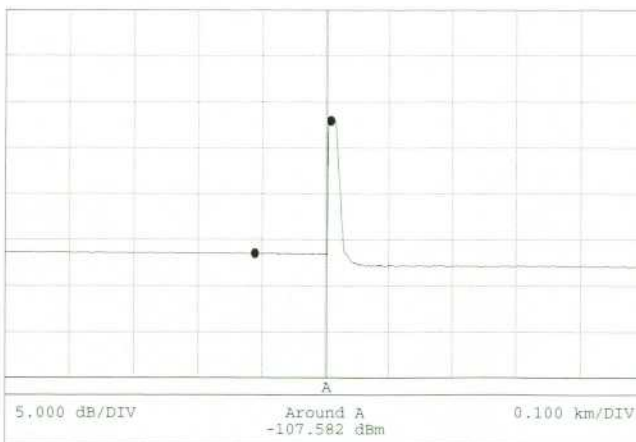
```
Marker Information:    A              1.145  km
                       B              3.997  km
                       Distance       2.852  km
                       Return Loss    29.244 dB
```

(b)

Fig. 7. Return loss measurement. (a) Measurement taken without reduced gain at the beginning, resulting in a wrong return loss value because of clipping. (b) A measurement taken of the same fiber with reduced gain at the beginning. The traces are identical, but there is a 5.3-dB difference in the return loss value from the value computed in Fig. 7a.

Analyzing OTDR Traces on a PC with a Windows User Interface

One of the tasks that is important to OTDR users is the ability to save measurement results on suitable media and to compare results from different measurement sessions. With this capability, users can obtain information about the aging of fibers, observe the effects of bending fibers very early, and do all the statistics that are relevant for evaluating the quality of the transmission link.

Besides offering printers for documenting and saving measurement results, there needs to be software that allows the user of an OTDR to do analysis and documentation tasks on a remote computer such as a PC.

The HP 81460SA (PC_OTDR) is a software package that enables users to communicate with the HP 8146A from a PC. This software offers the means to display OTDR measurement results, measure characteristic values like positions and losses, measure attenuation between events, perform Scantrace for finding and characterizing events, add comments to trace data, and do extensive compares for up to eight traces. All this software runs in the Microsoft®-Windows environment, which almost guarantees easy-to-use operation.

Fig.1 shows the software's main window and some of its child windows (Trace, Overview, and Marker). As the CUA standard suggests,* the PC_OTDR software has as its leftmost menu item the File menu which provides menus items for reading a trace from the disk, saving it, printing it, and exiting the program. Another menu item suggested by the CUA standard is the Help menu on the rightmost side of the main window. The help facility offers all the information necessary to operate the PC_OTDR software without a manual.

The menu items View, Analysis, and Events are PC_OTDR-specific menus. Within the View menu the user can select the child windows to be displayed, and set preferences such as trace colors and distance units. The Analysis menu offers the analysis mode, which displays the result in the Marker window. In the Analysis menu, the user can choose to display either the 2-point loss between markers A and B or the 2-point attenuation (or the least-squares approximation attenuation) between A and B. The Analysis menu can also be used to select the splice mode for positioning auxiliary markers to determine splice loss values and the return loss mode for evaluating the quality of connections.

* The IBM Common User Access (CUA) standard describes how Windows applications should look to make them consistent and easy to use.
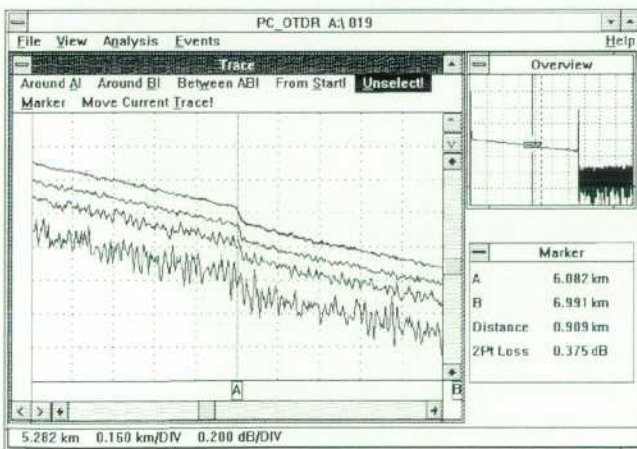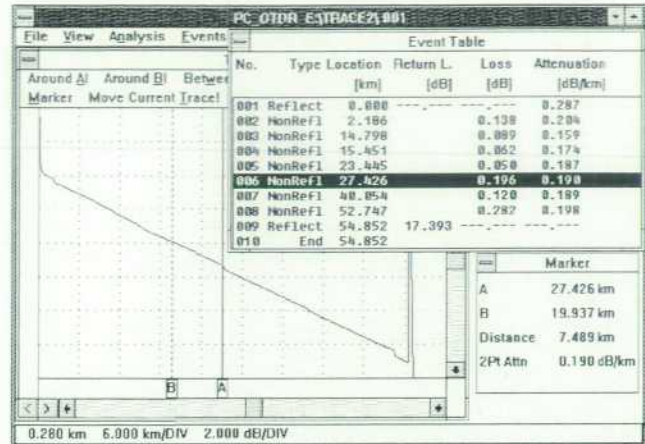
Fig. 2. Windows associated with running the Scantrace algorithm.

The Events menu allows the user to scan a trace for events and its characteristic values, jump between events, add additional events, and delete events from the list.

The child window Trace provides a zoomed-in or zoomed-out display of the traces from a measurement. Fig.1 shows as an example four traces of the same fiber, collected at different times. The top trace shows a measurement that was made directly after the installation of the fiber. Because of bending loss somewhere in the fiber, at about 3 km the power from the fiber became weaker over time resulting in the noisy bottom trace making it difficult to find the splice at marker A. By comparing up to eight traces the user can easily see how the fiber performs over the years. Another useful comparison is to compare traces that were measured with different pulse widths (e.g., 5 ns versus 100 ns) to see the influence of pulse width on resolution.

The Overview window shows where the zoomed-in portion of the current trace shown in the Trace window is located relative to the whole fiber.

The Marker window mentioned above lists the positions of markers A and B, the distance between them, and the result of the analysis mode that was chosen in the Analysis menu.

As with the OTDR, the user can run Scantrace with the PC_OTDR software. The result of such a scan is shown in Fig. 2. The Event Table window lists the types of events and their associated values. With just one mouse click on a single event the user can jump directly into an event to look at details in the Trace window.

Other window features like informative dialog boxes allow the user to easily select traces to be displayed or enter comments and trace information when saving a trace on a disk.

Wilfried Pless
Project Manager
Böblingen Instrument Division

Microsoft is a U.S. registered trademark of Microsoft Corporation.

Fig. 1. The main window of the HP 81460SA software and some of its child windows.

Return Loss Measurement

The return loss of optical components is the ratio of the incident optical power (P_{in}) to the reflected optical power (P_{back}):

$$\text{Return Loss} = 10\log (P_{in} / P_{back}) \qquad (1)$$

Reflections in high-speed transmission lines cause a lot of transmission errors. Therefore, measuring return loss is more and more important. In OTDR measurements the incident power is not known, but we can calculate the incident power by measuring the backscattered signal if we know the scatter coefficient of the fiber. Applying this concept to equation 1 yields the following equation for calculating return loss:

$$RL = C - 10\log (pw/1 \ \mu s) - 10\log \left[10^{(P_{refl} - P_{bs})/5} - 1 \right]$$

where C is the fiber's scatter coefficient, pw is the pulse width of the launch pulse, P_{refl} is the reflected power level, and P_{bs} is the backscattered power level.

This means that we can measure the return loss of a connector with an OTDR if we can measure the peak power level of the reflection caused by the connector and if we know the fiber's scatter coefficient. For the HP 8146A we cannot use standard OTDR measurements because the peak power level exceeds the measurement range of the OTDR's receiver/amplifier section and causes clipping. Some OTDRs must take a separate measurement with reduced gain to measure return loss. The HP 8146A OTDR takes a short measurement with reduced gain at the beginning of every measurement. Only high power levels are of interest, so we don't have to do much averaging. The power levels that will cause clipping in the high-gain measurement are saved in the register database. Every time a user wants to measure the return loss of clipped reflections, these saved power levels are used instead of the actual clipped values. Fig. 7 shows the difference in the return loss value of a measurement taken with and without clipping.

High-Performance Optical Return Loss Measurement

Although high-performance optical return loss measurements pose some tough technical challenges for fiber optics engineers, careful selection of appropriate test equipment and correct setup make precise measurements readily achievable. A new return loss module for the HP 8153A lightwave multimeter simplifies these measurements.

by Siegmar Schmidt

High-speed digital systems and analog cable television systems using fiber-optic media need to employ laser sources with narrow linewidths, such as distributed feedback (DFB) lasers. The narrower the linewidth of a laser, the more sensitive to backreflection it is. If a component reflects too much light back to the laser transmitter, the modulation characteristics and the spectrum of the laser change. This degrades performance in both digital and analog systems. Fabry-Perot lasers can also be affected, depending on their quality and the application. Therefore, reflection measurements on such components become more and more important in R&D and manufacturing.

Reflections in optical systems can come from a variety of sources. Fresnel reflections occur at connectors, splices, fiber ends, bulk optic interfaces, and detector surfaces. For example, reflection from a noncontact fiber connection (a Fabry-Perot resonator) can theoretically vary from 0% to 15% depending on the distance between the fiber endfaces, because of constructive and destructive interference.

In fiber optics it is common to use a logarithmic quantity called the return loss for measuring such optical reflections. It is defined as ten times the negative logarithm of the reflectivity R, which is the ratio of the backreflected optical power to the incoming optical power at a component's input.

$$RL \text{ in } dB = -10\log R = -10\log(P_{back}/P_{in}). \qquad (1)$$

This article describes a method for measuring optical return loss that is both highly accurate and easy to perform.

Return Loss Measurement Method

The following equipment is needed to measure the return loss of an optical component:

- A laser source
- A fiber-optic coupler
- An optical power meter.

The light emitted by the laser source is guided to the test port using the fiber-optic coupler. The light power that is reflected back is guided to the detector of the power meter. Fig. 1 shows the experimental setup. The test port for connector measurements is a master connector to which the connectors under test are connected. For measurements on pigtailed components, the test port is the bare fiber end,

onto which the components are spliced. The slanted connector and the splice in Fig. 1 represent discontinuities between the coupler and the test port that contribute to the parasitic reflections. The parameters K_1 and K_2 are the coupling coefficients of the fiber coupler in the forward and reverse directions, respectively. P_L is the output power of the laser source, and P_D is the power reaching the detector.

Three power levels have to be measured to determine the return loss of a device under test. The first value is the detector power P_{ref} for a known reference reflection R_{ref} attached at the test port. The second value is the detector power caused by parasitic reflections of the setup itself (P_p). The third power level is the detector power with the device under test attached (P_{meas}). Fig. 2 shows the first three steps of the return loss measurement.

Step 1. Measuring the detector power with reference reflection attached (P_{ref}). A known reflectance of R_{ref} at the coupler output port is used to effect an absolute calibration. The optical power at the detector is:

$$P_{ref} = (P_L K_1 K_2)R_{ref} + P_p. \qquad (2)$$

P_{ref} is sum of the detector power caused by the reference reflection and the power offset P_p at the detector caused by the parasitic reflections.

Step 2. Measuring the detector power of the unwanted parasitic reflections (P_p). The unwanted parasitic reflections P_p can be measured by terminating the fiber close to the front of the port. This can be done by wrapping the fiber five times around the shaft of a screwdriver or similar object with a diameter of approximately 5 mm. This creates some 80 dB of insertion loss in the fiber and therefore a two-way loss of
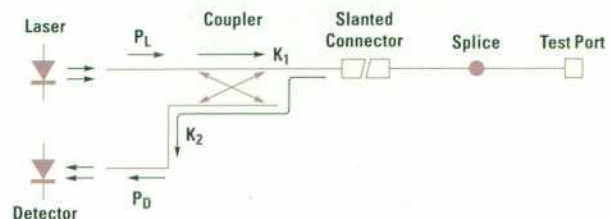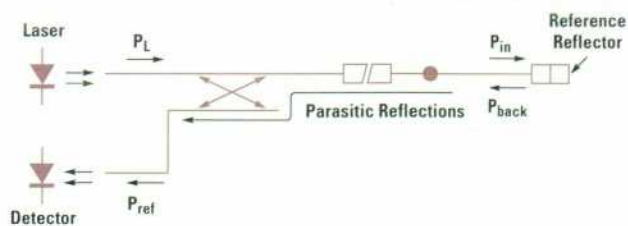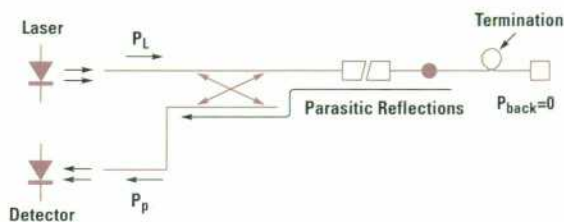

Fig. 1. Experimental setup for optical return loss measurement.

Step 1: Measuring the Detector Power with Reference Reflector Attached.

Step 2: Measuring the Detector Power of Unwanted Parasitic Reflections.

Step 3: Measuring the Detector Power with the Device Under Test Attached.
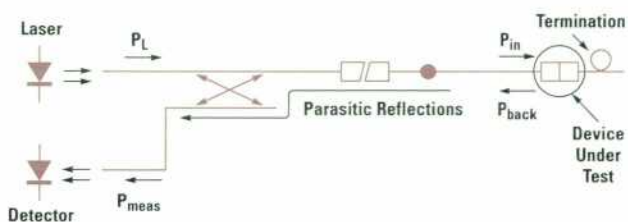

Fig. 2. Steps 1, 2, and 3 of the return loss measurement.

some 160 dB. Since the reflectivity at the test port is zero under this condition, all the power reaching the detector now comes from the parasitic reflections. P_p includes the coupler directivity (direct coupling from port 1 to port 2), reflections from events between the coupler and the test port, and the light scattered back by the fiber itself. The last item should not be forgotten, because 9 meters of single-mode fiber corresponds to a return loss value of approximately 60 dB, and even 1 meter corresponds to some 69 dB of return loss.

Step 3. Measuring the detector power with the device under test attached (P_{meas}). In this step, the device under test is attached to the test port and the fiber is terminated closely behind it. The detector power is now determined by the sum of the power reflected from the device under test and the parasitics.

$$P_{meas} = (P_L K_1 K_2)R_{dut} + P_p. \tag{3}$$

Since it is usual to talk about the return loss of a connector pair, the master connector at the test port is marked as a part of the device under test in step 3 of Fig. 2.

Step 4. Calculating the return loss. A combination of equations 1, 2, and 3 yields the following formula for the return loss of the device under test:

$$RL_{dut} = -10\log[(P_{meas} - P_p)R_{ref}/(P_{ref} - P_p)]. \tag{4}$$

Since the laser power level (P_L) and the characteristics of the fiber coupler are calibrated out in equation 4, only the applied reference reflection value R_{ref} has to be known. A return loss test set should include software that enables the

user to take the calibration measurements easily and that automatically calculates the return loss.

Measurement Uncertainty

Accuracy of the Reference Value R_{ref}. A perpendicular glass-air surface has a reflectivity of 0.035, corresponding to a 14.6-dB return loss for a refractive index $n_{glass} = 1.46$.

$$R_{ref} = [(n-1)/(n+1)]^2. \tag{5}$$

A perpendicular cleave is a good reference if a reliable cleaving tool is used. An open connector should not be used as a reference, since its return loss may vary up to 1 dB (25%) from the ideal value. The reason is that the roughness of the endface depends on the polishing process. For connector return loss measurements, it is better to use a gold-plated connector as the reference. Such a device theoretically offers a reflectivity of 0.98 for the glass-to-gold surface, independent of the polishing process. Because of the nonperfect mating between the connector and the gold reflector, a reflectivity value of 0.96 (0.18 dB return loss) is typically achieved, with a variation of ±2%.

$$R_{ref} = [(n_{gold} - n_{glass})^2 + k^2]/[(n_{gold} + n_{glass})^2 + k^2] \tag{6}$$

where: $n_{gold} = 0.419$
$\quad\quad\quad n_{glass} = 1.46$
$\quad\quad\quad k = 8.42$ (imaginary part of the complex refractive index of gold)
$\quad\quad$ wavelength = 1319 nm.

Polarization Dependence of the Fiber Coupler. In single-mode fibers, two perpendicular polarization states are guided by the fiber. Any kind of movement of the fiber creates mechanical stress, resulting in birefringence. This causes a phase shift between the two polarization states and the resulting polarization of the light in the fiber changes. This can cause a change in the splitting ratio or coupling ratio of a fiber coupler. If the fiber between the coupler output port and the device under test is moved, this also changes the coupling ratio.

The best available couplers offer a polarization dependence of ±1%. However, this ±1% is related to the input power of the coupler. For a 3-dB coupler, the polarization dependence at one of the output ports is ±2%. The total polarization dependence is therefore ±4% because the light has to pass through the coupler twice (downstream and upstream). This is the main reason for fluctuations in the display of a return loss test set when the user moves a patchcord and thereby changes the state of polarization in the fiber.

Power Level Stability of the Laser Source. For all steps of this measurement a constant power level from the laser source is necessary. Any change in power level will influence the calculated return loss value. Therefore, a stabilized laser source is needed.

During reference calibration with the open fiber or the gold reference, a strong reflection back into the laser occurs. It is essential to protect the laser source against this strong reflection, to prevent output power changes. This can be done by putting either an optical isolator or an attenuator between the laser source and the coupler. Optical isolators show excellent isolation with low loss, but at a very high price. On the other hand a 7-dB attenuator together with the 3-dB coupler provides 20 dB of isolation at low cost. Since
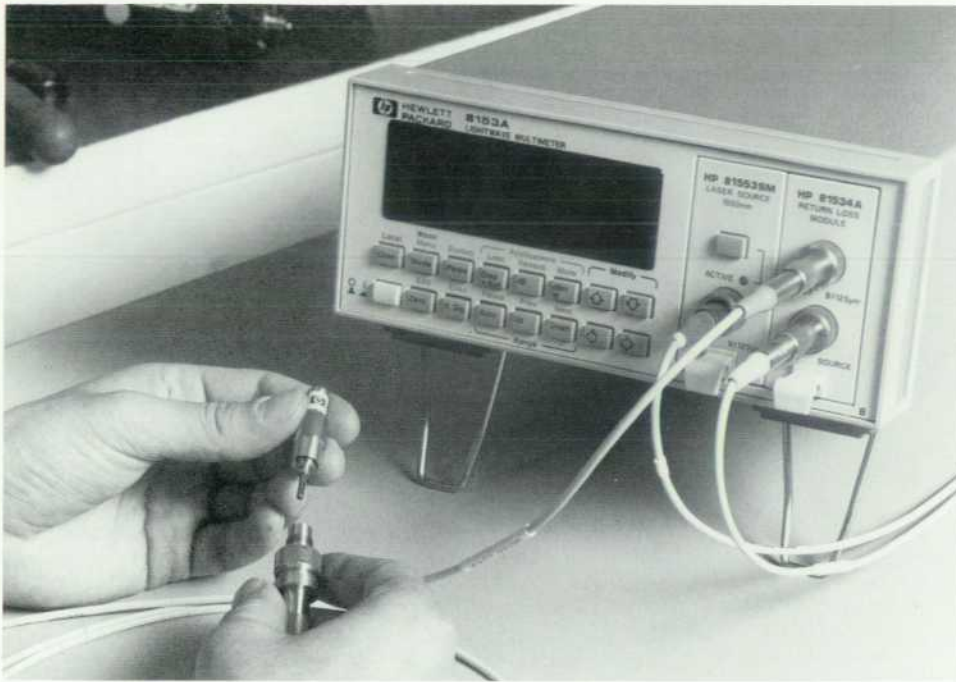
Fig. 3. The HP 8153A lightwave multimeter with laser source and return loss plug-in modules for high-performance return loss measurements.

the power budget usually is not the limiting factor for a return loss measurement and 20 dB is enough isolation for most Fabry-Perot lasers, the attenuator solution is a good cost-effective choice.

Linearity and Long-Term Stability of the Detector. Linearity errors contribute directly to the measurement uncertainty. Therefore, it is important that the detector and the amplification circuits show very good linearity over all measurement ranges. The amplifier usually contributes most to nonlinearity since the transimpedance of the amplifier is switched when the range is changed. This causes step nonlinearities between the ranges. If several ranges are between the level of the reference reflection and the level of the reflectivity of the device under test, these switching nonlinearities add. The detector unit, therefore, should be carefully calibrated for linearity to ensure precise measurements.

Good long-term stability means that the detector unit shows very low drift with time. Low drift makes it possible to measure for a long time before the setup has to be recalibrated.

Dynamic Range of the System. The laser source output power and the receiver sensitivity must offer enough dynamic range to keep the return loss signal well above the noise and display it with adequate resolution even for high return loss values.

Interference Effects. If a laser with a coherence length longer than twice the distance from the coupler to the device under test is used, interference modulation of the detected power at the receiver will occur. Light coming directly from the laser interferes with light coming from the device under test because these two light waves have a fixed phase relationship. The system behaves like a Michelson interferometer. Movement of the fiber will cause a change in the polarization of the interfering waves, resulting in a fluctuating power level at the detector.

Interference occurs when both waves have the same polarization. For perpendicular polarizations, this effect does not happen. The effect shows a maximum if both waves have the same amplitude. For a 3-dB coupler, this means that maximum interference occurs if the return loss of the device under test is 6 dB less than the coupler directivity.* For example, if the directivity is 70 dB, then the maximum interference effect occurs for a return loss of 64 dB. For lower return loss values, the interference effect will be present but not so pronounced.

* In Figs. 1 and 2, a 3-dB coupler will send half of the reflected power to the laser port and half to the detector port. Directivity is a measure of the cross talk between the laser port and the detector port. A directivity of 70 dB means that the laser power seen at the detector port is 70 dB below the laser input power.
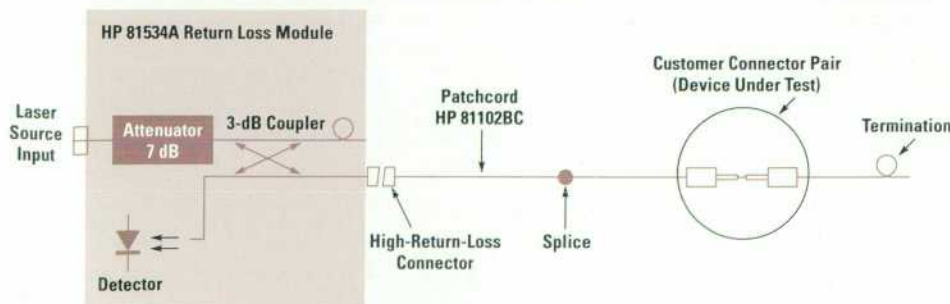

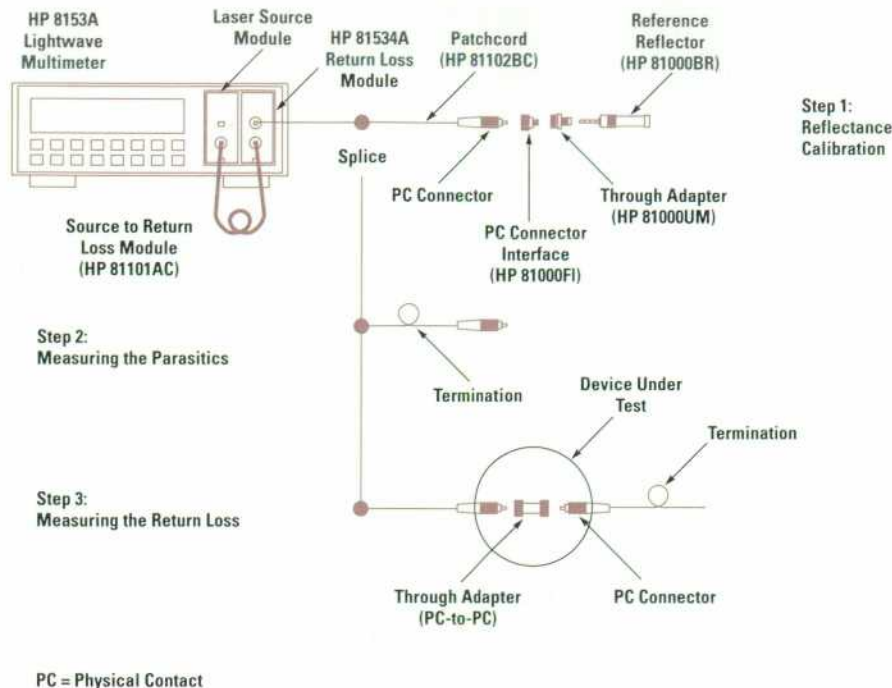**Fig. 4.** Return loss module design.

Fig. 5. Setup for return loss measurements of a PC/PC connector pair.

One possible solution is to increase the fiber length between the coupler and the device under test until it is longer than the coherence length of the laser source. The two light waves will then have no fixed phase relationship, resulting in noncoherent addition of their intensities. However, the spacing should not be exaggerated, since a fiber 9 meters long contributes 60 dB of return loss because of its backscatter.

High-Performance Return Loss Test Set

Hewlett-Packard now offers the HP 81534A return loss module for the HP 8153A lightwave multimeter, which is HP's platform for optical power and loss measurements.[1] The return loss test set is capable of measuring return loss up to 60 dB in the wavelength range from 1250 to 1600 nm. Accuracies of ±0.40 dB and ±0.65 dB are specified for measurement ranges of 0 to 50 dB and 50 to 60 dB, respectively.

Fig. 3 shows the HP 8153A lightwave multimeter with laser source and return loss plug-in modules for high-performance return loss measurements. The instrument can also be configured as a power meter, a 1-channel or 2-channel laser source, or a loss test set. Users therefore have the convenience of all standard optical measurement capabilities in a single instrument.

Fig. 4 shows the return loss module design. The module consists of an input connector for a laser source, an attenuator to protect the source against reflections, a 3-dB coupler, a high-return-loss output connector, and a detector. The user can choose either a plug-in laser source module or an external laser source.

The front-panel connector of the return loss module is a slanted noncontact high-return-loss connector with 65 dB of return loss. Adapter cables (HP 81109AC or HP 81102BC) with the same connector are used as interfaces and ensure both flexible and abrasion-free interfacing to the device under test. A pigtail output is also available as an option. It offers extended measurement range to 65 dB, at the expense of flexibility.

A valuable accessory is the gold-plated HP 81000BR reference reflector, which provides an accurate and stable 0.18-dB reference with just 0.1-dB uncertainty for connector return loss measurements. This external referencing, together with the built-in software, makes it possible to take a precise reference measurement at the plane of the device under test. All parasitic reflections, both inside the instrument and outside, can be calibrated out at the push of a button.

Fig. 5 shows the procedure for measuring the return loss of a PC/PC connector pair.* Steps 1 and 2 only have to be done once. It is only necessary to retake the reference measurement if the setup is modified.

Reference

1. B Maisenbacher and W. Reichert, "A Lightwave Multimeter for Basic Fiber Optic Measurements," *Hewlett-Packard Journal*, Vol. 42, no. 1, February 1991, pp. 58-63.

* PC = physical contact.

High-Speed Time-Domain Lightwave Detectors

The HP 83440 Series unamplified p-i-n lightwave detectors are designed for the best possible pulse performance. They are dc coupled and have bandwidths of 6, 20, and 32 GHz. They mate directly with high-speed sampling oscilloscopes.

Randall King, David M. Braun, Stephen W. Hinch, and Karl Shubert

Fiber-optic systems used in the telecommunications industry typically carry information as intensity-modulated digital pulses at rates from less than 100 megabits per second to 2.5 gigabits per second. Development of even faster systems at 10 and 20 Gbits/s is underway at research labs around the world. Current production testing and development of next-generation systems require specific types of optical test equipment. One important example is the time-domain lightwave detector.

Much information about the performance of a fiber-optic system can be gained from accurate information about the shape of optical pulses in the time domain. For instance, telecommunication systems often use a directly modulated laser as a source. The output of such a source (Fig. 1) is far from ideal. Excessive overshoot or ringing, high levels of timing jitter, and slow rise or fall times can all lead to erroneous detection of digital ones and zeros. Accurate characterization requires a measuring system with a bandwidth sufficient to capture the aberrations as well as the fundamental data stream.

The most common approach to studying optical pulses requires first converting the optical signal to an equivalent electrical signal and then displaying the waveform on an oscilloscope. For accurate reproduction of arbitrary input data streams, the converter must achieve constant gain and linear phase response from dc to the highest frequency present at the input. The best pulse performance is currently obtained with high-speed lightwave detectors based on unamplified p-i-n photodiodes. The addition of electrical amplification, while improving sensitivity, degrades the pulse response. The modest output of unamplified detectors can be a problem because a communications system's multivalued nonrepetitive data streams cannot be simply time-averaged to reduce noise. The choice between high sensitivity and the best pulse performance must be made for each application.

The recent advent of erbium-doped fiber amplifiers gives some users the opportunity to amplify in the optical domain and then use unamplified p-i-n detectors. The extremely high bandwidth and low noise of these amplifiers makes this an excellent approach. The drawbacks are the current high cost of erbium-doped fiber amplifiers and their restriction (at least at present) to 1550-nm operation.

The HP 83440 Series unamplified p-i-n lightwave detectors (Fig. 2) are designed specifically for customers who want the best possible pulse performance and do not need high sensitivity. They are dc coupled and have bandwidths of 6, 20, and 32 GHz. They are intended to mate directly with high-speed sampling oscilloscopes. They combine p-i-n photodiode technology (see page 85) with careful optical, electrical, mechanical, and manufacturing process development.

Detector Mechanical Design

The HP 83440 detectors are compact and rugged instruments that attach directly to an oscilloscope input. The form factor is inline: optical signal in one end and electrical signal out the other. This allows the use of multiple detectors on one test set. The optical input uses the Diamond HMS-10/HP connector.[1] This bulkhead connector has become the standard optical interface in HP's lightwave test equipment because of its high reliability, long lifetime, and good repeatability. The optical input can accept a variety of connector types by selecting different adapters.

The RF output of the detector screws to the input port of the oscilloscope, providing the sole mechanical support of the

Fig. 1. Typical output waveform of a directly modulated laser.

Ch. 2 = 7.000 mVolts/div   Offset = 22.62 mVolts
Timebase = 600 ps/div   Delay = 17.9520 ns

17.9520 ns   20.9520 ns   23.9520 ns

Fig. 2. Four HP 83440 Series lightwave detectors mounted on an HP 54124T oscilloscope.

detector. The APC 3.5-mm male connector was chosen because of its SMA compatibility, mode-free operation to 34 GHz, and suitability as a make-and-break test connector. The 32-GHz detector uses the APC 2.4-mm connector for frequency response to 50 GHz.

Fig. 3 is an exploded view showing the component parts of an HP 83440 detector. The optical connector flange provides one end cap for the instrument. The microcircuit serves as the other end cap. The dc supply provided by the user is regulated and limited on the printed circuit board before connection to the microcircuit. Protection of the photodiode from power supply related damage is a significant convenience to users who previously used component-level detectors. The extruded aluminum body has locating slots for the printed circuit board, optical fiber, and sheet-metal lid. The endplates are screwed into the extrusion, capturing the printed circuit board and lid.

Component Mechanical Design

From the beginning of the project, we wanted the photodiode package to be hermetic. The mesa InGaAs photodiode structure can be quite sensitive to moisture, showing increased dark current and noise. The usual semiconductor reliability problems are also a concern when water vapor is present. Hermeticity, however, is a matter of degree. Any microcircuit will eventually equilibrate with its external environment. The question is how long that process will take. In microcircuit production, this corresponds to choosing a maximum permissible leak rate. For the HP 83440 project, we originally assumed that we would use military leak testing procedures (MIL-STD-883C is the de facto industry standard). However, this specification could allow the microcircuit to equilibrate to ambient conditions within several weeks.[2] We considered this unacceptable and tightened the leak rate requirement by several orders of magnitude. This ensures many years of protection for the device, but requires special calibration and testing procedures.

To meet this stringent standard, the microcircuit package must be sealed with glass and metal. The body and lid are machined from stainless steel, then gold-plated for solder wettability and electrical conductance. Glass-to-metal seals are soldered into the microcircuit body for the dc and RF package feedthroughs. A lens is soldered into the microcircuit lid to provide a hermetic optical feedthrough. This allows the optical fiber to be attached with epoxy, since it is outside the hermetic wall.

After the photodiode and other circuit elements are die-attached to the microcircuit floor and wire-bonded, the lid is soldered to the body in a dry, helium atmosphere. A 48-hour high-temperature vacuum bakeout ensures the removal of
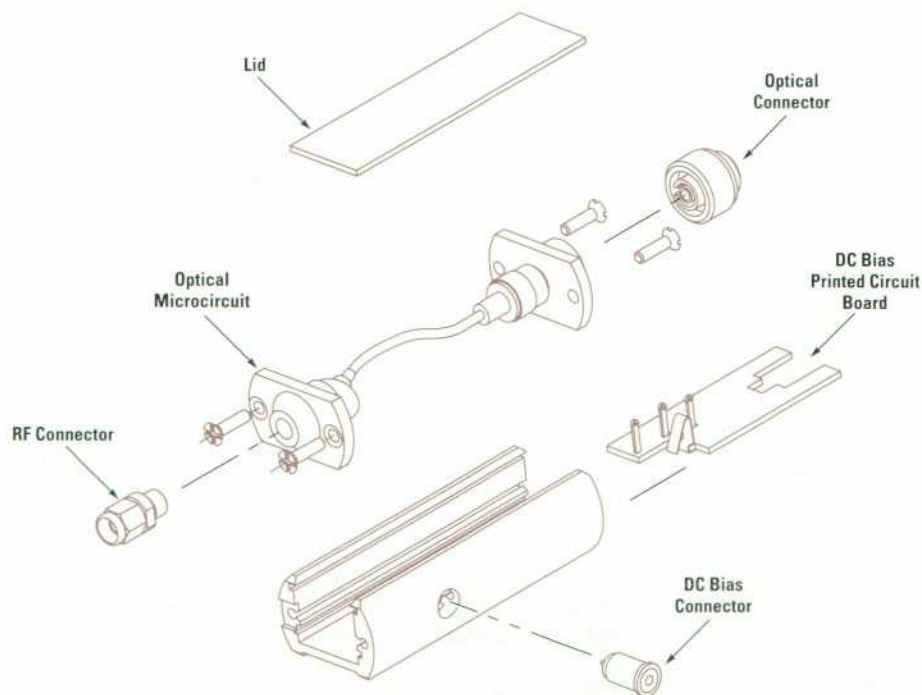

Fig. 3. Internal components of an HP 83440 Series lightwave detector.

InP/InGaAs/InP P-I-N Photodetectors for High-Speed Lightwave Detectors

The HP 83440 family of lightwave detectors uses custom InP/In$_{0.53}$Ga$_{0.47}$As/InP p-i-n top-illuminated mesa photodetectors to absorb incoming infrared light and convert it to photocurrent. These devices allow light with wavelengths from 1.2 to 1.6 μm to pass through the antireflection coating and the top p-type InP layer and be absorbed in the intrinsic InGaAs active layer below. The absorption of photons creates electron-hole pairs in the active layer. These carriers are swept out by a reverse bias, resulting in a photocurrent.

The photodetector epitaxial material is grown by organometallic vapor phase epitaxy (OMVPE) on InP:S substrates (see Fig. 1). A buffer layer of undoped InP is used to facilitate the growth of the lattice-matched intrinsic InGaAs active layer and the p-doped InP:Zn layer is grown on top. The device contains a metal contact ring to the p-layer, an antireflection coating, polyimide passivation, and a plated gold bond pad.[1] The mesa structure is used to achieve low capacitance for high-speed applications.

Both the RC time constant of the device and the carrier transit time across the InGaAs layer determine the frequency response of the photodiode. A low capacitance is achieved by having a thick intrinsic layer and a small area, while a short transit time calls for a thin intrinsic layer.[2] HP lightwave detectors contain photodiodes designed to optimize this trade-off for specified 3-dB frequency responses from 6 GHz to 32 GHz.

Devices like the one shown in Fig. 2 are used in the HP 83440D and have measured 3-dB optical bandwidths in excess of 39 GHz. These devices have a 14-μm
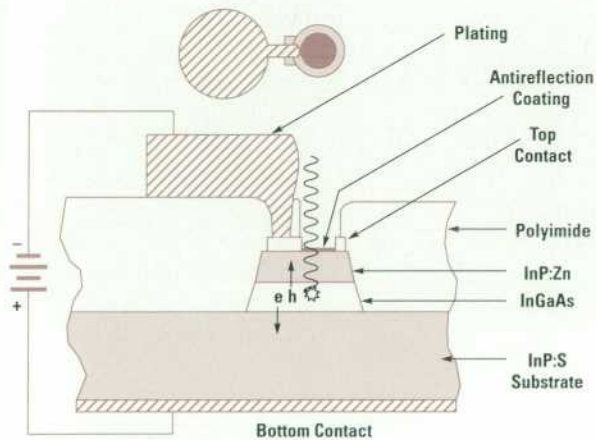

Fig. 2. Scanning electron micrograph of the photodiode used in the HP 83440D lightwave detector.

Fig. 1. Photodetector cross-sectional view. Incoming light is converted to electron-hole pairs in the InGaAs intrinsic layer, resulting in an electrical current.

active-area diameter and are designed for low dark current, low capacitance, low optical reflections, and high dc responsivity. Measured dark currents at −3V are subnanoampere (2×10^{-5} A/cm^2) and capacitance values measured at 1 MHz are approximately 0.07 pF (1.4×10^{-9} F/cm^2). Optical reflections from the top surface of the device are under 2% at 1300 nm and 1550 nm. The thinner i-layer required to achieve high-speed performance limits dc responsivity (the ratio of photocurrent output to optical power input) somewhat because of the shorter absorption length, especially at longer wavelengths. Measured responsivities are 0.59 A/W at 1300 nm and 0.47 A/W at 1550 nm. The devices are highly reliable in HTOL (high temperature operating life) testing with MTTF (median time to failure) of $>6\times10^{7}$ hours at 55°C, and < 1 FIT (failure in 10^9 device hours of operation).

References

1. S. Sloan, "Processing and Passivation Techniques for Fabrication of High-Speed InP/InGaAs/InP Mesa Photodetectors," *Hewlett-Packard Journal*, Vol. 40, no. 5, October 1989, pp. 69-75.
2. J.E. Bowers, et al, "Millimetre-Waveguide-Mounted InGaAs Photodetectors," *Electronic Lettres*, Vol. 22, 1986, p. 633.

Susan Sloan
Project Manager
Microwave Technology Division

most absorbed moisture before sealing. Residual gas analysis results indicate that the moisture content is below the detection level of 100 ppm.

Detector Optical Design

The goal of the optical launch is to couple light from the input fiber to the photodetector with high efficiency, good alignment tolerance, and high optical return loss. Common types of coupling schemes include butt-coupling of the fiber directly to the photodiode, using a lensed fiber to focus the light, or using separate lensing. We decided against butt-coupling because of the tight alignment tolerance required for our small-area detectors. Lensed fibers were rejected because their short focal lengths make them sensitive to axial motion. We selected a single graded-index (GRIN) cylindrical lens as best meeting our design objectives.
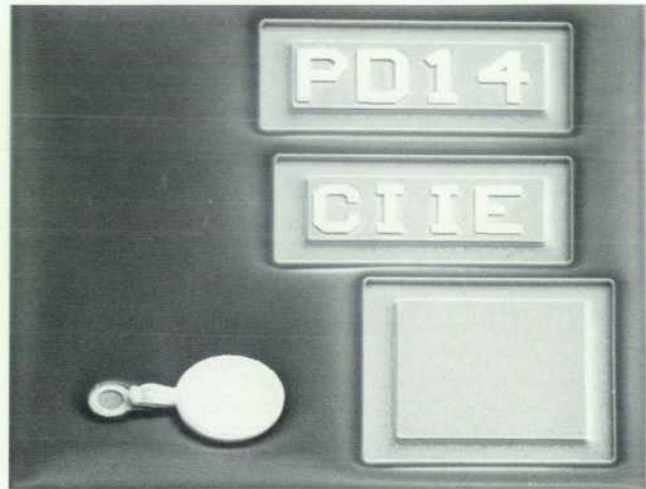
The input fiber is polished at a bevel and the photodiode is tilted with respect to the optical axis. One endface of the lens is beveled and both faces are antireflection-coated. This results in optical return losses that are typically greater than 50 dB at each interface. This is significantly better than the optical connector, which limits the overall instrument specification to 33 dB.

For the 6-GHz and 20-GHz products, the GRIN lens surfaces are planar and 1:1 imaging of the fiber endface is used. The active area of the 32-GHz photodiode is 14 micrometers in diameter and is too small for this approach. Instead, we use a planoconvex GRIN lens whose convex endface reduces spherical aberration. Combined with a magnification of more than 2:1, this arrangement provides good fiber alignment tolerance and high efficiency. One drawback is that the

photodetector must be placed quite accurately with respect to the optical axis or the GRIN lens will distort optical rays that are too close to the periphery of the lens.

The alignment of the optical fiber to the photodetector is made actively while monitoring the photodiode output. The fiber is then locked in place using a specialized high-stability epoxy. Extensive environmental strife (stress + life) testing was performed on prototypes to ensure the performance and reliability of the attachment method.

Detector Electrical Design

The major objective of the HP 83440 electrical design was to optimize the time-domain performance by minimizing pulse aberrations. By designing the instrument to connect directly to the oscilloscope and by placing the photodiode as close as possible to the connector, signal distortion from unnecessary components is eliminated. Careful design of the bias circuitry avoids resonances. As a result the HP 83440 family has excellent performance in both time and frequency domains (see "Calibration of Lightwave Detectors to 50 GHz," page 87).

High-speed photodiodes, because of their small size, are sensitive to electrostatic discharge damage. The power supply connection can withstand a ten-thousand-volt discharge. However, the RF connector cannot be protected without degrading performance. Caution must be exercised during the connection process, but a protective cap is supplied for use during storage.

Summary

The HP 83440 Series is a family of high-speed unamplified p-i-n photoreceivers designed for optimum time-domain performance. Attaching directly to sampling oscilloscopes, they find applications in the design and characterization of fiber-optic telecommunication systems. Their careful design and extensive reliability testing ensure a long life while providing state-of-the-art optical time-domain measurements.

Reference

1. W. Radermacher, "A High-Precision Optical Connector for Optical Test and Instrumentation," *Hewlett-Packard Journal*, Vol. 38, no. 2, February 1987, pp. 28-30.

2. J.G. Davy, "How to calculate the true permissible leak rate and how to raise it by four orders of magnitude," *IEEE Transactions on Components, Hybrids, and Manufacturing Technology*, Vol. CHMT-8, no. 3, September 1985, pp. 359-365.

Calibration of Lightwave Detectors to 50 GHz

Because they operate at much higher frequencies than previous products, new methods had to be found to test and calibrate the HP 83440 Series lightwave detectors. Three systems were developed. Their results agree closely.

by David J. McQuate, Kok Wai Chang, and Christopher J. Madden

The HP 83440 Series lightwave detectors described in the article on page 83 are a family of optical-to-electrical converters that includes models with bandwidths above 20 GHz. To test and calibrate these detectors, a higher-frequency test system was required. In this article we describe three systems that can be used to characterize high-speed lightwave converters. The first is a time-domain system that measures a photoreceiver's response to a short optical pulse. In the second system, two lasers are heterodyned to generate a test signal for a photoreceiver. The third system establishes an optical modulator as a calibrated source, which then is used to measure a photoreceiver's bandwidth. We present results that show good agreement among the systems on measurements of a photoreceiver's frequency response.

Optical Impulse Test System

Picosecond pulses are generated by a system consisting of a mode-locked Nd:YAG laser and a fiber-grating pulse compressor (Fig. 1). The laser produces 80-ps FWHM (full width at half maximum amplitude) pulses at an 80-MHz rate, a wavelength of 1060 nm, and an average power of 20 watts. The pulse compressor uses self-phase modulation and positive group velocity dispersion in single-mode fiber to broaden the pulse spectrum and linearly frequency modulate (chirp) the pulse as it propagates through the fiber.[1]

The diffraction grating pair introduces a time delay proportional to wavelength. When the chirped and spectrally broadened pulse is passed through the gratings, the pulse is compressed to about 2 ps FWHM.
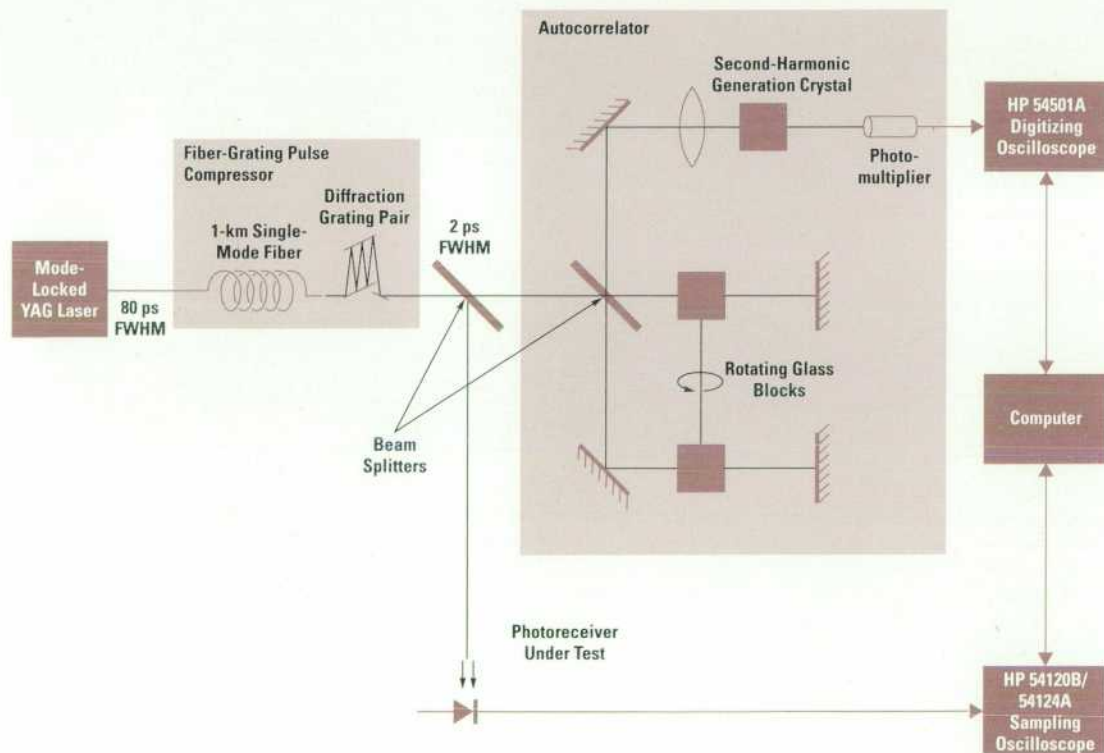

Fig. 1. Optical impulse response measurement system for photoreceiver characterization. An 80-ps FWHM pulse from a mode-locked YAG laser is compressed to about 2 ps FWHM by a fiber diffraction grating compressor. The width of the compressed pulse is measured by an autocorrelator. Digital oscilloscopes record the outputs of the autocorrelator and the photoreceiver being measured.

We cannot measure the shape of such a short pulse directly, but we can measure its autocorrelation function, from which we can calculate the power spectral density of the pulse and make estimates of its width. The autocorrelator splits the input beam into two paths, which pass through rotating rectangular glass blocks arranged to introduce a periodically swept differential delay. The two beams then meet in a LiIO$_3$ crystal which generates the second harmonic (at 530 nm), with an amplitude proportional to the product of the intensities of the two beams. This shorter-wavelength light is detected by a photomultiplier tube. The output signal traces out the optical pulse's autocorrelation function as the glass blocks rotate.

An HP 54501A digitizing oscilloscope records the output of the autocorrelator. The Fourier transform of this time record is the power spectral density of the optical impulse. Our measurements show a drop in power of only three decibels at 60 GHz.

Measurement of Photoreceiver Impulse Response

Once we have characterized the optical impulse, we can measure a photoreceiver's response to it. The optical impulse is focused on the photoreceiver. An HP 54120B sampling oscilloscope with an HP 54124A 50-GHz test set records the receiver's response. The measured trace is the convolution of the optical impulse with the impulse responses of the oscilloscope and the photoreceiver (Fig. 2).

The Fourier transform of the measured trace is the power spectral density of the impulse, but filtered by both the oscilloscope and the photoreceiver. The photoreceiver's
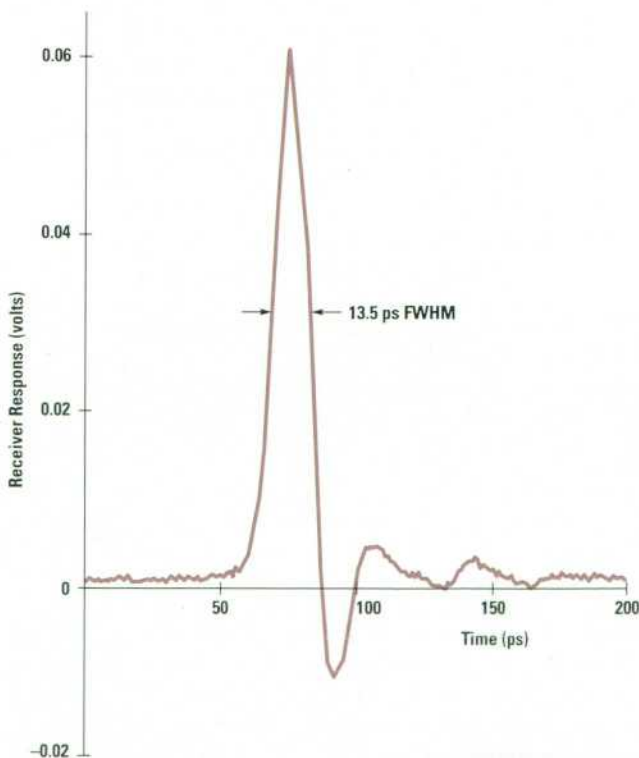

Fig. 2. The response of an HP 83440D lightwave detector and HP 54120B/54124A sampling oscilloscope to the compressed optical pulse. Some of the ringing and overshoot is attributable to the photodetector, and some to the oscilloscope.

frequency response can be obtained by dividing the measured spectrum by the optical pulse's power spectral density and by the oscilloscope's frequency response. The latter can be obtained by CW measurements using a microwave synthesizer and a microwave power meter, or by using two similar sampling oscilloscopes to measure each other's sampler impulse responses.[2]

Optical Heterodyne Test System

A second system for characterization of lightwave receivers to 50 GHz is shown in Fig. 3. An optical heterodyne source was built using a pair of diode-pumped Nd:YAG ring cavity lasers whose nominal wavelength of 1320 nm could be varied by changing the laser crystal temperature. The output beam from each laser passes through an optical isolator, a shutter, and a half-wave plate. The two beams are then combined in a fiber-optic 3-dB coupler/splitter. The isolators protect the lasers from feedback resulting from optical reflections. The shutters allow measurement of each individual laser's average power. The half-wave plates allow rotation of each laser's optical polarization. Good polarization alignment is obtained using an HP 8509A polarization analyzer and is maintained using a 3-dB coupler made from polarization preserving fiber. The output power (P_1 and P_2) is typically 1 mW from each laser at each of the coupler's outputs. Previous dual-YAG heterodyne systems measured photoreceiver frequency response to 22 GHz[3] and 33 GHz.[4]

Let the difference between the laser frequencies be f_d. If the laser outputs are linearly polarized and aligned, the optical power modulation envelope seen by a photoreceiver is:

$$P_{opt} = P_1 + P_2 + 2\sqrt{P_1 P_2}\cos(2\pi f_d t).$$

If $P_1 = P_2$ the resulting signal is 100% modulated at the difference frequency.

The difference frequency f_d is tuned by adjusting one laser's temperature and leaving the other's fixed. It can be tuned continuously over about 25 GHz before the laser hops to a different longitudinal mode. Since the mode spacing is about 15 GHz, a wider scan can be obtained by "stitching" together the continuous tuning curves from several adjacent modes. For a 50-GHz span, five curves are used. The overall tuning rate is about 1 GHz/°C.

A calibration of the temperature-versus-frequency tuning characteristic is done just before the measurement of a photoreceiver. An HP 71400C lightwave signal analyzer is used. Since it has a 22-GHz bandwidth, the calibration is done in three overlapping tuning ranges. During six months of testing, the repeatability of the frequency calibration was about 50 MHz. The drift of the difference frequency was measured at 15 MHz in 30 minutes. The linewidth is specified at <3 kHz.

In the test system, one of the coupler/splitter's outputs is connected to the photoreceiver to be tested while the other is used for monitoring laser power. The electrical signal from the photoreceiver being measured passes through an attenuator (which provides a dc bias path) and is measured with a microwave power meter (HP 8487D/437B). A measurement of the frequency response involves scanning the difference frequency and measuring the change in output microwave power.
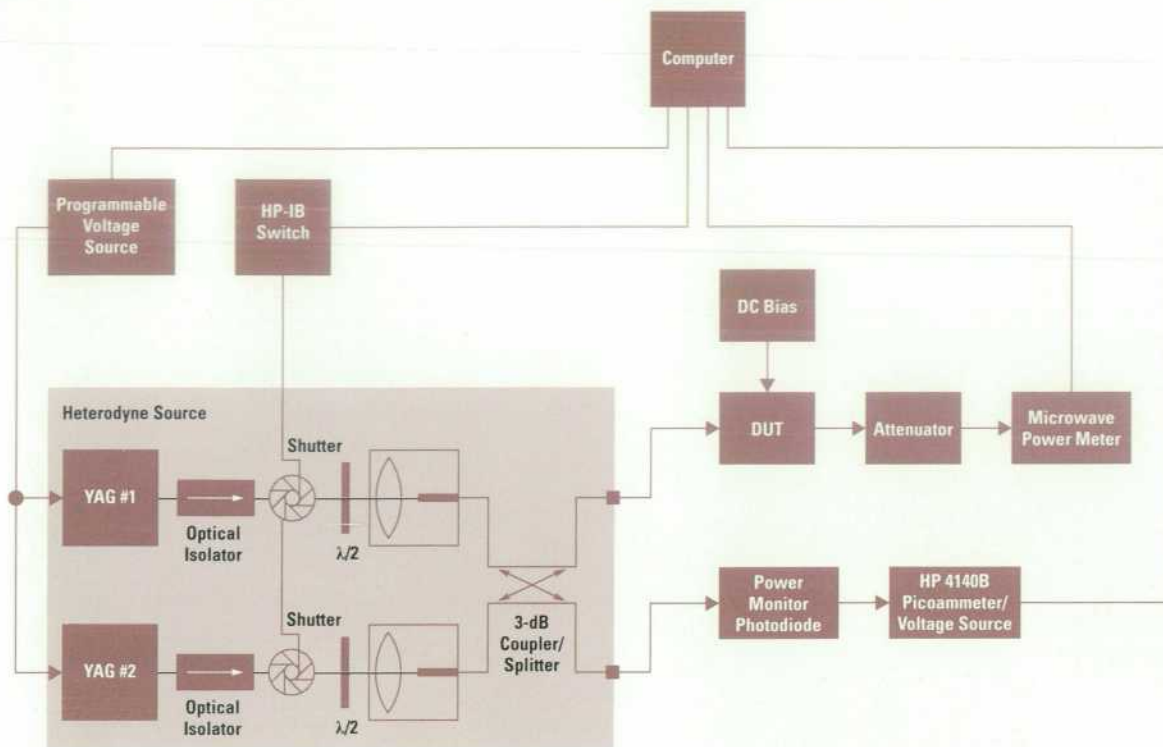
Fig. 3. Dual YAG heterodyne frequency response measurement system. Infrared light from a pair of temperature-tuned diode-pumped YAG ring lasers is combined in a 3-dB single-mode fiber coupler. The envelope of the optical power varies at the difference frequency. The response of the photoreceiver being tested is measured using a microwave power meter while the difference frequency is swept.

A photodetector produces a current proportional to the optical power received. The ratio of output current to input optical power is its responsivity, R_d, in amperes per watt. For an input optical power of $P_{RF\ optical}$, the peak photocurrent is $R_d P_{RF\ optical}$, and the electrical power delivered to the detector's load resistor, R_{load}, is $P_e = i^2 R_{load}$ or

$$P_{RF\ electrical} = \left(R_d P_{RF\ optical}/\sqrt{2}\right)^2 R_{load}.$$

Since we have a heterodyne source, we substitute $P_{RF\ optical} = 2\sqrt{P_1 P_2}$. We solve for responsivity, explicitly showing its frequency dependence, take the ratio of responsivity at a given measurement frequency f_m to that at the lowest measurement frequency f_0, and convert to decibels. Then the responsivity relative to that at the lowest frequency is:

$$R_{dB\ electrical} = P_{dBm\ electrical}(f_m) - P_{dBm\ electrical}(f_0)$$
$$- 10 \log \frac{P_1(f_m)P_2(f_m)}{P_1(f_0)P_2(f_0)}.$$

Corrections are also made at each frequency for the variation in the optical power output of each laser, and for the actual loss in the attenuator. Residual ripple in the response measurement is caused by standing waves resulting from microwave reflections.

Modulator-Based Frequency Response System

The frequency response of an optical receiver can also be determined by measuring its response to a calibrated modulated optical source. In this third system, a lithium niobate Mach-Zehnder interferometer,[5,6,7] used as an optical amplitude modulator, is characterized so that it becomes a calibrated source. We'll first describe the modulator and its calibration, and then show the system of which it is a part.

A voltage applied to the modulator's electrodes alters the relative phase of the light in the two arms of the interferometer, which in turn controls the amount of light transmitted through it. Its transfer function varies sinusoidally with the applied voltage. If we apply both a dc bias voltage, V_b, and a sinusoid with radian frequency ω, the transmitted light is:

$$I(t) = \frac{I_0}{2}\left[1 + \cos\left(\pi\frac{V_b + E(\omega)V_p\cos(\omega t)}{V_\pi}\right)\right],$$

where: $I(t)$ = transmitted light power
  I_0 = maximum transmitted light power
  V_b = dc bias voltage
  $E(\omega)$ = a frequency dependent modulation "efficiency"
  V_p = peak signal voltage applied to the modulator
  V_π = characteristic switching voltage of the modulator.

We can select the operating point on the modulator's transfer curve by adjusting the dc bias. The modulation "efficiency" decreases with increasing modulation frequency for two reasons. First, the modulation signal travels more slowly down its transmission line than the optical signal in its waveguide. The two tend to get more out of phase with each other towards the end of the modulator as the modulation frequency increases. Second, the transmission line loss increases with increasing frequency so that the modulation voltage becomes weaker.

By expanding the above expression in a Bessel series, effectively transforming it to the frequency domain, we can

examine the spectral content of the modulated light. We use the identity:

$$\cos[z\cos(x)] = 2\sum_{k=1}^{\infty}(-1)^k J_{2k}(z)\cos(2kx)$$

and identify the Bessel function argument as:

$$z = \pi\frac{V_b + E(\omega)V_p}{V_\pi}.$$

We are interested in three special cases in which we select a single spectral component and set the modulator bias to maximize it. In each case the infinite sum reduces to a single term. These three expressions allow us to measure the modulator's frequency dependent efficiency and use it to calculate the modulated optical power at any harmonic of any given modulation frequency.

Modulator Calibration. In case 1, the modulator is biased to minimum transmission and two modulation signals are applied with frequencies ω_1 and ω_2 and peak voltages V_{p1} and V_{p2}. Among other signals there will be a difference frequency component

$$I(\Delta f) = I_0 J_1\left(\pi\frac{E(\omega_1)V_{p1}}{V_\pi}\right)J_1\left(\pi\frac{E(\omega_2)V_{p2}}{V_\pi}\right).$$

If we place the two modulation signals very close in frequency, $E(\omega_1)$ is essentially the same as $E(\omega_2)$. We measure I_0, V_π, the applied voltages V_{p1} and V_{p2}, and the optical power at the difference frequency, $I(\Delta f)$, and then solve this expression numerically for $E(\omega)$.

By stepping ω, we determine $E(\omega)$ for the whole range of modulation frequencies. We keep the difference frequency low and constant during these measurements so that we can use an inexpensive photoreceiver whose frequency response we need not know.

Fundamental Operation. In case 2, the modulator is biased at its half-power transmission point. At the modulator's output, the fundamental frequency component of the modulated light is:

$$I = I_0 J_1\left(\pi\frac{E(\omega)V_p}{V_\pi}\right).$$

Given $E(\omega)$ and V_π, a measurement of V_p and I_0 allows us to calculate the magnitude of the modulated light at any given modulation frequency.

Second-Harmonic Operation. When the modulator is biased at the minimum of its transfer curve and modulation is applied, the power in the second harmonic is:

$$I = I_0 J_2\left(\pi\frac{E(\omega)V_p}{V_\pi}\right).$$

As above, if $E(\omega)$ and V_π are known and we have measurements of V_p and I_0, we can calculate the modulated light power at the second harmonic. Second-harmonic operation allows us to modulate light at frequencies higher than those for which we have amplifiers with which to drive the modulator.

Modulator-Based Frequency Response Measurement
The calibrated optical modulator is placed in the system shown in Fig. 4, which also contains a CW semiconductor laser with optical isolator, a microwave amplifier, and a vector network analyzer (HP 8510C with HP 8517A 50-GHz test set and HP 83651A synthesized source), which provides a microwave source and receiver.

The microwave source is modified by adding a coupler to provide a sample of the synthesized signal just before the final frequency doubler. This signal, amplified by the microwave amplifier, drives the microwave input of the optical
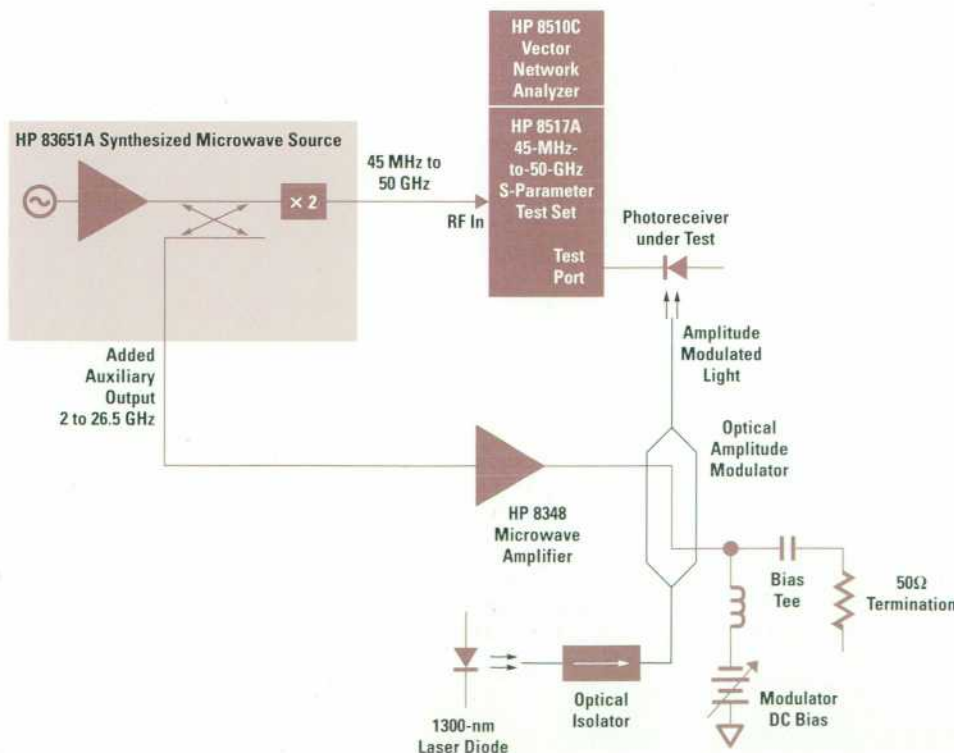

Fig. 4. Lightwave HP 8510 frequency response measurement system. A calibrated optical modulator modulates light from a diode laser, producing either the fundamental or the second harmonic of the microwave drive signal. The HP 8510 network analyzer measures both the output electrical reflection coefficient of the photoreceiver being tested and its response to the modulated light.

modulator. When the system is operating below 26.5 GHz, the modulator is operated in fundamental mode. Above that frequency, the optical modulator doubles the modulating frequency, producing, for example, light modulated at 50 GHz when electrically driven at 25 GHz. The normal output of the synthesizer provides the microwave reference signal for the test set.

In characterizing a photoreceiver, the network analyzer is first used in its native electrical-to-electrical mode to measure the photoreceiver's electrical reflection coefficient. Then the modulated light is turned on and the network analyzer is used as a calibrated power meter to measure the photoreceiver's electrical response to the calibrated optical source. A standard vector network analyzer full two-port calibration removes the effect of standing waves caused by the photoreceiver's output impedance mismatch.

Comparison of the Systems

Each of the three systems has its advantages. The optical impulse system allows direct measurement of the impulse response of a photoreceiver-oscilloscope pair. If the oscilloscope's impulse response can be accurately determined, the photoreceiver's impulse response can be closely estimated, since the optical impulse is so much narrower. The measurement is fast. The time required to calculate the Fourier transforms might easily exceed the time it takes to obtain the data. Because the autocorrelator provides a time record of only about 120 ps, we have data on the impulse spectrum only above about 8 GHz. This determines the measurement's low-frequency limit and its frequency resolution. However, the measurement frequency range extends above 100 GHz.

The heterodyne technique's measurements are most easily referenced to U.S. NIST standards. It is also the one most easily extended to higher frequencies. A higher-frequency microwave power meter is required, and the frequency-versus-temperature curves need to be extended. In its present form, frequency accuracy and repeatability limit the heterodyne technique's frequency resolution to about 50 MHz. Increased frequency accuracy can be obtained by measurement of the difference frequency while a photoreceiver's frequency response is being measured, or by phase-locking to an external reference. The system tends to be slow because the laser wavelength is tuned thermally.

The optical modulator system benefits from its constituent vector network analyzer. Frequency resolution is limited only by the synthesized microwave sources, so that resolution on the order of one hertz is possible. Using this system, a microcircuit cavity resonance about 50 MHz wide was easily seen. This resonance has been eliminated in newer photodetectors. Measurement of the photoreceiver's vector electrical reflection coefficient makes it possible to eliminate the effect of standing waves on the frequency response measurement. Time-domain characterization of a photoreceiver, which is available with the HP 8703A, is possible if the phase response of the measurement system is characterized. Like the heterodyne technique, the optical modulator system's measurements are ultimately referenced to power meters, optical and electrical, and thence to NIST. This system can also be used to characterize electrical-to-optical converters once a photoreceiver has been characterized. Measurements made on the system are repeatable because of the synthesized microwave source and stable microwave

test set. The measurement speed depends on the means used to measure the microwave drive to the optical modulator. A system could be built which would operate at the same speed as a standard HP 8510 measuring microwave s-parameters.

Comparison of Measurement Results

Fig. 5 shows excellent agreement on the frequency response of an HP 84330D lightwave detector, whose electrical bandwidth is specified to be at least 32 GHz, as determined by four measurement systems. Below 20 GHz the HP 8703A and the modulator-based system show very similar results. These two systems are very similar in concept. The 50-GHz system uses higher electrical and optical power, so the signal levels are farther above the noise floor; this results in lower random variation in the measurement results.

The dual-YAG data was taken in five slightly overlapping bands. The small differences in responsivity measured at the overlap points indicates good repeatability and low random variation. The measurement made on the optical impulse system is consistent with the others, within estimated uncertainties.
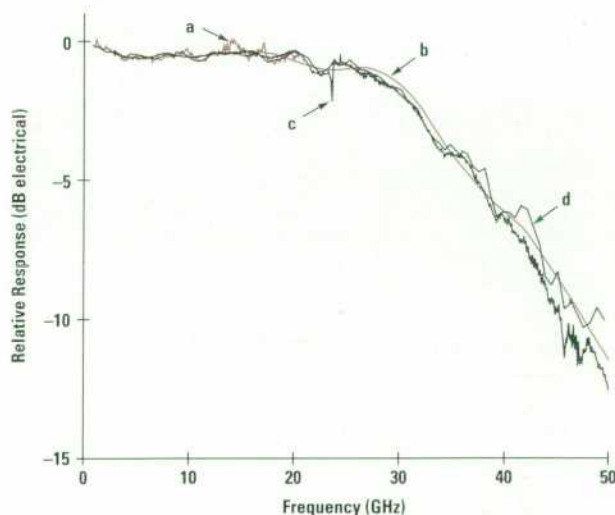
Fig. 5. Frequency response of an HP 83440D lightwave detector. (a) Data from an HP 8703A lightwave component analyzer (130 MHz to 20 GHz). (b) Data from the optical impulse response system (10 GHz to 50 GHz). (c) Data from the lightwave HP 8510 system (2 GHz to 50 GHz). (d) Data from the dual YAG heterodyne system (1 GHz to 50 GHz).

References

1. A.E. Siegman, *Lasers*, University Science Books, 1986, pp. 388-392.
2. K. Rush, S. Draving, and J. Kerley, "Characterizing High-Speed Oscilloscopes," *IEEE Spectrum*, Vol. 27, no. 9, September 1990, pp. 38-39.
3. T.S. Tan, et al, "Optical Receiver and Modulator Frequency Response Measurement with a Nd:YAG Ring Laser Heterodyne Technique," *IEEE Transactions on Microwave Theory and Techniques*, Vol. MTT-37, no. 8, 1989, p. 1217.
4. R.T. Hawkins II, et al, "Comparison of Fast Photodetector Response Measurements by Optical Heterodyne and Pulse Response Techniques," *Journal of Lightwave Technology*, Vol. 9, no. 10, October 1991, p. 1289-1294.
5. R. Jungerman, et al, "High-Speed Optical Modulator for Applications in Instrumentation," *Journal of Lightwave Technology*, Vol. 8, no. 9, September 1990, pp. 1363-1370.
6. R.L. Jungerman and D.J. McQuate, "Development of an Optical Modulator for a High-Speed Lightwave Component Analyzer," *Hewlett-Packard Journal*, Vol. 42, no. 1, February 1991, pp. 41-50.
7. R. Jungerman and D. Dolfi," Frequency Domain Optical Network Analysis Using Integrated Optics," *IEEE Journal of Quantum Electronics*, Vol. QE-27, no. 3, March 1991, pp. 580-587.

Authors

February 1993

6   Photonics Technology

Waguih S. Ishak

Waguih Ishak was born in Cairo, Egypt and attended universities in Egypt and Canada before joining HP Laboratories in 1978. He received a BSc degree in electrical engineering from Cairo University in 1971 and a BSc degree in mathematics from Ain Shams University in 1973. His MSc and PhD degrees in electrical engineering were awarded by McMaster University in 1975 and 1978. At HP, he designed surface acoustic wave low-loss filters for several products. Later, he managed research teams responsible for transferring the SAW technology, shockline technology, and photonics technology used for many HP synthesizers, oscilloscopes, and lightwave instruments. He currently manages the photonics technology department and has responsibility for technology transfer for more than ten HP products in the areas of RF, microwave, and communications test. He has written about 40 journal and conference papers on magnetic bubble memories, SAW devices, and magnetostatic wave devices. He is named an inventor in six patents and one pending patent on magnetostatic wave and SAW technologies. In 1990, he presented a paper on MSW technology by invitation to the USSR Academy of Sciences. Waguih is married and has two sons. He coaches youth soccer and sings in his church choir.

Kent W. Carey

R&D project manager Kent Carey received his BS degree from the University of California at Berkeley in 1976 and continued his studies at Stanford University, from which he received an MS degree in materials science in 1977. He joined HP in 1978 to do research aimed at improving the crystal quality of epitaxial silicon on sapphire substrates while continuing to work toward his PhD degree in materials science from Stanford, which he received in 1981. His research in the areas of organometallic vapor phase epitaxy of III-V compound semiconductors and photonic device processing has contributed to the development of several products, notably the HP 71400A lightwave signal analyzer, the HP 8702A/B and HP 8703A lightwave component analyzers, and the dual detector for the HP 8704A precision reflectometer. Since 1986, he has managed the optoelectronic devices group at HP Laboratories. He's the author or coauthor of more than 20 articles and conference papers and his work has resulted in a patent related to solid-state diffusion. A California native, Kent is married and has two children. His outside interests include wine tasting and studying Japanese.

Steven A. Newton

With HP laboratories since 1978, Steve Newton is project manager of the fiber and high-speed optics group. He has managed projects leading directly to five HP products: the HP 8145A optical time-domain reflectometer, the HP 11980A fiber interferometer, the HP 81210/310LI optical isolators, the HP 8504A precision reflectometer, and the HP 8509A/B polarization analyzers. He has a BS degree in physics from the University of Massachusetts (1976) and MS and PhD degrees in applied physics from Stanford University (1978 and 1984). He has contributed 45 publications and conference papers on fiber-optic devices, circuits, signal processing, and measurements and is named an inventor in ten patents on the same topics. He's a member of the IEEE and the Optical Society of America, for which he has served on several program committees. Steve was born in Teaneck, New Jersey. He is married, and outside of work, he enjoys sports and music.

William R. Trutna, Jr.

Author's biography appears elsewhere in this section.

11   Tunable Laser Sources

Bernd Maisenbacher

R&D project manager Bernd Maisenbacher contributed to the development of pulse and function generator products after joining HP in 1981, and then worked on various projects for lightwave power meters, sources, and attenuators. A project manager since 1986, he led the R&D team for the HP 8167A/68A tunable light sources and earlier was responsible for the HP 8153A lightwave multimeter, the HP 81210LI and 81310LI optical isolators, and the HP 8140A handheld loss test set. He is named as an inventor in two patents related to micropositioning and a circular filter wheel, both developed for the HP 8157A/58A optical attenuators. Bernd was born in Pforzheim, Germany and attended the University of Stuttgart, from which he received a Diplom Ingenieur in 1981. He lives in the Black Forest area and is married. He lists tennis, skiing, hiking, and bike riding as his outside interests.

Robert Jahn

An R&D project engineer at HP's Böblingen Instrument Division, Robert Jahn was a firmware engineer for the HP 8167A/68A tunable light sources, working on software design, hardware and software control, and the user interface. Earlier, he

developed the scan trace, user interface, and HP-IB and RS-232 capabilities for the HP 8146A optical time-domain reflectometer. He also was the firmware engineer for the HP 8153A lightwave multimeter. Born in Landsberg in the Bavarian area in Germany, he has a Diplom Ingenieur awarded in 1989 by the University of Dortmund. He has been with HP since 1989. Robert and his wife live in Stuttgart. His leisure activities include bike riding, billiards, and personal computers.

Michael Pott

Michael Pott joined HP in 1989, the same year he completed work for his Diplom Ingenieur in electronics at the University of Dortmund. He contributed to the firmware design for the HP 8153A lightwave multimeter, and later worked on the hardware design, user interface, and firmware for the HP 8167A/68A tunable light sources. His professional interests include software engineering methods and computer hardware. Michael was born in Hamm, Westfalen, Germany. He is married and enjoys personal computers, photography, and travel.

Edgar Leckel

Author's biography appears elsewhere in this section.

20 Laser Design and Wavelength Calibration

Emmerich Müller

With HP since 1981, project manager Emmerich Müller was responsible for optomechanical design of the external cavity laser for the HP 8167A/68A tunable light sources. Previously, he contributed to the design of the HP 81519A optical receiver and the HP 81520A/21B optical heads. He also was project manager for the detector modules and lens interfaces for the HP 8153A lightwave multimeter. His work has resulted in several patents related to optomechanical design. A member of the International Society for Hybrid Microelectronics and a graduate of the Engineering School of Furtwangen, he received his Diplom Ingenieur in 1981. Born in Obereschach, Germany, Emmerich has two children and enjoys woodworking and sports.

Wolfgang Reichert

With HP's Böblingen Instrument Division since 1982, Wolfgang Reichert contributed to the mechanical design for the HP 8167A/68A tunable light sources. He also developed fiber-optic interfaces and accessories for the HP 8153A lightwave multimeter and currently works on enhancements to the tunable light sources as well as

on process development for optomechanical assemblies. Born in Sindelfingen, Baden-Württemberg, Germany, he has a Diplom Ingenieur in mechanical engineering from the Engineering School in Esslingen. His degree was awarded in 1982. He is named as an inventor in a patent on moving and positioning optical filters. Wolfgang is married and has two children. His outside interests include working on his home, volleyball, tennis, and alpine skiing.

Clemens Rück

A graduate of the University of Bonn, development engineer Clemens Rück has a degree in physics, awarded in 1989. He joined HP's Böblingen Instrument Division the same year, and contributed to the development of the HP 8167A/68A tunable laser sources. He's presently working on enhancements to these products, as well as designing optical systems. A native of Baden-Württemberg, Clemens was born in Freiburg and now lives in Bondorf. He is married and has three children, which he says occupy most of his spare time.

Rolf Steiner

Rolf Steiner has been with HP since 1990 and was the production engineer responsible for the HP 8167A/68A tunable laser sources. He received a Diplom Ingenieur from the Engineering School at Karlsruhe in 1989 and worked in the field of medical electronics before joining the HP Böblingen Instrument Division. Before attending the university, he served for fifteen months in the German army. A native of Nagold, Germany, Rolf is married and has one son. He breeds pheasants and doves and enjoys sports.

28 Laser Temperature Stabilization and Power Control

Horst Schweikardt

An R&D project engineer at HP's Böblingen Instrument Division, Horst Schweikardt has been with HP since 1972. He contributed to the hardware design of the HP 8167A/68A tunable laser sources and the design of the power meter modules for the HP 8153A lightwave multimeter. He also has served as a project leader for the HP 8152A optical power meter and the HP 81521B optical head, and has headed project teams for the HP 214B pulse generator and other products. He received his Diplom Ingenieur in electrical engineering from the University of Stuttgart in 1972. A native of Schwäbisch Gmünd, Baden-Württemberg, he is married and has two children. His hobbies include photography, mountaineering, and bowling.

Edgar Leckel

R&D project engineer Edgar Leckel was responsible for the hardware design, instrument architecture, calibration software, and development of measurement techniques for the HP 8167A/68A tunable laser sources. He received his Diplom Ingenieur in communications engineering from the University of Stuttgart in 1988 and joined HP the same year. Edgar was born in Hildrizhausen, Germany and is now a resident of the Black Forest region. He's married, likes to travel, and enjoys sports such as hiking, swimming, and soccer.

32 Dual-Output Laser Module

Roger L. Jungerman

Roger Jungerman's special interests include fiber optics, integrated optics, and acoustics. He contributed to the development of the laser module for the HP 8167A/68A tunable laser sources. He studied physics at the University of California at Santa Cruz (BA 1978) and applied physics at Stanford University (MS 1983 and PhD 1985). At Watkins-Johnson Company, he worked on thin-film coating development, and then joined HP's Microwave Technology Division in 1985. One of his first assignments was developing surface acoustic wave devices. Currently, he is working in lightwave R&D. Roger is the author of 20 journal articles and 20 conference papers on fiber optics, optical modulators, microscopy, and microwave acoustics. His work has resulted in three patents, two on optical modulators and one on a scanning optical microscope. He is a member of the IEEE, the SPIE, and the Optical Society of America. Roger was born in Sacramento, California. He is married and enjoys bicycling and hiking.

David M. Braun

Author's biography appears elsewhere in this section.

Kari K. Salomaa

Kari Salomaa graduated from the Massachusetts Institute of Technology with a BSME degree in 1973. Before coming to HP in 1982, he was a mechanical designer for several companies, working on a diverse range of products from electromechanical transducers to artificial kidneys. He contributed to the development of the tunable external cavity laser for the HP 8167A/68A tunable laser sources and earlier worked on optical modulators and optical receivers. He is named as an inventor in a patent on an automated serial diluter developed for Cetus Corporation. Kari is a native of Helsinki, Finland and currently lives in Jenner, California, where he serves as community fire captain.

35 External-Cavity Laser Research

William R. Trutna, Jr.

Project manager Rick Trutna joined HP in 1980. He worked on IC process development during the first four years of his HP career, then moved to HP Laboratories, where he contributed to the development of the HP 8145A optical time-domain reflectometer. He was project manager for the group that developed the HP 8167A/68A tunable laser sources. Rick is a member of the IEEE and is the author of 20 articles on optics, lasers, fiber optics, and integrated circuit processing. His work has resulted in eight patents on the same topics. Born in Pasadena, Texas, he studied electrical engineering at the University of Texas at Austin (BSEE 1973) and at Stanford University (MSEE 1974 and PhD 1979). He also did a year of postdoctoral work on laser isotope separation of uranium at the Max-Planck Institut für Quanten Optik in Garching, Germany. Rick is married, has two sons, and enjoys hiking in addition to spending time with his family.

Paul Zorabedian
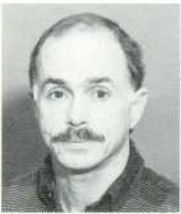
With HP Laboratories since 1981, Paul Zorabedian has a BS degree in physics from Yale University (1974) and MS and PhD degrees in applied physics from Stanford University (1976 and 1982). He investigated laser re-growth of silicon films before joining the HP Labs photonics technology department, where he worked on the receiver for the HP 8145A optical time-domain reflectometer. His contribution to the HP 8167A/8168A tunable laser sources was the external-cavity semiconductor laser. He has written a dozen technical papers, is named as an inventor in four patents related to external-cavity lasers, and is a member of the Optical Society of America and the IEEE. Paul was born in Providence, Rhode Island. His outside interests include swimming, bicycling, hiking, camping, kayaking, and ballroom dancing.

39 Low-Coherence Reflectometer

D. Howard Booster

R&D project manager Howard Booster has held several positions since joining HP in 1974. He was responsible for analog and microcircuit design on the HP 8672 and HP 8340 microwave sources, and then managed the team that introduced the HP 8340 to manufacturing production. From 1984 to 1990, he established and managed the quality engineering department for HP's Lightwave Operation, and most recently was R&D project manager for the HP 8504A precision reflectometer. A graduate of Stanford University, he received a BSEE degree in 1974 and an MSEE degree in 1975. He is a native of Corvallis, Oregon, is married, and has three

daughters. His leisure interests include Scottish fiddle music and classical and pop piano. He is a member of the San Francisco Scottish Fiddlers.

Harry Chou

Author's biography appears elsewhere in this section.

Michael G. Hart

Development engineer Mike Hart works at the HP Lightwave Operation and was responsible for firmware development for the HP 8504A precision reflectometer. Since coming to HP in 1984, he has developed firmware for the HP 8753 network analyzer and the HP 8702 and HP 8703 lightwave component analyzers. Most recently, he developed software for the HP 8509 lightwave polarization analyzer. An author of two previous HP Journal articles on lightwave instruments, his work has resulted in three patents related to lightwave component analyzers. His professional interests also include user interface design for instruments. Born in Sacramento, California, he is married, and has two children. He plays piano and organ and shares the organ playing duties at his church. He also enjoys horseback riding and spends part of his paycheck on his two horses.

Steven J. Mifsud

Born in San Francisco, Steve Mifsud studied mechanical engineering at the California Polytechnic State University at San Luis Obispo, graduating in 1982 with a BS degree in mechanical engineering. Before joining HP's Network Measurements Division in 1985, he designed hard disk drives at Shugart Corporation. He worked on the HP 85070A materials probe and was on the mechanical design team for the HP 8504A precision reflectometer at the HP Lightwave Operation. Steve is married and has two children.

Rollin F. Rawson

An R&D development engineer, Fred Rawson has contributed to the design of a series of HP instrument products, including sweep oscillators, scalar and vector network analyzers, and lightwave component analyzers. He was the hardware designer for the HP 8504A precision reflectometer. Fred was born in Laguna Beach, California and served in the U.S. Air Force for four years as a staff sergeant. He joined HP's engineering pool in 1960 before he graduated from San Jose State University with a BS degree in electrical engineering (1961). He and his wife have four children and three grandchildren. For relaxation, he collects and refurbishes Studebakers and collects U.S. postage stamps.

49 Diode Fabrication

Patricia A. Beck

Hardware engineer Patti Beck works at HP's Lightwave Operation and is responsible for process transfer between divisions for new lightwave products. Since joining HP in 1990 she has worked on semiconductor laser and diode design, fabrication, testing, packaging, and reliability. Born in Atlantic City, New Jersey, Patti has a BS degree in applied physics from Stockton State College (1980) and MS and PhD degrees, also in applied physics, from Stanford University (1983 and 1991). Her dissertation work advanced the art of silicon micromachined sensors. Before joining HP she held research positions at Kitt Peak National Observatory and at AT&T Bell Laboratories, where she conducted research on topics such as solar energy, robotics, low temperature semiconductors, and recrystallized and porous silicon. She is a member of the American Physical Society and the IEEE, has published several technical papers, and her work has resulted in patents in the areas of robotics and semiconductors. Her leisure activities include photography, charcoal sketching, travel, hiking and backpacking, the arts, other sciences and all varieties of puzzles.

52 Optical Reflection Measurements

Harry Chou

A design engineer with HP's Lightwave Operation, Harry Chou has worked on design, development, and testing of lightwave test instruments since joining HP in 1989. Past projects include the HP 8703 lightwave component analyzer and the HP 8504A precision reflectometer. More recently, he has been responsible for testing the HP 8509 polarization analyzer. He studied electrical engineering at the Massachusetts Institute of Technology, from which he received BS (1981), MS (1983), and PhD (1989) degrees. His doctoral research was in the area of optically pumped solid-state laser materials. From 1983 to 1984, he was with Codenoll Technology Corporation, where he was responsible for fabrication of semiconductor light sources. He is the author of two HP Journal articles and has published papers in the areas of lasers, light sources, and interferometry. His work has resulted in a patent on optical fiber measurement. Harry is married and enjoys hiking, sailing, skating, and visiting museums with his wife.

Wayne V. Sorin

A native of British Columbia, Canada, Wayne Sorin joined HP Laboratories in 1985. His academic degrees include a bachelor of science (1978) and a bachelor of applied science in electrical engineering (1980) from the University of British Columbia.

He continued his studies at Stanford University, from which he received an MSEE degree in 1982 and a PhD degree in 1986. His work at HP involves research and development on optical fiber-based measurement systems. He demonstrated the technical feasibility of a precision reflectometer, which was the basis for the HP 8504A precision reflectometer, and transferred the technology to HP's Network Measurement Division. Wayne has authored or coauthored 24 publications on optical fiber-based devices and systems and is listed as inventor or coinventor in nine patents on the same topic. He's a member of the IEEE and is currently interested in applications of low-coherence interferometry. Wayne is married and has a seven-year old son. He likes tennis and an occasional game of golf.

60 All-Haul OTDR

Josef Beller

Project leader Josef Beller has been with HP since 1987. He received a Diplom Ingenieur in electrical engineering from the University of Stuttgart in 1982, and worked at the university as a research associate in digital signal processing while completing his doctoral degree (1987). He contributed to the design of the data acquisition and digital signal processing hardware for the HP 8146A optical time-domain reflectometer, and now heads a team working on OTDR enhancements. He is the author of several papers on low-noise digital filters and noise reduction techniques, and his work has resulted in a patent related to the signal processing technique used in the HP 8146A OTDR. Josef enjoys woodworking, making furniture, reading, backpacking, and hiking.

Wilfried Pless

Project manager Wilfried Pless attended Ruhr University at Bochum and received his Diplom Ingenieur in 1982. With HP since 1983, he worked on the first fiber-optic products developed at the Böblingen Instrument Division, the HP 8150A 850-nm laser source and the HP 8151A optical power meter. He also contributed to the development of the signal processing technology for the HP 8145A optical time-domain reflectometer. After that he led the software team for the HP 8153A lightwave multimeter and then became project manager for the HP 8146A OTDR. He's now a project manager for photonic equipment and is the author of HP Journal articles related to the HP 8151A and the HP 8153A. Born in Haltern in Westfalia, Germany, Wilfried is married and has five children; the youngest are twins. His hobbies include music and everything having to do with personal computers.

63 OTDR Signal Processing

Josef Beller

Author's biography appears elsewhere in this section.

69 OTDR Receiver

Frank A. Maier

With HP since 1989, Frank Maier is R&D project manager for OTDR activities at the Böblingen Instrument Division. He was born in Waiblingen, Baden-Württemberg, Germany and attended the University of Stuttgart, from which he received a Diplom Ingenieur in 1988. He contributed to the development of the laser sources for the HP 8153A lightwave multimeter before working on receiver hardware and analog hardware troubleshooting for the HP 8146A. His professional interests include analog hardware, especially optoelectronics. Frank enjoys opera, theater, and good food and wine.

72 OTDR User Interface

Robert Jahn

Author's biography appears elsewhere in this section.

Harald Seeger

Software engineer Harald Seeger was born in Esslingen, Germany and attended the University of Karlsruhe, from which he received his Diplom Ingenieur degree in electronics in 1988. He has worked on several OTDR projects since joining HP's Böblingen Instrument Division in 1989. His contributions to the HP 8146A OTDR include work on the display and measurement firmware, the scan trace algorithm, and the PC software. Harald enjoys traveling and is interested in politics, ecology, and economics.

79 Optical Return Loss Measurement

Siegmar Schmidt

Optics specialist Siegmar Schmidt has been with HP's Böblingen Instrument Division since 1984. He has a degree in physics from the Friedrich Schiller University at Jena and worked in the field of optics before coming to HP. He has contributed to the development of the HP 8121OLI and HP 8131OLI optical isolators, the HP 8157A and 8158A/B optical attenuators, and the HP 81000AS/BS optical power splitters. One of his recent projects was a new return loss module for the HP 8153A lightwave multimeter. A patent has resulted from his work on a variable optical attenuator. Born in Jena, Thüringen, Siegmar is married, has two sons, and lives in the Black Forest region. His hobbies include boardsailing, swimming, and tennis.

83 Time-Domain Lightwave Detectors

Randall King

Hardware design engineer Randy King was born in Port Jervis, New York. He received a BS degree in physics from the University of Oregon in 1979 and an MSE degree in interdisciplinary engineering in 1983 from the University of Washington. More recently (1991) he completed work for an MS degree in engineering management from the National Technical University. Before joining HP in 1984 he designed oceanographic instruments and was a technician at Kitt Peak National Observatory. On his first HP assignment at the Signal Analysis Division, he was a reliability physics engineer. Later, he managed environmental test and reliability physics laboratories for the Network Measurements Division. He contributed to the receiver design of the HP 83440 Series lightwave detectors. Randy has written two papers on reliability physics and is a coauthor of two others on astronomy. He enjoys a variety of outside activities, including kart racing, hiking, gardening, mountain biking, and sailing.

David M. Braun

A native of Shawano, Wisconsin, hardware design engineer David Braun received a BSEE degree in 1978 and an MSEE degree in 1980 from the University of Wisconsin. After joining HP in 1980, he worked on test and process development for a high-speed photodetector and on development of a GaAs power MESFET. He contributed to the mechanical design and optical launch design of the HP 83440 Series lightwave detectors and the laser antireflection coating process for the HP 8167A/68A tunable laser sources. David is the author or coauthor of five articles and a conference paper on photodetector antireflection coating design and measurement, GaAs MESFET design, and optical receiver design. Two patents have resulted from his work on low-reflectivity surface relief gratings for photodetectors. He is a member of the Optical Society of America. He is married, has three sons, and enjoys bicycling, gardening, and basketball.

Stephen W. Hinch

R&D program manager Steve Hinch has held several positions since coming to HP in 1974. As a production engineer, he supported work for a number of spectrum and network analyzer products. Later, he was production engineering manager for microelectronic components. As corporate manager for HP's surface mount technology program, he supervised the design and consolidation of HP's surface mount manufacturing sites. After serving as R&D section manager for microwave accessories he

assumed his current position, in which he is responsible for lightwave time-domain measurement instruments in HP's Lightwave Operation. Steve's BS and ME degrees were awarded concurrently in 1974 by Harvey Mudd College, Claremont, California. A member of the Optical Society of America and the Surface Mount Technology Association, Steve is the author of a book on surface mount technology as well as numerous technical articles. He is married and has two children. His leisure interests include swimming, mountain biking, backpacking, and large-format photography.

Karl Shubert

With HP since 1979, Karl Shubert was R&D project manager for the HP 83440 Series lightwave detectors. Earlier, he was an engineering supervisor and manufacturing section manager for fabrication of thin-film circuits and surface acoustic wave devices. He graduated in 1979 from California Polytechnic State University at San Luis Obispo with a BSME degree. Karl is married and has two daughters. His favorite pastimes include cabinetry, gardening, white water rafting, cross-country skiing, winemaking, and cooking.

David J. McQuate

A design engineer at HP's Microwave Technology Division, David McQuate received a BS degree in physics from Ohio University in 1970 and MS and PhD degrees in the same field from the University of Colorado at Boulder (1974 and 1977). He joined HP in 1978. Past projects include microwave spectrum analyzer design, GaAs FET characterization and modeling, optical modulator design, and design of a computer-aided fiber pigtailing system. He contributed to the design and characterization of photoreceivers for the HP 83440 Series lightwave detectors. Currently, he is working on a 50-GHz lightwave production frequency-response test system. David and his wife have two daughters. His leisure activities include music synthesizers, bicycling, backpacking, cross-country skiing, and gardening.

Kok Wai Chang

Born in Hong Kong, Bill Chang attended National Chung Kung University in Taiwan, from which he received a bachelor of science degree in physics in 1977. He also studied physics at Cambridge University, England, for which he received a certificate of postgraduate study in 1978. His PhD in physics was awarded by Texas Christian University in 1982. He was a research associate at the University of Texas at Arlington before joining HP in 1984. Past HP projects include work on an optical isolator, a fiber measurement technique, and magnetostatic wave devices. He is currently working in the area of high-speed optical testing and was involved in testing and calibrating the HP 83440 Series lightwave detectors. Bill has written 20 papers in the areas of molecular spectroscopy, magnetostatic wave devices, optical isolators, and fiber-optic measurement and is named an inventor in five patents related to MSW devices and one on an optical isolator. He is a member of the IEEE and the Optical Society of America. He is married and has two sons and is a fan of the Oakland A's baseball team.

Christopher J. Madden

Chris Madden completed work for his PhD degree in electrical engineering at Stanford University in 1990, the same year he joined HP. A member of the technical staff at HP Laboratories, he is working on the design, modeling, and testing of high-frequency p-i-n and FET devices and circuits for the HP 83440 Series lightwave detectors. He is the author of several articles on picosecond electronics and optoelectronics and is a member of the IEEE. He moved to California from his home town near Boston, Massachusetts in 1981.

HEWLETT PACKARD